AN ABSTRACT OF THE THESIS OF

James Barr Ridlon (Name of Student) for the Ph. D. (Degree)

in Oceanography (Geological) (Major) presented on November 24, 1968 (Date)

Title: Bathymetry and Structure of San Clemente Island, California, and Tectonic Implications for the Southern California Continental Borderland

Abstract approved: Redacted for privacy

John W. Byrne

Five lithologic units, ranging in age from Middle Miocene to Recent, are defined on the basis of continuous seismic reflection profile records. Two of the units are Miocene sedimentary and volcanic rocks that have been truncated to form a major unconformity (post-orogenic surface) related to the most recent major tectonism of the region. The remaining units are post-orogenic unconsolidated sediments.

The fault pattern offshore is generally related to that exhibited on the island. The pattern conforms to a wrench-fault system hypothesized by Moody and Hill (1956) modified by a general north-south tensional fracturing. The San Clemente Fault is assumed to be the primary wrench fault of the system. Anomalies in the thicknesses and the structure of the unconsolidated sediment and rock units tend to confirm the structural model.

A canyon (Eel Ridge Canyon) off the west side of San Clemente Island appears to have been caused by pivotal faulting and erosion, and represents a boundary between different structural trends north and south.

A prominent terrace around the island is postulated to have been wave-cut during and since the Late Pleistocene. The island has been tilted slightly to the west by Recent tectonism.

A steep magnetic gradient off the east side of the island is considered the consequence of faulted volcanic flows comprising the island itself and a deep basic rock mass responsible for a large positive magnetic anomaly off the northwest side. Other magnetic anomalies reflect major structural trends.

Earthquake epicenter data suggest a recent and possibly cyclical occurrence of fault activity in the northern Continental Borderland region and the study area. Fault offsets at the sea floor and earthquake epicenters along the San Clemente fault zone imply recent adjustments along the fault.

Wrench-fault movement resulting from a simple shear or shear couple is considered to have caused the zone of brecciation along the San Clemente Fault and produced the fault-trace curvature so evident in a series of en echelon, northwest-striking major faults of the Borderland. Tensile release during periods of wrench-fault development has been a fundamental factor in the structural development of the Borderland basins. The entire structure of the Continental Borderland is believed to have developed by right-lateral movement along the series of wrench faults. These faults are believed to have resulted from a translation

of force by sea-floor spreading originating on the East Pacific Rise in the Gulf of California region. This force is considered to have moved a northern Continental Borderland crustal plate westward by east to west release along major wrench faults bordering the north and south ends of this plate.

Sediments, transported along channels developed along faults in the island block, were deposited in basins developed by faulting and folding of the pre-orogenic rocks. Transportation appears to have been by means of turbidity-current flows, sand flows, and slides. A maximum average depositional rate of 35 to 47 centimeters per 1,000 years is estimated for post-orogenic sediments.

The following findings are suggested for inclusion in the Neogene history of the island: (1) the top 365 meters of Miocene andesitic lavas were deposited above sea level and tend to become slightly more basic in composition with depth; (2) subsidence of the island region and temporary sea-level stand(s) occurred after the deposition of the volcanic rocks, with possible periods of foundering to about the Late Pliocene; (3) emergence, lengthy subaerial exposure, and a period of partial submergence took place from about Late Pliocene through Early Pleistocene; (4) a north-south compressive force developed or recurred across the Borderland during Late Pliocene, developing the present northwest-southeast and east-west wrench-fault systems that have been intermittently active to the present time; (5) much of the present Borderland topography formed during the Pleistocene to Recent.

Bathymetry and Structure of San Clemente Island, California, and Tectonic Implications for the Southern California Continental Borderland

by

James Barr Ridlon

A THESIS

submitted to

Oregon State University

in partial fulfillment of
the requirements for the
degree of

Doctor of Philosophy

June 1970

APPROVED:

Redacted for privacy

Professor of Oceanography
in charge of major

Redacted for privacy

Chairman of Department of Oceanography

Redacted for privacy

Dean of Graduate School

Date thesis is presented November 24, 1969

Typed for James Barr Ridlon

ACKNOWLEDGMENTS

Obtaining marine data is a team effort requiring a high standard of cooperation among scientific personnel and with the ship's crew. The author is particularly grateful to D. W. Scholl and R. E. von Huene, now with the U. S. Geological Survey, Menlo Park, California, whose guidance during the planning stages of the cruises, assistance at sea, and interpretation of data greatly contributed to the success of this investigation.

The author acknowledges especially the critical review of the manuscript by his major professor, Dr. John V. Byrne, and Dr. L. Kulm, Department of Oceanography, and Dr. H. Enlows, Department of Geology, Oregon State University, Corvallis, Oregon.

Special thanks are due J. R. Curray, Scripps School of Oceanography, University of California, La Jolla, California; D. G. Moore and E. L. Hamilton of the Naval Undersea Research and Development Center, San Diego, California; and C. F. Austin and P. St.-Amand of the Naval Weapons Center, China Lake, California, who offered valuable suggestions and critical appraisal of the interpreted results.

J. C. Vedder and P. G. Smith of the U. S. Geological Survey, Menlo Park, California, identified fossils from deposits on San Clemente Island and from samples recovered by the CURV (cable-controlled undersea research vehicle) instrument. J. K. Pringle of the Naval Weapons Center, China Lake, aided by doing a petrographic analysis of some of the submarine volcanic rock samples.

Excellent radar tracking by members of the Naval Undersea Research and Development Center San Clemente Island range personnel contributed

to the success of the sea operations. E. Beasey of the Naval Weapons Center, China Lake, provided maintenance and assisted in the operation of the profiling equipment on the reconnaissance survey.

The skill and outstanding cooperation of the personnel from the Naval Undersea Research and Development Center, Pasadena, California, who operated the CURV instrument, are recognized.

The exemplary cooperation of Captain D. Patterson and the crew of the MV Defiance and the operators of the MV Duchess and the tug, YTM-759 is acknowledged.

The study reported herein was conducted as part of a broad survey of the San Clemente ocean area, as a basis for plans to use the ocean floor. The survey was conducted by the Naval Weapons Center, financed in large part by independent research and exploratory development funds provided by the Director of Navy Laboratories. The author appreciates the substantial support of the Naval Weapons Center, which made this report possible.

TABLE OF CONTENTS

TABLE OF CONTENTS (CONTINUED)

LIST OF FIGURES

LIST OF FIGURES (CONTINUED)

LIST OF FIGURES (CONTINUED)

LIST OF FIGURES (CONTINUED)

LIST OF TABLES

BATHYMETRY AND STRUCTURE OF SAN CLEMENTE ISLAND, CALIFORNIA, AND TECTONIC IMPLICATIONS FOR THE SOUTHERN CALIFORNIA CONTINENTAL BORDERLAND

I. INTRODUCTION

SCOPE OF INVESTIGATION

San Clemente Island, off the coast of southern California (Figure 1), was selected early in 1966 by the U. S. Naval Ordnance Test Station (now the Naval Weapons Center), China Lake, California, as a possible site for a permanent, manned, under-the-sea-floor installation with direct sea-floor access for marine environment studies. Initial marine investigations during 1966 involved geophysical and geological surveys (Appendix I). The first of two surveys (Figure 1) was a nearshore continuous-seismic-reflection-profile reconnaissance around the island. This survey employed a 30- to 120-kilojoule low resolution system (Appendix II) along survey lines 4 to 5 nautical miles in length positioned normal to the island and separated by approximately 1 nautical mile. The second survey was a 750- to 3,000-joule high resolution detailed seismic-profiling survey (Appendix II) of the seaward portion of two favorable areas, Eel and Lost Points,[1] on the western side of the island. This survey was coordinated with topographic and geologic studies on the island related to the intended drill site. The second survey involved SCUBA diving to a depth of 45 meters to investigate and sample rock

---

[1]The concentrated profile grids off Eel and Lost Points are identified in this paper as the "Eel Point Grid" and the "Lost Point Grid."

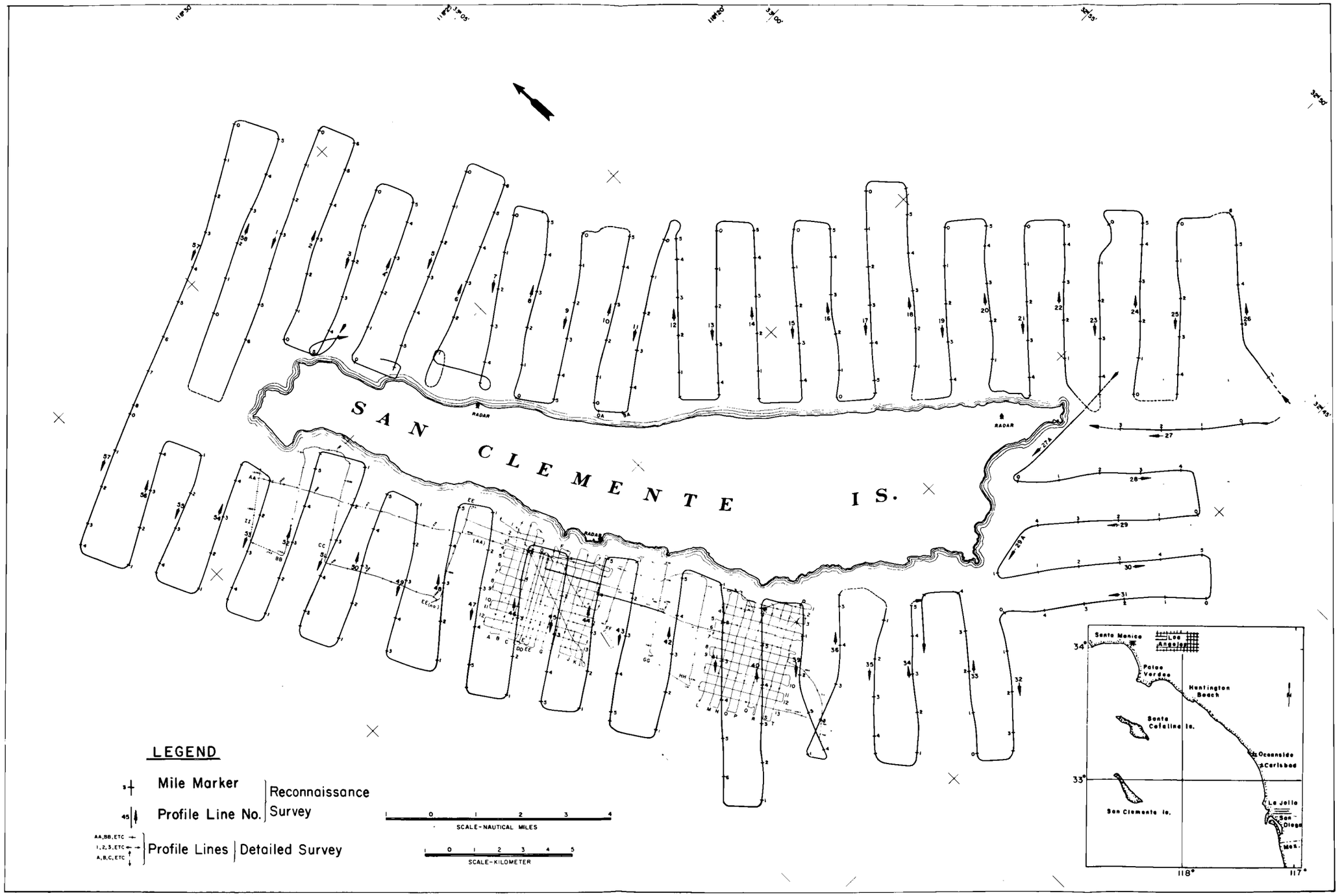

Figure 1. Index map and ship's tracks for acoustical Reflection Profile Surveys, San Clemente Island, July and August 1966.

outcrops as well as surface sampling (snapper) of sea-floor sediments at depths greater than 45 meters (Figure 2). These surveys are referred to in this paper as the Reconnaissance Survey and Detailed Survey, respectively.

The Reconnaissance Survey made possible the delineation of general offshore sea-floor topography, subbottom structures, and rock types that would influence the site selection. The Detailed Survey provided offshore geologic information for potential sites at Eel and Lost Points. The nature and structure of the shallow rock units were also resolved by the Detailed Survey.

Survey methods relative to instrumentation, navigation, and related geological considerations, and water sound velocity data are detailed in Appendices II and III. Water depth and rock unit thickness data, interpreted from the profile records, are listed in Appendix IV.

Additional structural and sedimentation information was taken from continuous seismic profiles of a 1964 cruise on the U.S.N.S. Gear by personnel from the U. S. Naval Ordnance Test Station.

A supplementary aeromagnetic survey was initiated in December 1966 and January 1967 to measure the total intensity of the earth's magnetic field in the area studied.

PURPOSE OF INVESTIGATION

Data from the surveys are used in this paper to (1) define the offshore rock units and relate these to the rocks on the island and others of the immediate offshore region; (2) relate bathymetry to the structural nature of the island block; (3) identify the structure of the

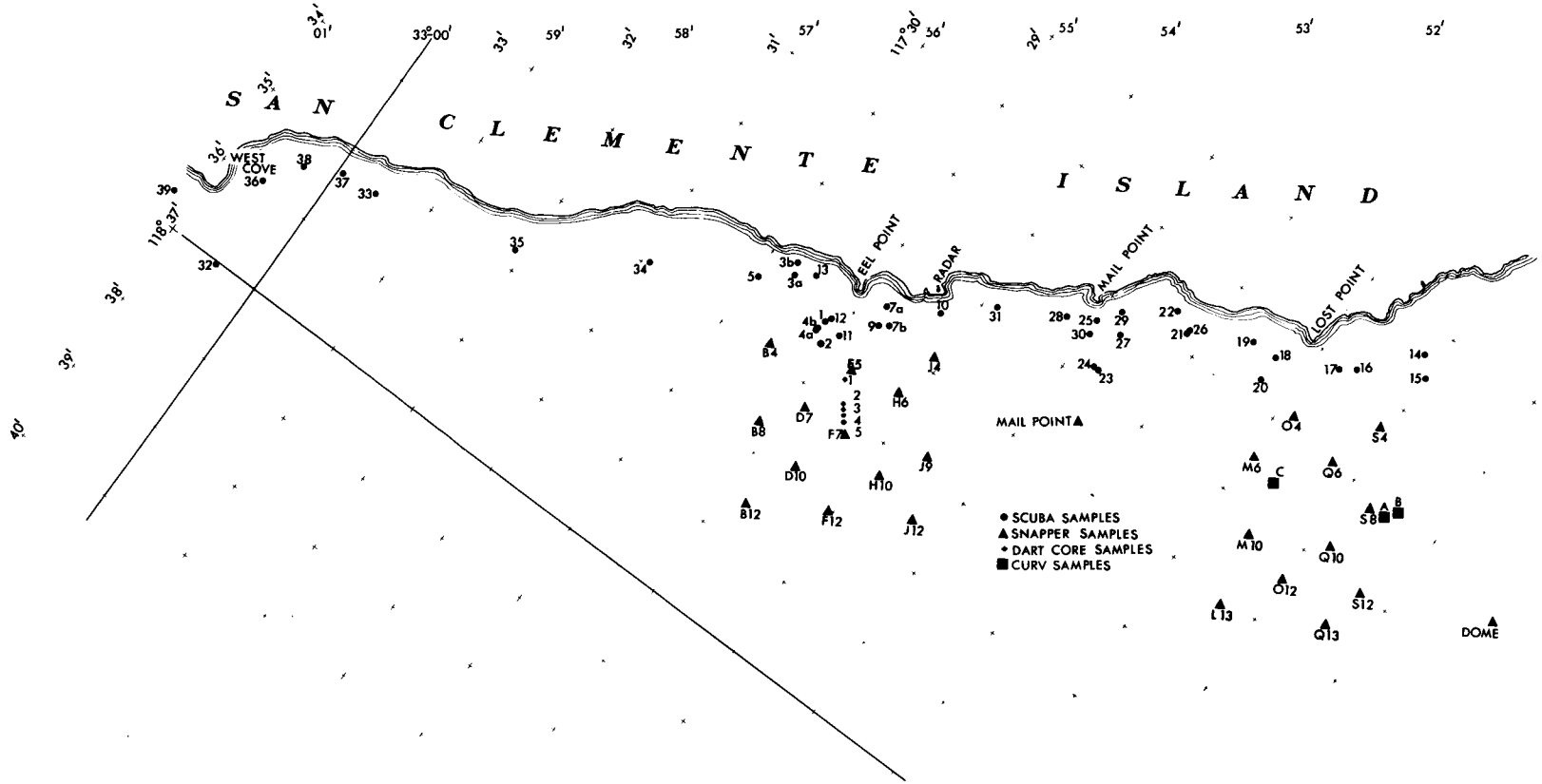

Figure 2. Sea-floor sample locations, Detailed Survey.

island block with a best-fitting structural model; and (4) propose this model as the mode for the geologic development of the San Clemente Island block in relation to the origin of the surrounding borderland region. To further implement this study, bottom samples from the Detailed Survey coupled with information taken from cores of other surveys are used to identify the mode of sediment transport and consequent fill in adjacent basins; magnetic and seismic data are also incorporated as aids to the study.

The objective of the study is to provide a better understanding of the geologic history of the Continental Borderland off the coast of southern California.

PREVIOUS INVESTIGATIONS

The geology of San Clemente Island is known mainly from reconnaissance studies. Smith's paper (1898) describes the general geologic features in considerable detail. Olmsted (1958) refined the areal geology of Smith and furnished additional data on the age and lithology of the rocks and sediments described by Smith. Mitchell and Lipps (1965) reported on some vertebrate fossil and the general depositional environment of the sedimentary rock exposures over the island. Merifield and Lamar (1967) made a detailed structural survey of two 6-km^2 areas around Eel and Lost Points. The author has made a general reconnaissance of parts of the island to ascertain further structural relationships.

Bathymetric data of the nearshore area around the island are known from U. S. Coast and Geodetic Survey soundings, publications of Shepard and Emery (1941), Emery (1960), and Gaal (1966). Subbottom data consist

of a few widely separated seismic-reflection reconnaissance profiles made during the 1964 cruise of the U.S.N.S. Gear.

REGIONAL GEOGRAPHIC SETTING

The submarine basin and range province between the coast and the continental slope off southern California were named the Continental Borderland by Shepard and Emery (1941), a term which is used in this paper. This area is also classified as a basin-ridge complex province of the continental margins by Heezen (1963).

San Clemente Island is the southernmost of a series of islands within the northern portion of this borderland area. The center of the island is at approximately 32°50'N latitude and 118°30'W longitude.

II. GENERAL PHYSIOGRAPHY AND GEOLOGY

SAN CLEMENTE ISLAND

The island is the upper part of a tilted, gently domed and faulted block of the earth's crust that is elevated more than 1.6 kilometers relative to the floors of adjacent sea basins (Olmsted, 1958). The upper part of this block is composed principally of volcanic rocks (Olmsted, 1958; Harrison et al., 1966). Although the surface of the island is principally volcanic rocks, some 16 isolated patches of Miocene marine sedimentary rocks (from a few to about 90 meters thick) are preserved in down-thrown fault blocks (Olmsted, 1958; Mitchell and Lipps, 1965).

The northeast side of the island is fronted by a steep slope, (Figure 3a and b), presumably a fault-line scarp (San Clemente Fault). The island portion of this scarp averages 15 degrees in dip, but in some areas steepens to slightly more than 30 degrees (Olmsted, 1958). Slump scars and slumps are noted along part of this scarp. In contrast, the remainder of the island has a gently dipping slope to the southwest, averaging less than 5 degrees of dip (Olmsted, 1958). Together, these slopes give the island a cuesta-like appearance. The southwesterly dipping slope is interrupted by more than 20 wave-cut terraces or step-like benches (Figure 3b) that represent former relative stands of sea level (Olmsted, 1958).

Northeastward-trending stream courses have moderate to steep gradients and are shallow to deeply incised. The drainage down the southwest-dipping slope is confined to generally straight V-shaped canyons

(a)

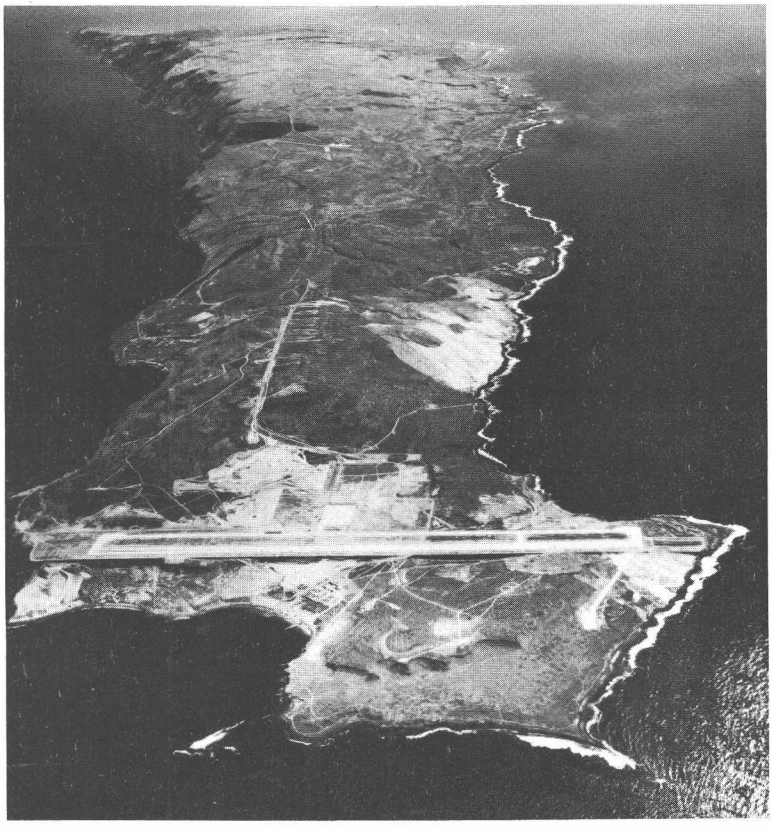

(b)

(Figure 3a); however, the courses are shallow and mostly ill-defined at the upper reaches of the slope.

OFFSHORE REGION

San Clemente Island is bordered on the north and northeast by the Santa Catalina Basin, on the west by the San Nicolas Basin, and on the south to southeast by the San Clemente Basin (Figure 4). Other prominent features are the San Clemente Escarpment and San Clemente "Rift" Valley (Shepard and Emery, 1941, Chart 1) immediately off the east and southeast side of the island block, and the San Clemente Ridge (Gaal, 1966), a submerged continuation of the island block northwestward to near the Osborne Bank.

Various authors report rock and sediment samples of Eocene, Miocene, Pliocene, and Pleistocene ages from the adjacent basins, submerged ridges, and banks (see, for example, Emery, 1960; Krause, 1965; Uchupi, 1961).

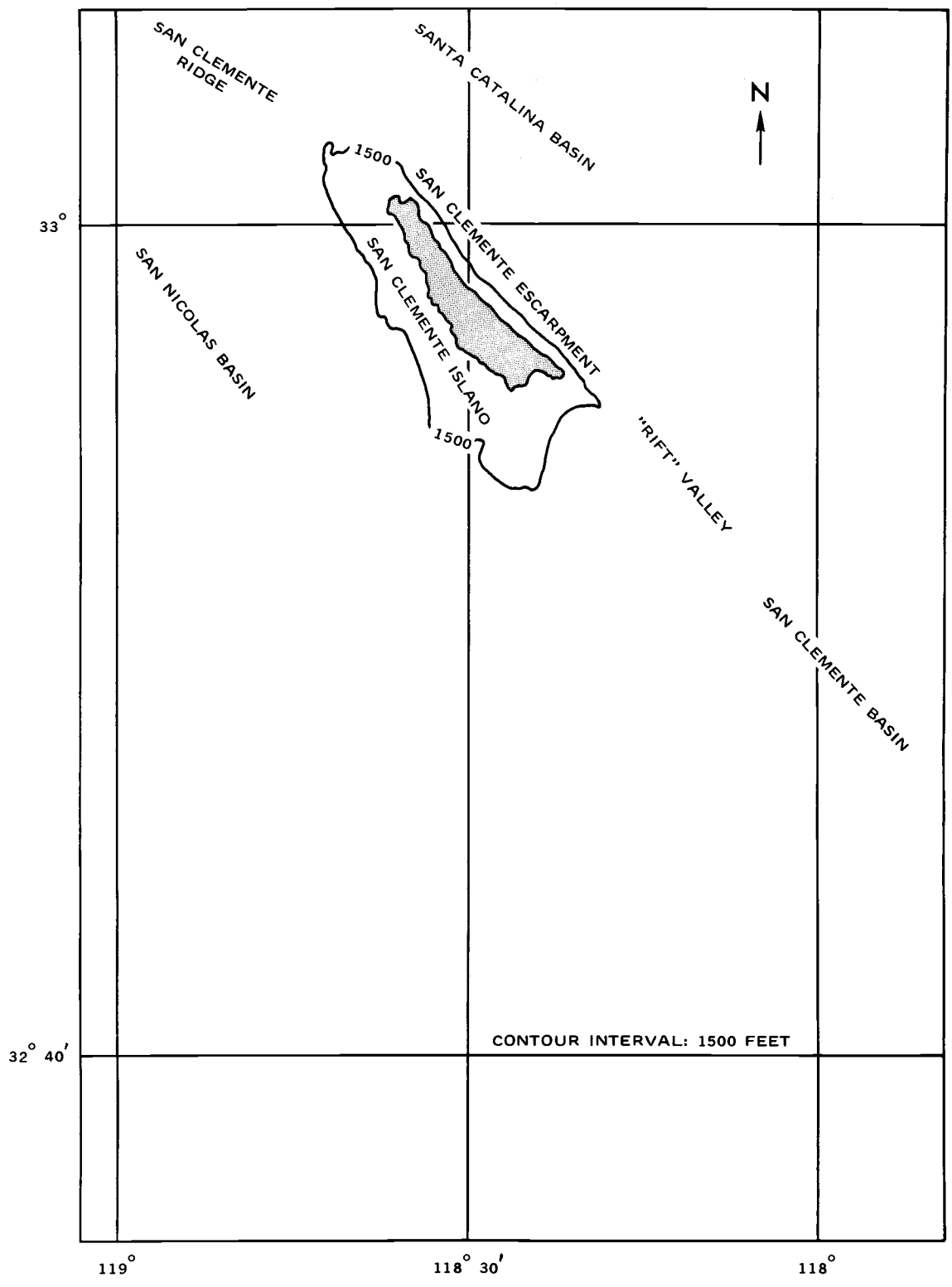

Figure 4. Regional physiographic features.

III. BATHYMETRY

The dominant topographic and bathymetric trend in the Continental Borderland is northwest-southeast. There is an equally important but subtle east-west trend (Shepard and Emery, 1941; Emery, 1960; Gaal, 1966; Krause, 1965; Moore, 1966). The San Clemente Island crustal block follows the strong northwest-southeast topographic trend but also demonstrates a subtle northeast-southwest topographic trend across the central part of the crustal block.

The waters surrounding San Clemente Island at a distance of 5 kilometers from shore range in depth from 250 (west side of island) to 1,200 meters (east side of island). Depths in excess of 1,800 meters are noted within 25 kilometers of the southeast end of the island. The proximity of deep water emphasizes the relief of this island block above the surrounding basins.

Gaal (1966) roughly outlined the physiographic provinces of the Santa Catalina Basin. The San Clemente Island crustal block forms the southwest border of the Basin. The bathymetry of the study area can be divided into three distinct major geomorphic types (Figure 5): (1) irregular topography generally representing the San Clemente Slope of Gaal but divided by a prominent shallow marine shelf; (2) the major offshore shelf averaging slightly more than 100 meters below sea level and broad off the west side and ends of the island; and (3) the basin-trough area, mostly equivalent to the San Clemente apron and southern part of the Santa Catalina Basin Plain of Gaal, including some perched troughs occupying this apron province. The Emery Seaknoll and Southern Plateau, identified by Gaal, are placed under the irregular topographic area as are smaller

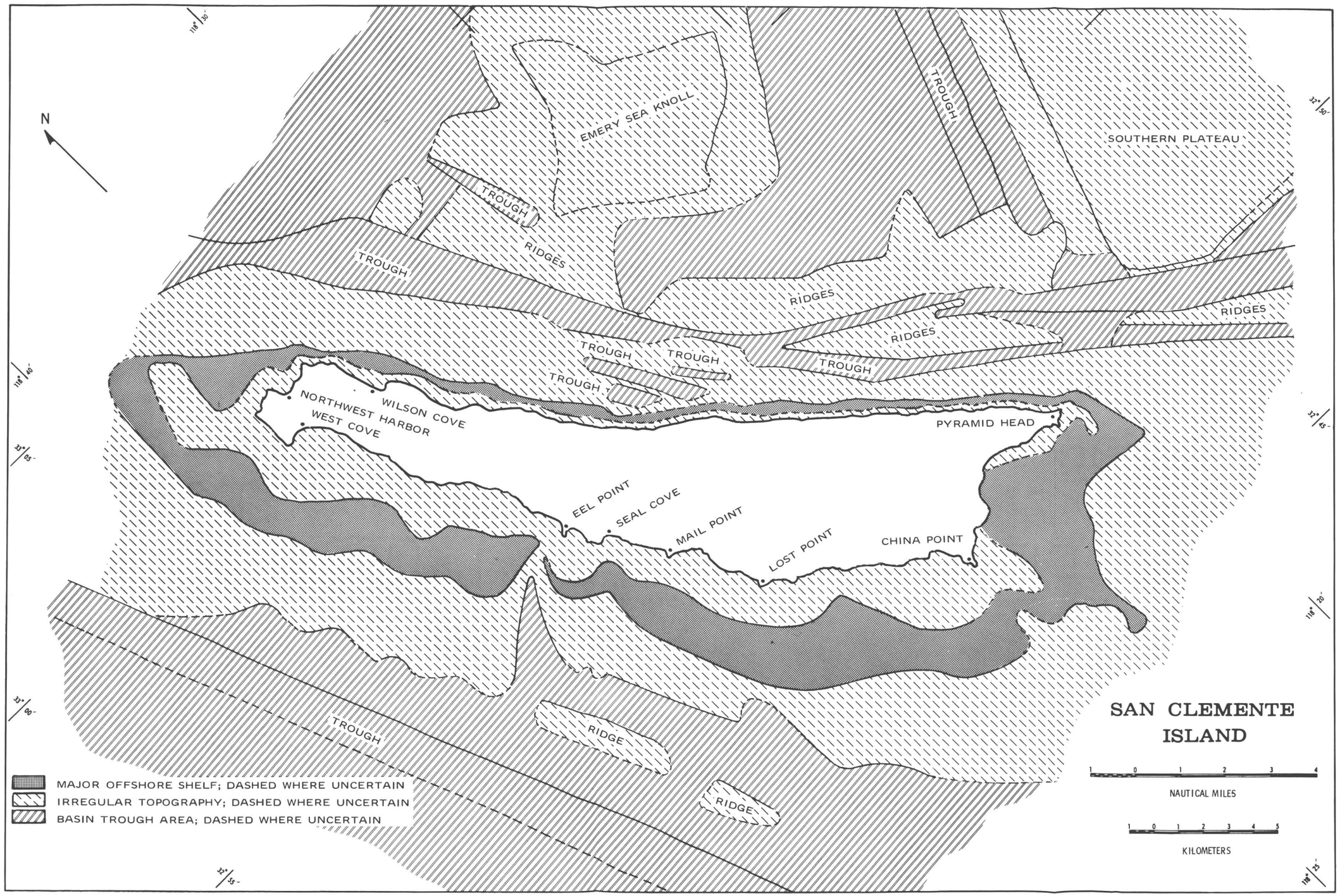

Figure 5. Physiographic map of the San Clemente Island crustal block region.

high areas within the basin-trough area. The term "apron" may be fitting for certain areas since some Pleistocene (?)-Recent sediments form slopes and fans as shown by some of the seismic profiles around the island.

PROMINENT FEATURES AND TRENDS

Several prominent submarine geomorphic features are distinguished in the area of study (Figures 5 and 6). Of primary importance is the San Clemente Escarpment along the east side of the island. Near sea level the escarpment is interrupted by the marine shelf, approximately 1/2- to 3/4-kilometer wide along this side of the island. From the seaward end of the shelf the sea floor slopes steeply to a depth slightly more than 1,000 meters. A representative example of the slope along the northern part of the island block is shown in Figure 7. The average slope at this location is about 21 degrees. The average slope along the entire east side of the island is 18 degrees. However, calculations based on pressure data made by the writer in 1962 for that part of the escarpment south of Wilson Cove indicate dips up to 27 degrees. Local dips as steep as 35 degrees have been measured by inclinometer during a deep submersible vehicle survey (von Huene, 1967). Based on the seismic profile data, the entire slope has a dip variance ranging from 12 to 21 degrees. The average strike of this major feature is N40°W. However, the escarpment exhibits a slight northeast concavity along the central to northern end of the island (note Figure 3).

A second major feature is the offshore shelf. This shelf broadens around the ends of the island and is prominent along the southwest side. Its geomorphic expression is similar to the elevated benches cut into the

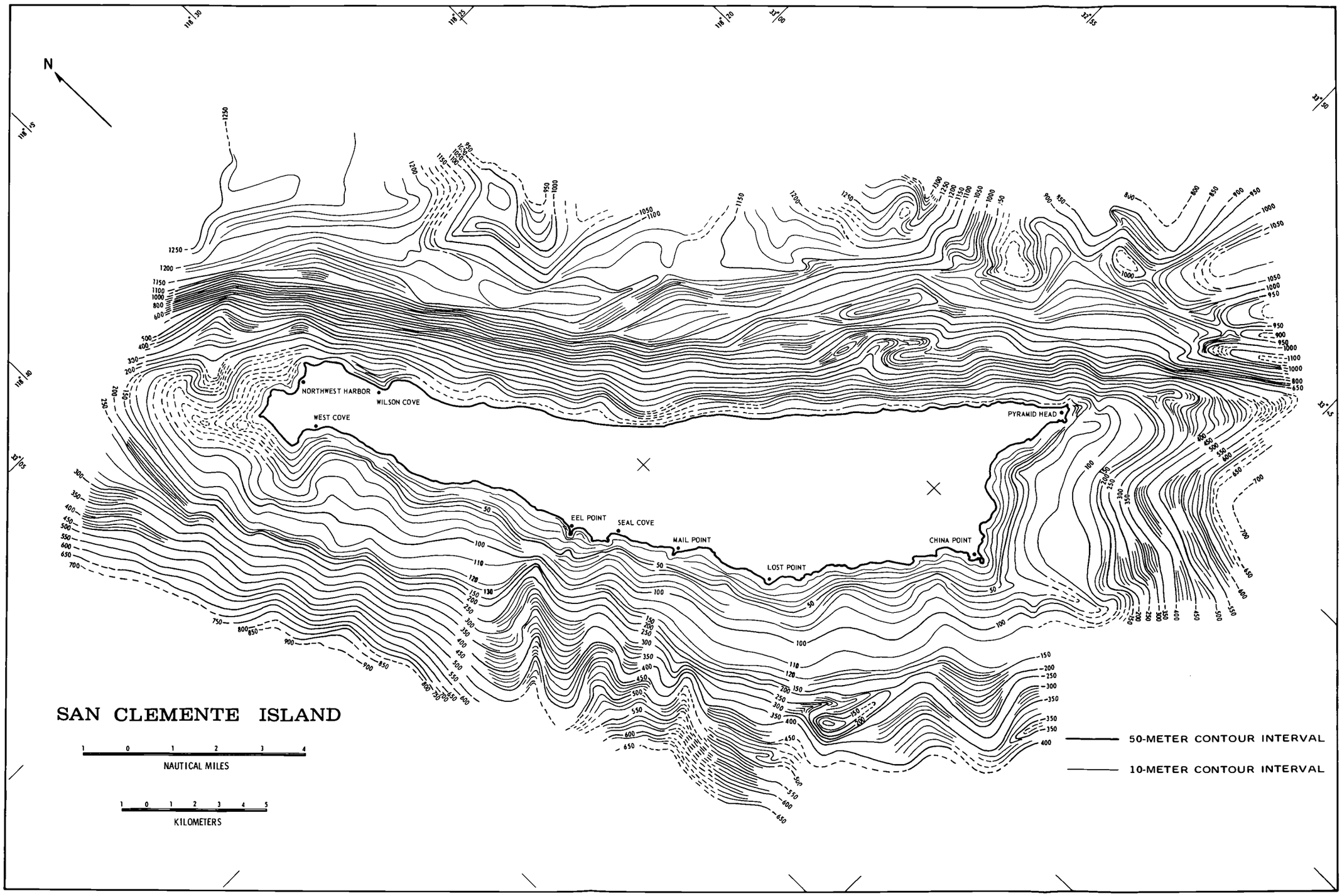

Figure 6. Bathymetry of the San Clemente Island block region. Shallow, nearshore data (between end of profiles and shore) taken from the U. S. Coast and Geodetic Survey Chart 5111.

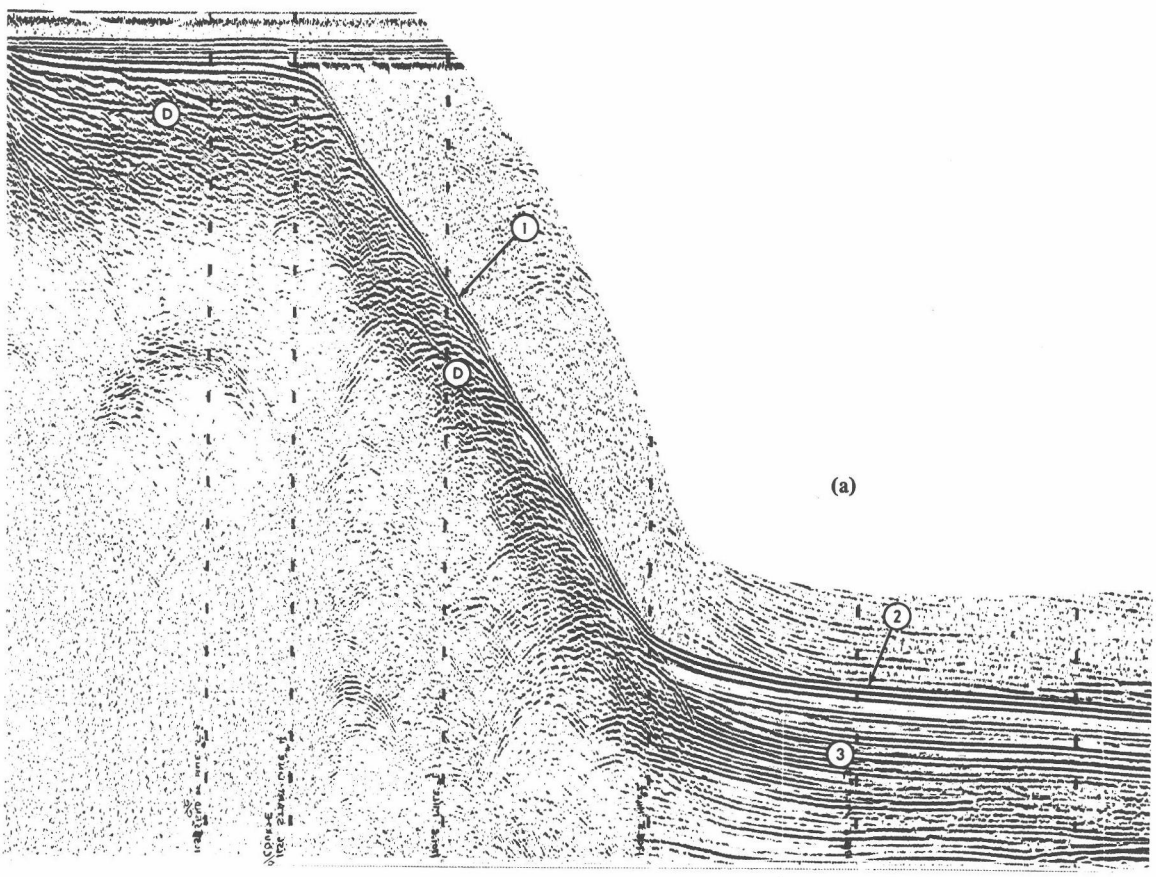
D
1
D
(a)
2
3

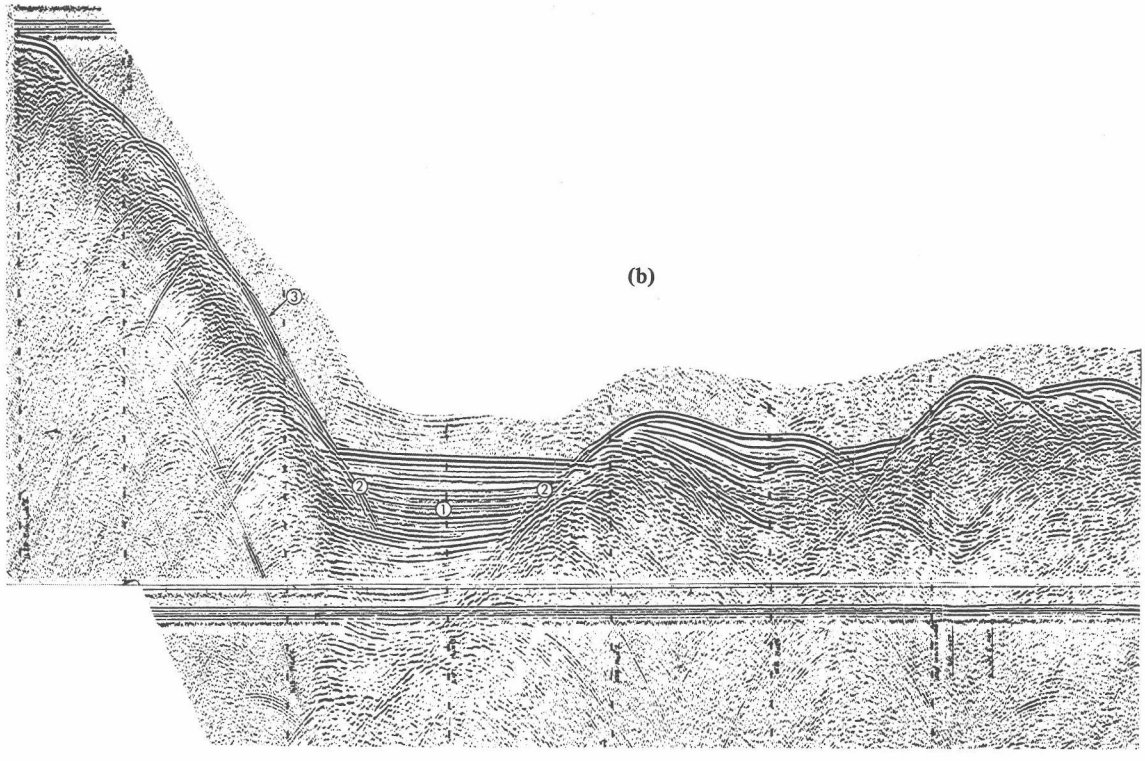
3
(b)
2
1
4

southwest flank of the island. The shelf is generally smooth and averages a nearly 1-degree slope. It ranges from about 0.35 to 3.70 kilometers in width along the western side of the island, with an average width of nearly 1.9 kilometer.

At the seaward terminus (between 120 to 130 meters of depth) of the marine shelf along the western side of the island the slope steepens sharply to about 15 to 17 degrees and continues to a depth of roughly 400 meters, where it assumes a moderate incline of 3 to 5 degrees. Shoreward, the major marine shelf is terminated by a steeper and more irregular surface related to the volcanic topography on the island.

Off the east side of the island the slope grades abruptly into a submarine basin-trough zone. The basin-trough zone is a third major feature. The highs and depressions of this zone (Figure 6) have been developed by faulting and folding of crustal rocks. The linear bathymetric trends of this zone are aligned mostly north-south or northwest-southeast. These trends are most striking along the northeastern edge of the surveyed area in the vicinity of the Emery Seaknoll and the Southern Plateau (Figure 5). The topography between the island and the Emery Seaknoll along the basin-trough area, tends to slope downward in a northwest and southeast direction. The western border of the Emery Seaknoll appears more irregular than shown heretofore on bathymetric maps. Gaal (1966) described this basin high as subrounded, conical with relatively steep slopes--all of which suggest a volcanic structure. However, Gaal also reported that the highly irregular topography of the southwestern slope suggests a breached or faulted portion of the structure.

A fan-shaped pattern of three ridges is apparent to the southeast of Pyramid Head, at the edge of the mapped area. A trough, bordering the

southwest side of the westernmost ridge, is the only linear depression of the basin-trough zone that lacks a flat bottom. According to profile records, this trough appears to be relatively devoid of sedimentary fill.

The Emery Seaknoll, the more shallow central part of the basin-trough zone, shoaling off the central southwestern side of the island, inferred upward bowing of the island (Olmsted, 1958), and the bathymetric high southwest of Lost Point are related to the subtle northeast-southwest secondary trend of this area.

Bathymetric data around the island indicate that numerous gullies are cut into the seaward slope off the marine shelf and sometimes into the shelf proper. The re-entrant caused by a canyon off Eel Point forms a complete break in the shelf; the canyon and shelf break are considered important features of the island's structural genesis.

A less outstanding, yet important, bathymetric feature of the submarine slope off the west side of the island is a volcanic high approximately 7 kilometers southwest of Lost Point. This feature is shown in U. S. Coast and Geodetic Survey Chart 5111 where it appears as two separate highs aligned approximately N70°W. This alignment is maintained in Figure 6 but is interpreted as a single, elongated high. In addition, there is a general tendency for the island offshore slope region along the western side of the island to become steeper from north to south. This change becomes prominent about midway the length of the island. The area to the north is also more uniform in slope than that to the south. Major re-entrants, protuberances, and depressions are also more prominent to the south.

GENESIS OF SEA-FLOOR TOPOGRAPHY

Deep-sea topographic features are considered to be less modified by erosion, compared with those on land. Thus, fault-controlled features such as ridges, troughs (or grabens), crustal blocks, and crustal folding may be interpreted more readily as essentially linear and sharply defined features. These considerations have strongly influenced the interpretation of Figure 6.

Subbottom profiles indicate that faulting is the major factor controlling the geomorphology of the area. Many of the high areas and depressions appear to be offsets of formerly more extensive linear features.

The dissection of the southwestern slope is probably the consequence of both faulting and erosion. The erosional pattern appears to follow the fault trends, at least partially, and may have developed largely during the Late Pleistocene fluctuations of sea level. Erosional development along the northwestern slope may have resulted largely from slumping, sand flows, and turbidity currents, which have partly followed fault zones.

According to the theory of Bradley (1958) the major San Clemente Island marine shelf was probably cut during slow submergence. It is probably a wave-cut terrace of Late Pleistocene age (Curray, 1964, 1965; Emery, 1960; Shepard, 1963b). Shallower terraces, representing sea level stands of the Recent transgression (see, for example, Curray 1960, 1961, 1965; Shepard, 1963a and 1963b; Shepard and Seuss, 1956; van Andel and Sachs, 1964) may be present along the nearshore submarine volcanic outcrop area. Emery (1958, 1960) has postulated two shallower submerged terraces for San Clemente Island. However, these are not readily

apparent, possibly because many of the profiles do not reach close enough to shore. Two possible terrace levels noted on a few of the profiles may be related to shallower sea level stands. These are located at depths of about 28 to 30 meters and 55 to 64 meters. The lower level approximates the lower terrace noted by Emery; the upper corresponds to Curray's upper Holocene regression. Emery's diagram (1960, p. 35) shows the two upper terrace levels as being discontinuous. Data from the present study suggest that some of the discontinuous sections are related to oblique faulting which has offset sections of the major terrace.

IV. STRATIGRAPHY

GEOLOGIC UNITS

A synthesis of the high-resolution profiling records shows a succession of four rock units based on the acoustic character and geometry of the records (Figure 8a). These units are identified on most of the Detailed Survey profile records by unconformable relationships and the intensity of their profile traces. They are referred to as Units A, B, C, and D, on the basis of superposition, and can be followed over the entire area surveyed off Eel and Lost Points (note Figure 1). Units B, C, and D are definable on the Reconnaissance Survey records for the west side and ends of the island block.

Three of the units are considered hard rock units; the fourth, A, is unconsolidated surficial sediment. Units B and C are inferred to be sedimentary rocks and Unit D, volcanic rock. The sedimentary rock units dip gently to moderately seaward (2 to 15 degrees) and are truncated at the offshore terrace. A fifth sedimentary unit, Unit X, is defined on the reconnaissance records at the slope and basin-trough zone. It appears to be a seaward equivalent of Units A and B.

Distinctive acoustic and geologic characteristics for each of the lithologic units are summarized below. Some geologic inferences are presented. Units C and D are related to previously defined rock units by sampling and correlation. Unit B is related to previously defined units by inference.

Stratigraphic unit thicknesses, as taken directly from the profile records, are relative (acoustical) thicknesses. To obtain an "apparent

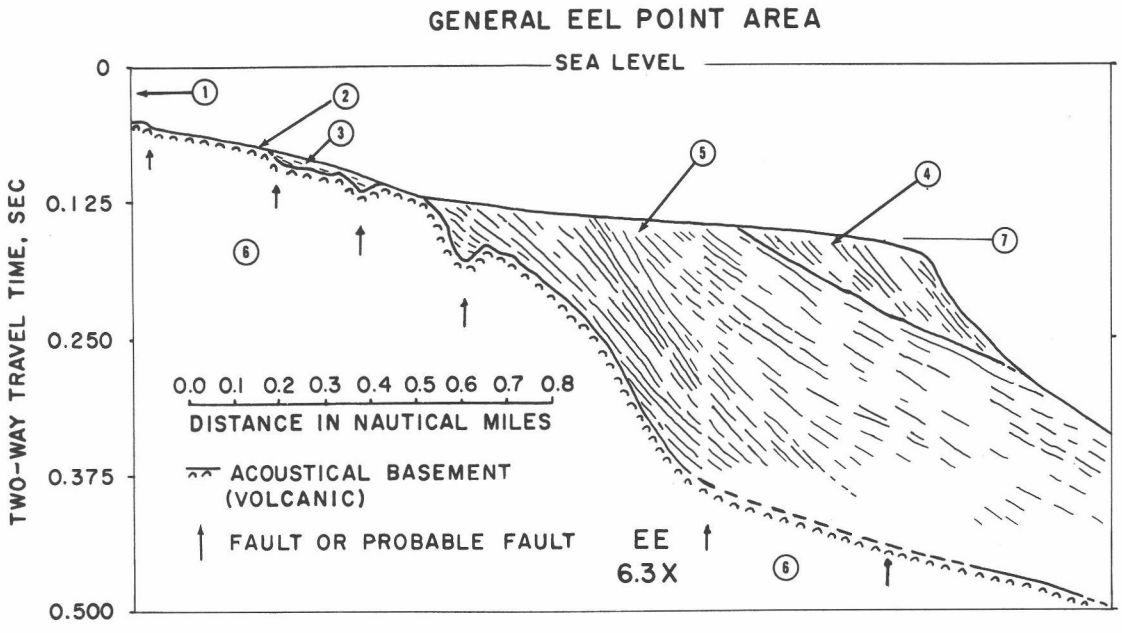
GENERAL EEL POINT AREA
SEA LEVEL
0
0.125
0.250
0.375
0.500
TWO-WAY TRAVEL TIME, SEC
0.0 0.1 0.2 0.3 0.4 0.5 0.6 0.7 0.8
DISTANCE IN NAUTICAL MILES
ACOUSTICAL BASEMENT
(VOLCANIC)
FAULT OR PROBABLE FAULT
EE
6.3X
1
2
3
4
5
6
7

(a)

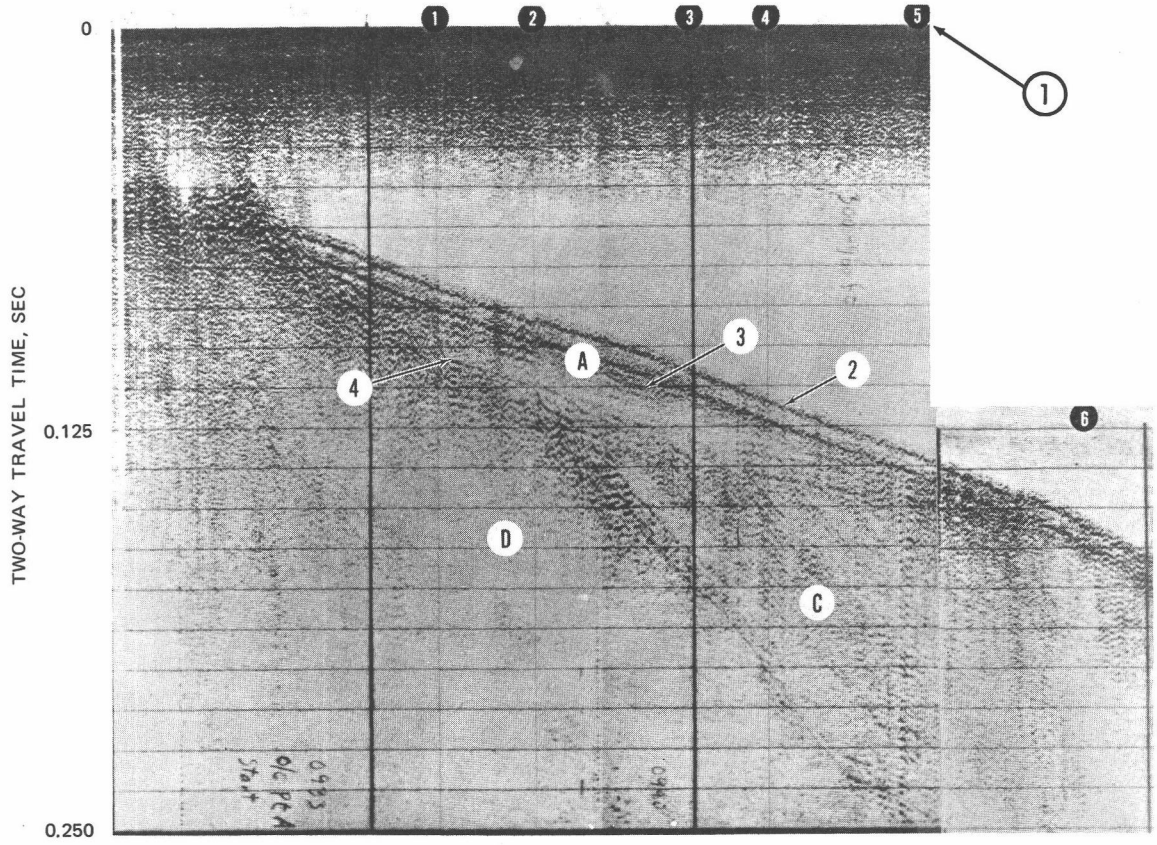
0
0.125
0.250
TWO-WAY TRAVEL TIME, SEC
1
2
3
4
5
6
A
C
D

(b)

true thickness" (Appendix III), a correction based upon the ratio of the average velocity of sound in the lithologic unit to that of the velocity of sound in seawater is applied. This correction is referred to as the seismic-interval-velocity correction factor. Various bases of interpretation are adopted to arrive at the average interval velocity for each lithologic unit.

Unit D

This unit is equivalent to the volcanic rocks on the island (andesite and dacite). With the exception of the region along the northeast side of the island the upper surfaces of the volcanic rocks dip seaward under Unit B and Unit C at angles from 5 to 10 degrees. Unit D is the most widespread of all the described units. This unit comprises all of the irregular topography shoreward of the wave-cut terrace and most of the San Clemente Escarpment. The depressions of this nearshore surface are filled to varying degrees by the very coarse bioclastic debris of Unit A. The seaward limit of this exposed surface is usually at the contact with Unit C and is coincident with the inner boundary of the wave-cut terrace as defined in this paper. Generally, the volcanic rocks of Unit D are exposed farther seaward off points of land than off coastal embayments. The unit is also locally exposed immediately seaward of the wave-cut terrace along the west side of the island (Figures 9 and 10).

The Emery Seaknoll has been determined from dredge hauls to be composed of volcanic rock (Gaal, 1966). Profile interpretation corroborates the conclusion by Gaal and further indicates that much of the northern

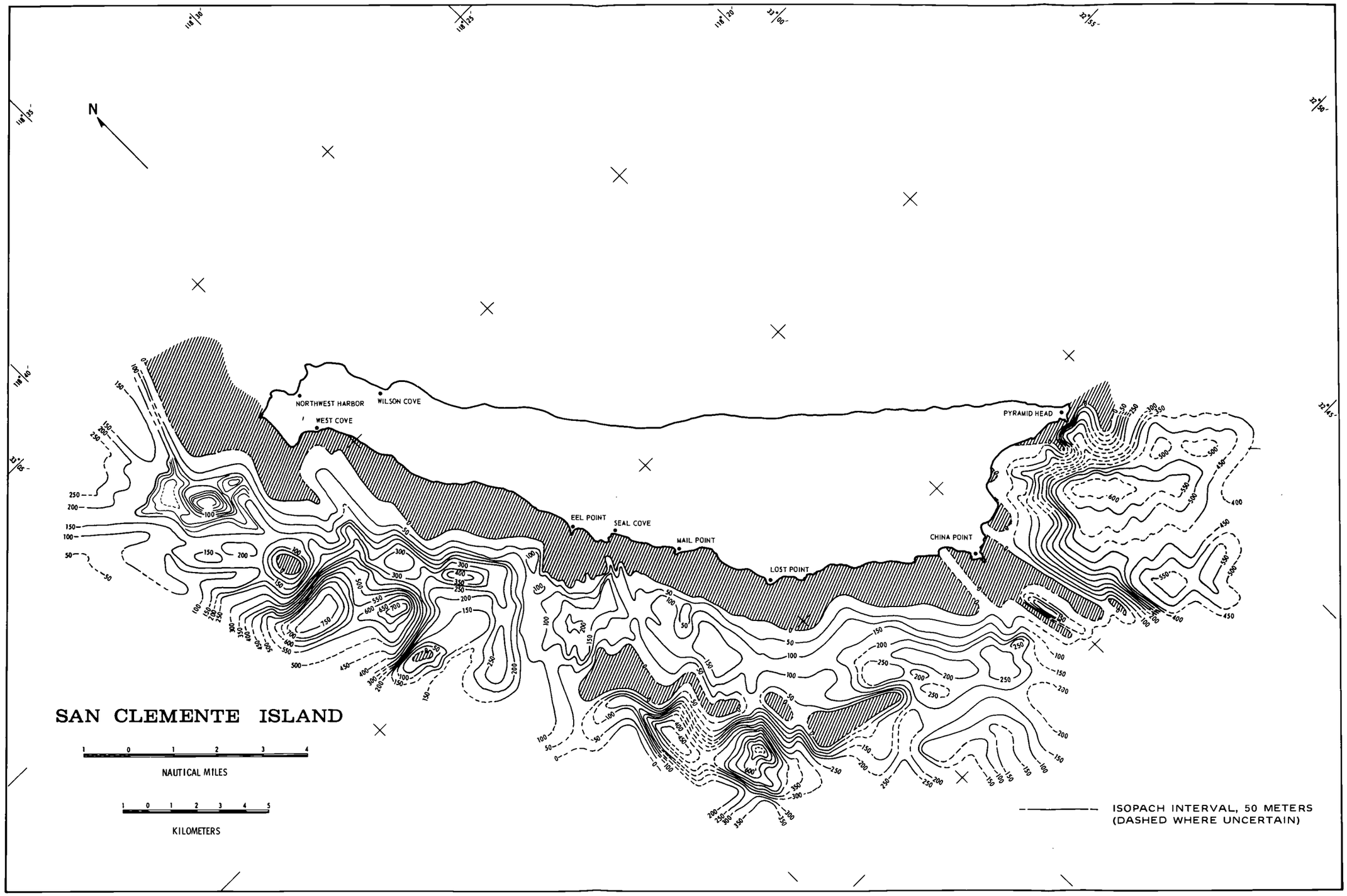

Figure 9. Isopach map of Unit C, Reconnaissance Survey. Irregular nature of the contours off Eel and Mail Points area is the result of composite control from both seismic profile surveys. Crosshatched areas are exposures of volcanic rocks (Unit D).

part of the Southern Plateau is also volcanic rock. Various minor outcrops of the basin area seaward of the San Clemente Escarpment are isolated crustal blocks exposed by presumed faulting.

Submarine observations and samples from SCUBA-diving operations show the volcanic rock to be hard, brittle, extensively jointed, and with variability in structure and texture, as do the terrestrial equivalents described by Olmsted (1958), Merifield and Lamar (1967), and Lamar et al. (1967). Petrographic study of the samples indicates that the majority of these have an average plagioclase feldspar phenocryst composition near the andesine-labradorite border. From a total of 32 thin sections examined, 22 show maximum albite-twin-extinction angles on sections normal to the 010 plane ranging from 21 to 35 degrees (An_{42} to An_{56}). Ten of these indicate a sodic-labradorite composition, and 12 are of calcic-andesine composition. According to Johannsen's classification (1931), 12 of the 32 samples are andesite and 22 are basalt. However, due to a variable degree of zoning within the plagioclases and the proximity to the An-border between andesine and labradorite, a more precise identification should be made. The petrographic analysis generally agrees with the interpretation by Olmsted (1958) and Lamar et al. (1967), wherein the island andesites contain plagioclase phenocrysts that are mostly andesine or sodic labradorite.

A preliminary analysis of thin sections from a 1,200-foot core taken at Eel Point during the early part of 1967 (Austin, 1967) indicated an andesitic composition for all of this section, with plagioclase phenocrysts composed of very calcic andesite. However, detailed study of the core by Lamar et al. (1968) showed an oscillatory zoning from An_{47} to

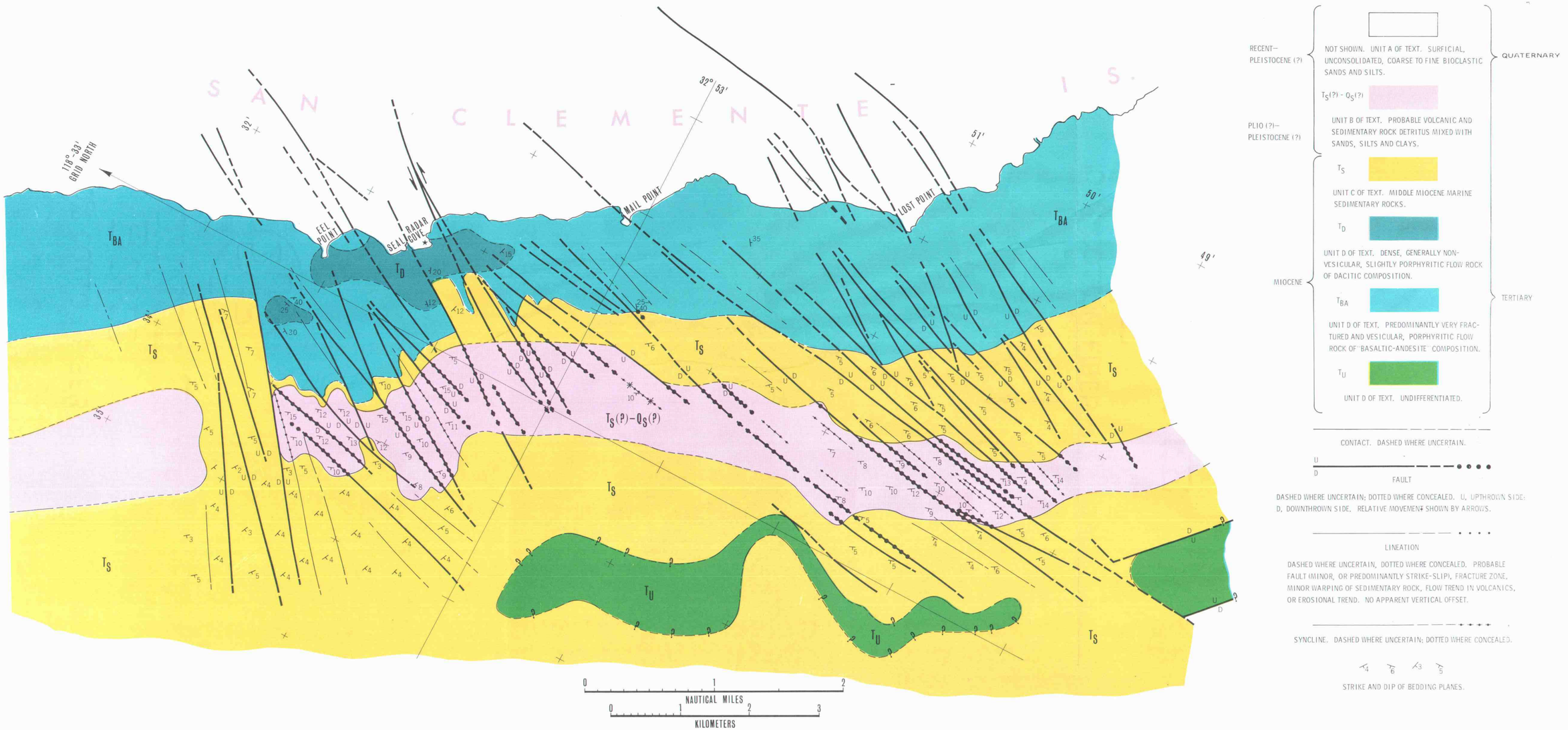

Figure 10. Geologic map of Detailed Survey area.

An_{78} with an average composition of An_{60}. The microlitic plagioclase was mostly andesine of An_{40} to An_{48}.

The above analyses suggest that the andesitic type of volcanic rock becomes more basic in composition at depth and seaward of Lost and Eel Points.

Five of the submarine volcanic rock samples are identified as dacite. These were used to outline a general seaward extension of the dacite on the island (Figure 10).

The San Clemente Island volcanic rocks are said to be of probable Miocene age (Olmsted, 1958). Potassium-Argon dating by the Geochron Laboratories, Inc., Cambridge, Massachusetts,[2] establishes dates of 15.7 ($\pm$0.8) x 10^6 and 15.5 ($\pm$0.7) x 10^6 years for the 40- and 1,158-foot depths, respectively, from samples taken from the 1,200-foot onshore test hole. These dates, uniformity of rock composition, and the absence of definite soil zones or unconformities between volcanic flows suggest that volcanic rocks on the upper part of the island had a common magmatic source. The volcanic rocks of the island can be confidently projected seaward beyond the wave-cut terrace on the basis of diver-collected samples and the subbottom profile records.

---

[2]A letter dated 26 September 1967 from the Geochron Laboratories, Inc., Cambridge, Massachusetts, states that an analysis of two samples (40- and 1,158-foot levels) from the island's 1,200-foot test hole shows the volcanic rocks to be olivine pyroxene basalt.

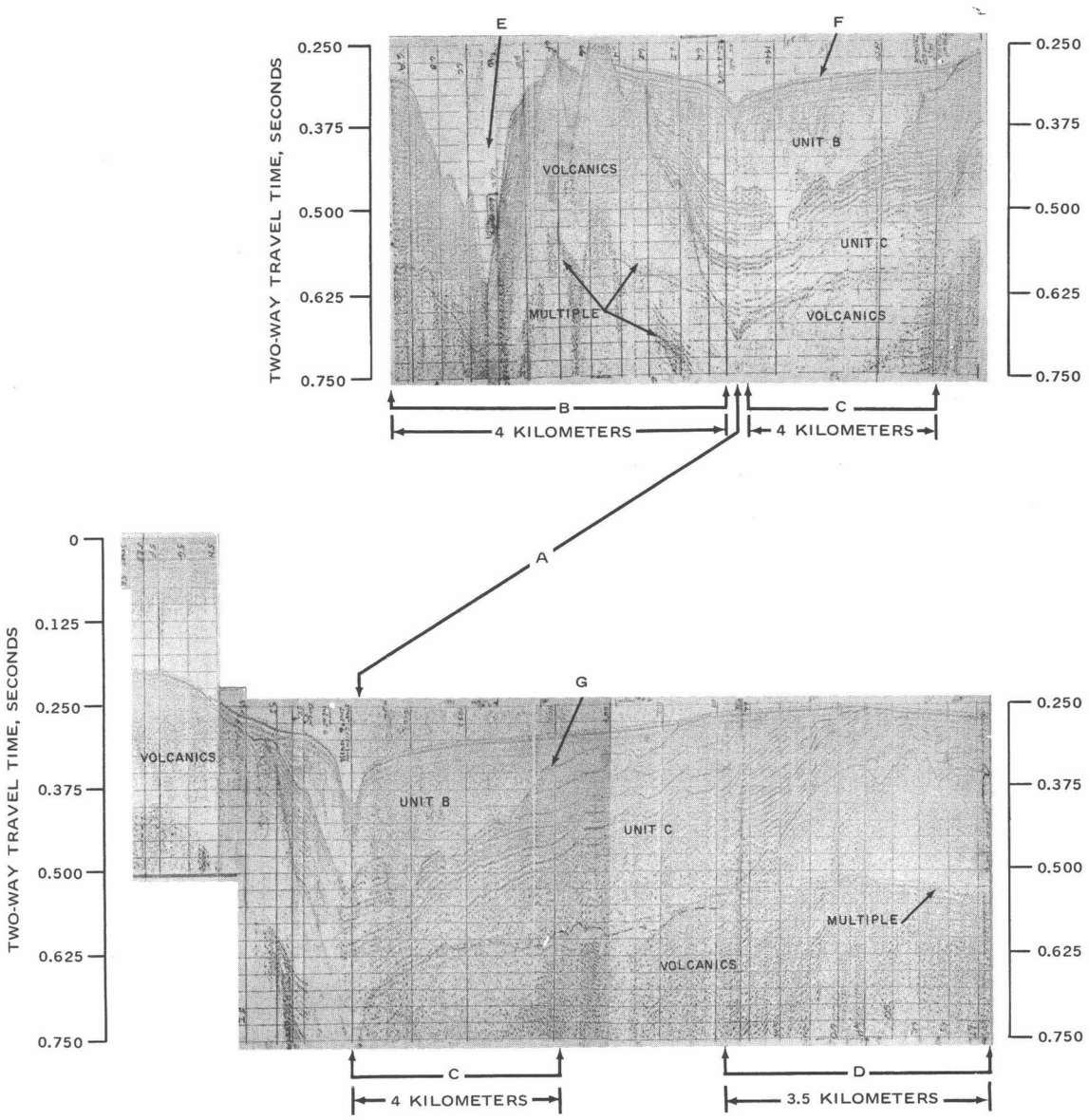

Figure 11. Profiles 5 and 6 and an extension of Profile 6, Eel Point Grid, and Profile 6 of Lost Point Grid (see Figure 1). A indicates equivalent position of profiles (same wave-cut terrace gully), B is Profile 6, C is extension of Profile 6 of Eel Point Grid, D is Profile 6 of Lost Point Grid, E is canyon, F is sea floor and wave-cut terrace, and G is unconformity between Units B and C. Vertical exaggeration, 22:1.

Unit C

Differentiation of this unit from that of Unit D (below) for the east side of the island was too difficult for definitive analysis because of the complex nature of the structure, side echoes, and overlap of multiples (Appendix III). Unit C is a sedimentary rock unit and has a much greater areal extent both landward and seaward than Unit B. The unit is characterized by strong, parallel reflectors and the erosional and structural unconformity at its upper boundary. The unconformity is pronounced off the Mail Point area where a pre-Unit B canyon, cut into Unit C, is filled by Unit B sediments (Figure 11). This unconformity is irregular and widespread over the entire west side of the island.

A major feature conceivably related to this unconformity is the submarine canyon cut through the insular terrace off Eel Point. The canyon begins off a submarine extension of Eel Point tentatively referred to as Eel Ridge. The canyon is herein named Eel Ridge Canyon. The subbottom profile records show that Unit C increases in thickness from south to north across Eel Ridge Canyon (Figure 12). Furthermore, north of the canyon, Unit C is divisible into two and possibly three subunits (note Figure 8a). Roughly the lower one-third to one-half of the thicker northern section contains strong reflectors that appear to correspond to the entire unit south of the canyon. The upper subdivision generally lacks the strong reflectors characteristic of the lower part and lies parallel to subparallel to the lower subunit. This implies an unconformable relationship and a more complete stratigraphic sequence within this section of Unit C. Records north of the canyon show that the greater thickness and the stratigraphy of this unit appear to be maintained close

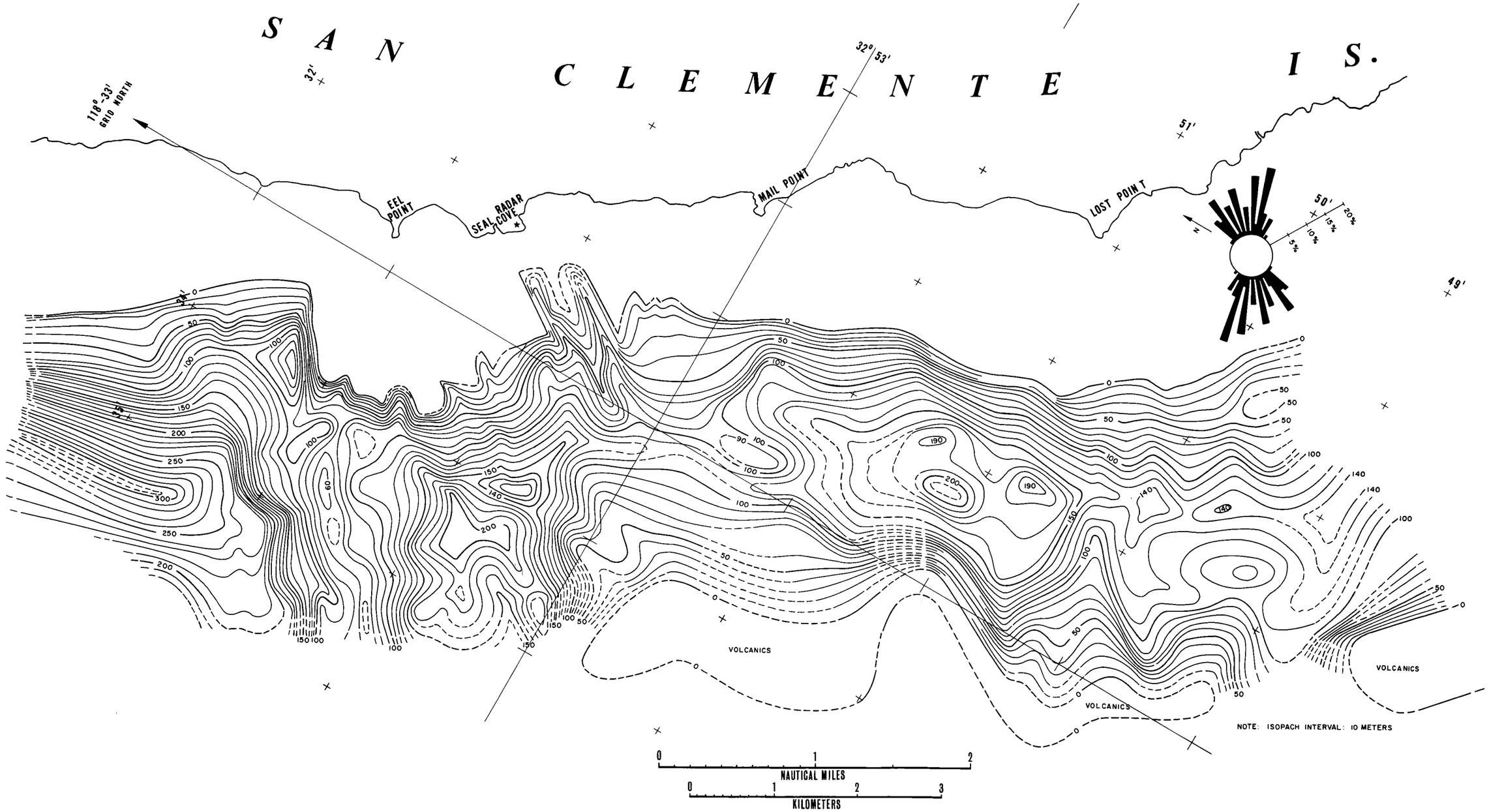

Figure 12. Isopach map of Unit C, Detailed Survey. Rose diagram represents 10-degree increments of the dip strikes of Unit C sediments taken at the intersections of the seismic profiles.

to the northern end of the island. At this point the unit thins and has the appearance of the lower subdivision characterized by strong reflectors. Unit C rests unconformably on Unit D and is readily distinguished from Unit D on the profiles.

Two large outcrop samples of Unit C were recovered off Lost Point at a depth of about 105 meters by the cable-controlled underwater research vehicle (CURV).[3] These rocks are a slightly altered, fossiliferous, finely crystalline limestone. Based on the classification of Folk (1962) this rock is a biomicrite with some alteration to microspar. The classification of Leighton and Pendexter (1962) categorizes this rock as a micritic-skeletal limestone. Accessories include very scattered quartz grains (silt to sand size) and some clay-like material. Ubiquitous foraminiferal and mollusk fragments are the dominant bioclasts. Both of the rock samples contain numerous pholad (boring clam) bore holes.

Microfossils from the CURV samples indicate a late Middle Miocene (Luisian) age for this part of Unit C (Smith, 1967). Macrofossils and microfossils taken from sedimentary rocks exposed on the northern and east-central parts of the island are also of this age. A bathal depositional environment has been postulated for the fossils from the sedimentary units at the northern end of the island (Vedder, 1967). Macrofossils from the east-central part of the island suggest a subtropical, shallow-water depositional environment (Mitchell and Lipps, 1965). It is interesting to note that a change in stratigraphic sequence within

---

[3]CURV, a pamphlet issued by the U. S. Naval Ordnance Test Station, Pasadena, California (now the Undersea Research and Development Center).

the sedimentary rocks at one locality on the east-central part of the island divides these sediments into deep-water (upper part) and shallow-water (lower part) environments.

Island field work provides some possible evidence for the nature of the lithology of Unit C off the West Cove area. Unit C is preserved close to shore in this area (Figure 9). Along the shore and mixed with a predominance of volcanic cobbles and boulders are cobbles of thinly stratified, buff to greenish gray (5GB8/1 to 5Y-5GY6/1), finely crystalline, dense, well-indurated dolomite. Because of the proximity of Unit C offshore and the apparent lack of well-indurated sedimentary rocks in the other stratigraphic units, it is assumed that these rocks represent remnants of Unit C. This part of Unit C may be correlative with the Miocene section at Wilson Cove (see Olmsted, 1958) where a shale unit contains a cementing material of dolomite (Vedder, 1967).

Figure 9 shows seven zones of major thickness of Unit C. These are (1) two zones that are located southwest of West Cove; (2) a third that is illustrated by elongate, nearly rectangular isopach lines immediately southeast of the first two zones; (3) a fourth and fifth zone west of Mail and Lost Points that trend northeast, and (4) two zones off the south end of the island. The first two zones are a composite of essentially one northwest-trending zone that appears to have been cut by erosion and apparently offset by faulting. This composite part of Unit C lies between two slightly exposed volcanic highs and constitutes a major depression fill for this area. The third zone represents a Unit D graben fill. The fourth and fifth zones also can be considered a composite of what was once a single zone apparently offset by faulting and altered by erosion. The configuration of the sixth and seventh zones

suggests preservation by faulting, as are the terrestrial equivalents of Unit C in this area.

Unit B

This unit is observed only on the profiles for the west side and ends of the island. On the east side of the island some Reconnaissance Survey profiles do not reach the wave-cut terrace while others disclose an apparent lack of the unit. Conceivably, some minor deposits of the unit are present along this side of the island.

Unit B is considered a semiconsolidated sediment[4] which rests unconformably on the eroded and faulted surface of Unit C at the outer terrace area (Figures 8a and 11). This unit is possibly a Pliocene (?)-Pleistocene accumulation of erosional debris of volcanic and sedimentary rock origin derived mainly from the island. The unit has a lens-like outline on the reflection profiles normal to the island, with the thickest part at the outer edge of the submerged terrace. It appears to be truncated at the terrace. Acoustically, it lacks strong internal reflections but enough horizons are observed to indicate the attitude. Figure 11 shows faint, intermittent reflectors that tend to dip slightly toward the thicker part of the unit, thus suggesting a canyon or gully sediment fill origin that was later truncated by wave action to develop part of the submerged terrace. Seaward the dips of reflectors within the outer part of this unit essentially parallel the seaward slope off the terrace. This suggests that the outer part of the terrace was formed by sedimentary progradation.

---

[4]Based upon an unsuccessful test hole attempt through Unit B and Unit C off Mail Point in August 1967.

Figure 13 shows some suggestion of the geomorphic depressions present at the major unconformity between Units B and C. The more irregular (detailed) nature of the isopach lines off Eel and Lost Points is the result of composite thickness data from the Detailed and Reconnaissance Surveys. Doubtless, this type of control outside of the Detailed Survey area would reveal much more irregularity in the configuration of the isopach lines.

Unit A

This unit was definable only on the detailed survey profile records. It is the youngest unit and is possibly Pleistocene (?)-Recent in age. This unit consists of unconsolidated sediment resting on the insular terrace and slopes. Several fair to good parallel reflectors within this unit are present on the profiles, and the unit lies mainly in isolated pockets close to shore (Figures 8 and 14). The sediments in these pockets unconformably overlie Unit D and in some areas part of Unit C. Profile data suggest that the pockets are interconnected to some degree. Figure 8 also shows a minor unconformity present about 5 meters below the sea floor. The maximum thickness of Unit A is in the order of a few tens of meters. Seaward, Unit A is thinner and can only be defined on the records as faintly scattered stringers and patches below the masking caused by the multiple trace of the sea-floor return signal. Detailed Survey profile data indicate an average of close to 10 meters in thickness at this area of the terrace.

Samples of the nearshore sediment of Unit A (note Figure 2) consist of coarse to very coarse, predominantly bioclastic sand that ranges compositionally from 100% bioclastic material to a mixture containing up to 50% volcanic rock (probably andesitic) fragments. The

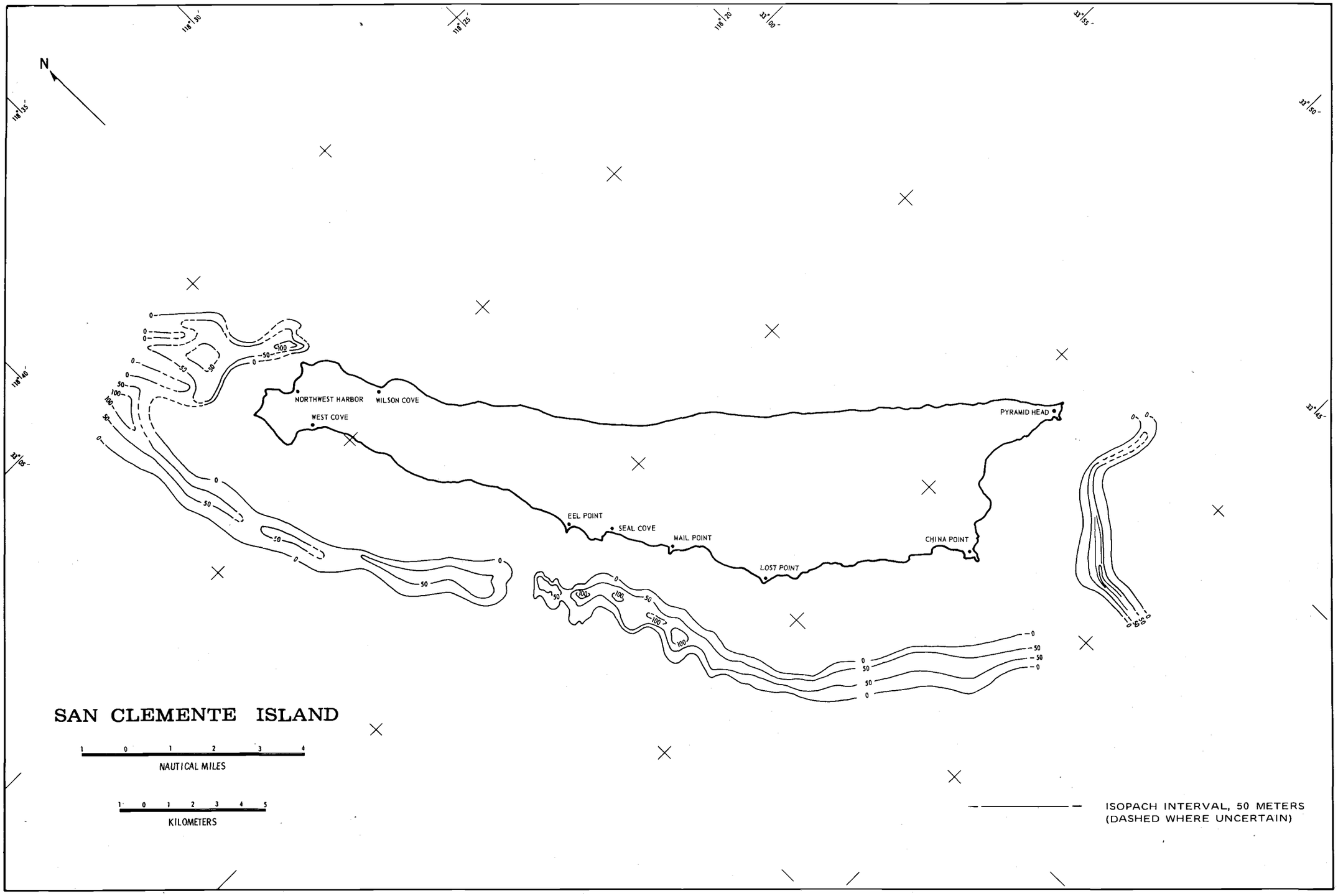

Figure 13. Isopach map of Unit B, Reconnaissance Survey. Irregular nature of isopach lines off Eel and Lost Points area is the result of the composite data control from both of the seismic profile surveys.

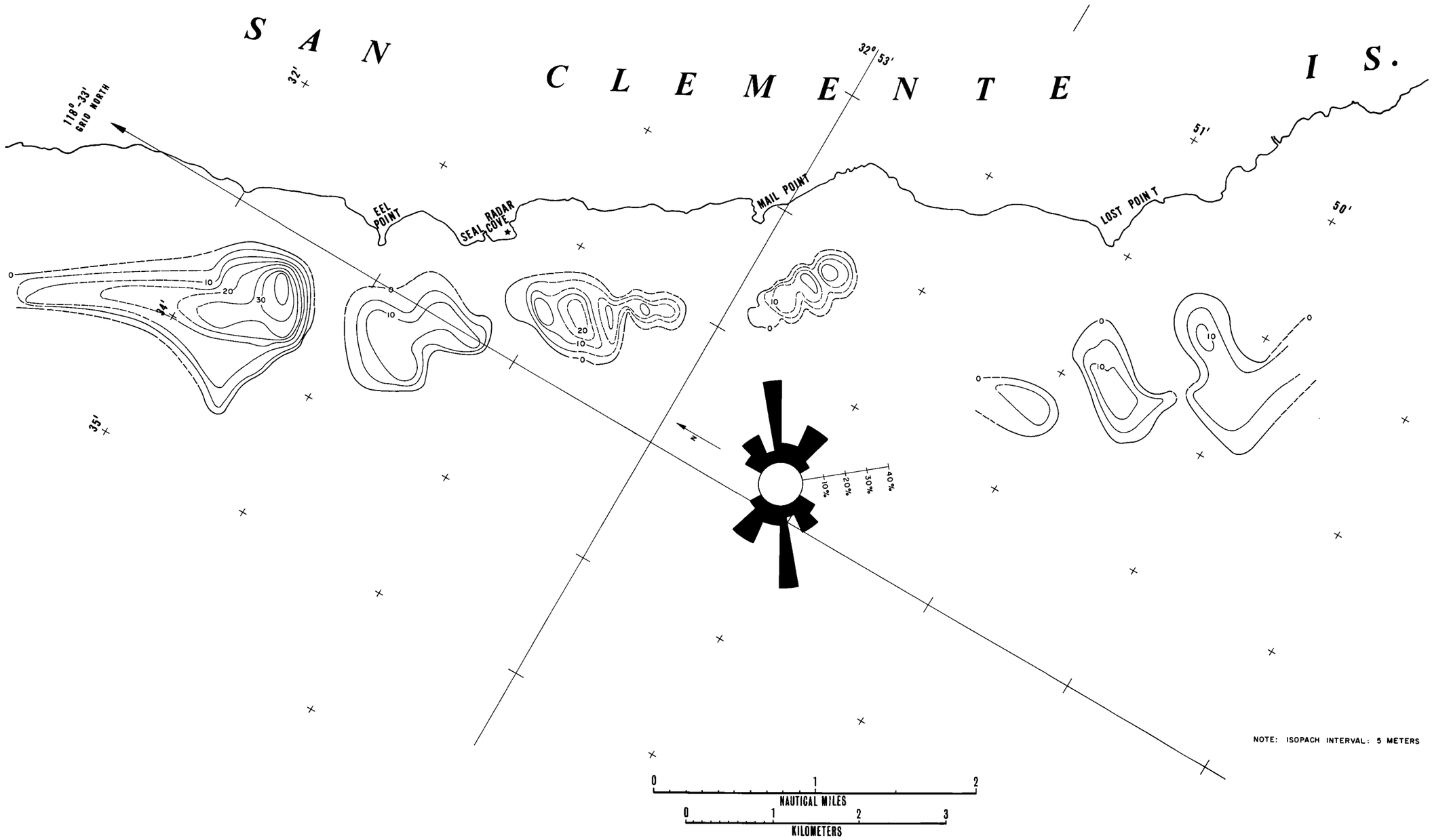

Figure 14. Isopach map of Unit A. Rose diagram represents 10-degree increments of the dip strikes of Unit A sediments taken at the intersections of the seismic profiles.

unit grades seaward to an olive gray, fine to medium grain, bioclastic (mostly foraminiferal), silty sand on the terrace and terrace foreslope, becoming more silty with depth. The bioclastic debris consists of Foraminifera, various amounts of rock fragments (1 to 30%), sponge spicules, echinoid fragments, fecal pellets, and bryozoan, pelecypod, and gastropod shell fragments. Ostracods are rare. Glauconite occurs as fillings and coatings of Foraminifera and other biota fragments, and as small coating and filling fragments. The sediment appears richer in glauconite seaward of about 70 to 80 meters of depth, which coincides with the transition zone between the coarser nearshore sediment and the more seaward finer, highly foraminiferal, silty sands on the terrace and terrace slopes.

The seismic-interval-velocity correction factor used for determining the thickness of Unit A is taken from the many velocity measurements of shelf sands compiled by Hamilton (1967a). Hamilton's maximum velocity-correction factor for shelf sands is 1.2; this factor was used for Unit A because relatively high velocities are normally encountered in calcareous and volcanic rocks as well as in marine sediments containing high percentages of these materials.

Only the main nearshore pockets of the coarse to very coarse sand of Unit A are isopached (Figure 14) in order to emphasize the structural relationship and sediment transport in the area of study. Unit A is removed from the Detailed Survey geologic map (Figure 10) in order to show the underlying units and structure.

Unit X

The description given by Moore (1966) in his classification of the Continental Borderland's stratified rocks and sediments is used to describe this unit. Moore's strata are divided into pre-orogenic and post-orogenic units. This division is based on the internal structures and their relationships to adjoining faults and basement or volcanic rock masses. The division relates highly folded and faulted strata and volcanic rocks, mainly of Miocene age, to that of the subsequent bathymetric depression fill. Unit X comprises the post-orogenic strata seaward of the wave-cut terrace and includes the fan, apron, and basin-depression deposits of the area studied (Figure 15). Only the major parts of this unit are isopached (Figure 16) in order to show the areal distribution of the unit with respect to the structural trends. The zero isopach line represents (as for Unit A) an approximated pinch-out of the major deposits of the unit. The unit actually extends beyond this as relatively thin deposits, mostly comprising hemipelagic sediment overlying bathymetric highs, that are not definable on the seismic profiles.

A surficial part of Unit X undoubtedly corresponds in age to Unit A. Part of the subjacent section probably correlates with Unit B. The profile correlation was too tenuous to specifically relate the two units. However, Unit X is noticeably subdivided into two and possibly three subunits by unconformities (Figure 17) in parts of the basin areas. These subdivisions are believed to correspond to Unit A and at least part of Unit B, and possibly the lowest zone relates to a period of Pliocene deposition which could conceivably be related to a lower part of Unit B.

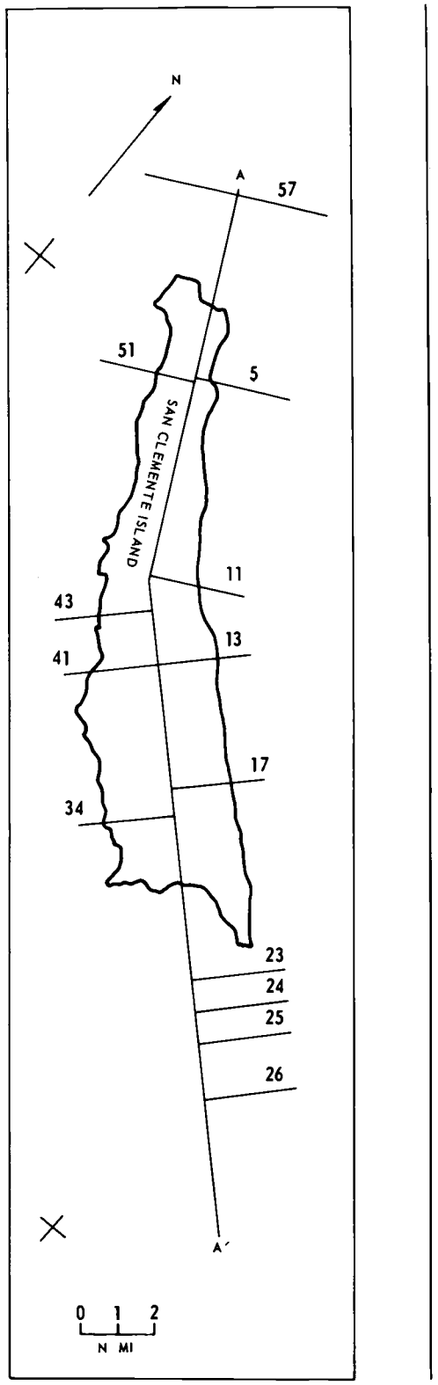
N
A
57
51
5
SAN CLEMENTE ISLAND
11
43
13
41
17
34
23
24
25
26
A´
0 1 2
N MI

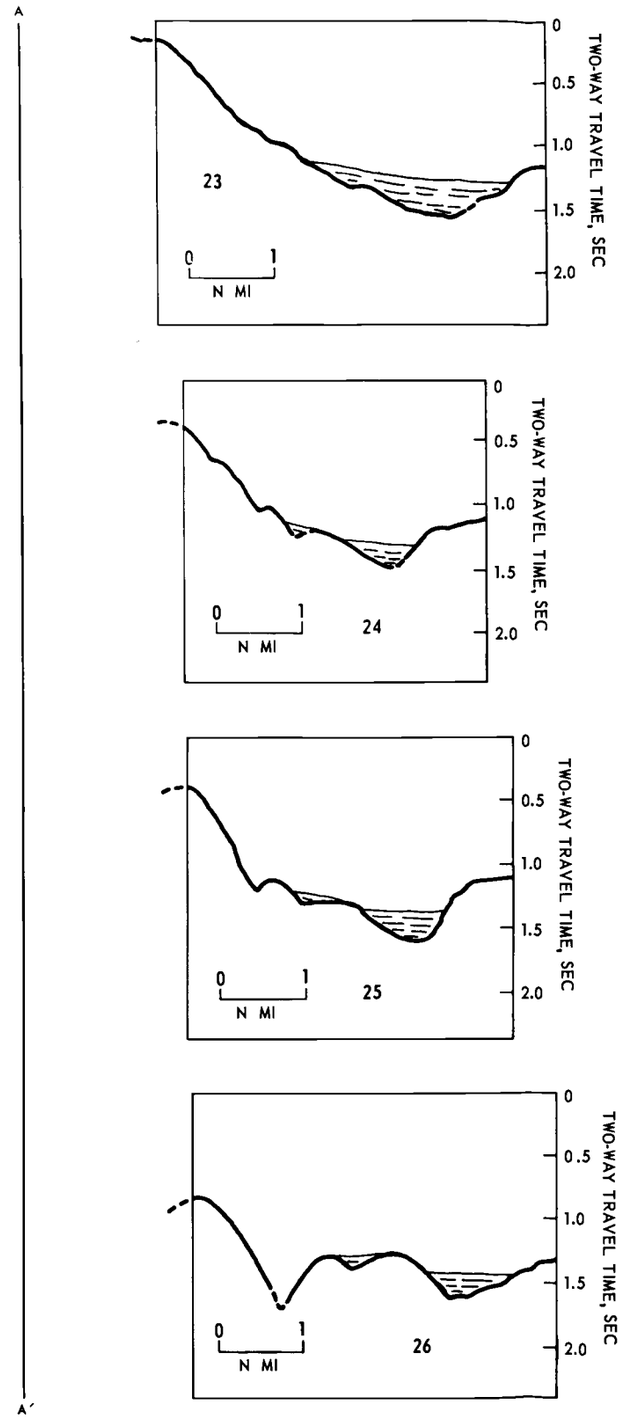
A
A´
23
24
25
26
0 1
N MI
TWO-WAY TRAVEL TIME, SEC
0
0.5
1.0
1.5
2.0

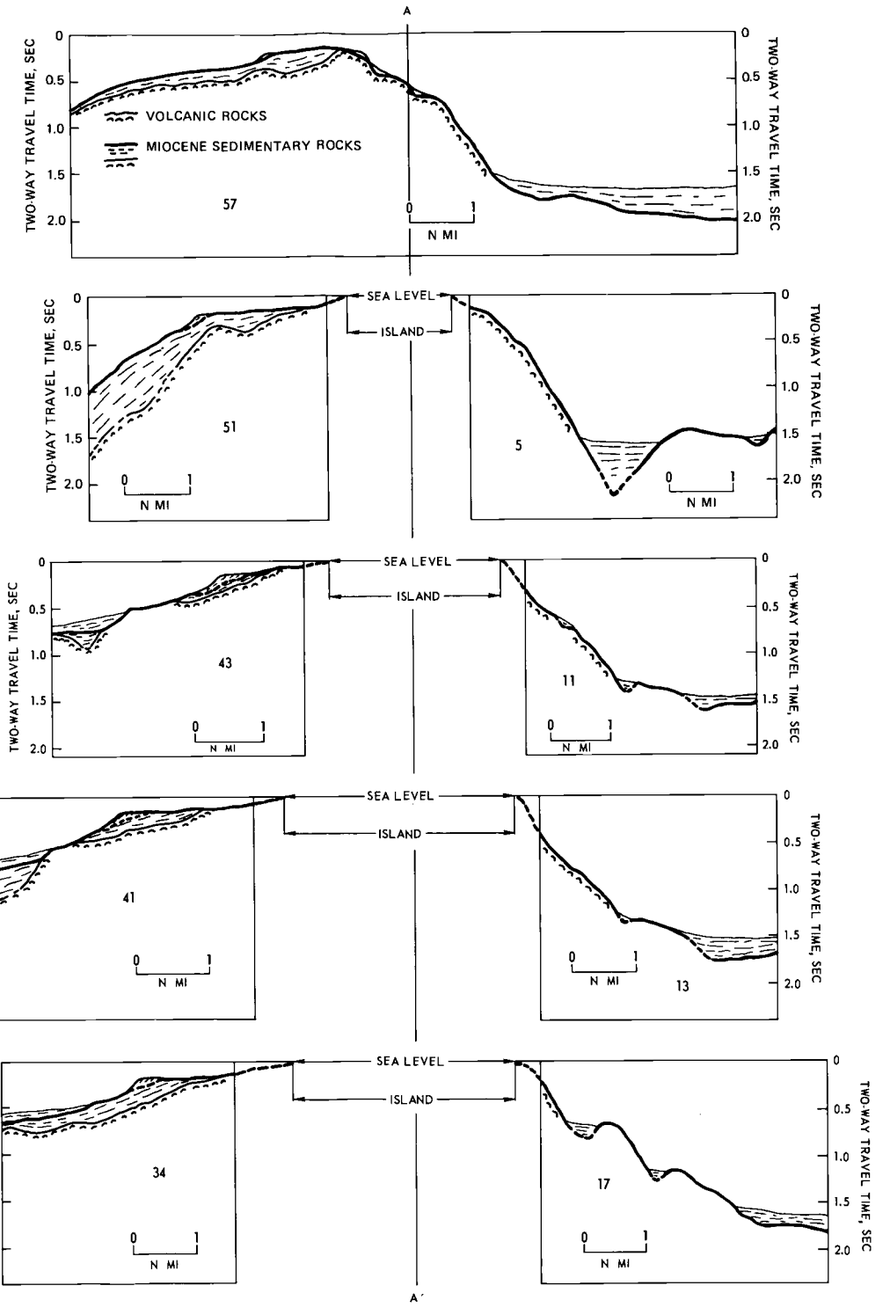
A
A´
VOLCANIC ROCKS
MIOCENE SEDIMENTARY ROCKS
SEA LEVEL
ISLAND
57
51
5
43
11
41
13
34
17
0 1
N MI
TWO-WAY TRAVEL TIME, SEC
0
0.5
1.0
1.5
2.0

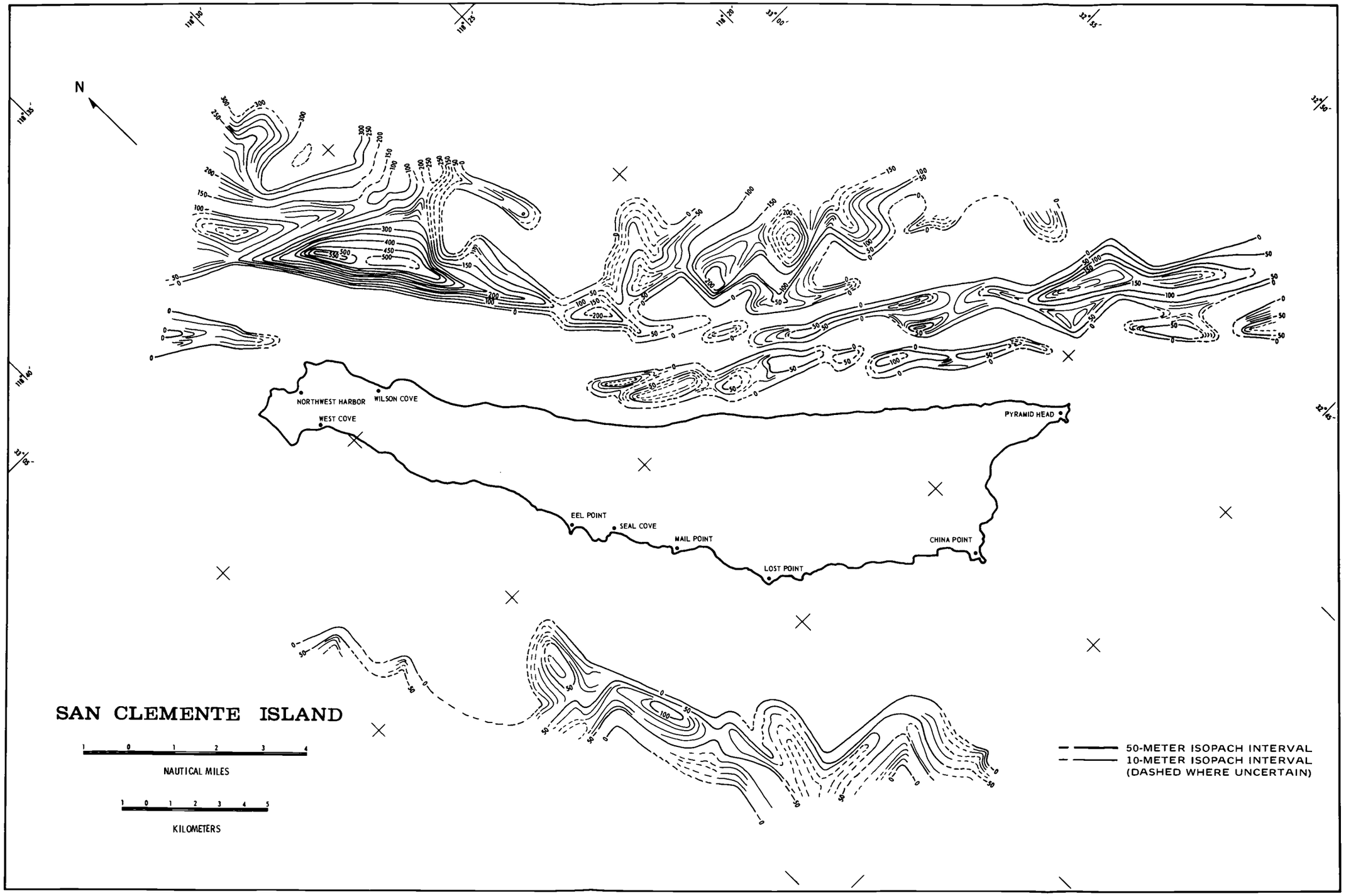

Figure 16. Isopach map of Unit X.

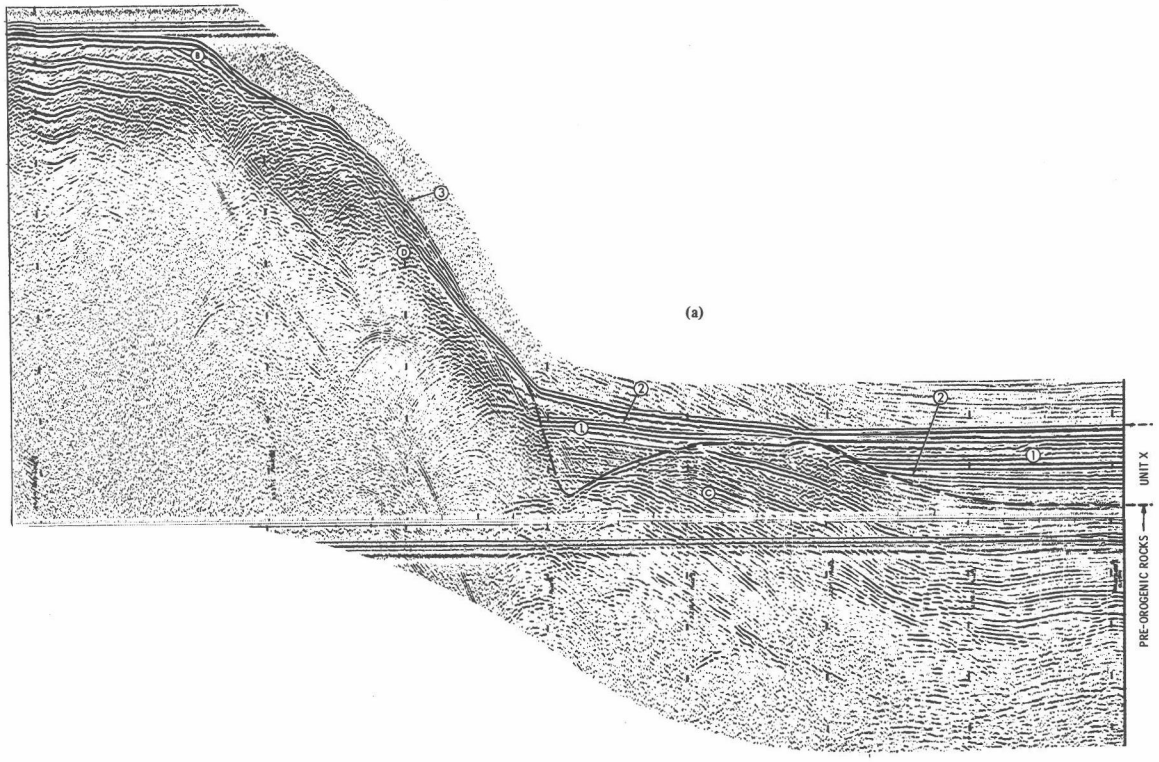
(a)
UNIT X
PRE-OROGENIC ROCKS

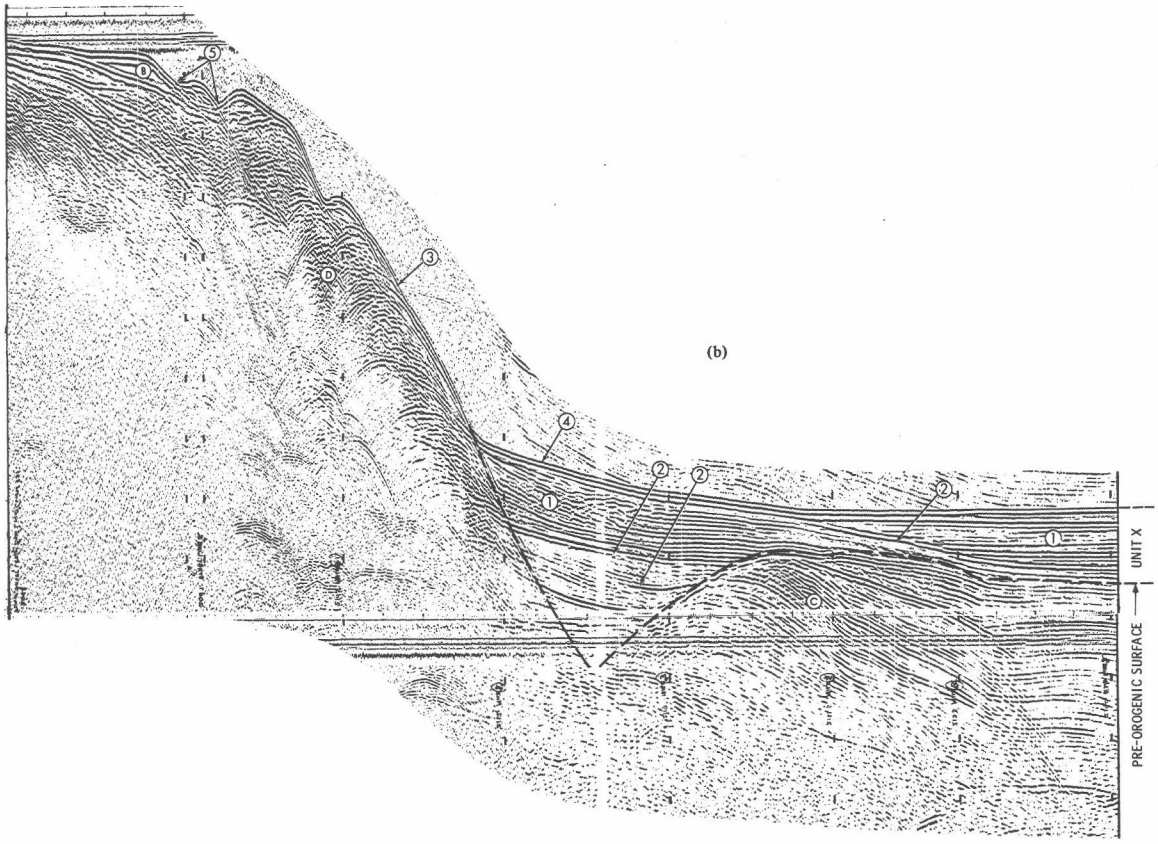
(b)
UNIT X
PRE-OROGENIC SURFACE

Gaal (1966) reported two post-orogenic sedimentary unconformities near the margins of the Santa Catalina Basin that he believed are Pliocene to Recent in age. However, Moore (1966) contends that all of the post-orogenic sediments are Pleistocene or younger in age.

The outlines of the deposits of Unit X (Figure 16) are commonly linear and abruptly terminated. The planar sediments of this unit are clearly outlined in the perched troughs along the escarpment. Much of the upper part of the elongate section on the shelf off Northwest Harbor, interpreted as Unit B (Figure 13), may be equivalent to Unit X.

A maximum thickness of slightly more than 550 meters is recorded in the triangular-shaped basin deposit off the Wilson Cove area. Most other deposits along the San Clemente fault zone have maximum thicknesses less than 300 meters. The maximum thickness of Unit X deposits off the west side of the island is 100 meters. These deposits are interpreted as a combination of apron and minor fan deposits (Menard, 1955). Isopach configurations along this side of the island suggest trends of sediment transport that follow the underlying geomorphic pattern that is principally controlled by structure.

V. STRUCTURAL GEOLOGY

FAULT EVIDENCE IN AREA OF STUDY

Structural interpretations in this study are based on previous investigations coupled with continuous seismic profiling. Integration of internal structure and topography is used to differentiate fault scarps from the flanks of folded sedimentary structures (Appendix III). Stratigraphic and geomorphic features of the offshore region are used to further emphasize the structural aspects.

Anomalous Fault Trends

Major faulting, apparent from all survey data around the island, is generally related to that on the island. Anomalous trends in the isopach intervals of the geologic units are attributed primarily to faulting.

A tectonic map of the San Clemente Island block region (Figure 18) was made with the objective of showing small as well as large faults or probable faults in order to indicate stress trends. Ridges and linear depressions or anticlinal-synclinal folds are shown by the same symbol; it is often difficult to differentiate small features of this type on the profiles due to the "velocity effect" (Appendix III). Where faults could be confidently projected to those on the islands, they are tied together by dashed lines. Island faulting is mainly taken from Olmsted (1958), with modifications resulting from the work of Merifield and Lamar (1967) and the author's field and aerial photographic interpretations.

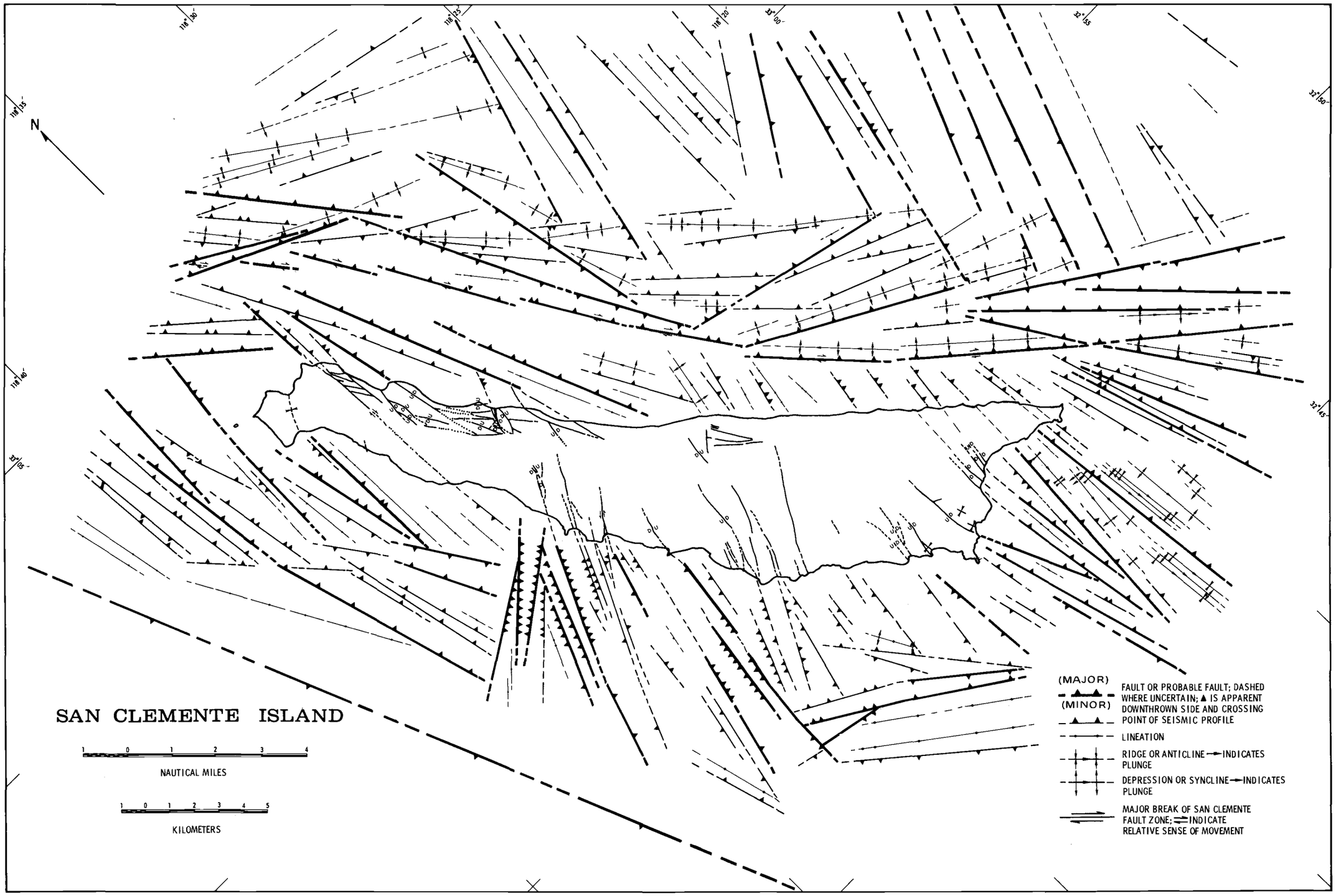

Figure 18. Tectonic map of San Clemente Island block region. Island structure from Olmsted (1958), Merifield and Lamar (1967), and field reconnaissance of writer.

A major fault trend to the northwest (approximately N40°W) that represents the San Clemente fault zone is particularly evident along the east side of the island. The main fault of the San Clemente fault zone is represented as the break and trough at the base of the San Clemente Escarpment (Figures 18 and 15, Profiles 5, 11, 13). A second major fault trend cuts obliquely across the island block in a more northerly direction. The faults of this trend are pronounced immediately off the northern one-third and the south end of the island. A third major fault trend is northeasterly and is evident both to the east of the San Clemente fault zone and on the central and south parts of the island crustal block.

Statistical Analysis of Fault Trends

The use of faults and other displacements to reconstruct stress fields is often tenuous and far from simple. Statistical treatment of the data is one method that allows elimination of local deviations. Rose diagrams of various sections of the region of study (Figure 19, Table 1) indicate that three structural trends exist. Together, these trends can be explained as due to horizontal compressional stress with the principal axis oriented in a northerly direction and about 30 degrees to the long axis of the island. Specifically, the rose diagram of Figure 19a shows two major fault-strike trends. One trend averages N40°W, which is considered a principal shear direction. This trend is similar to that of the San Clemente Escarpment (Shepard and Emery, 1941, Chart 1) and the San Clemente Fault as defined by Moore (1966, Figure 13). The average of the second trend is N13°E. The rose diagram of

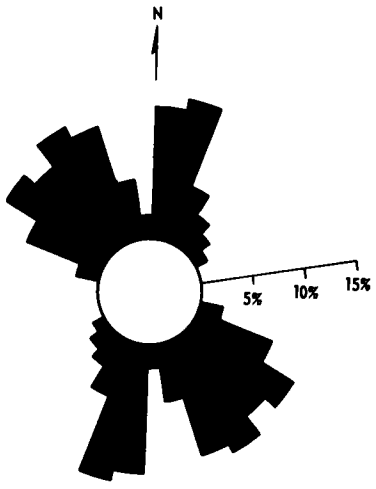

(a)

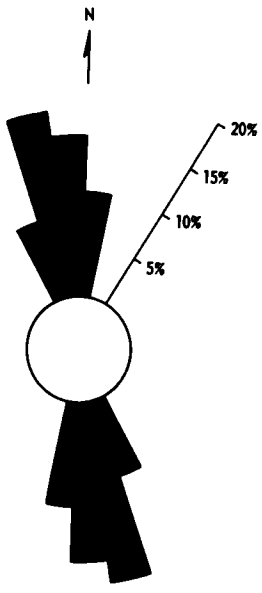

(b)

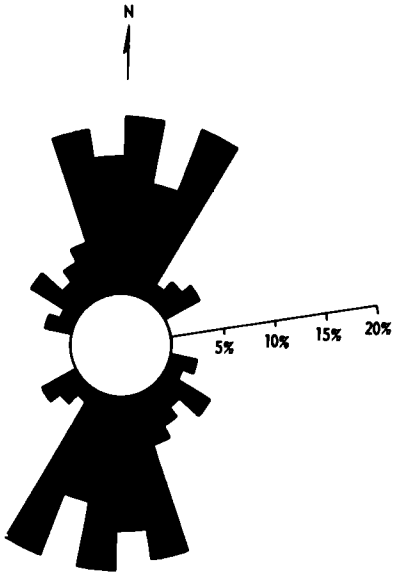

(c)

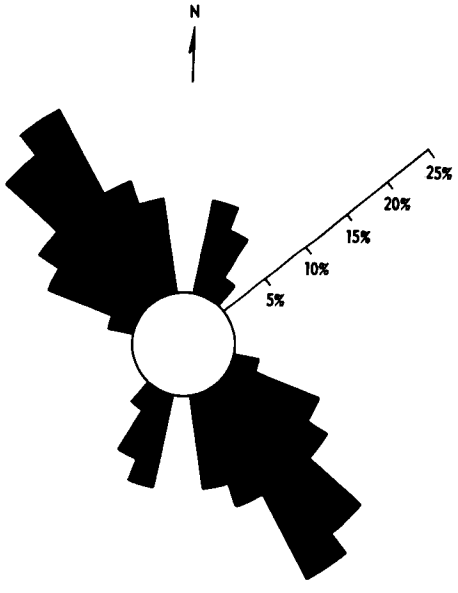

(d)

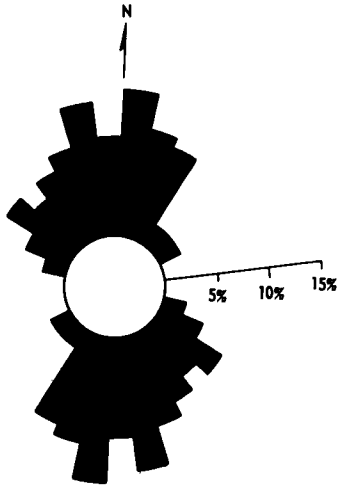

(e)

TABLE 1. FREQUENCY OF OCCURRENCE OF FAULTS, SAN CLEMENTE ISLAND BLOCK REGION, SHOWN IN DIAGRAMS OF FIGURE 19.

Azimuth	NE side of island		South end of island		SW side of island		Reactivated fault		Total faults	
	Frequency of occurrence	% of occurrence	Frequency of occurrence	% of occurrence	Frequency of occurrence	% of occurrence	Frequency of occurrence	% of occurrence	Frequency of occurrence	% of occurrence
N70°-80°W	2	2.22	••	•••	2	2.56	1	2.27	4	2.13
N60°-70°W	7	7.78	••	•••	1	1.28	4	9.10	8	4.25
N50°-60°W	10	11.12	••	•••	4	5.13	5	11.36	14	7.45
N40°-50°W	9	10.00	••	•••	2	2.56	8	18.18	11	5.85
N30°-40°W	11	12.22	••	•••	3	3.84	9	20.45	14	7.45
N20°-30°W	10	11.11	3	15.00	4	5.12	5	11.36	17	9.04
N10°-20°W	5	5.55	7	35.00	12	15.39	4	9.09	24	12.77
N-10°W	2	2.22	6	30.00	10	12.82	••	•••	18	9.57
N-10°E	11	12.23	4	20.00	13	16.67	••	•••	28	14.89
N10°-20°E	12	13.33	••	•••	8	10.25	4	9.10	20	10.64
N20°-30°E	5	5.56	••	•••	13	16.66	3	6.82	18	9.57
N30°-40°E	3	3.33	••	•••	1	1.28	1	2.27	4	2.13
N40°-50°E	2	2.22	••	•••	2	2.56	••	•••	4	2.12
N50°-60°E	1	1.11	••	•••	3	3.84	••	•••	4	2.12
Total	90	100.00	20	100.00	78	99.96	44	100.00	188	99.98

Figure 19b has an average trend of N10°W; that of Figure 19c has three trends that average N18°W, N7°E, and N24°E. Figure 19d, based on what is believed to be recent offsets of the sea floor at basin and trough fills, exhibits two trends, a major one averaging N42°W and a secondary trend with an average at N20°E. The rose diagram of all the fault strikes (Figure 19e) and the averages of the fault trends of Figure 19a, b, and c exhibit three anomalous trends (Figure 20). The averages of the trends of Figure 20 result in a pattern (Figure 21), the included angles of which very closely coincide with the theoretical angle (frictional effects considered) between primary shear faults (Hafner, 1951; Anderson, 1951; and others), but modified by tensile fracturing between the directions of primary shear.

Faulting in the Detailed Survey area exhibits certain characteristics of distribution that support and augment some of the structural conclusions in this paper. All discernible faults in the detailed area strike north to northeast and generally follow the onshore fault trend of this area (Figure 10). The strikes of the faults have a dominant trend between N20°E and N35°E with the mean near N25°E (Table 2). A secondary trend is noted between N5°E and N15°E. The dominant fault trend is most evident north of Seal Cove; that of the secondary trend is more apparent to the south. A slight southeast to northwest clockwise rotation of the overall fault pattern is evident.[5] There is, in addition, a marked tendency for Unit C to show a similar rotation of the dip azimuth seaward of the Eel and Lost Point offshore areas. The fault

[5]This fault pattern rotation is noted slightly on rose diagrams compiled by Merifield and Lamar (1967) for the Lost and Eel Point areas.

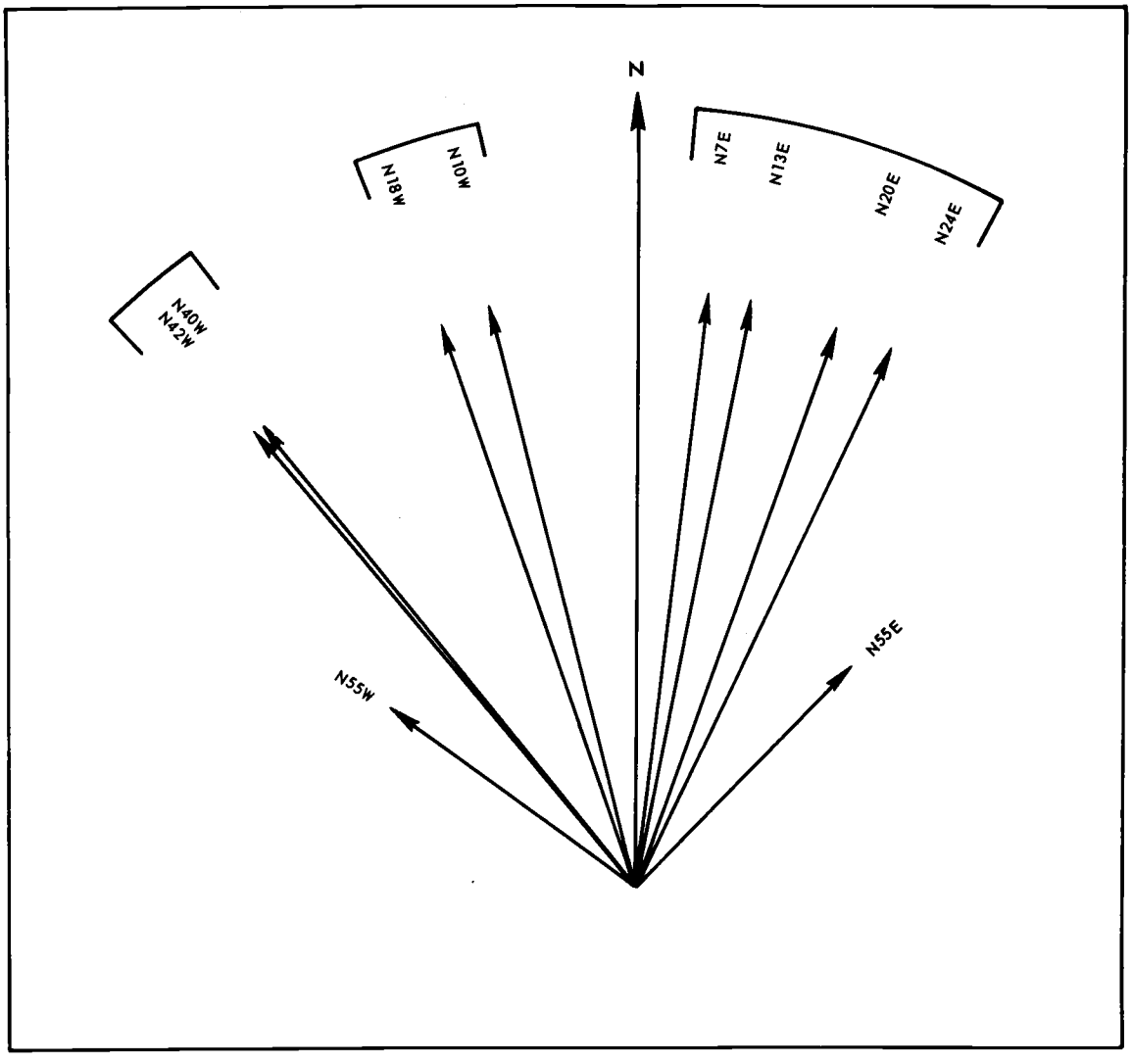

Figure 20. Clustering of averages of fault trends in rose diagrams of Figure 19.

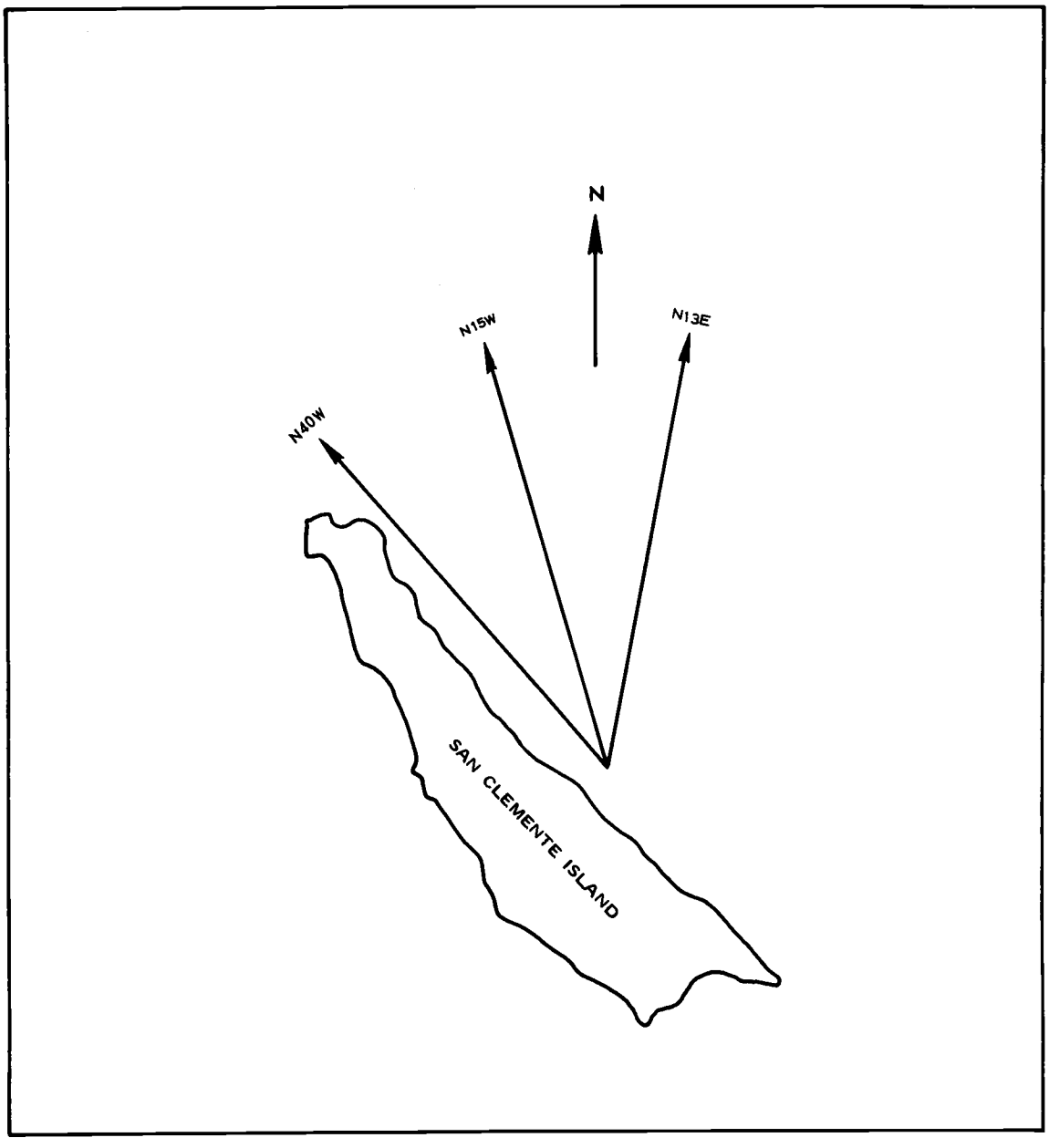

Figure 21. Resultant of averaging the fault strikes for each of the clusters in Figure 20, to give three principal trends.

TABLE 2. STRIKE INTERVALS OF FAULTS, DETAILED SURVEY AREA.

Strike interval	Frequency of occurrence	% of occurrence
N-5°E	1	1.8
N5°E-N10°E	6	10.7
N10°E-N15°E	8	14.3
N15°E-N20°E	5	8.9
N20°E-N25°E	10	17.9
N25°E-N30°E	5	8.9
N30°E-N35°E	10	17.9
N35°E-N40°E	3	5.4
N40°E-N45°E	5	8.9
N45°E-N50°E	1	1.8
N50°E-N55°E	1	1.8
N55°E-N60°E	1	1.8
Total	56	100.1

rotation ends abruptly at the northwest side of Eel Ridge Canyon (note also Figure 18). The Seal Cove area is structurally interesting because of a major inlier of Unit C preserved by a series of faults (Figures 10 and 12). In addition, one of the two island faults that are shown to have a horizontal component of movement (Merifield and Lamar, 1967) projects into the northern side of Seal Cove. This horizontal movement, shown in Figure 10, is left-lateral and tends to substantiate the necessary relative horizontal movement to preserve the inlier as it is positioned to the south of the island fault. Preservation of the inlier may also be due to seaward vertical displacement. Profile line K and a continuation of Profile line HH-GG-FF (not shown in Figure 1) indicate an apparent vertical (graben) displacement of 60 to 70 meters across the series of offshore faults concentrated in this area. This suggests either pivotal faulting seaward from the island or the disguising of similar throw in the onshore volcanic rocks by terrace fill and the development of post-fault wave-cut terraces so evident on this side of the island.

Anomalous Stratigraphic Trends

Major pockets of Unit A (Figure 14) reflect the principal depressions in the nearshore volcanic rock. Further, the geometric configuration of these deposits tends to align with the faulting trend. The depressions are believed to be caused by faulting and possibly weathered out breccia and curved, flow banding zones in the volcanic rocks. Noteworthy are the three deposits of Unit A off the Eel Point and Seal Cove area. Eel Ridge is believed to be due to faulting and possibly preservation by the tougher dacite covering. This ridge acts as a barrier to the general

longshore currents resulting from the southeasterly current flow and the prevailing wave train and swell patterns from the west to northwest (Emery, 1960). The resulting deposit to the north of Eel Ridge has a maximum thickness of nearly 40 meters and is positioned at the head of Eel Ridge Canyon where faults trend seaward close to the axis of Eel Ridge Canyon. The deposit opposite Seal Cove is considered the result of deposition in the fault trough that preserved the inlier of Unit C. The configuration of the Lost Point Grid and Mail Point area deposits is coincident with the fault trends of these areas.

The predominant dip of the nearshore pockets of sediments is about 2 degrees seaward. The general trend of the dip is shown by the rose diagram in Figure 14.

The offshore terrace is essentially flat; it represents much of the upper surface of Unit B. As a consequence, the isopach trends in Figure 13 reflect the deposition of Unit B on the unconformable and faulted surface of Unit C. Faulting in Unit C is particularly defined by the three thick zones of Unit B immediately to the south of Eel Ridge Canyon. Here, two faults have also affected Unit B, as indicated by the first two thick zones. These are the only faults that appear to have affected Unit B, except possibly for those that follow the trend of Eel Ridge Canyon (note Figure 10). However, it is suspected that minor reactivation of some pre-Unit B faults (or later faults) has been absorbed by incompetence within the bedding of Unit B and is not revealed on the profile records. This is suggested where some of the Eel Point and Lost Point Grid profile records normal to the island show the wave-cut terrace (at Unit C) slightly offset by faulting (Figure 22).

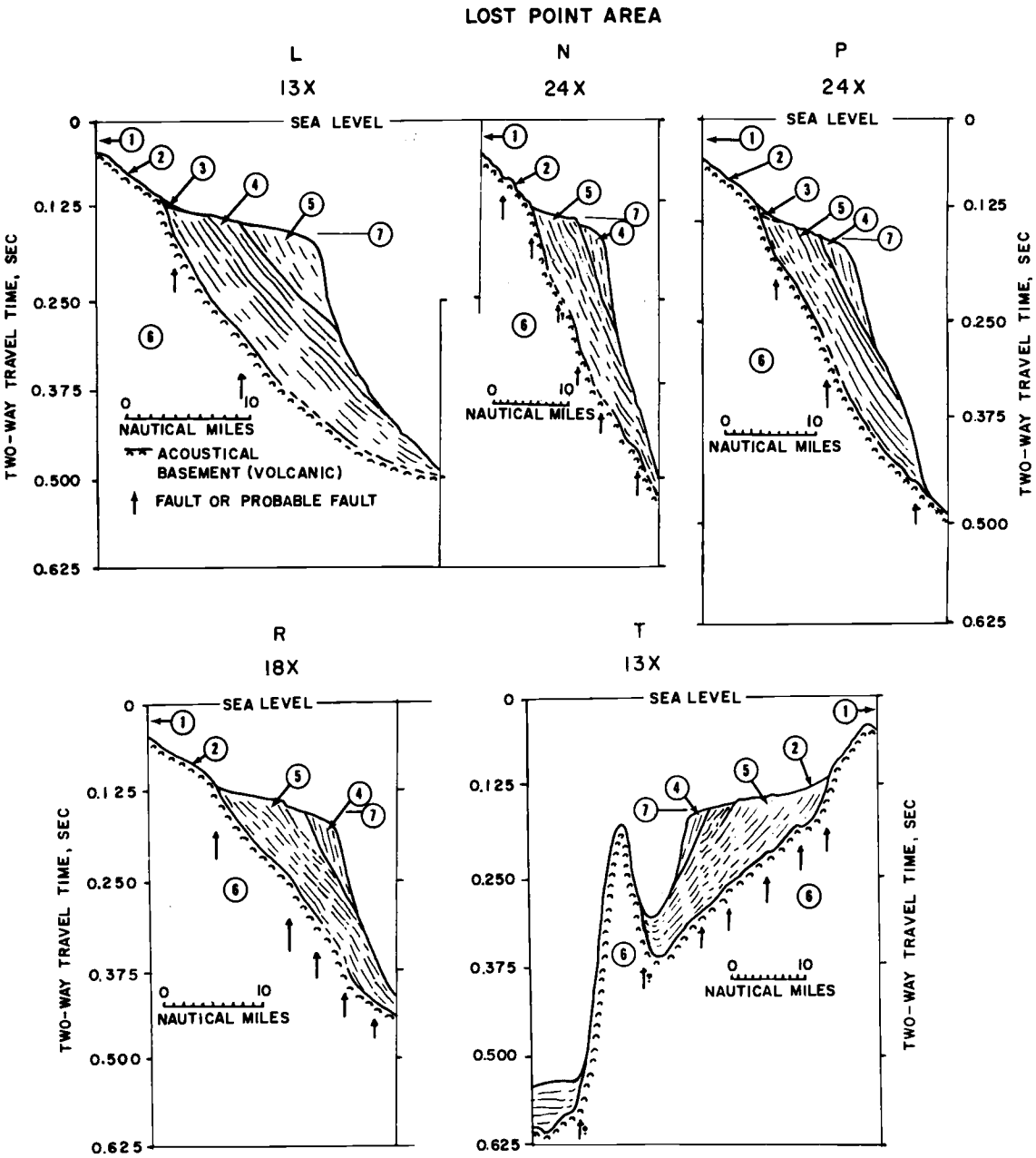

Figure 22. Line drawings of Profiles L, N, P, R, and T, Lost Point area. (1) Shoreward, (2) sea floor, (3) Unit A, (4) Unit B, (5) Unit C, (6) Unit D, and (7) wave-cut terrace. Note offsets of terrace related to faulting. In one case (Profile N) the offset appears to be at the contact of Units B and C. (See Figure 1 for location of profiles.)

Erosion as well as faulting of Unit B is suspected in much of the study area. This is particularly noticed in the area immediately south of Eel Ridge Canyon. However, the possibility that deposition was never complete enough in this area to reach the average elevation and width of the wave-cut terrace must be a consideration. The profile records of the Eel Point Grid parallel to the shore indicate erosion as well as a faulted surface, since gullies appear to be incised into the wall of the canyon. In conjunction with this, the break in continuity of Unit B across the canyon is likely the consequence of erosion as well as faulting in the canyon area. Evidence of erosion of Unit B near its seaward edge is shown by the extension of Profile 6 (Figure 11).

An embayment of Unit B between the Eel and Lost Points area is attributed to the inferred pivotal or lateral faulting seaward from the Seal Cove area.

The majority of the dips of Unit B in the Detailed Survey area lies between S45°W and S70°W. This trend is similar to that of Unit A, suggesting a similar mode of transportation and deposition for both units.

Figure 13 broadly depicts the offshore structural fabric along the west side and the ends of the island. However, from evidence presented in the Detailed Survey, the structural outlining is primarily due to deposition on the unconformity at the post-orogenic surface. Closer spacing of the data would permit a better definition of any isolated depressions such as those revealed by the Detailed Survey.

The lower part of the northwest-trending deposit off the north end of the island may be a remnant of pre-orogenic strata preserved by faulting. A clear-cut definition of Unit B was difficult and tenuous on parts of the profiles of this area.

The only separation of Unit B along the west side of the island is at Eel Ridge Canyon. This break further emphasizes the contrast in the geomorphic and structural nature of this area over that of the remaining side of the island.

Figure 12 shows that faulting and erosion have strongly affected Unit C. The inlier of the Seal Cove area is well outlined. Further, a net right-lateral movement is suggested in the faulting aligned with the north side of Eel Ridge, placing Unit C much closer to shore along the northern side of Eel Ridge Canyon. However, pivotal faulting, accompanied by a subsequent stripping of Unit C over the Eel Ridge Area, could accomplish the same effect. The pivotal fault hypothesis is strengthened by the presence of a thicker section of Unit C to the north of the canyon. Unit C thins along the axis of Eel Ridge Canyon. The thinning implies considerable erosion of Unit C, probably following the development of the canyon axis faults.

Development of a canyon in Unit C (Figure 11) is indicated by the isopach trend seaward of the inlier of Unit C in the Seal Cove area. The association of this trend with the isopach interval of Unit B for the same area more clearly defines the canyon.

Outcrops of Unit C on the submarine terrace are only observed on the Detailed Survey records of the Lost Point area (Figure 22). These outcrops align with the fault pattern of this area. It is presumed that

faulting followed the bedding on the basis of competency, but the profiles normal to the island disclose a much steeper dip than would be developed by bedding plane faults. The Lost Point area outcrops are confidently related to a series of relatively parallel faults of small throw that cut this area. These outcrops interrupt the uniform slope of the offshore terrace (except for interfilling by Unit A sediments) and suggest either a post-terrace faulting or lack of sufficient deposition of Unit A sediments to cover the outcrops. Post-terrace faulting is more likely, since (1) a smoother surface of Unit C exists across the terrace in most other areas and (2) a single terrace offset of 5 to 8 meters is linear across most profiles of the Lost Point area normal to the island.

The dip of Unit C in the Detailed Survey area is generally southwestward (Table 3). A noticeable and somewhat uniform spread in the major rose diagram peaks (Figure 12) is related to the aforementioned marked tendency for the strike of the faults in this area to have a general southeast to northwest clockwise rotation. As a consequence, the individual (fault) blocks have apparently rotated to change the attitude of the dip in such a manner as to allow the dips to rotate in the same direction as the faults.

Isopach anomalies shown in Figure 9 tend to substantiate the faulting shown on the geologic map of Figure 10. A pronounced change in the isopach trends is noted north and south of the Eel Point-Lost Point area; the areas to the north and south are similar by containing northwesterly and northerly trends, respectively. The area between Eel and Lost Points contains northerly to northeasterly trends. Also, the major exposure of volcanic rock seaward of the wave-cut terrace is more clearly defined and better illustrates the structural control disclosed

TABLE 3. DIPS AND AZIMUTHS OF DIP OF UNIT C, DETAILED SURVEY AREA.

Dip,[a] degrees	Frequency of occurrence	% of occurrence	Azimuth of dip	Frequency of occurrence	% of occurrence
1	..	...	S10°W	1	0.5
2	..	...	S15°W	14	6.7
3	13	6.2	S20°W	12	5.7
4	60	28.6	S25°W	23	10.9
5	74	35.2	S30°W	7	3.3
6	16	7.6	S35°W	2	1.0
7	16	7.6	S40°W	16	7.6
8	8	3.8	S45°W	2	1.0
9	2	1.0	S50°W	24	11.4
10	13	6.2	S55°W	1	0.5
11	4	1.9	S60°W	14	6.7
12	2	1.0	S65°W	1	0.5
13	..	...	S70°W	29	13.8
14	1	0.5	S75°W	5	2.4
15	..	...	S80°W	34	16.2
16	..	...	S85°W	11	5.2
17	1	0.5	West	3	1.4
18	..	...	N85°W	10	4.8
19	..	...	N80°W	..	...
20	..	...	N75°W	1	0.5
Total	210	100.1		210	100.1

[a]Mean is 5 1/2 degrees.

by the Detailed Survey data. The relatively thick deposits of Unit C southwest of West Cove appear to have right-lateral offset. The Unit C fault-depression fill immediately north of Eel Ridge Canyon has apparently been severed by the northerly and northwesterly striking faults. A possible part of the fill is shown immediately to the north where it has been offset by one of the north-striking faults. The two thicker deposits off Mail and Lost Points are dissected by a right-lateral offset if these portions are considered to have been together before faulting. An apparent offset is present near the center of the thick deposit off Lost Point. Presumably, the two thicker sections of Unit C off the south end of the island have been dissected and preserved by faulting, as are their island complements. Some normal faulting is suggested by a predominance of blocks downthrown to the southeast. Normal faulting in this area is especially fitting for the cluster of faults immediately off Pyramid Head. The horsts to the south of China Point and off Pyramid Head are probably the result of tensional stress followed by normal faulting.

Profile interpretation suggests that blocks and ridges of Unit C are preserved along the entire San Clemente fault zone. These are shown as exposed upthrown as well as buried crustal blocks that are presumed to be underlain by volcanic rock. Some profiles indicate a thickness of Unit C in this zone corresponding to a sound velocity of roughly 0.6 second one-way travel time (approximately 400 meters).

Some of the broader structural trends of the island block are well delineated in Figure 23. Normally, evidence of faulting should be better preserved by the cover of Unit C, providing the surface separating

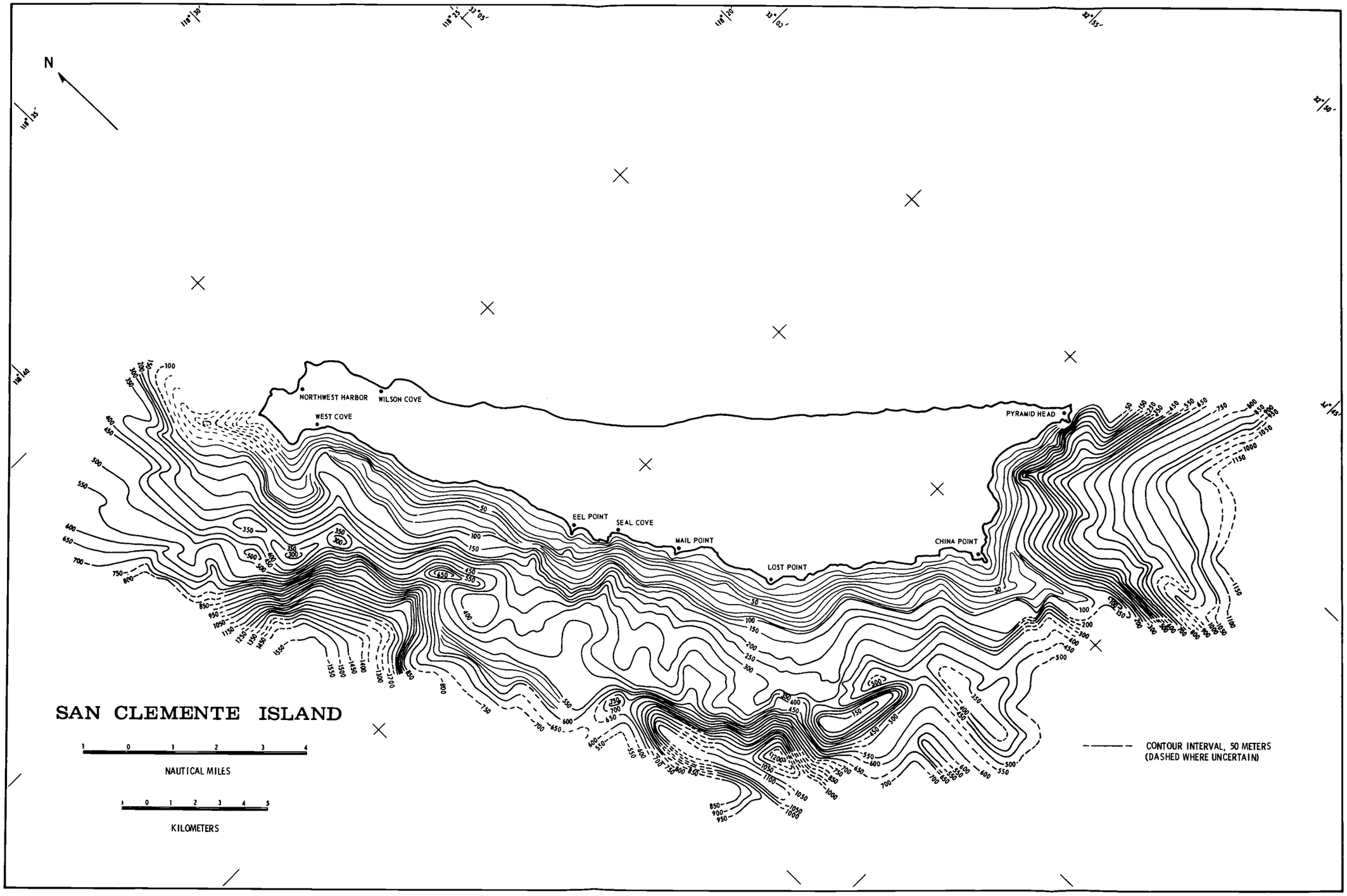

Figure 23. Structure contour map on the surface of Unit D, Reconnaissance Survey. Datum taken at sea level, with 10-meter contours between datum and the 100-meter line. Note tendency of surface to flatten seaward of the 300-meter contour along the west side of the island.

Units C and D does not represent too great a hiatus. An interesting feature that suggests a hiatus between these units is the tendency for the sloping volcanic rock surface to "flatten" beneath and slightly seaward of the present submerged terrace. This may represent the remnant of a pre-Unit C wave-cut terrace. The volcanic topographic highs off West Cove emphasize the major depression that has preserved the thicker parts of Unit C in that area. Other major features previously mentioned but reviewed here are (1) an elongate, north-trending topographic high immediately west of the Detailed Survey area with an adjacent trough to the east, (2) a pronounced southeast-trending topographic high off Lost Point, and (3) a complementary high to the west of (2) and (3). These topographic highs show trends, cutoffs and offsets that strongly suggest structural control aligned with the inferred faulting in this area. Conceivably, these may also be vents for the volcanic flows that comprise the upper part of the island block. This is especially suggested for the high off West Cove that is believed responsible for a major magnetic high in this area (Emery, 1960; Harrison et al., 1966; Gaal, 1966; and this paper). In conclusion, structural trends contained in some areas shown in Figure 23 do not correspond very well with the equivalent areas in Figure 9; this reflects, in part, the extent of erosion on the surface of Unit C.

Because of the difficulties encountered in profile interpretation for the east side of the island, only maps of the post-orogenic sediments (Unit X) and of the post-orogenic surface (note Figure 15) are used in the structural analysis.

Figure 24 best illustrates the general overall tectonic pattern for the east side of the island. Intersections of faults at various angles are clearly outlined by the linear trends and sharp discontinuities of the topographic highs and lows along the San Clemente fault zone. Futhermore, some of the geometric patterns suggest that more extensive faults are present, either as separate faults or as extensions of those defined in Figure 18. Some northeast-striking faults suggest that left-lateral offsets have affected (crossed) the main fault zone much more than is shown by Figure 18; this impression has also been suggested for Figure 6. The contour patterns along the submerged part of the San Clemente Escarpment subtly reflect the interpreted fault pattern. The patterns are marked by a change of trend midway of the island. However, the area along the escarpment across from Eel and Mail Points may be affected more by the northeast-trending faults than is indicated by Figure 24. The trough fills by Unit X sediments (Figure 16) further suggest this by offsets in these deposits. The deepest part of the post-orogenic surface in the area studied is at the base of the San Clemente Escarpment off Wilson Cove. Depths to slightly greater than 1,700 meters are recorded in the triangular-shaped depression. The general shoaling nature of the main fault zone off the central part of the island is also evident. Most of the pre-orogenic surface along the San Clemente Escarpment is volcanic rock and is, therefore, considered the equivalent to Unit D. Ridges of this surface form breaks in the escarpment that are considered of fault origin. These ridges act as natural dams to sediment transport.

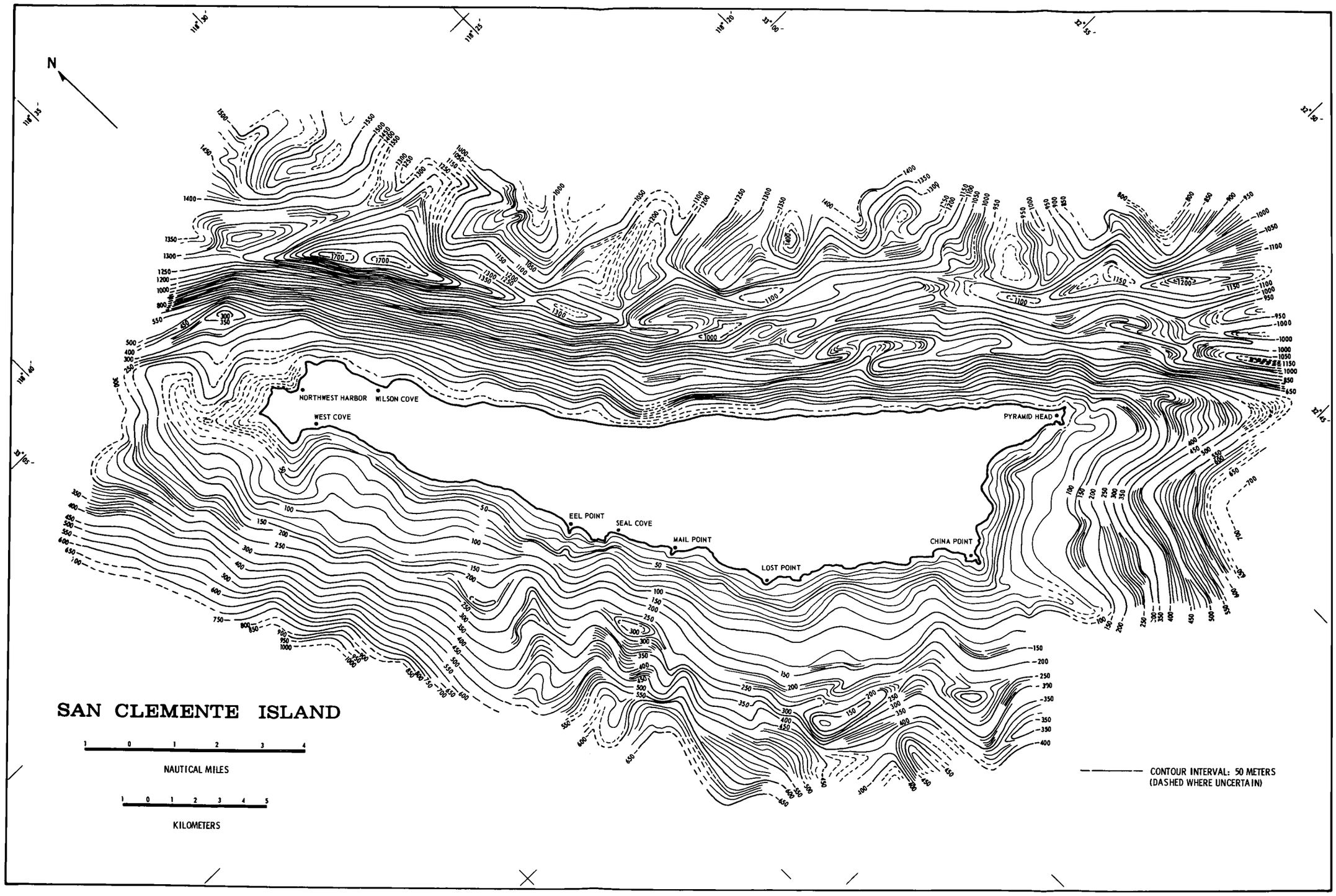
N
NORTHWEST HARBOR
WILSON COVE
WEST COVE
PYRAMID HEAD
EEL POINT
SEAL COVE
MAIL POINT
LOST POINT
CHINA POINT
SAN CLEMENTE ISLAND
1 0 1 2 3 4
NAUTICAL MILES
1 0 1 2 3 4 5
KILOMETERS
CONTOUR INTERVAL: 50 METERS
(DASHED WHERE UNCERTAIN)

Figure 16 further substantiates the structural fabric along the San Clemente fault zone. Offsets stand out very clearly. A combination of pivotal, normal, and thrust faulting to develop minor fault slices is considered responsible for some of the trends along the fault zone and adjacent basin areas. Specifically, as in Figures 18 and 24, the effect of intersections by lateral faulting is indicated by right- and left-lateral offsets around the southwest flank of the Emery Seaknoll. In addition, the upthrust of crustal blocks and the development of depressions are strongly suggested. The effect of fault intersection across the entire San Clemente fault zone by the northeast-striking faults is also more readily seen than is apparent in Figure 18. Noted here are the right-lateral offsets in the perch troughs that are prevalent along the San Clemente Escarpment. The troughs, elongated northwest-southeast, are conceivably the consequence of slump blocks resulting from weak zones developed by the northeast and north-to northwest-striking faults.

NATURE OF STUDY AREA FAULTING

The main purpose of this section is to analyze the structure of the San Clemente Island crustal block by a study of faulting, folding, and uplift in the light of lateral faulting. The main basis for tectonic interpretation is the plan view of fault strikes and the inferred relationship of these faults to the segmentation of crustal blocks, folds, and ridges as interpreted from the seismic profiles. The interpretation is supplemented by and compared to the concepts of other authors. A dynamic approach to the problem is very difficult. Consequently, the

geometric relations have been used for a qualitative approach to the problem. Considering the degree of uncertainty attending this indirect method, substantial agreement with the theoretical application results from both statistical and geometric model analyses. Different interpretations may be applied, but the evidence strongly suggests that the lateral-fault tectonic system is the most applicable for the area studied.

General Theory

Many authors are in controversy relative to the types of tectonic movement in the earth's crust and the interpretation applied to areas of study (for example, Nevin, 1949; Hubbert, 1951; Billings, 1954; Beloussov, 1962, and others). Certain concepts are presented briefly for their importance and relationship to this paper's analysis of the origin of the San Clemente Island block.

Anderson (1951) treated the interrelation of thrust, wrench,[6] and normal faulting and elaborated on the association of wrench and thrust faults. Moody and Hill (1956) evaluated newer concepts of fault dynamics based on pure (rotational) shear and emphasized the importance of wrench faulting, with its consequential thrust faulting and anticlinal folding (Figure 25). According to these authors, the San Andreas Fault and the associated fault zones of southern California and adjacent areas appear to be related to this form of tectonic movement. Maxwell and Wise (1958)

---

[6]Synonymous with strike-slip, transcurrent, and, in the broader sense, lateral fault. The particular terminology is used in this paper when related to a certain author's usage.

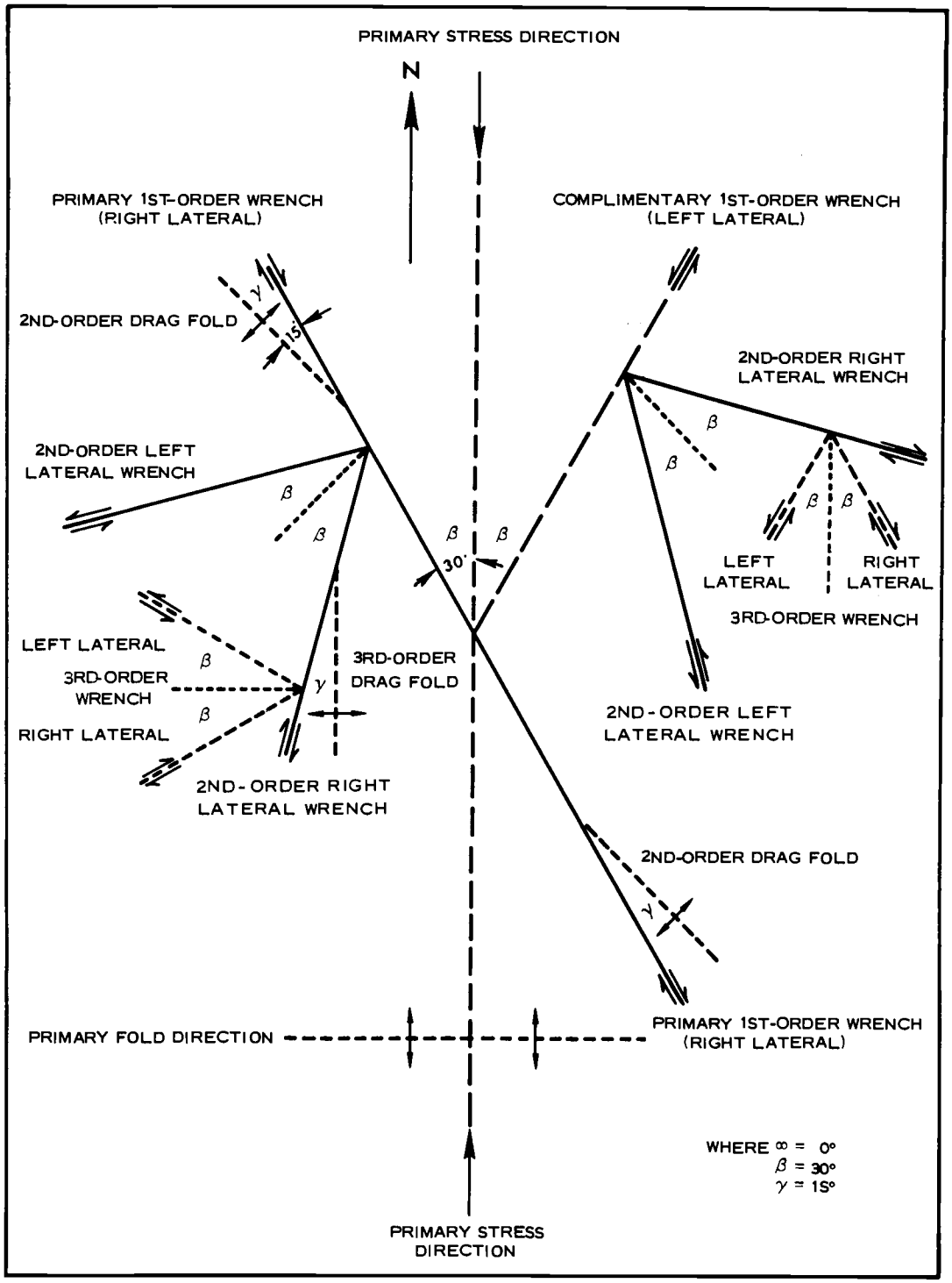

Figure 25. Plan of wrench-fault system under north-south compression (adopted from Moody and Hill (1956)).

suggest that simple (non-rotational) shear by a couple would result in zones of widespread brecciation with large shearing movements accommodated along a single wrench fault or zone of parallel wrench faults. Furthermore, extensive zones of brecciation will not occur under pure shear because conjugate fractures will relieve the forces involved. An important conclusion of these authors for the present study is that small forces are involved under conditions of simple shear, larger forces under conditions of pure shear. They suggest that one mechanism to develop the forces necessary for pure shear could be subcrustal viscous flow, possibly caused by convection currents. According to McKinstry (1953), curves or irregularities in a master strike-slip fault will set up nonuniform distribution of stress with movement along the fault and shears of the second order will tend to form where the fault diverges the greatest from parallelism with the initial force direction. An important conclusion related to the present study is that if tension fractures develop, they should be parallel to the major axis of compressive force.

Other authors have also evaluated the importance of wrench faulting and applied this type of fault mechanism to various areas of the world (for example, Cotton, 1956, 1957; Kingma, 1958; St.-Amand and Allen, 1960; Prucha, 1964; Chinnery, 1966; and Garfunkel, 1966).

San Clemente Fault Zone

Shepard and Emery (1941) show a bathymetric reversal in the direction of slope of the scarp along the strike of the San Clemente Fault from the island to 40-Mile Bank. These authors tend to favor a horizontal right-lateral shift of about 40 kilometers to explain this

phenomenon and give several reasons for this concept over that of pivotal faulting. Allen et al. (1960) believe that the San Clemente Fault is a continuation of the Agua Blanca Fault to the south with a presumed right-lateral displacement of up to at least 11 kilometers along the latter fault. These faults have the same sense of movement as that of the San Andreas and San Jacinto Faults of the coastal area.

Although many of the Continental Borderland's inferred fault scarps have considerable throw, these throws are considered relatively small compared to the postulated lateral movement along such as the San Clemente-Agua Blanca Faults and those in the southern California-Baja California region. Furthermore, the last increment of wrench fault movement in many cases is believed to be essentially vertical (Anderson, 1951; Moody and Hill, 1956) and simulates a high-angle normal or high-angle thrust fault. Referring specifically to the San Clemente Island block relief, local relief may also result from lateral faulting if a high area is brought into juxtaposition to a low area (Cotton, 1956), accompanied by buckling of the moving block (Cotton, 1956), or thrust faulting (Cotton, 1957). Kingma (1958) suggested that a block may be squeezed up if caught between two strike-slip faults. In addition, shape change and shifting of crustal blocks may result from wrench faulting (Moody, 1962). This could have caused certain blocks to collapse, forming present basins such as those surrounding the San Clemente Island block and the development of the San Clemente Escarpment.

Wrench faults are generally characterized by steeply dipping fault planes, but wrench faults with much less dip than 70 degrees have been

described in the literature (Moody and Hill, 1956). The fact that the San Clemente Escarpment has a maximum slope of slightly more than 30 degrees is not considered a major obstacle to the consideration of the wrench-fault hypothesis. Slumps and slump scars indicate that the slope has been modified since its inception. Erosion has undoubtedly had some modifying effect. The seismic profile records suggest that this fault tends to steepen slightly with depth, although this is not conclusive due to the hyperbolic nature of acoustic response from bathymetric troughs.

The most striking property of large lateral faults is the consistent straightness, or smooth and gradual curvature of the fault (St.-Amand, 1958). This is supplemented by a trough along the strike of the fault that is usually sediment filled. Small-scale features attributable to smaller-scale faulting are often found in the trough. Examples are the thrusting of minor fault slices and the formation of small grabens. St.-Amand concludes that any fault having a straight trace more than a few miles in length has undergone lateral movement. All of the properties above are evident along the San Clemente fault zone.

Seismic epicenter evidence (Gaal, 1966; Allen, 1967) indicates that the zone representing the San Clemente Fault has been relatively active since 1934, the beginning year for recording epicenter data. The earthquake foci are believed to be several kilometers in depth (Shor and Raitt, 1958). If these foci are associated with the San Clemente Fault, as is suggested, this fault must extend to several kilometers in depth. Lateral faults are believed to be normally

deep-seated, particularly those that are large primary lateral faults (Anderson, 1951; Moody and Hill, 1956).

From the considerations above, the San Clemente Fault is inferred to be a lateral fault. Arguments in favor of this are sufficiently important to justify making the basic assumption that this fault represents the primary shear direction of the essentially horizontal compressional stress pattern (Figure 25) such as that postulated by Moody and Hill.

Structural Model for Study Area

The rose diagrams (Figure 19) provide a reasonable statistical basis for the above postulated stress pattern by the assumption that the San Clemente Fault is the primary horizontal shear direction. These diagrams provide a close analogy between the average of the fault strikes and the theoretical application. According to Moody and Hill's theoretical wrench-fault system, the N40°W trend is considered the primary first-order right-lateral wrench fault and N13°E is the direction of the complementary first-order left-lateral wrench fault. The N15°W trend corresponds to the primary stress direction, which also corresponds to tensile fractures as defined by Beloussov (1962) and shown in Figure 26a. The shear pattern closely corresponds to the definition of the basic San Andreas Fault shear-stress pattern by Moody and Hill.

A positive empirical assessment of the pattern of faulting in various parts of the study area tends to justify the model. Using

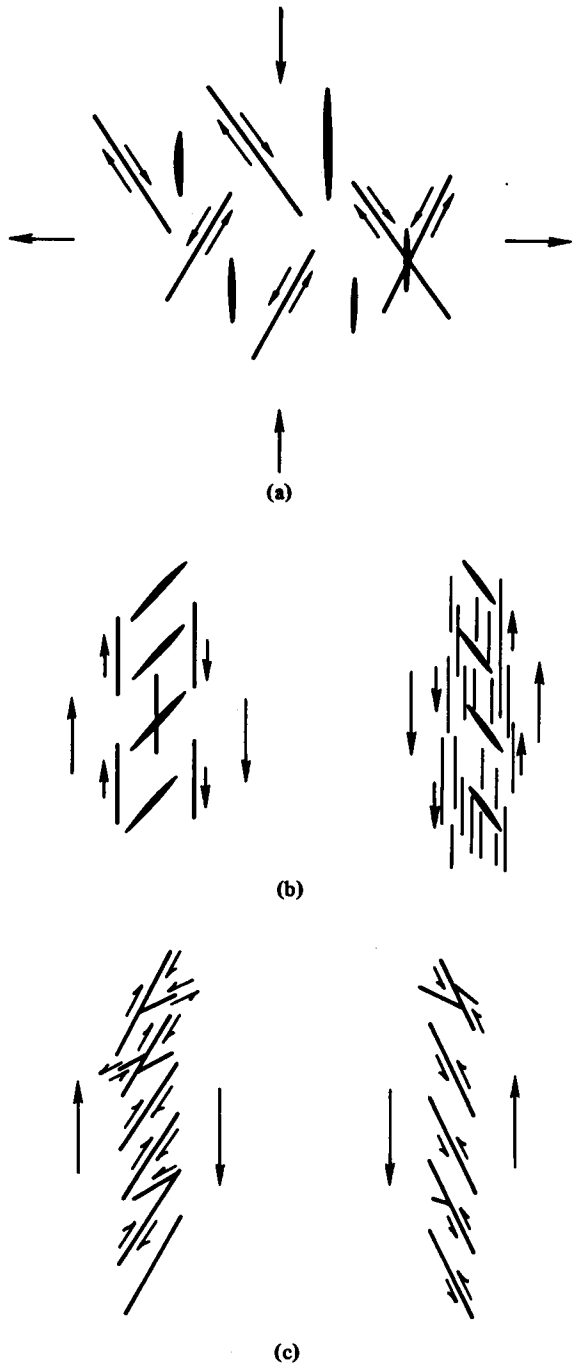

Figure 26. Tectonic stress pattern after Beloussov (1962). (a) Tension-compression, (b) shear formation produced by a couple with formation of a system of en echelon joints, and (c) same as "b" with the formation of a system of en echelon shear fractures. Fine lines are shear fractures; heavy lines are tension fractures. Arrows show direction of displacement.

N15°W as the principal compressional stress direction, much of the offshore and island faulting is readily associated with a tensile-component modified version of Moody and Hill's wrench-fault system.

An example of offshore tensile faulting is shown by the many faults off the south end of the island where normal or pivotal faulting has developed, resulting in a slight crustal block rotation with the downthrown side to the east. The many north- to northwest-striking faults north of Eel Ridge Canyon are considered to be of tensile-strain origin. This area contains a graben and horst assemblage that provides a criterion for this interpretation. Some offsets by north- to northwest-trending faults along the northwestern part of the studied San Clemente fault zone may be attributable to east-west tension resulting in slight dilation, perhaps related to a shear couple (Figure 26b). Some of the faulting within the offshore area between Pyramid Head and Eel Ridge Canyon may also have developed from a shear couple.

The major fault across the northern end of the island (Figure 18) that has right-lateral displacement (Olmsted, 1958) is related to second-order right-lateral wrench faulting. A second fault (Figures 10 and 18), intersecting Seal Cove and having a left-lateral sense of movement (Merifield and Lamar, 1967), is closely aligned with the second-order left-lateral direction. According to Olmsted (1958), movement on the island faults appears to be chiefly vertical, but on many of the other faults the movement has been strike-slip. This implies a combination of lateral and normal (or thrust) faulting. However, Merifield and Lamar (1967) state that the faults studied in the central part of the island dip steeply and that the rake of striations on slickensided gouge zones

shows a dominance of oblique movement more in the horizontal than vertical direction. The steepness of dip and the horizontal movement correspond more to a near-horizontal compression related to wrench faulting.

Merifield and Lamar (1967, p. 11) state in their description of faulting at the central part of the island that,

> "In the cases where the sense of movement could be demonstrated, the north-northeast to northeast-trending faults have moved in a left-lateral sense and the north-northwest-trending faults have moved in the right-lateral sense."

These senses of movements are consistent with the stress model proposed for the study area.

The complex series of faults along the eastern side of the island is considered to be a combination of lateral shear and tensile faulting with resulting slide or slump blocks so prevalent along this side of the island.

Olmsted has related the sympathetic faults between the two main northward-trending faults near Wilson Cove to tensional stress. In this sense, the two main faults would then be essentially shear-derived (couple?) and are related to second-order right-lateral wrench faulting.

Lineations across the island at N75°-85°W (Figure 27) may be second-order right-lateral wrench faults. This interpretation is strengthened by some apparent right-lateral offsets along the shorelines of the island.

An example of offshore horizontal movement is shown by the series of en echelon offsets of the main San Clemente Fault that are consistent with left-lateral faulting. Faults are not shown that cause these offsets. The offsets are presumed to be related, at least in part, to the northeast-striking faults along the northwest and southeast sides of the Emery Seaknoll, and those cutting the escarpment. This series of faults

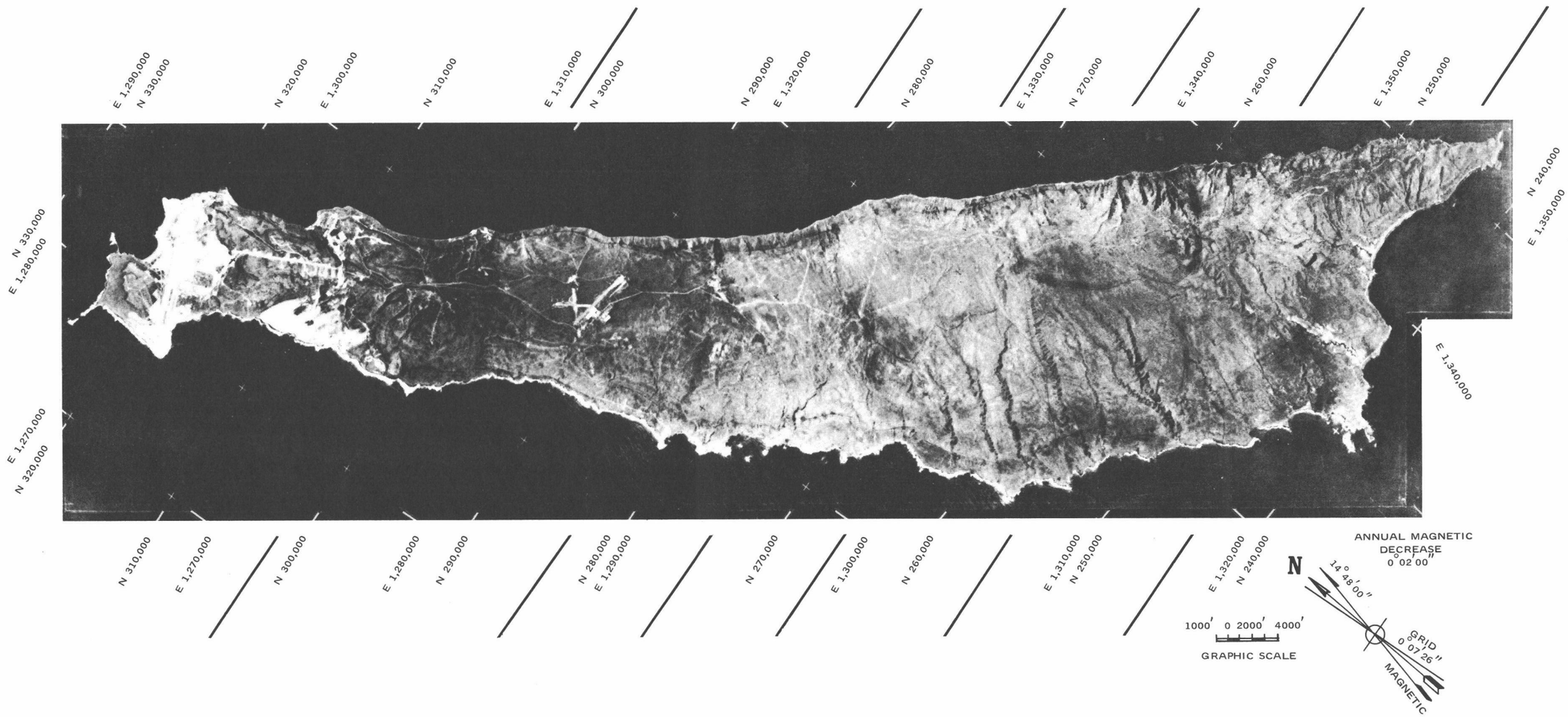

Figure 27. Photomosaic of San Clemente Island. Heavy solid lines outside of border indicate approximate trend of west-northwest lineations on the island that are suggestive of second-order right-lateral wrench faults.

readily corresponds to the complementary first-order shear direction. The 10- to 15-degree bifurcation of the San Clemente Fault, off Pyramid Head may have resulted from a combination of first-order right-lateral wrench faulting and thrust faulting developed by second-order drag. The area between the Emery Seaknoll and the island has several examples of varied, apparent offsets. This area illustrates the complexity that could result from lateral shear between two opposing topographic highs. In plan view, the fault pattern tends to "rotate" around the west side of the Emery Seaknoll, the smaller of the highs. The effects of both tension and shear may be present in this area. Compression was (and is) probably greatest in the zone between the Emery Seaknoll and the island, resulting in the upthrust of the island block and complex fracturing.

Extrapolation of the several northwest- and northeast-striking faults at the northwestern end of the study area will lead to intersections that well illustrate the pattern of primary shear directions.

A further analogy to the postulated stress pattern is shown by an analysis of the ridges and folds off the east side of the island. Most of these features have northwesterly strikes. Under the Moody and Hill system, these features are considered second-order drag folds or ruptures (reverse or thrust fault ridges). A few more northerly-trending features close to the Emery Seaknoll are presumed to be compression ridges (Moody and Hill, 1956) related to the primary wrench fault.

The gentle folding off the southern end of the island (Figure 28) is parallel to subparallel with the associated faulting. These folds presumably resulted from either drag folding (third-order) or drag by the series of fault blocks that rotated eastward in a counterclockwise

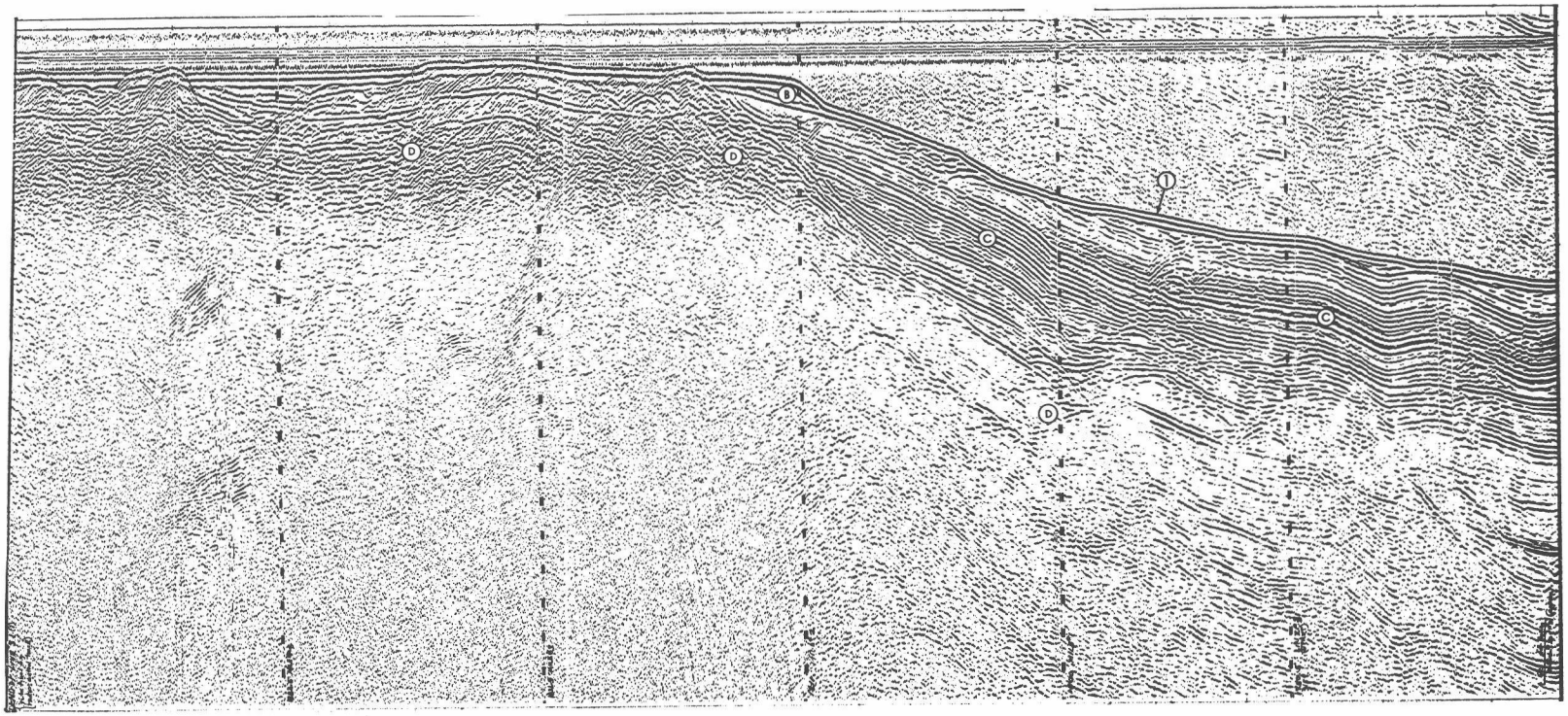

Figure 28. Reconnaissance Survey Profile 31 showing (B) Unit B, (C) Unit C, (D) Unit D, and (1) sea floor. Note the gentle folding of Unit C in areas of the lettering of this unit and the breaks in the continuity of the reflectors suggesting faulting.

direction. The syncline between Northwest Harbor and West Cove is related to second-order drag by complementary left-lateral wrench faulting.

The drag-fold interpretation is strongly supported by statistical analysis. According to Moody and Hill, the value of the critical angle, γ, (note Figure 25) has not been determined satisfactorily. However, generally it varies between 5 and 30 degrees with an average of 15 degrees. Figure 29a and Table 4 show that the majority (80%) of these tectonic features have formed between 30 and 60 degrees (γ = 0 to 30 degrees) from the postulated primary-stress direction. The remaining folds, being within 30 degrees northwest-southeast of the primary-stress direction, may be compression ridges. Table 4 and Figure 29b show that 75% of these folds or ridges are aligned within 10 degrees northeast-southwest of the primary-stress direction. These features may be readily assigned to the third-order drag-fold phenomenon as noted in Figure 25; they correspond to the correct side of the primary first-order wrench fault and the position of the second-order right-lateral wrench fault.

Finally, the proposed structural model is evaluated on the basis of the apparent lateral offsets of other faults and folds (shear type) and the development of horsts, grabens, and rotational faulting (tension type). Figure 29c and 29d exhibit trends that tend to substantiate the basic structural model. The major trend of Figure 29c represents mostly those faults associated with the San Clemente fault zone. The northeasterly trend, representative of the complementary shear direction, would be emphasized if those faults that apparently offset the main break of the San Clemente fault zone could have been defined. The major trend in Figure 29d is close to the N15°W trend illustrated in Figure 21. Most

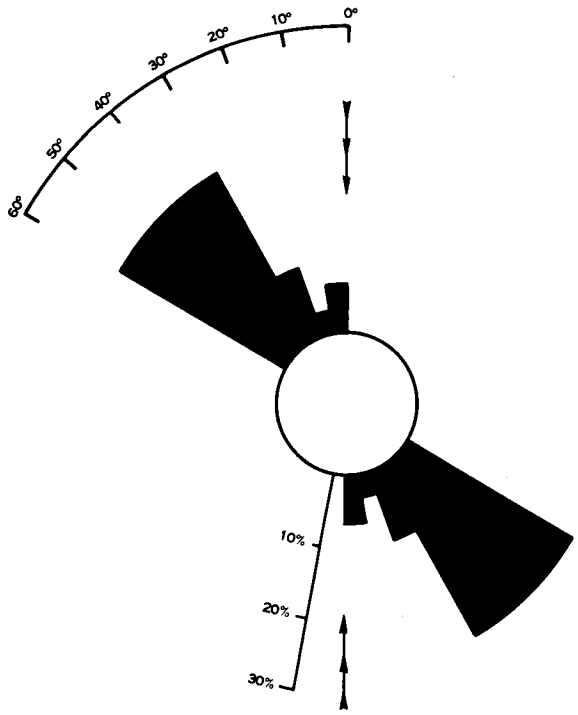
0°
10°
20°
30°
40°
50°
60°
10%
20%
30%

(a)

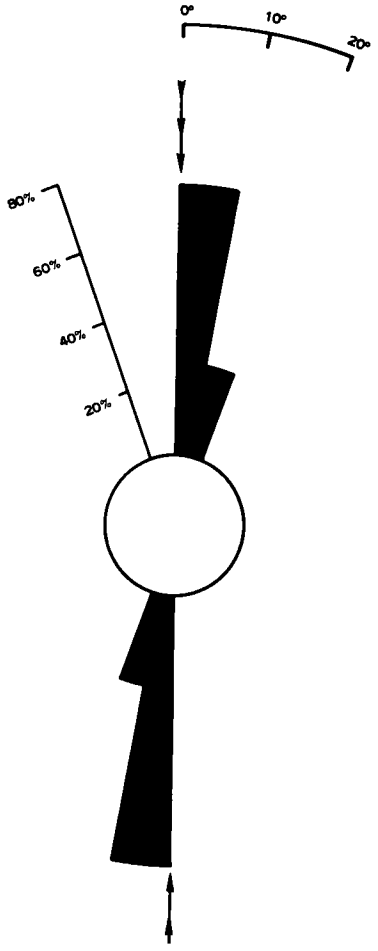
0°
10°
20°
80%
60%
40%
20%

(b)

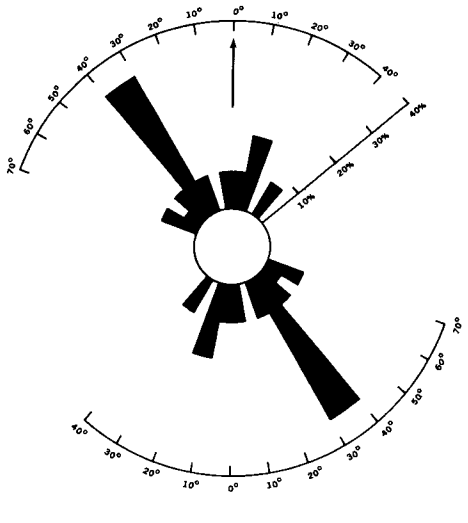
0°
10°
20°
30°
40°
50°
60°
70°
10%
20%
30%
40%

(c)

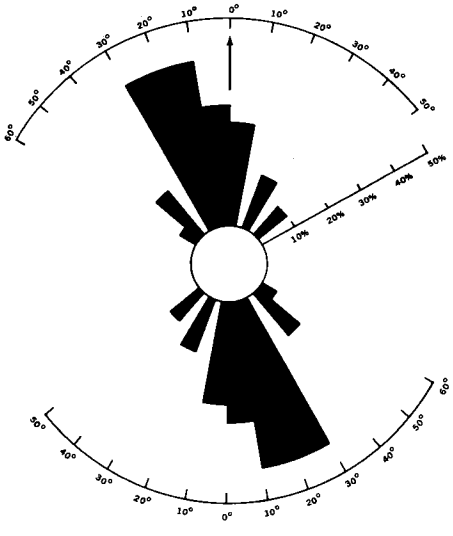
0°
10°
20°
30°
40°
50°
60°
10%
20%
30%
40%
50%

(d)

TABLE 4. OCCURRENCE OF SECONDARY STRUCTURES (FOLDS OR RIDGES) ALONG THE SAN CLEMENTE FAULT ZONE AND OFF THE SOUTHERN END OF ISLAND.

Degrees from γ[a]	Frequency of occurrence	% of occurrence
San Clemente Fault Zone		
0-10	2	6.67
10-20	1	3.33
20-30	3	10.00
30-40	8	26.67
40-50	8	26.67
50-60	8	26.67
Total	30	100.01
Southern End of Island		
0-10	9	75.00
10-20	3	25.00
Total	12	100.00

[a]See Figure 25 for angle γ.

of the northeasterly secondary trend in Figure 29d represents rotational faulting postulated for the Eel Ridge Canyon area and the faults forming the graben-like depression between the Emery Seaknoll and the Southern Plateau.

SUPPLEMENTARY TECTONIC CONDITIONS AND FEATURES

Uplift, Doming, and Tilting

There is no strong evidence of primary folding on the island block. Consequently, the uplift of the entire block, complemented by doming and tilting, must represent some response to the primary compressional force. Various authors have related crustal-block uplift to lateral faulting. Buckling, thrust faulting, squeezing between strike-slip faults, and shape change and shifting are given as causes for uplift.

Bowing of the surficial dacite flows capping the central part of the island is noted by Merifield and Lamar (1967). These authors suggest a 0- to 15-degree westerly to southwesterly dip of the volcanic rocks on the west flank of the island and, by limited observation, a 10- to 30-degree northeasterly dip of the volcanic rocks on the steep east flank. Possibly, the latter dip is the result of drag along the San Clemente Fault.

Rotation of the northeast fault pattern offshore in the Detailed Survey area, culminating at Eel Ridge Canyon (Figure 30a), may have been partly caused by the upbowing of the island block. According to Beloussov (1962) both shear and tension fractures may be formed by bending and upwarping. This may develop stretching that varies widely in

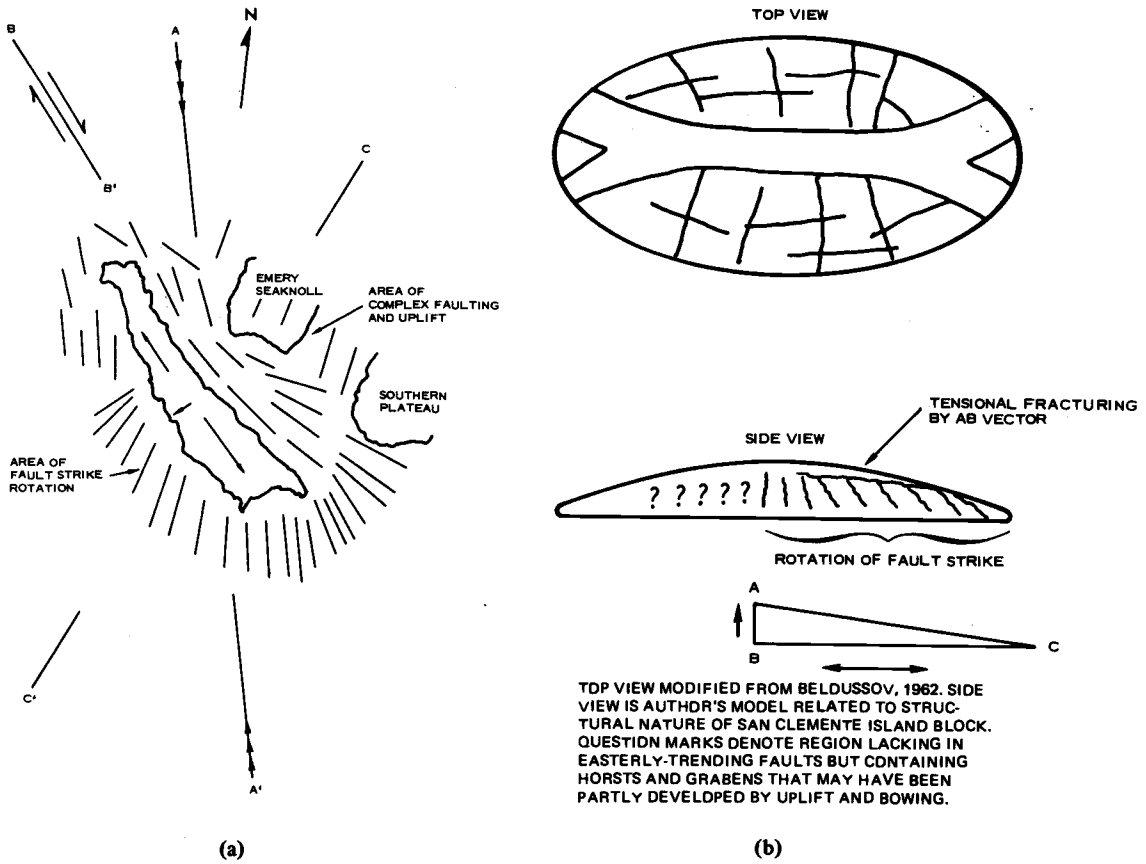

Figure 30. Sketch of proposed upbowing and subsequent fracturing of San Clemente Island block. (a) Plan view showing principal horizontal compression direction A-A' and main trends of offshore faulting. B-B' is primary first-order wrench-fault direction, and C-C' is the trend of the bathymetric high. (b) Model showing relationship of tension stress to compressional stress by upbowing of island. AB vector is component of uplift and BC is component of compression representing the principal compression direction.

intensity depending on the shape of the uplifts. Under these conditions, the northwest-striking faults and lineations off China Point could be related to tension as shown in Figure 30b. A graben in this area is one criterion for this conclusion. In some cases, one of the fracture systems predominates, most frequently the radial (shear) pattern. Accordingly, this could be the case for some of the northeast-trending fractures southeast of Eel Ridge Canyon. Also, some of the north- to northwest-striking faults associated with horsts and grabens northwest of the canyon may have been developed by uplift as well as tension from horizontal compression. In conclusion, a complex structural pattern could result from a horizontal compression that has caused upbowing of a crustal block as well as direct horizontal shearing in the block. This may be the case here, considering the attitude of the longitudinal axis of the island block relative to that of the inferred primary-stress direction, where further compression has acted on the block after some uplift has occurred.

Shear Couple Model

The major fault zone along the west base of the island block was obtained from the 1964 U.S.N.S. Gear survey profiles. This fault zone is also shown by Moore (1966). The strike of this feature is N22°W and may be interpreted as a tensile feature associated with uplift of the island block. On the other hand, certain criteria strongly suggest that it is a second primary wrench fault that complements the San Clemente Fault. The seismic profiles show a wide trough along this zone that is relatively straight for several kilometers (note Figure 18). The trough appears to contain small crustal blocks associated with faulting.

It is suggested that, under the assumed direction of primary stress the San Clemente fault zone and the complementary zone mentioned above comprise the main primary shear fractures of a shear couple encompassing the island block. This may be the reason for a strong expression of inferred northerly striking tensile faults as well as the spread of azimuth in the complementary first-order shear fracturing, (Figure 20). Kingma's and Lensen's interesting models (1958; 1958a) pertaining to the development of horsts and grabens are particularly adaptable to this study and possibly to the Continental Borderland topographic features. The San Clemente Island block has been uplifted and tilted in a direction (see next section) that may be related to right-lateral movement (along the San Clemente Fault) under conditions postulated by these authors. However, for this shear mechanism to be valid the subparallel primary shear zones must intersect at depth. This can only be assumed at this time.

Offshore Terrace Structure

The major offshore terrace has been postulated as being wave-cut during the Late Pleistocene. Subbottom profile data indicate that this terrace has been affected by Recent tectonism.

Reference is made here to Figures 5 and 8a. For consistency, definition of the seaward edge of the terrace is taken at a point on each profile derived from the intersection of lines projected from the average slope of the terrace and upward from the steepest part of the slope off the seaward end of the terrace. The shoreward edge is defined as the contact of Unit C and Unit D. This definition of the terrace is chosen because (1) a uniform slope of the terrace exists across Units B and C,

(2) this zone probably represents much of the period of low sea-level stand before the sea's transgression to its present level, and (3) this permits a better structural analysis of the terrace. The inner depth of the terrace along the east side of the island is taken at the first point of major shoreward slope change.

Post-terrace faulting is indicated by sea-floor and subbottom reflection line offsets at positions along the terrace on several of the Detailed and Reconnaissance Survey profile records (note Figures 15 and 22). Figure 31 and Table 5 show a marked elevation break at those profiles covering the Eel Ridge Canyon area. This implies decided post-terrace faulting with as much as 30 to 50 meters of apparent throw at the northern wall of the canyon. Faulting and erosion of the terrace in the Eel Point Grid area are also implied by the narrowness of the terrace on several of the grid's lettered profiles, particularly in the vicinity of the canyon. Post-terrace faulting oblique to the terrace is further suggested by the configuration at that part of the depth diagram representing the Lost Point Grid area. An overall slight northwestward tilting of the terrace is suggested. This direction of apparent tilt is maintained from the Lost Point area to the canyon. Of interest is the break in the trend of the tilt at the canyon, since this is the area where a major change in fault-strike trend is apparent (Figure 18).

A net effect of post-terrace faulting is suggested by some of the offsets shown in Figure 32, particularly at the inner depths, since this appears to have been the approximate shoreline immediately preceding the more rapid phase of the Holocene transgression across the volcanic rocks to the present sea level.

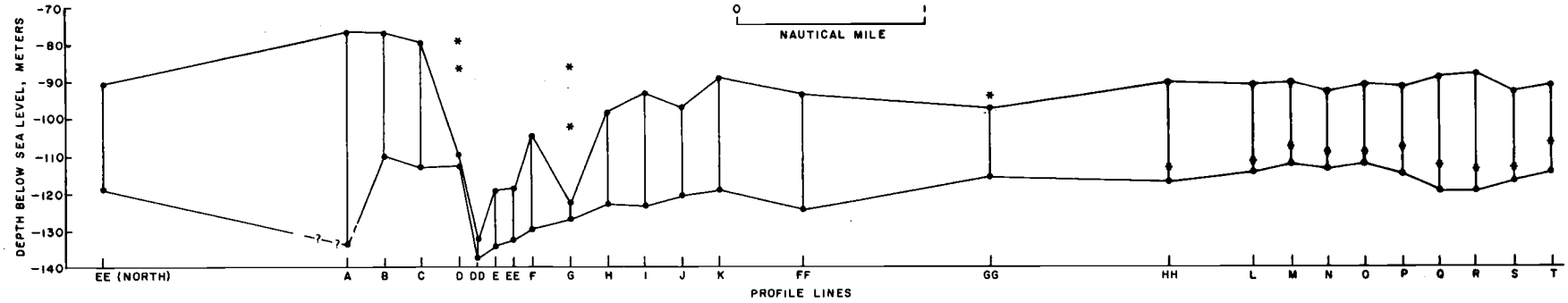

Figure 31. Depth of the major offshore terrace along the Detailed Survey area. Asterisks indicate reconstructed depths from fault offsets showing on the profile terrace outline. The upper line connecting the vertical profile lines represents the depths at the shoreward limit of the terrace as defined. The lower connecting line is the depths at the seaward limit as defined. Asterisks denote depths corrected for faulting (see Table 5).

TABLE 5. DEPTHS OF OFFSHORE TERRACE ALONG DETAILED SURVEY AREA.

Profile line	Present depth, meters		Corrected for faulting, meters	
	Inner depth	Outer depth	Inner depth	Outer depth
EE (no.)	90.8	119.0	....	....
A	76.3	134.1 (?)	....	....
B	78.0	109.8	....	....
C	79.3	112.8	....	....
D	109.8	112.8	79.3 (?)	86.6 (?)
DD	132.8	137.1	....	....
E	119.5	134.1	....	....
EE	118.8	132.5	....	....
F	114.0	129.4	....	....
G	122.3	126.9	86.5	101.9
H	98.1	123.1	....	....
I	93.3	123.8	....	....
J	96.9	120.8	....	....
K	89.0	119.0	....	....
FF	93.3	124.3	....	....
GG	97.6	115.9	94.5	....
HH	90.8	112.8	....	117.0
L	91.6	111.6	....	115.0
M	90.8	107.3	....	112.8
N	93.3	109.0	....	114.0
O	91.6	109.1	....	112.2
P	92.1	107.3	....	114.8
Q	89.6	112.8	....	119.5
R	88.5	114.0	....	120.0
S	93.3	113.4	....	117.0
T	91.6	117.0	....	115.2

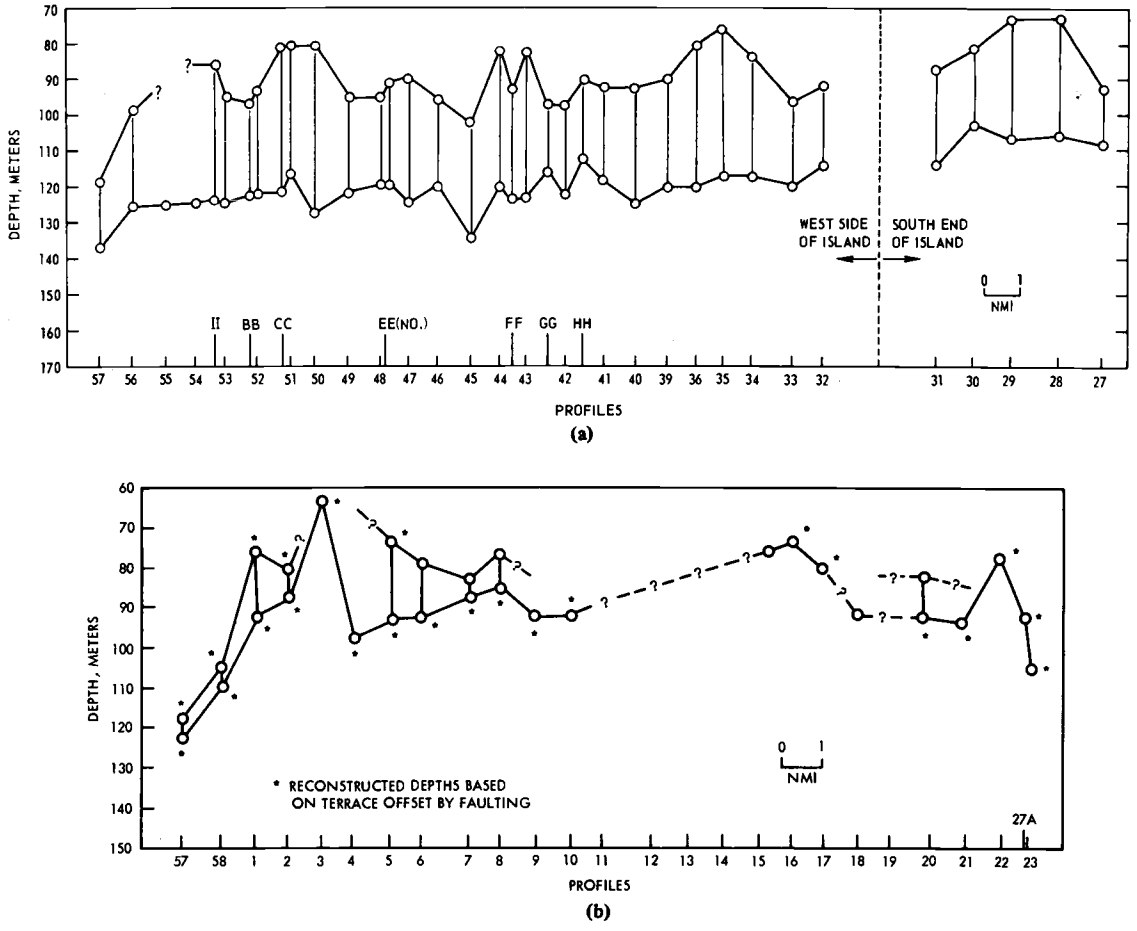

Figure 32. Offshore terrace depth diagrams, Reconnaissance Survey. (a) Profiles along the west side and south end of the island. West side includes partial data from the Detailed Survey. (b) East side of island. Lack of data along the middle of island is due to profile surveys missing the narrow terrace close to the island.

The shallow depth at the outer end of the terrace off Wilson Cove, shown by Reconnaissance Survey Profile 3, corroborates the sense of throw for the major fault (Olmsted, 1958) projecting from the island to form part of this cove. The effect of the northwest-striking fault pattern is indicated by the rapidly increasing depths across Profiles 2, 1, 58, and the east part of 57. The faults have apparently developed a major offset in the terrace of this area (see, for example, Profile 57, Figure 15). The effect of northeast-striking faults is perceptible at the west end of Profile 57. The sharp break in the southerly shoaling of the terrace between Profiles 8 and 11 (Figure 32b) may be related to slump-block activity and a northwest-striking fault (Figure 18). The sudden deepening of the terrace in the area of Profiles 23, 27A, and 27 relates to the cluster of northerly-striking faults off Pyramid Head that have produced downthrown blocks to the southeast.

No mention is made by either Olmsted (1958) or Merifield and Lamar (1967) of offset terraces on the island. The fact that offshore faulting (west side) has apparently offset the terrace suggests that (1) the faulting is more lateral and any offset is disguised by erosion and alluvial fill on the island or (2) the faulting is of the pivotal type with very little apparent throw on the island. Pivotal faulting is indicated in the Eel Ridge Canyon area by data from the Detailed Survey profiles.

A slight northwestward tilting is suggested in Figure 32a. The estimated degree of tilt is roughly 6 meters per 20 kilometers. Slight tilting to the northwest is also suggested in Figure 32b by the alignment of the outer-terrace depths along Profiles 4 through 17. This

part of the terrace is considered to have less offset by faulting than the remaining areas to the north and south.

The outer terrace depths for the west side of the island range from 113 to 137 meters with an average of 121.9 meters. The average for the inner depths is 91.1 meters, with a range of 80 to 118 meters (Table 6). The average terrace slope is very nearly 1 degree. Eighty percent of the outer depths along the west side of the island show depths within 5 meters of the average. This suggests that a reasonable approximation of the original (pre-fault, pre-tilt) outer terrace depth in this area is 122 meters. The outer edge of the terrace on the east side of the island ranges from 70 to 123 meters of depth, of which only three measurements are greater than 94 meters in depth (Table 6). Here, the average of 21 outer depth measurements is 90.3 meters. However, the 19 measurements made with confidence average 91.1 meters. It is concluded that 91 meters is a reasonable approximation of the original outer depth along this part of the terrace.

The difference in depths of the terrace for both sides of the island suggests a slight southwesterly component of tilt of the island block. Although based on insufficient data, a southwesterly tilt is also suggested by the profile terrace data off the southern end of the island. Based on the average of 0°07' for continental shelves (Shepard, 1963a) the near 1-degree average for the west side of the island also suggests that westward tilting has occurred since the inception of the terrace. The southwesterly component of tilt is calculated as 1/4 degree, based on the average horizontal distance across the island (4.8 nautical miles) between outer terrace positions. Calculations based upon the terrace data above

TABLE 6. DEPTHS OF OFFSHORE TERRACE.

Profile no.	Present depth, meters	
	Inner depth	Outer depth
West Side of Island		
57	118.6	137.3
56	99.6	125.8
55	....	124.4
54	....	124.4
II	85.4	123.0
53	95.2	124.4
BB	96.4	122.0
52	93.7	121.4
CC	80.8	121.5
51	80.6	117.0
50	80.6	127.5
49	95.2	121.4
48	95.2	120.0
EE (North)	90.8	119.0
47	89.3	124.4
46	....	120.0
45	102.5	134.6
44	82.0	120.0
FF	93.3	124.3
43	82.0	122.9
GG	97.6	115.9
42	97.9	122.9
HH	90.8	112.8
41	92.4	118.6
40	92.4	124.4
39	90.7	120.0
36	80.6	120.0
35	76.1	117.1
34	83.5	117.1
33	96.7	120.0
32	92.2	114.2
Average	91.1	121.9

TABLE 6. (CONTINUED)

Profile no.	Present depth, meters	
	Inner depth	Outer depth
East Side of Island		
57	118.6[a]	122.9[a]
58	105.3[a]	109.7[a]
1	76.0[a]	92.2[a]
2	80.4[a]	87.7[a]
3	....	62.9[a]
4	....	98.0[a]
5	73.2[a]	93.6[a]
6	79.0	92.2[a]
7	82.4	87.7[a]
8	76.0	85.0[a]
9	....	92.2[a]
10	....	90.7[a]
11	....	....
12	....	....
13	....	....
14	....	....
15	....	76.0[a]
16	....	73.2[a]
17	....	80.4[a]
18	....	90.7[a]
19	....	....
20	81.9	92.2[a]
21	....	93.6[a]
22	....	77.6[a]
27A	....	93.6[a]
23	....	105.3[a]
Average		90.3
South End of Island		
27	93.6	108.3
28	~73.2	105.3
29	~73.2	106.8
30	81.9	102.4
31	87.7	114.1

[a]Reconstructed depths; see Figure 32b.

show that the fulcrum of the northeast-to-southwest tilt is close to the northwesterly axis of the island and that the net tilt is roughly westward.

Gaal (1966) noted from bathymetry that the submarine terraces of some of the Continental Borderland islands have a deeper western margin. Emery (1958) also noted that tilting may be the cause of the difference of depths of the terrace on either side of San Clemente Island. Emery (1958, 1960) postulated a regional west-to-south tilting of the borderland based on submerged terrace measurements. However, the tilting of the San Clemente Island block only partly conforms to these authors' data. Conceivably, crustal block segmentation and a resulting block shift have given different structural histories to various crustal blocks or groups of blocks in the Continental Borderland. Thus, the San Clemente Island block tilting need not conform entirely to tilting of the other islands or to the regional trend.

The average depth for the outer end of the terrace on the east side of the island is the same as the average for the inner depth at the western margin of the island. This suggests that Smith (1898) and Olmsted (1958) could be correct in their interpretation for upward bowing of the island volcanic rocks; it also attests to the writer's conclusion that tilting post-dates the cutting of the major submarine terrace. A suggestion of both post-terrace upbowing and tilting is shown by profile data on the slopes of the offshore terrace along both sides of the island. The average of a few profile slopes for the east side of the island is about 1/2 degree. This slope, the near 1-degree average for

the west side of the island, and the estimated 1/4-degree component of southwesterly tilt of the island block tend to support both conclusions.

A gradual tilt of the island block of 5 degrees over geologic time (minimum by Olmsted) would make the uppermost island terrace slope slightly greater than 5 degrees. On the other hand, if upbowing is considered, the return to a more gentle slope is possible. There are no known precise measurements made for the true slopes of the island terraces. Doubtless, the variable alluvial and colluvial fill and post-terrace faulting would tend to complicate the efforts for precise meaurements. The writer has made a Brunton compass measurement on the first two major terraces above sea level on the west side of the island. The slope angle is nearly 2 degrees, almost an order of magnitude greater than the slope of the submarine terrace. This suggests considerable tilting or upbowing between the development of these island terraces and the offshore terrace. It is concluded that post-Pleistocene tilting and possibly upbowing of the island block have taken place.

The tilt since late Wisconsin time is used, statistically, to estimate the time period for the entire tilt of the island block based on a general 5- to 10-degree southwesterly dip of the island volcanic rocks (Olmsted, 1958). To do this, it is necessary to assume that the island volcanic rocks were initially horizontal and that there has been a constant rate of tilt. On the basis of 18,000 years since the low stand of sea level (Curray, 1965; Emiliani and Flint, 1963) and the general southwesterly dip of the volcanic rocks, a total time of 360,000 years minimum and 720,000 years maximum is required for the entire westward tilt of the island block.

It has been suggested by some authors that the Pliocene-Pleistocene boundary be redefined on the basis of events recognizable in deep-sea sediments, especially extinctions of pelagic organisms (Emiliani and Milliman, 1966). Some extinctions at 600,000 to 800,000 years B. P. (Emiliani, 1955; Emiliani et al., 1961) appear to coincide with the last reversal of the earth's magnetic field dated at about 700,000 years (Hays and Opdyke, 1967; Opdyke et al., 1966). Other times of very pronounced faunal changes have been estimated by sedimentation rates based on radiometric dating and related to climatic changes (Ericson et al., 1963, 1964) as well as magnetic reversals (Berggren et al., 1967). These data place the Pliocene-Pleistocene boundary at approximately 1 1/2 to 2 million years. Assuming 1 1/2 to 2 million years for the age of the Pleistocene Epoch, it is concluded that the entire westerly tilt of the island block has taken place within the latter part of the Pleistocene.

With the acceptance of the conclusions above on the time of the tilt of the island block, and relating this to a vertical (physiographic) offset of the San Clemente Escarpment of roughly 1,500 meters, it is concluded that the average rate of throw is about 1/3 meter per 1,000 years. The time relationship of the tilt and vertical offset to Pleistocene time is considered reasonable and compatible, since the series of terraces on the island is believed to have been cut during the Pleistocene (Emery, 1958, 1960; Olmsted, 1958; Mitchell and Lipps, 1965).

The narrowness of the terrace along the east side of the island may be due to either (1) less erosion of the more resistant volcanic rocks compared to the softer Miocene sedimentary rocks, or (2) to the terrace being a remnant resulting from faulting. The writer concurs mainly with

(2) above since, according to Emery (1960) and Moore (1967), the San Clemente Fault break at this level of the island probably had taken place before the end of Wisconsin time. However, some loss of the terrace has probably resulted also from slide or slump-block activity.

It is concluded that, on the basis of the evidence presented here, much of the present geomorphic and structural nature of the San Clemente Island block probably developed during Pleistocene time. However, the relationship of the net tilt of the island block to that of the primary compressional force proposed in this paper is not fully understood. Conceivably, the tilt is associated with both upward bowing in response to lateral compression and a shear couple encompassing the island block.

Origin of Eel Ridge Canyon

Substantial data in this study indicate that Eel Ridge Canyon may be classified as a fault-controlled canyon or tectonic valley (Shepard, 1965). Major faulting is apparent along the axis of the canyon, and there is no significant land valley aligned with the canyon. A graben has formed as a consequence of opposing fault throw across the canyon fault zone. The canyon has a V-shaped transverse profile (Figure 33), is related to faulting on land, and has relatively straight walls. It also has a fairly well developed tributary pattern with no apparent basin depressions along its axis; this is contrary to Shepard's (1965) definition for fault-controlled canyons. Shepard's definition may refer mainly to oblique faulting relative to the axis of a canyon. A combination of parallel and oblique faulting appears to be responsible for both the axis of the canyon and some of its tributaries.

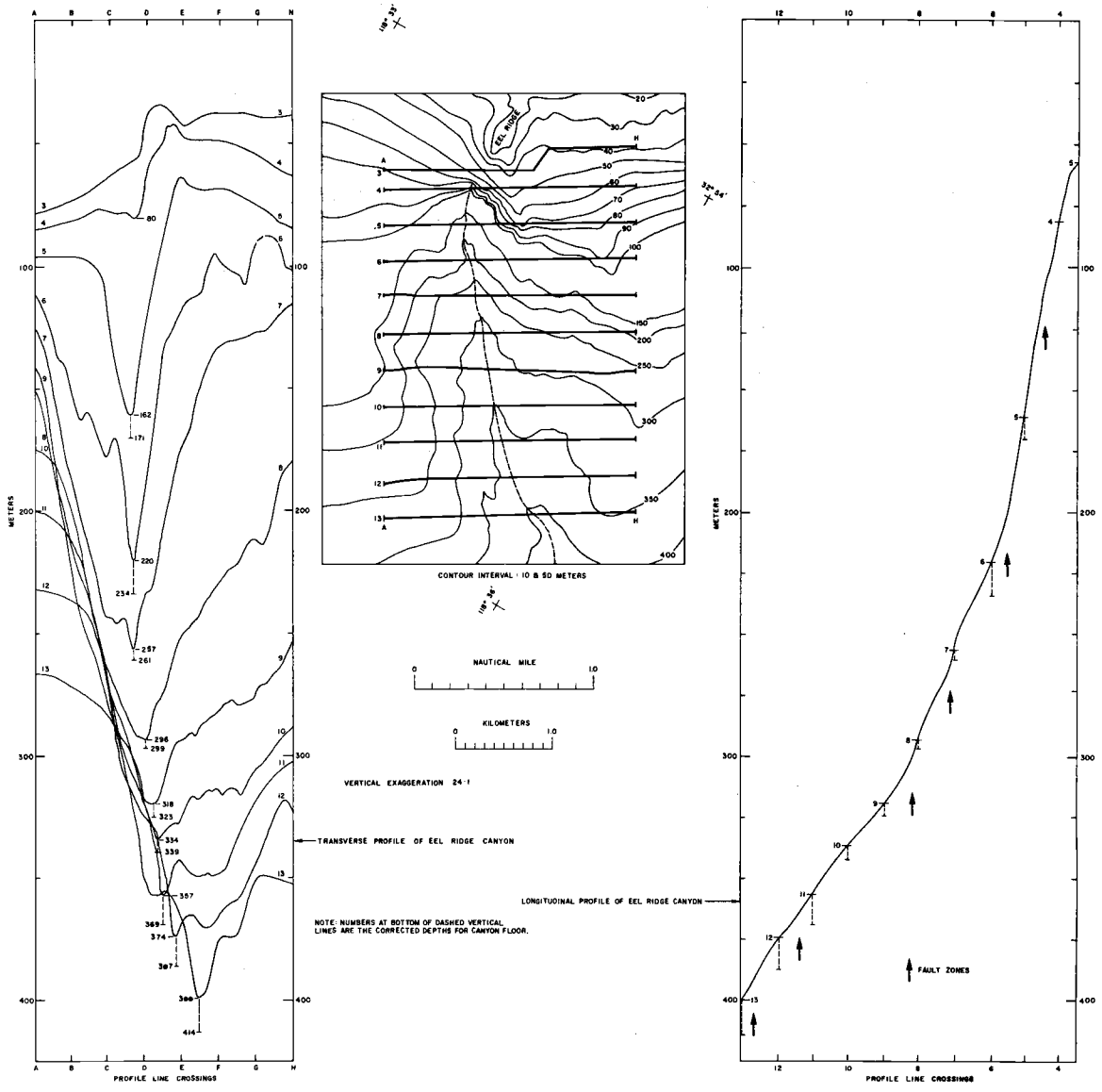

Figure 33. Longitudinal and transverse profiles of Eel Ridge Canyon.

The effect of oblique faulting is manifested as breaks in the slope of the canyon floor on the longitudinal profile. Three major changes in slope are as follows: (1) about 12 degrees from Profiles 4 to 6, (2) 5 degrees from Profiles 6 to 9, and (3) 3 degrees from Profiles 9 to 13. The northward-striking faults are considered responsible for these slope changes.

The faults parallel to the canyon axis have apparently cut a set of northwest-striking faults that form a fault trough filled with Unit C sediments on the north side of the canyon. This trough is recognizable in Figure 12.

The degree of apparent throw on one of the faults paralleling the northern wall of the canyon is illustrated in Figure 34. The uppermost strong reflector of the lower subdivision of Unit C (Figure 35) is used as the reference for these measurements. A definite seaward pivoting is observed. A series of refraction points shown in Figure 35 may represent the plane of this fault with an apparent dip of 20 degrees, a rare recording with present-day echo-ranging techniques. The combination of this pivotal faulting, oblique faults, and erosion may be noted on the canyon transverse profile by the change in elevation of the tops of the north and south canyon walls. The south wall is higher shoreward of Profile 7 and becomes progressively much lower than the north wall seaward of this profile. Coexistent with this change is a general broadening of the canyon and a more gentle sloping of the southern wall. The northern wall generally maintains the same slope (about 10 degrees) from Profiles 7 to 13, but is slightly steeper shoreward of Profile 7. The slope of the canyon walls ranges from about 8 to 15 degrees, with an

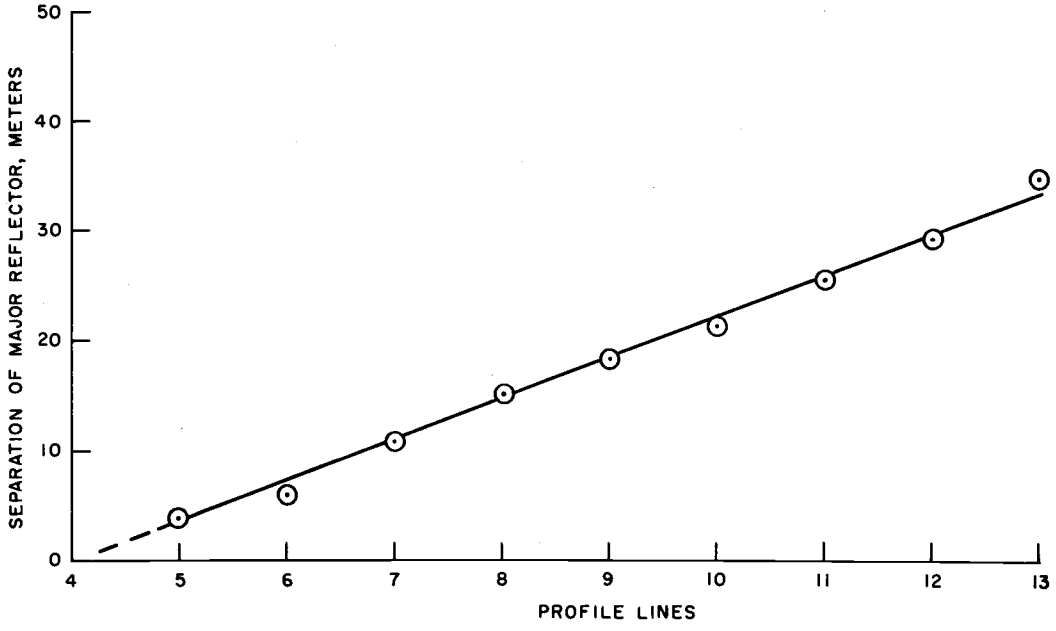

Figure 34. Apparent offset of major reflector of a fault paralleling the northern wall of Eel Ridge Canyon.

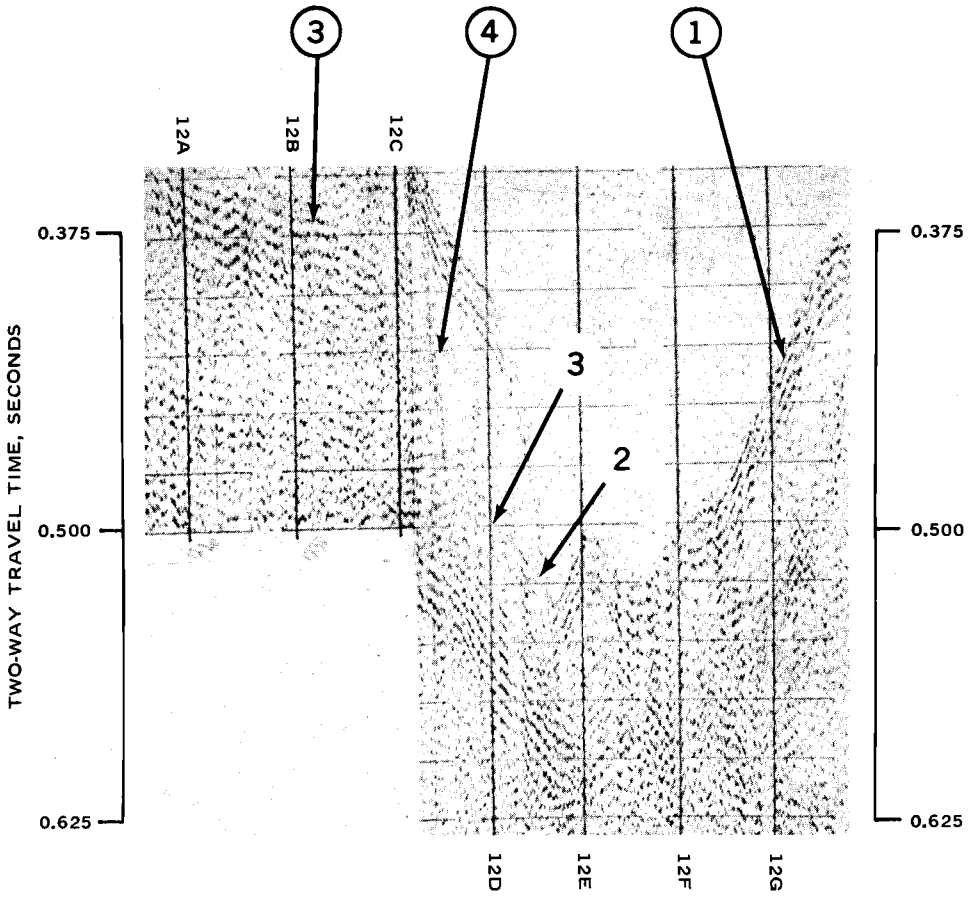

Figure 35. Portion of Profile 12 of Eel Point Grid showing offset of major reflector by faulting. (1) Sea floor, (2) axis of canyon, (3) major reflector, and (4) possible refraction pattern of fault plane.

average of 11 degrees. The average gradient is 6 degrees. The width of the canyon averages approximately 1 nautical mile from rim to rim and ranges from about 1/2 to 1 1/2 nautical miles in width. The maximum relief, taken from the north wall, is about 200 meters (Profile 9). The canyon heads at a point slightly seaward of Eel Ridge, approximately 0.9 nautical mile from shore and about 90 meters in water depth. It terminates in a sea fan disclosed by the seaward ends of the reconnaissance profiles.

Removal of Unit A from the head of the canyon places the canyon head at about 100 meters of depth, which is close to the upper limit of the wave-cut terrace. Emery (1960) reasons that if a submarine canyon was cut before that of an associated shelf, the shelf would have been cut along re-entrants into the canyon as well as the seaward side. A canyon cut later would have its shelf break progressively shallower as shore is approached. Eel Ridge Canyon does not show the re-entrant feature in the bathymetry of the Detailed Survey area, but a semblance of re-entrance is indicated at the head of the canyon by the removal of Unit A in this area (note Figure 14). Conceivably, the canyon was already present and its head aerially exposed or very close to sea level during Late Pleistocene time. The depression marked by the major pocket of Unit A sediments next to Eel Ridge may represent part of the terrace along the re-entrant at the head of the canyon. Apparently post-terrace faulting or differential erosion have disguised a clear-cut definition of the relative age of the canyon to that of the terrace.

It is not known to what extent the origin of Eel Ridge Canyon is due mainly to tectonism or to erosion dissecting the area along old faults.

From the thinning of Unit C across the axis of the canyon, it is assumed that erosion has been important in modifying the canyon to its present form. The presence of the sea fan, mostly seaward of the area studied, provides evidence that considerable sediment has been channeled down the canyon from the concentration of sediment obstructed by Eel Ridge at the head of the canyon. Erosion of canyons probably occurs as a result of sediment drift along the shore that builds up rapidly to form unstable masses subject to slump, sand flows, and turbidity currents (Emery, 1952). Conditions for such erosion of Eel Ridge Canyon exist where a net littoral drift has piled up the accumulation of Unit A shown in Figure 14 However, recent active transport of sediment was not apparent by television viewing of the walls and bottom of the canyon from the CURV instrument in the general area between Profiles 5 and 8. Scouring of the canyon walls was not observed. In fact, no outcrops of Unit C were observed. Very coarse sand and debris were observed near the head of the canyon. There is not a noticeable change in the general sediment trend across the canyon as delineated by snapper sampling of the very coarse to coarse, fine to very fine sands. Thus, sedimentary evidence suggests that a period of quiescence exists at the present time relative to very active transport of sediment down this canyon.

The evidence presented suggests that the original geomorphic configuration of Eel Ridge Canyon was caused by faulting during the early stages of the island block's development and that the canyon has been maintained by both recurrent faulting and erosion by sediment transport down the canyon.

Origin of "Rift" Valley

The San Clemente Fault bifurcates at the southern end of the island. This is the northern end of what is termed the San Clemente "Rift" Valley by Shepard and Emery (1941). For unknown reasons, perhaps due to dislocation and nonelastic behavior, the strike of the San Clemente Fault has taken a smooth and gradual curvature from the south end of the "Rift" Valley to the north end of the island. As a consequence, it is logical to assume that due to tensional stress a "cross-strike separation" or "pull-apart feature" has developed to form the "Rift" Valley (Figure 36).

From bathymetry the "Rift" Valley is not apparent to the northwest along the Santa Catalina Basin. However, the fault zone adjacent to the San Clemente Escarpment is still broad and contains minor horsts and grabens. The lack of a rift valley to the northwest may be explained by a modification of the fault zone by the more northwesterly striking faults (Figure 18), greater sedimentation in this area, and the tendency for the fault to become linear. Bathymetry along this portion of the escarpment indicates a series of left-lateral offsets (see Shepard and Emery, 1941, Chart 1) that could be related to second-order left-lateral wrench faulting. These faults, along with the main fault and others associated with the development of the Southern Santa Catalina Basin, have possibly modified a rift zone valley.

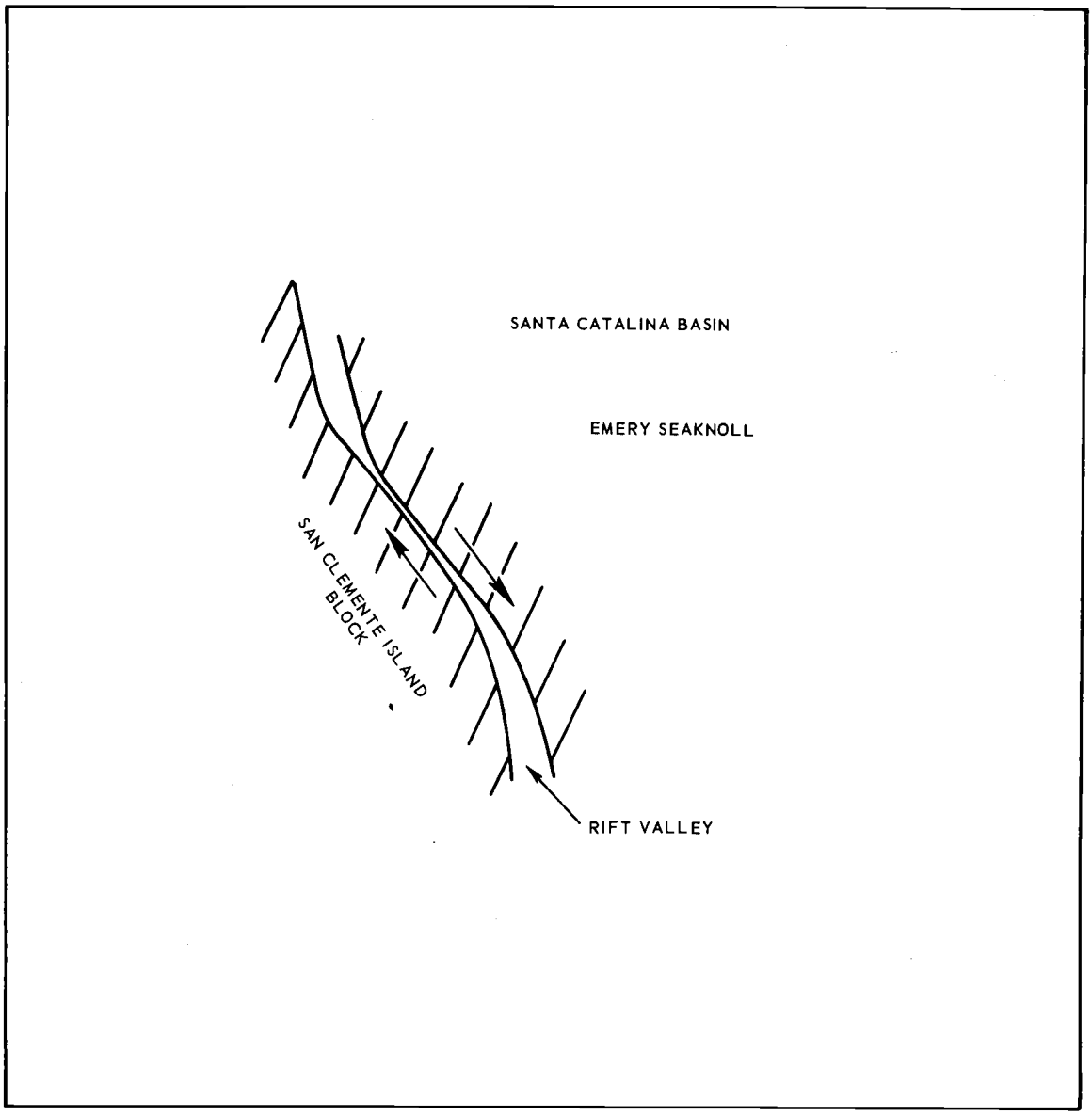

Figure 36. Sketch of proposed mechanism for "Rift" Valley separation along the San Clemente fault zone. Arrows denote direction of movement.

GEOPHYSICAL CONSIDERATIONS

Magnetism

The first published detailed magnetic studies in the northern Continental Borderland were made by Harrison and von Huene (1965), von Huene and Ridlon (1965), and Harrison et al. (1966), and in the southern Continental Borderland by Krause (1965).

The aeromagnetic survey in this study (Figure 37) is considered the most detailed of any made of an insular feature in the borderland region. Removal of the earth's regional gradient from the total magnetic intensity of the region (Appendix V) leaves a high of 1,100 gammas and a low close to 25 gammas for two principal features of the area (Figure 38). These anomalies are present in the residual anomaly map (Figure 39) but have a slight shift in position. The low closely conforms to the large triangular pre-orogenic structural depression filled with 550 meters of post-orogenic sediments. The high corresponds to the large volcanic high defined by seismic Profile 52 (Figure 40b and Figure 23). The major high becomes elongated east-west with a maximum 100-gamma "bulge" centered over the volcanic high, and the low is shifted to the south of the major pre-orogenic surface depression.

The principal high off West Cove was recognized by Emery (1960), Harrison and von Huene (1965), and Harrison et al. (1966). If the large mass of volcanic rocks in the San Clemente Island block is responsible for the magnetic anomaly, the maximum positive anomaly should occur off the southwest corner of the block (Harrison et al., 1966). The maximum of the residual-map high is positioned at the bathymetric exposure of

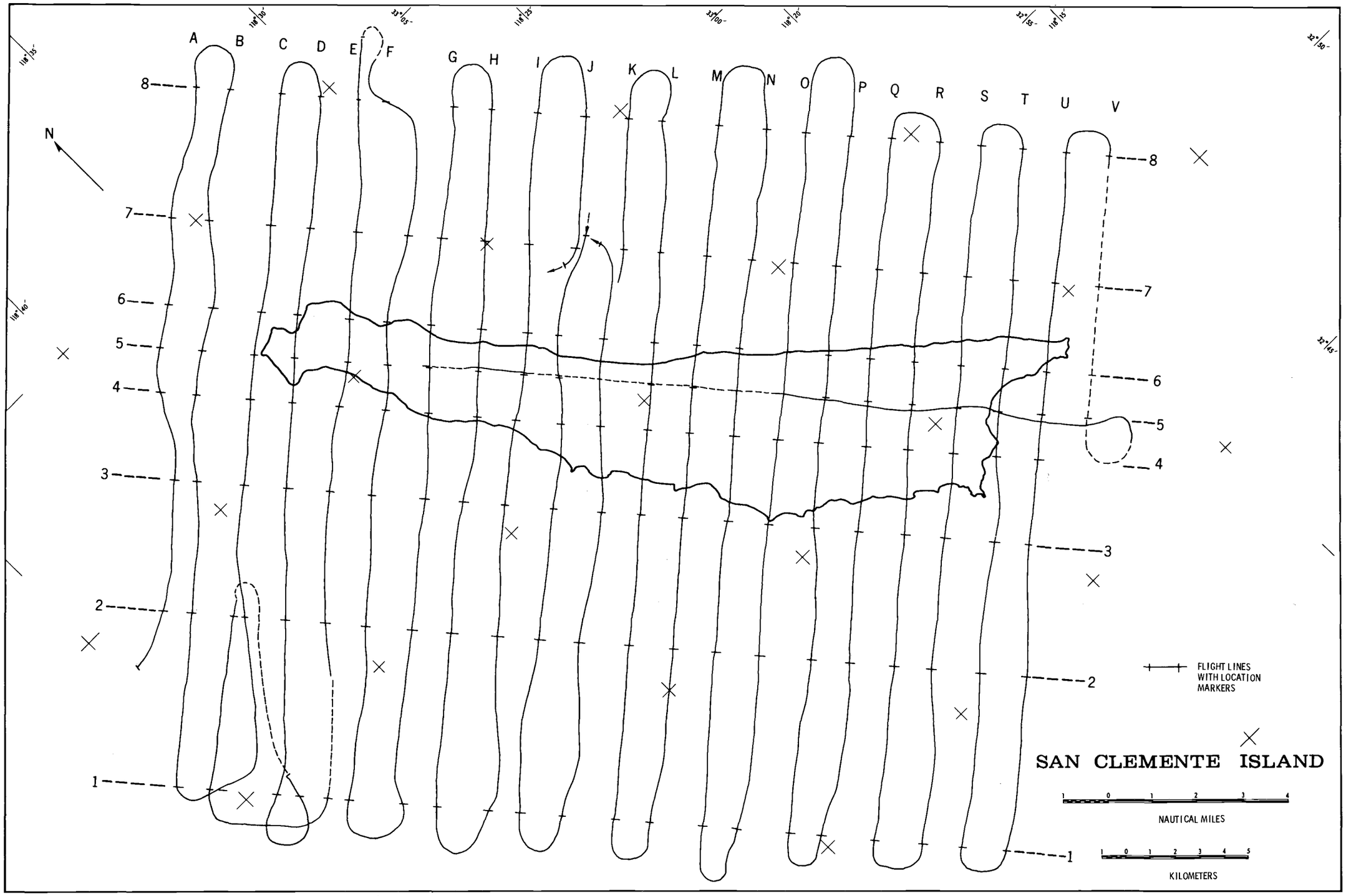

Figure 37. Flight lines of aeromagnetic survey. Radar control from island indicated by solid lines; lack of radar control and estimated flight position by dashed line.

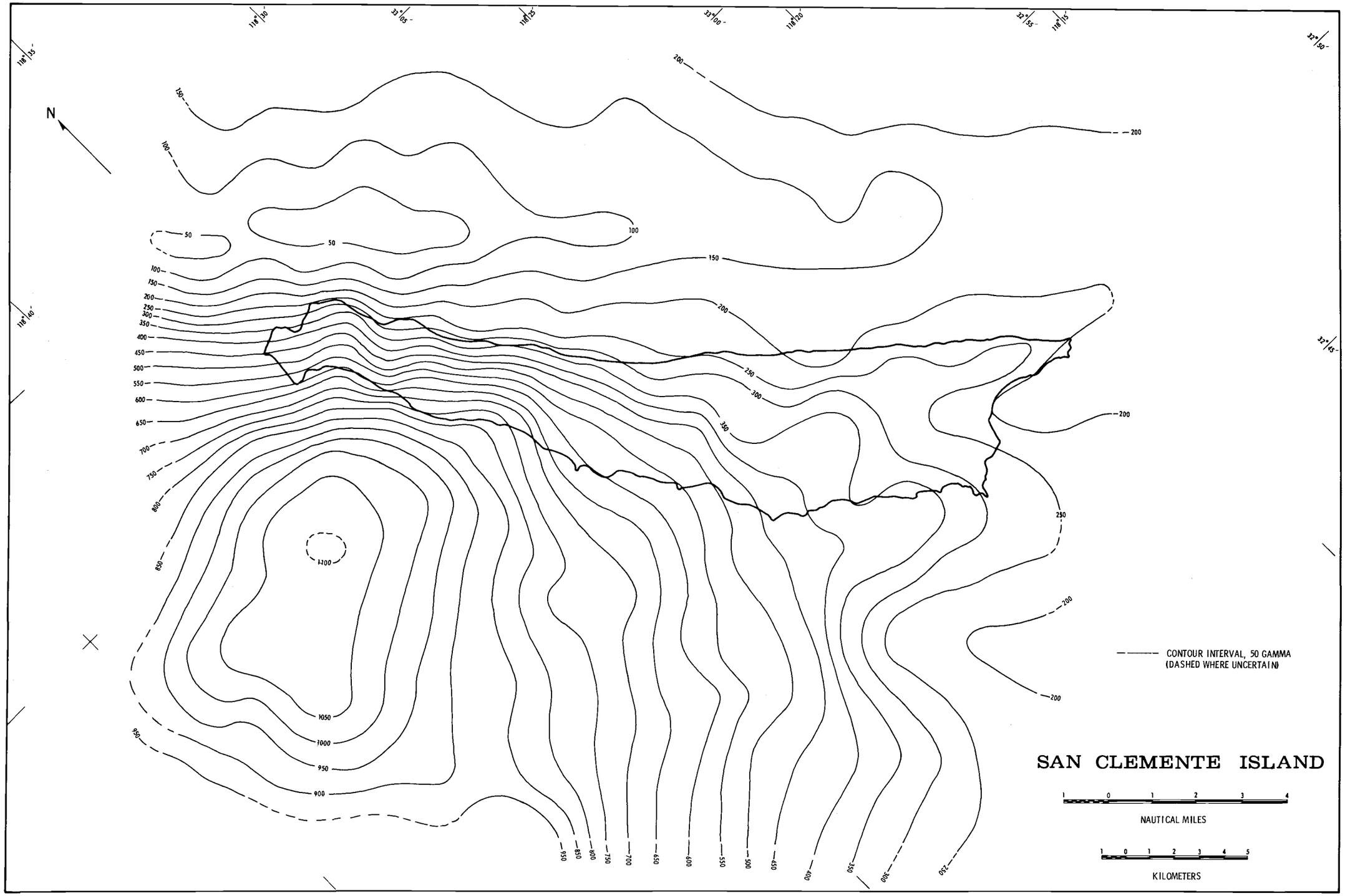

Figure 38. Magnetic anomaly map of the San Clemente Island block region. Compiled by graphic subtraction of the earth's smoothed regional magnetic field from the measured field.

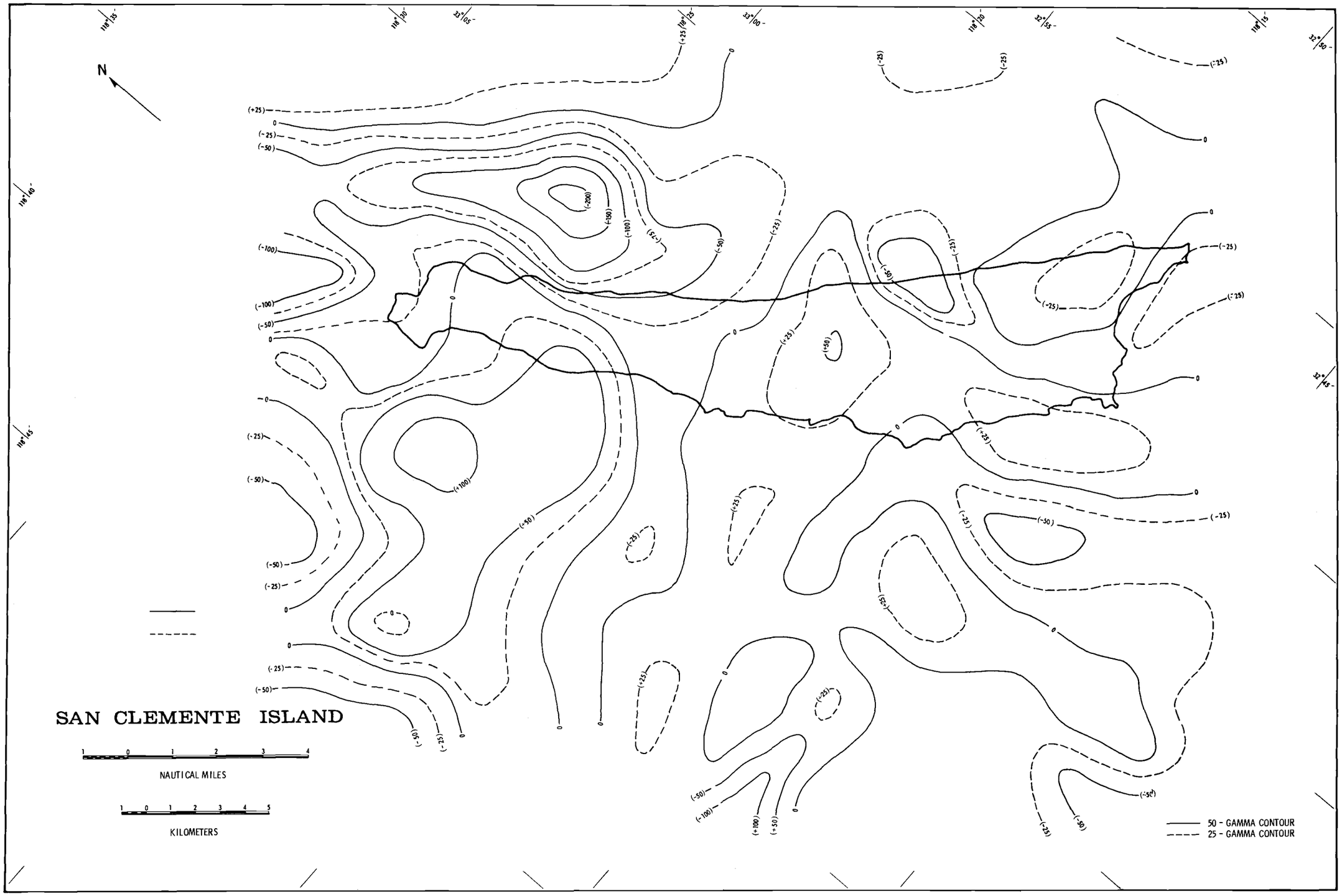

Figure 39. Residual magnetic anomaly map of the San Clemente Island block region. Compiled by use of the empirical grid-residual system (Nettleton, 1954).

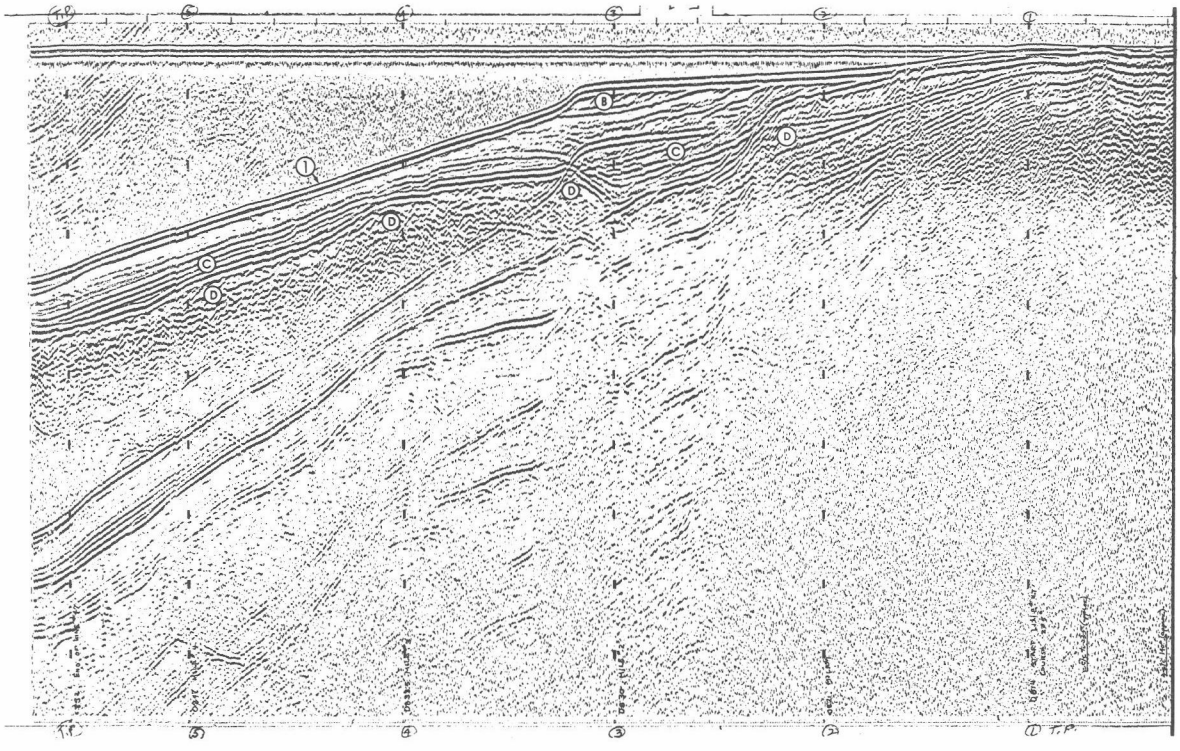

(a)

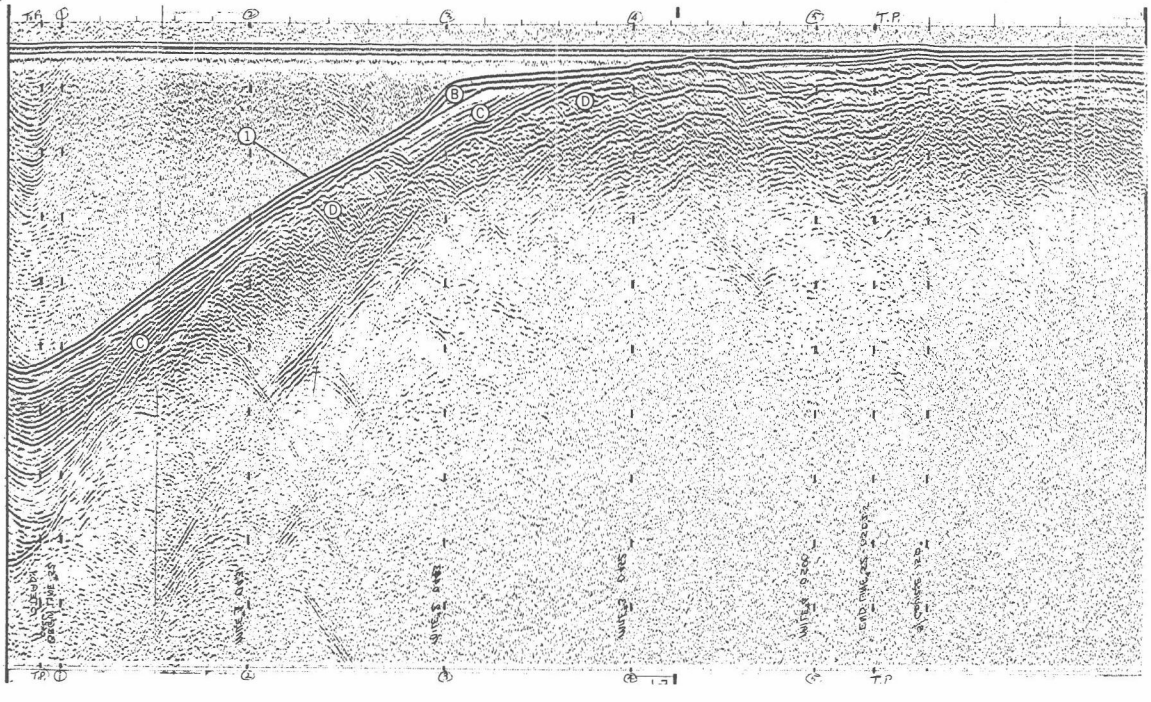

(b)

the volcanic high off West Cove and has a relatively steep magnetic gradient along the north slope. The east-west "wings" of the residual high may, however, correspond to a deeper source. Harrison et al. (1966) presumed a deeper source, although the near-surface rocks undoubtedly contribute something toward an anomaly. These authors postulated a depth of 6 kilometers to the top of such a positive anomaly, but admit that an infinite number of shallower magnetic bodies could be developed to fit equally well. According to Emery (1960), the magnetic intensity of this high is greater than that over outcrops of granodiorite and must therefore represent a basement more magnetic than granodiorite.

The flexures in the contours to the southeast of the major positive anomaly (Figure 38) correspond to the general northeast-trending fault pattern along this part of the west side of the island. A noticeable flexure at the Eel Point Canyon area is presumably related to the canyon faulting and the marked change in the fault pattern across this area. A change in the regional anomaly pattern along the west side of the island is also evident across the canyon area in Figure 39.

The compression of northeast-trending contours southeast of Lost Point closely corresponds to the northwest-trending volcanic rock high noted in the bathymetry and seismic profiles for this area. Figure 39 has a positive anomaly closely allied to this high. The negative anomaly immediately to the southeast aligns with a northwest structural trend (Figures 9 and 18) southwest of China Point. The negative anomaly is closely identified with the northwest-striking faults and structural lineations interpreted for this area.

The origin of the small positive residual anomalies (Figure 39) at the central and southern parts of the island is not known. Possibly deeper (thicker) masses within the volcanic rock sequence or zones of higher magnetic susceptibility are responsible. The positive anomaly at the center of the island corresponds to a compression of the contours shown in Figure 38, which in turn coincides with the dacite flow on the island. Since the magnetic properties of the island volcanic rocks have not been measured, it is not known whether this anomaly is related to the dacite flows.

The pronounced, elongate negative anomaly along the eastern margin of the island tends to conform to the post-orogenic surface and sediment fill trends (Figures 16 and 24). Major flexures in the contours are present where the complex zone of faulting exists between the Emery Seaknoll and the island. The general tendency for a more positive magnetic trend southeastward is likely related to a gradual surfacing of the magnetic source and the presence of the Emery Seaknoll and Southern Plateau volcanic rock highs. A slight negative anomaly (Figure 39) marks the elongate sediment basin between these volcanic rock highs.

The writer suggests that the steep magnetic gradient off the San Clemente Escarpment is the combined effects of (1) the margin of the mass of volcanic flows, (2) the postulated deep basic mass related to the large positive anomaly off West Cove, and (3) major faulting that has cut both the mass of volcanic rocks and a possible deeper basement rock of more basic composition.

Gravity

There were very few published data on gravity measurements for the southern California region until 1957 (Emery, 1960). Since that time, and particularly very recently (see, for example, Harrison and von Huene, 1965; von Huene and Ridlon, 1965; and Harrison et al., 1966), considerable surface-ship gravity work has been done for much of the northern Continental Borderland. Harrison and von Huene (1965) and Harrison et al. (1966) have based many of their gravity interpretations for the Continental Borderland on the seismic refraction data of Shor and Raitt (1958). The San Clemente Island block is interpreted as an igneous feature, specifically a thick mass of volcanic rocks with sharp boundaries possibly caused by faulting (Harrison and von Huene, 1965).

San Clemente Island is the only topographic high in the region that is not associated with a major Bouguer anomaly. This lack of anomaly is attributed to a vesicular texture or low density of andesitic rocks postulated for the upper part of the island block.

Seismicity

The Pacific Coast region of North America, a part of the circum-Pacific orogenic belt, is considered one of the major seismic areas of the world. Richter (1958) has sectioned this region into several seismic provinces. San Clemente Island lies within the offshore seismic province located south of the Channel Islands.

Most earthquake epicenters of the southern California region are concentrated in the land areas. The greatest concentration of seismic

activity in the northern Continental Borderland has been in the San Pedro Basin area (Figure 41) next to a similar concentration on land. The frequency of shock occurrence increases moderately from the center of San Clemente Island outward to roughly 60 kilometers, and then markedly from 60 to 90 kilometers. The marked increase is mostly due to an increase in activity in the San Pedro Basin area. The shoreward concentration tends to give a misleading aspect to the analysis of epicenter occurrence closer to San Clemente Island. The greatest concentration of epicenters within 40 kimoleters of the island occurs near and off the southeastern part of the island. The relatively high activity in this area is noted in the strain-release map of the southern California region of Allen et al. (1965). The two shocks of greater than 5.0 magnitude (Richter scale) in the entire compiled data occurred close to the island, one at Pyramid Head and the second at a point 37 kilometers southwest of China Point.

A period of relatively low but cyclical occurrence in seismic activity for the northern Continental Borderland is noted between the latter part of the 1930 decade and the present time (Figure 42a). The curves of Figure 42b and 42c show more clearly the tendency for a cyclical occurrence closer to San Clemente Island, which suggests a periodic (10- to 20-year cycle?) adjustment along major faults within the area. The 40-kilometer range was selected to cover only the major faults believed to be closely related to the structure of the San Clemente Island block region.

Attempts to correlate earthquake epicenters with known and inferred geologic structures in the southern California region have been made by

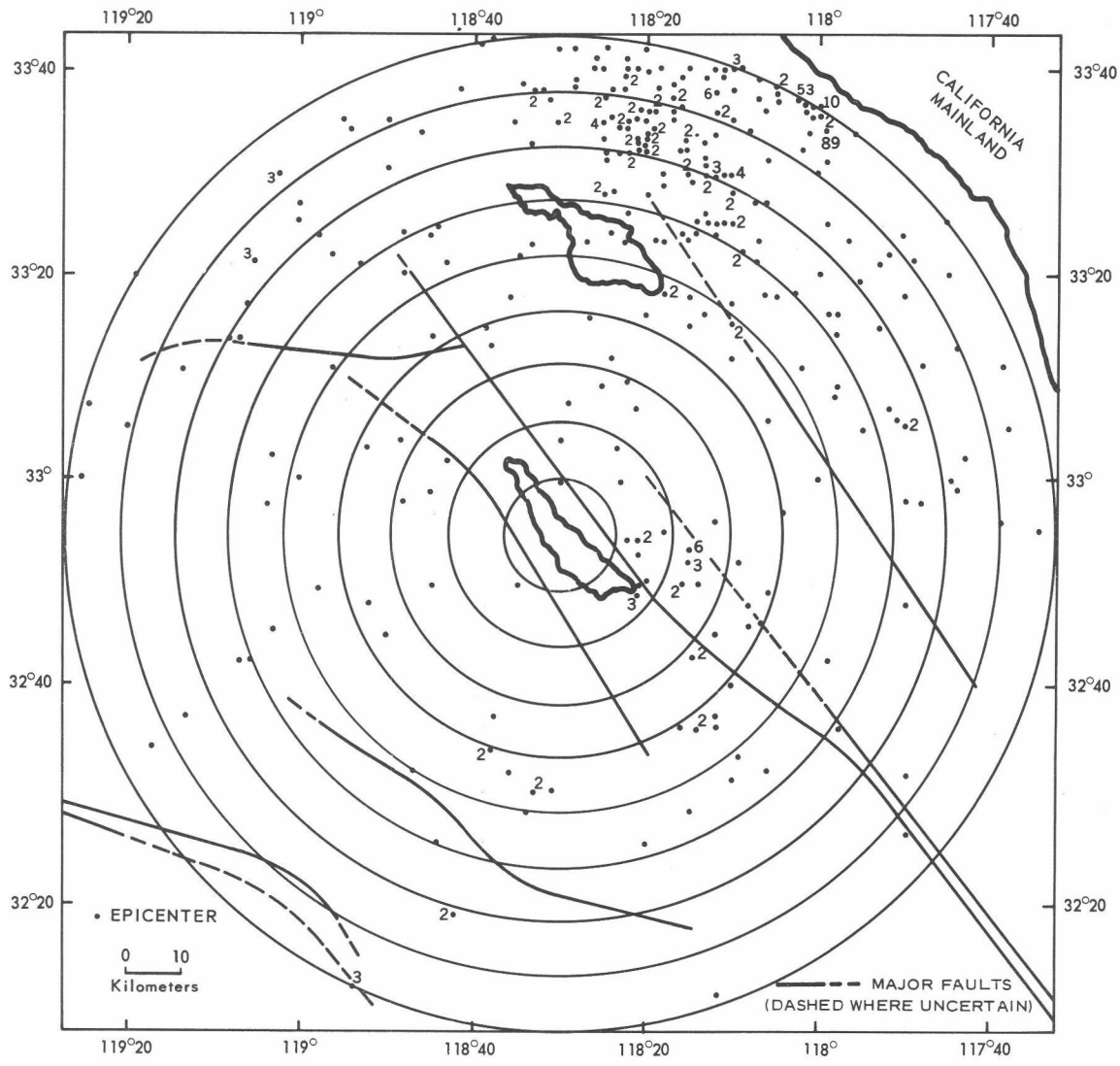

Figure 41. Epicenter map of earthquake shocks within 90-kilometer radius of San Clemente Island. Number of shocks greater than one noted by number next to location. Circles are increments of 10-kilometer "zero" position on island taken at 32°55'N, 118°30'W. Major faulting from Moore (1966).

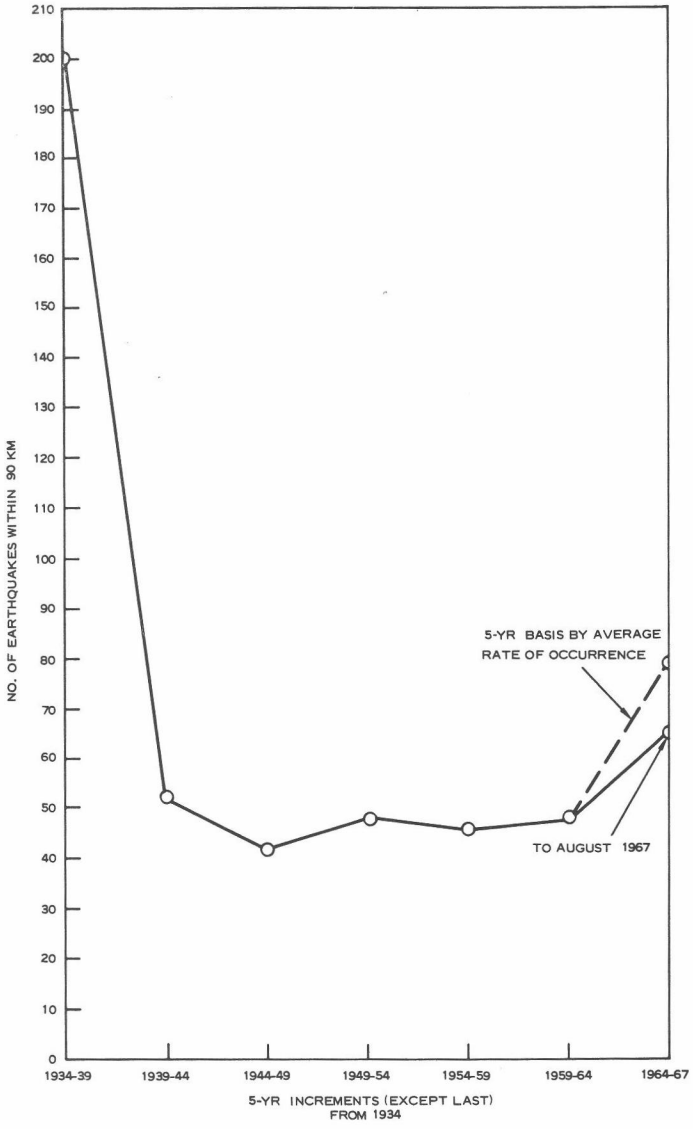
NO. OF EARTHQUAKES WITHIN 90 KM
210
200
190
180
170
160
150
140
130
120
110
100
90
80
70
60
50
40
30
20
10
0
1934-39
1939-44
1944-49
1949-54
1954-59
1959-64
1964-67
5-YR INCREMENTS (EXCEPT LAST) FROM 1934
5-YR BASIS BY AVERAGE RATE OF OCCURRENCE
TO AUGUST 1967

(a)

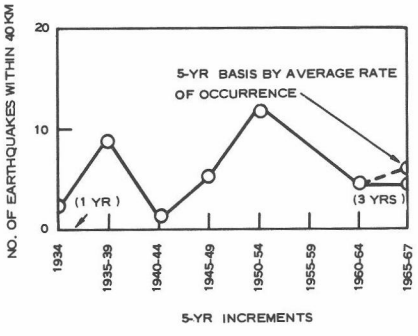
NO. OF EARTHQUAKES WITHIN 40 KM
20
10
0
1934
1935-39
1940-44
1945-49
1950-54
1955-59
1960-64
1965-67
5-YR INCREMENTS
5-YR BASIS BY AVERAGE RATE OF OCCURRENCE
(1 YR)
(3 YRS)

(b)

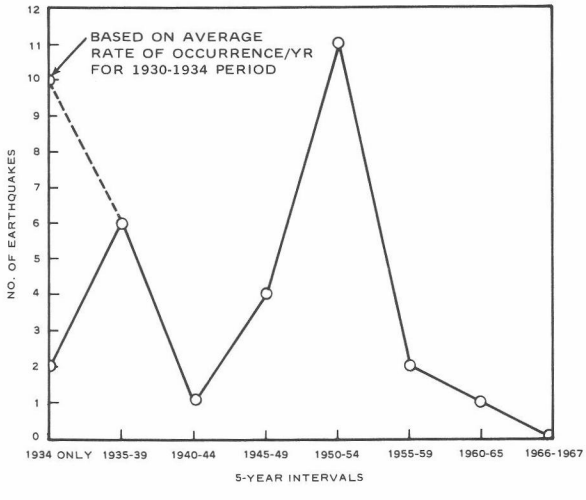
NO. OF EARTHQUAKES
12
11
10
9
8
7
6
5
4
3
2
1
0
1934 ONLY
1935-39
1940-44
1945-49
1950-54
1955-59
1960-65
1966-1967
5-YEAR INTERVALS
BASED ON AVERAGE RATE OF OCCURRENCE/YR FOR 1930-1934 PERIOD

(c)

many authors (for example, Wood, 1947; Clements and Emery, 1947; Emery, 1960; and Allen et al., 1965). Earthquakes associated with the San Clemente Fault, the Agua Blanca Fault, and the San Andreas-Gulf of California rift zone are frequent and large. The large deformations of the region at the present time are probably occurring along these zones (Krause, 1965).

Evidence of very recent fault activity is noted on several of the seismic profiles along the eastern side of the island. Certain offsets and change of dip of the post-orogenic sediments at the sea floor (Figure 43) are readily aligned with inferred faulting. Some of these features may have resulted from sedimentation processes (for example, channeling, onlap, deposition, and compaction), but fault alignment, the apparent lack of levees, and the equivalent elevation of some aligned offsets across the profiles tend to favor the recent fault activity interpretation. Some offsets are near or at the base of the escarpment. These offsets are next to small wedges (aprons?) of sediment possibly representing surges of sediment flow off the escarpment caused by fault activity. Periodic fault rejuvenation is also suggested on the profiles (Figure 7b) by a downward convexity in the reflectors at depths below the sea floor in the San Clemente fault zone. However, differential compaction could also account for at least part of this downwarping. The close relationship between the inferred recent fault activity and the epicenter locations in the area of study is illustrated in Figure 44. The greatest concentration of these features is obviously along the San Clemente fault zone (note Figure 19d). The only epicenter in the study area west of the island is close to the major complementary fault outlining the western

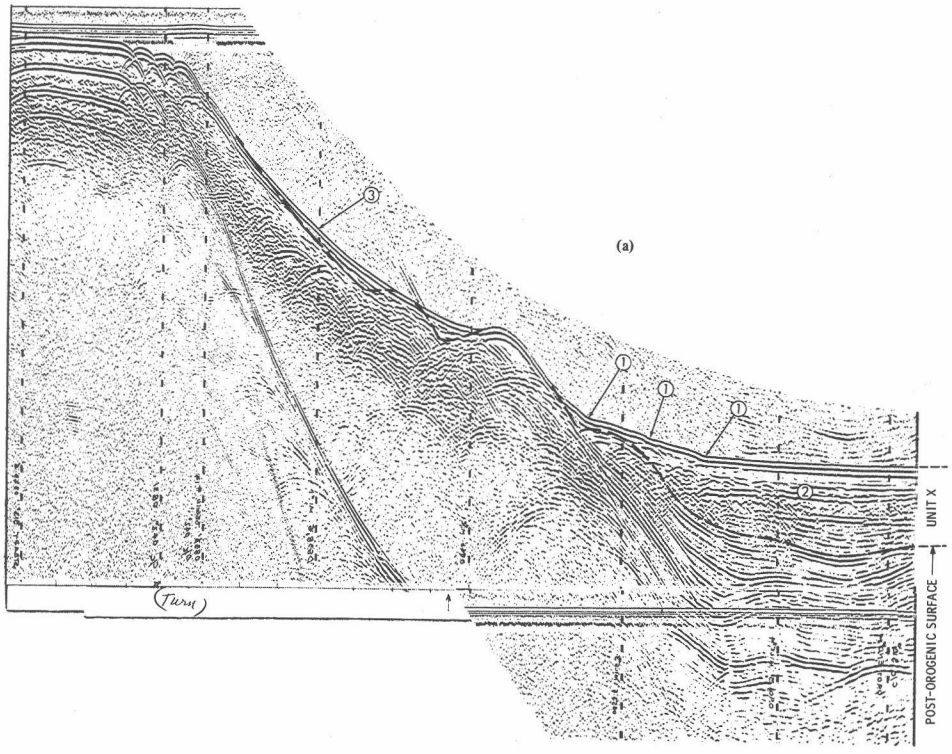
(a)
UNIT X
POST-OROGENIC SURFACE

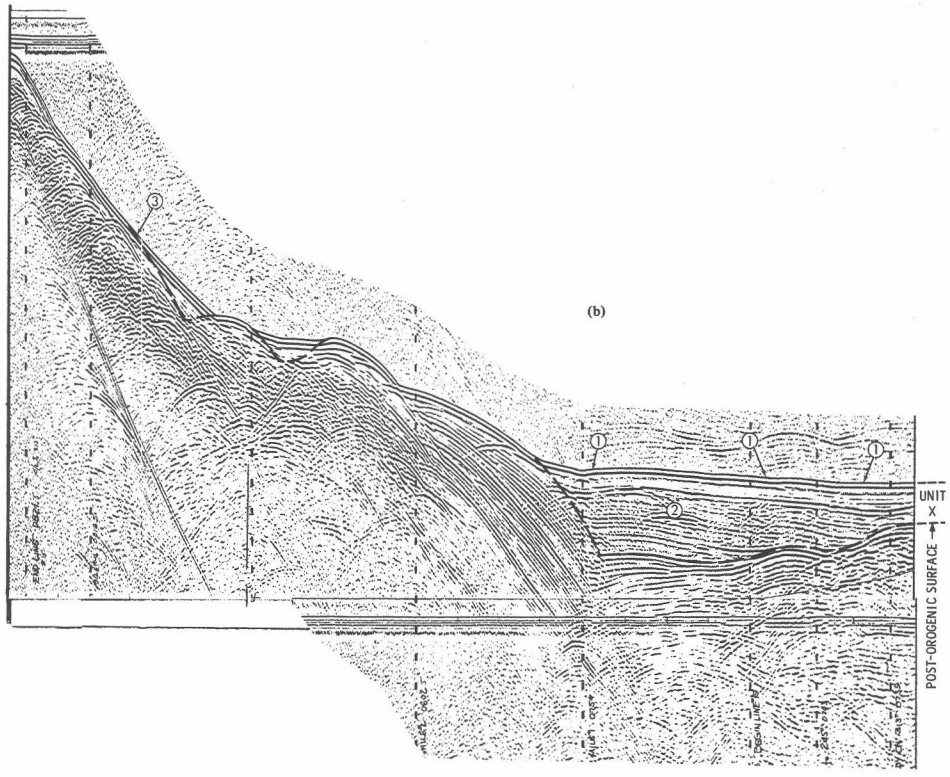
(b)
UNIT X
POST-OROGENIC SURFACE

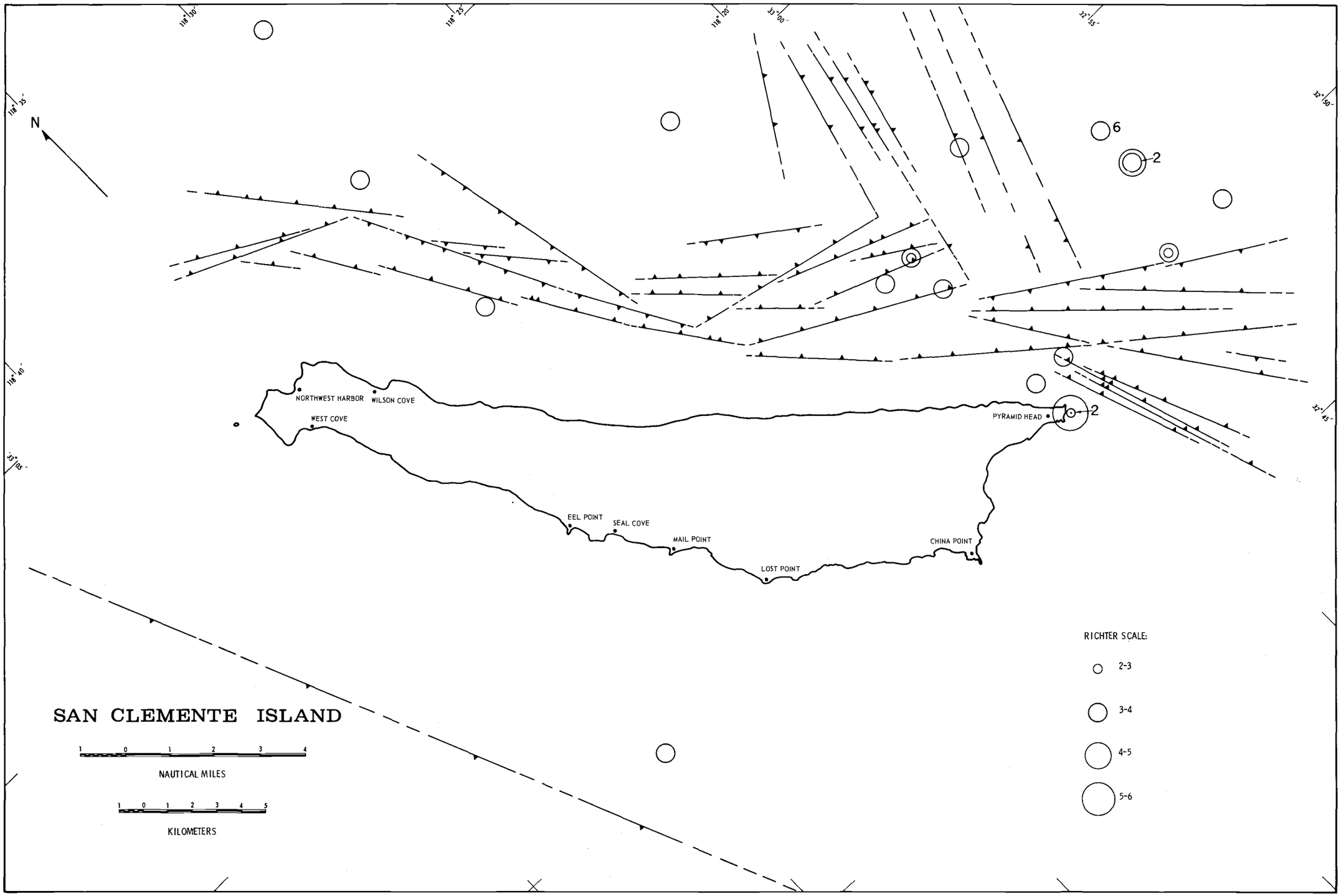

Figure 44. Recent fault activity and epicenter locations in the San Clemente Island block region. Number of shock occurrences greater than one is shown by number next to the location.

margin of the island block. Recent fault activity is not apparent in the basin sediments northwest of the Emery Seaknoll. The evidence above suggests that the area from the "Rift" Valley to the Emery Seaknoll has recently and periodically (Figure 42c) adjusted to local stress inequalities related to movement along the San Clemente Fault.

REGIONAL TECTONIC FRAMEWORK

Regional Tectonic Theories

In order to bring the structure of the San Clemente Island block into focus, it is necessary for a brief review of the forces postulated for the structural origin of the Continental Borderland.

Several authors have presented theories.

St.-Amand (1958, 1961) contended that (1) the Pacific Coast of North America is fringed with a series of right-lateral faults subparallel to the coastline, (2) this faulting forms a consistent pattern, and (3) this pattern is consistent with the observations of seismologists that many earthquakes are produced by lateral movement on faults. St.-Amand concludes that, by a consistent pattern of dextral movement, the Pacific basin is rotating counterclockwise. Benioff (1958) also postulates counterclockwise rotation of the Pacific basin relative to the continents.

Field study results and theoretical explanations for the broad structural nature of New Zealand geology and transcurrent faulting have been the subject of several papers (see Cotton, 1956, 1957; Kingma, 1958, 1959; Lensen, 1958a, 1958b, 1958c, 1959, 1960; and Suggate, 1960). Hatherton (1968) has shown by a comparative study of New Zealand and California that the geometry and absolute size of the structural provinces of these

areas appear to be very similar, and suggests that simple, regular physical forces are at work at the edges of continents.

Benioff (1962) proposed, by earthquake model, that the behavior of earthquake shocks is related to strike-slip faulting. According to Gutenberg (1941), study of the nature of the first impulse of earthquake waves on seismograms indicates a right-lateral displacement along the faults in the southern California region.

Menard's (1960) hypothesis on the East Pacific Rise related major lateral faulting to Rise activity resulting in northerly, elongate areas of fault blocks along the margin of the Pacific basin and North America. One of these fault-block areas is the Continental Borderland.

Hamilton (1961) proposed a mechanism involving a tensional component of strike-slip movement along California as the cause for the structural trend of the Continental Borderland. Krause (1965) reasoned that interaction between a counterclockwise rotating Pacific Ocean basin and the continent caused a zone of maximum tension to develop trending southwesterly in the southern Continental Borderland area with a general east-west dilation between the oceanic basin and the continent. Rusnak and Fisher (1964) propose a tilted crustal block of Tertiary sediments and volcanic rocks sliding northwestward due to uplift by batholithic intrusion. This structural model is basically proposed for the evolution of the Gulf of California but is also related to adjustment along parallel lateral faults of the North American Pacific Coast area. Krause and Rusnak and Fisher associate the tentional effects with Menard's hypothesis and correlate volcanic eruptions of Miocene time with resulting fissures. Moore (1966) supported the theory of shear between the Pacific

basin and the continent as the driving force responsible for the primary fault pattern and consequently the direct origin for much of the present Continental Borderland area. Moore cited left-lateral movement along an east-west structural grain coupled with right-lateral movement along the major northwesterly trend as the basic fault mechanism for origin of the Borderland structure. This is similar to Hill's hypothesis (1954) for the southern California region wherein north-south shortening is associated with east-west spreading along a system of primary faults. Here, two major sets of faults are represented, one trending northwest, the other east-northeast. The most prominent trend is northwest and includes the conspicuous and well-known San Andreas Fault. The east-west grain is best represented north of the Borderland by the Garlock Fault, and that to the south by the Agua Blanca Fault in Baja California (Allen et al., 1960). Rusnak and Fisher (1964) showed a similar northwesterly trend for the Gulf of California region.

Sykes (1968) and Isacks et al. (1968) cited a pattern of en echelon ridges present in the Gulf of California region; these authors related the earthquake mechanisms of this region to a series of northwesterly-striking transform faults with a right-lateral displacement to account for the displacement of Baja California relative to the mainland of Mexico. These authors also note that seismic activity is shallow under the condition of strike-slip movement, but that occasionally rather large shallow earthquakes are observed and some zones combine thrusting and strike-slip motion. Their slip vectors, derived from earthquake mechanism studies, show a northwest component of direction for the Continental Borderland region (see Isacks et al., 1968, Figure 3, p. 5861).

Hill and Dibblee (1953) showed the importance of lateral faulting for the southern California region in a treatise on major faulting.

Deep structures of the Continental Borderland are primarily based on the seismic work of Shor and Raitt (1958), and the compilation of geomagnetic and gravity data by Emery (1960), Krause (1965), Harrison and von Huene (1965), von Huene and Ridlon (1965), and Harrison et al. (1966).

The classic treatise of Shepard and Emery (1941) and later that of Emery (1954, 1960) related the offshore structural trends of the Continental Borderland to that of the onshore region of southern California. Subsequently, the work of Krause (1965) in the southern Continental Borderland region, and that of Moore (1966) for the entire Borderland area, have tended to support some of the main structural conclusions and theories presented by the earlier works.

Moore (1966) provided the most comprehensive study to date of the structural and lithologic trends of the entire Continental Borderland and the relationship of the structural trends to the northern Peninsular Range and Channel Islands Transverse Range structures. Moore postulated a five-part structural division of the Continental Borderland based on the major tectonic grains and areas where faulting or folding predominates. San Clemente Island borders on the west side of the inner (eastern) fault zone and lies within a zone described by Moore (p. 47) as "an oval shaped central belt of probable en echelon oriented major folds." Moore's work utilized previous investigations coupled with continuous seismic profiling as the basis for structural interpretations; integration of internal structure and topography was used to differentiate fault scarps from flanks of folded sedimentary structures.

Thus, a major tectonic role has lately been attributed to lateral faulting as the mechanism to explain much of the crustal movement for the Continental Borderland as well as other regions of the world (see also, for example, Alberding, 1957; Burton, 1965; Bagnall, 1964; Freund, 1965; Sugimura and Matsuda, 1965).

The main objective of this section of the present study is to relate the structure of the San Clemente Island crustal block to that of the Continental Borderland and to propose a hypothesis for the structural origin of the northern Continental Borderland. This may also serve as a general test for the usefulness of the lateral-fault hypothesis for the Continental Borderland region. Furthermore, an acceptance of the proposed structural working hypothesis involves broad geological implications concerning not only the structural origin of the northern Continental Borderland but possibly geotectonics concerning the effect of sea-floor spreading in this region.

Study Area Versus the Continental Borderland

The structural hypothesis presented in this paper may be used to explain the origin of certain geomorphic and structural features within the Borderland region. Some of the bathymetric trends of the northern Continental Borderland considered as fault scarps are broken by offsets such that the offset to the north of the break is found east or northeast (Shepard and Emery, 1941). A particular example of such an offset is located west of Forty-Mile Bank (adjacent to the "Rift" Valley of the San Clemente Fault), southeast of San Clemente Island. Under the stress model used in this paper, second-order right-lateral wrench faulting

could readily account for this offset. Others may be noted, particularly those northwesterly-trending offsets along the continental margin of the Borderland that may be considered first- and second-order right-lateral faults.

Moody and Hill (1956) treat only the pattern of pure[7] (uniaxial compressional) shear. The alternate of simple[7] shear or shear by a couple should be considered. First, the strong trend of inferred tensional faulting lends credence to a structural model involving some rotational type of stress-strain mechanism, such as a shear couple, but with variable normal forces to develop a broad zone of brecciation as well as the compressional features based on the model of Moody and Hill. Second, the lack of strong primary folding suggests the lack of large normal forces, at least during the formation of the island block. Thus, a simple shear (or shear couple) mechanism is suggested as a supplement or alternate, perhaps at least since Miocene time.

In relation to the development of basins in the borderland, a mechanism is suggested that is based on that proposed by Kingma (1958) for parts of New Zealand. Tension with consequent collapse along a series of parallel tension faults may occur near the expiring end of a transcurrent fault (Figure 45a). Subsequent sedimentation then fills in the depressions caused by the broken "undermass." The San Clemente Fault appears to die out at the northern end of the Santa Catalina Basin (see Emery, 1960; Moore, 1966). The deeper part of this basin borders the east side

---

[7]As postulated by Maxwell and Wise (1958).

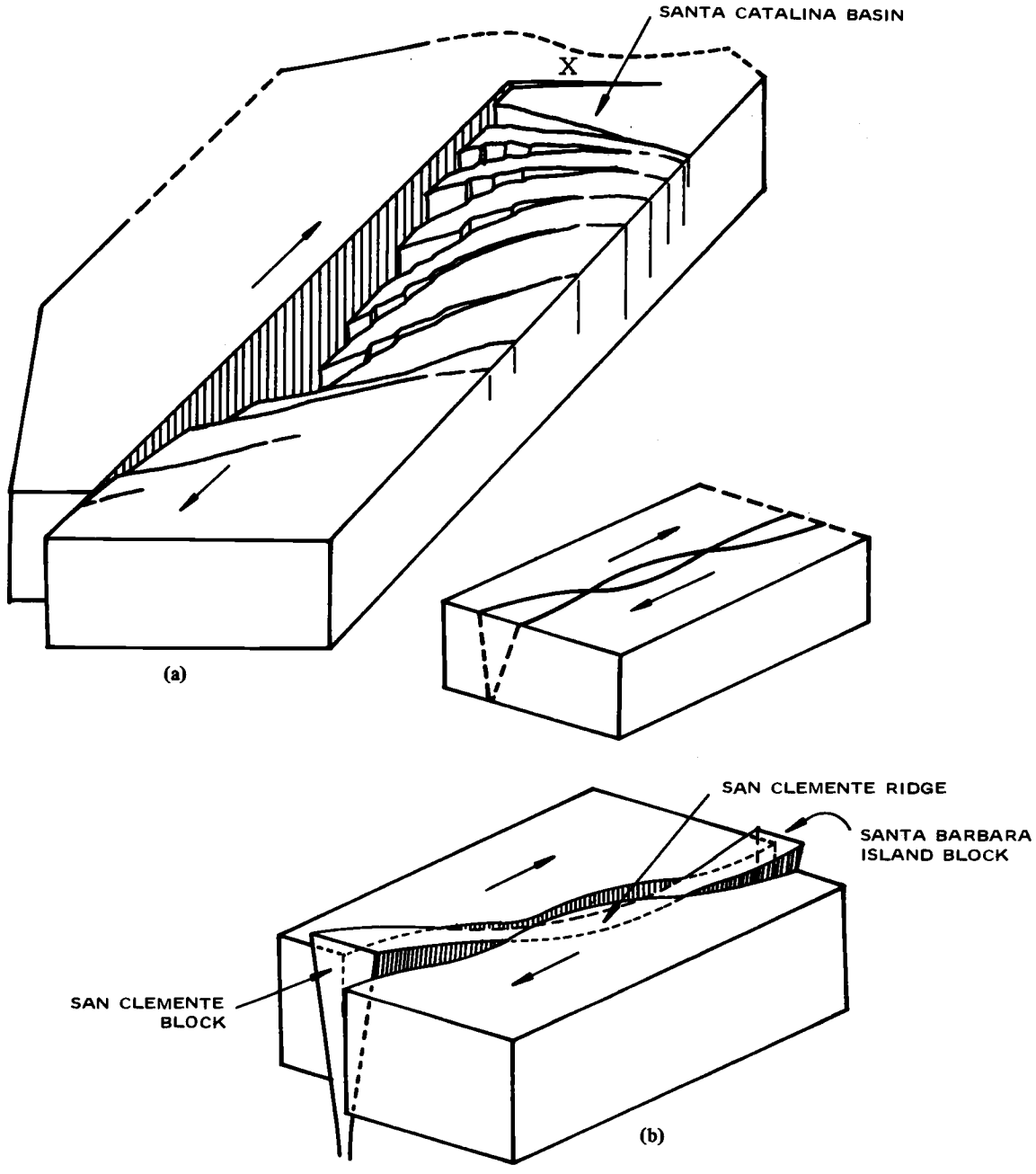

Figure 45. (a) Right-lateral wrench fault dying out at X; right side under tension with consequent collapse to form basin area. (b) Top: right-lateral wrench-fault zone before movement but after development of change in direction and that resulted from initial linear fracture. Bottom: view after movement to develop horsts and graben (modified from Kingma (1958)).

of the fault zone in this area and may have resulted from such a mechanism. Freund (1965) has postulated tension with normal faulting at an acute angle to the wrench fault. Chinnery's diagram (1966) suggests normal faulting essentially normal to the transcurrent fault. Inferred tension faulting in the present study is at a much smaller acute angle than proposed by Freund, unless some of the inferred complementary shear faults nearer the average strike of the tensile faults are rotated tensile fracturing (Lensen, 1958a) under a shear-couple condition.

Northeast-striking faults, inferred by Moore (1966), and other faults that can be inferred from bathymetry such as those along the steep escarpments at the northwestern borders of the San Nicolas and San Clemente Basins and the San Clemente block, suggest a rotation of secondary tensile faults between transcurrent faults (Lensen, 1958a). This assumption is based on the fact that many of the fractures other than those of the primary and complementary first-order shears have arisen as a consequence of the primary shear movement rather than from the stress that produced the first-order shear faults.

It is proposed on the basis of bathymetry, faulting inferred by other authors, the position of the faulting, and the structural model of this paper that major basins within the Borderland are tension depressions resulting from lateral displacements over a period of time. It is further proposed that the upthrow of the San Clemente Island block, as well as other islands and ridges of the Borderland, resulted from this lateral faulting under a shear couple.

Using the principle of uniaxial compression, most of the folding in the Borderland, as shown by Moore (1966), may readily be interpreted as

second-order drag folds along the major northwest-striking (primary wrench) faults.

At certain times and in certain areas, the compressional effects normal to the shear direction were probably small or negligible in order to develop the shear release and allow the development of the minor horsts and grabens so apparent in the San Clemente fault zone. At other times and areas, an increase of normal force allowed a development of the compressional features. Since the San Clemente fault zone appears to dominate the structural nature of the study area at the present time (Figures 18 and 44), it would seem that the more recent activity resulted from simple shear.

Kingma (1958) cited an example of horizontal rotation of the primary-stress direction related to transcurrent faulting during the New Zealand orogeny throughout Tertiary-Quaternary time. Figure 20 suggests the possibility of such a rotation by an examination of the averages of the postulated complementary first-order wrench and tensile faults. However, the primary first-order wrench-fault pattern does not indicate such a rotation. It appears, then, that there has not been a pronounced change in the principal stress direction for the area studied, and probably for the Borderland region, since the inception of the present fault system.

A theoretical explanation for the time-special sequence of the occurrence of curved-strike traces related to transcurrent faulting is given by Chinnery (1966). According to Chinnery, secondary faulting must be associated with the end of the master shear fault. He proposed six basic major modes of secondary faulting and applied these to

predicting or explaining the curvature, location, and strike of the secondary faults in a given area. An important assumption made by Chinnery is that the theoretical results assume that the ground behaves as an elastic solid and that these results are only applicable on a short time scale (i.e., to a single movement on a fault). Also, the development of the master fault may be traced by locating the ends of the shear zone at various times in the past. Chinnery further states that individual movements or sets of movements may not occupy the total length of the fault. In cases of uniaxial compression and simple shear (Figure 46a) a master fault that once ended at a certain point will tend to be extended along a curve (Figure 46b). The San Clemente Fault does, in fact, follow a pattern similar to that in Figure 46b. This curvature is shown by Moore (1966) and Figure 41, whereby the fault tends to curve broadly along the "Rift" Valley and again to the southeast where the San Clemente and Agua Blanca Faults merge. If this reconstruction is valid, the San Clemente-Agua Blanca fault system has had recurrent movement resulting in extensions of the fault zone. Successive main ends of the fault system at certain periods of time would be in the areas of the "Rift" Valley, at Forty-Mile Bank, next to the Pacific Ocean side of Baja California, and in the vicinity of Santa Barbara Island if one considers by bathymetry that the San Clemente Fault continues to Santa Cruz Island of the Channel Islands. This analysis can also be applied to major fault-trace curvatures of other major northwest-striking faults in the Borderland and the adjacent southern California land area.

With respect to repetitive fault movement, Kingma (1958) suggested that the spasmodic and uneven transcurrent movement along fault zones is

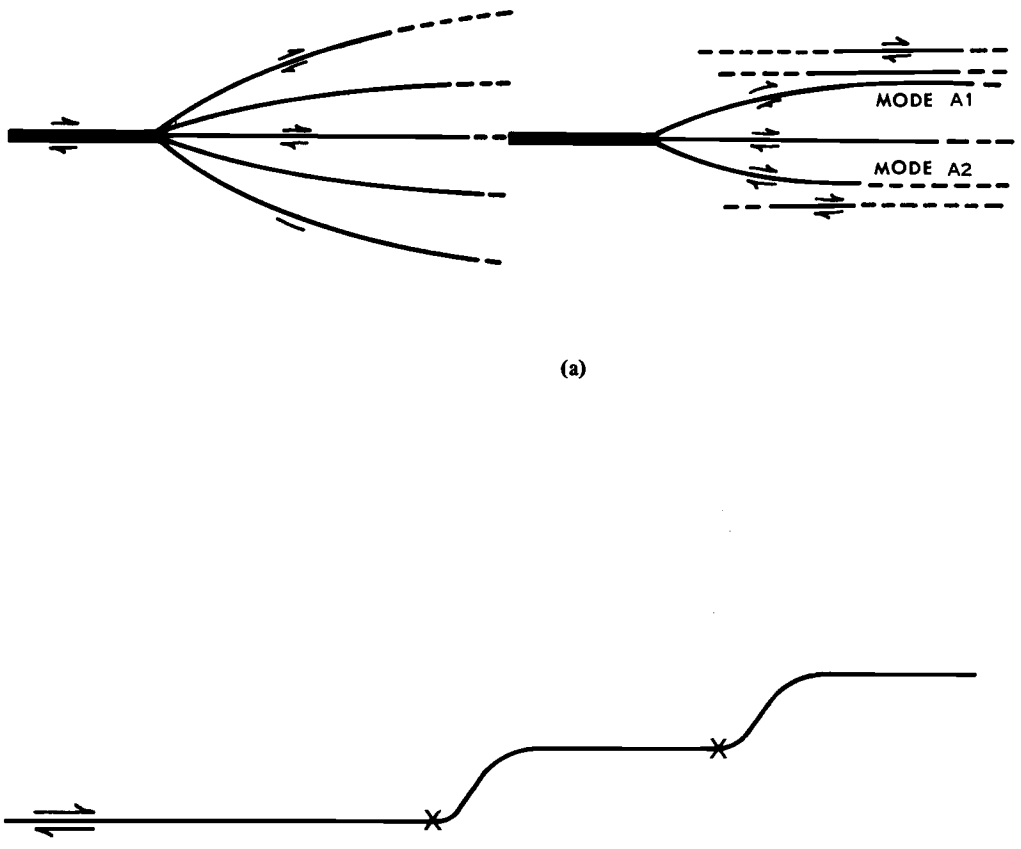

Figure 46. Transcurrent fault movement (from Chinnery (1965)). (a) The left-hand pattern relates to the formation of the master and secondary faults, respectively, under condition of simple shear; the right-hand pattern to that from uniaxial compression (pure shear). (b) Maximum shear-stress curves for the case of uniaxial compression where A1 mode is more likely than the A2 mode. Similar curvature of the fault trace is postulated for simple shear. Thus, a fault that once ended at a point marked by a cross will extend itself as shown.

responsible for the development of elongate, upthrown crustal blocks and secondary basins, as proposed above (Figure 45b).

The present author rejects east-west (tensional) spreading as the major factor for the development of the basins and ridges in the Borderland region. Admittedly, considerable east-west, left-lateral displacement for the Santo Tomas Fault (Krause, 1965) separating the north and south parts (considered small crustal plates) of the Borderland is evidence for such a conclusion. However, the present writer contends that north-south compression, resulting mainly in primary shear, is the principal factor responsible for the present topographic features and that tensional release is a secondary or complementary response that developed the basins along the major northwesterly striking lateral-shear faults. The strike-slip motion along these shear faults has developed the ridge system (block relief) by topographic offset and buckling, squeezing up, or shape change of the moving block.

The major east-west faults shown by Moore (1966) and Krause (1965) are used by the present writer for postulating movement by the northern Borderland acting as a crustal plate that is partitioned or "vertically laminated" by the northwest-striking wrench faults. This crustal plate has moved westward essentially as a unit in response to north-south compression, accompanied by a gradual right-lateral offset along the primary wrench faults and minor adjustments by complementary lateral fault movements. Normally, a north-south compression with shear failure would require a left-lateral displacement somewhere along the northern edge of the Borderland. Bathymetry immediately west of the Channel Islands suggests that such is the case. On the other hand, crustal plate

movement of the northern Borderland, as implied, requires that this plate move westward relative to the crust to the north. Conceivably, the crustal plate to the north has moved westward under similar stress conditions and at a faster rate than the Borderland plate, resulting in an apparent left-lateral displacement.

Menard's concept (1960) of mantle convection current flow at the East Pacific Rise as the driving force for tectonic movement in the Gulf of California-Continental Borderland region has been recently used (Moore and Buffington, 1968) to postulate a prototype gulf in the Gulf of California during the period of 4 to 10 million years B. P. The reactivation of the East Pacific Rise started about 4 million years B. P. with further opening of the gulf in a northwesterly direction and development of a series of en echelon transform faults (see also, Larson et al., 1968). It is postulated that the north-south horizontal compression proposed in this study is derived possibly from the action of this convection cell whereby the transform faults manifest the movement primarily in the series of northwest-striking primary wrench faults within the crustal plate forming the northern Continental Borderland. Furthermore, the primary shear faults developed northwestward in a spasmodic and uneven manner in response to the convection cell forces with shear stress building up at the ends of these faults at intervals of geologic time to further propagate the faults. This tectonism developed the bathymetric pattern of ridges and basins as a result of predominantly simple shear under a shear couple (in most, if not all cases) and a responding tensile strain that allowed the collapse of small crustal blocks. Most of the present structural nature of the Borderland is

believed to have developed since Late Pliocene, with much of this structure occurring during Pleistocene-Recent time.

It is concluded that the present structure of the San Clemente Island block region was caused by a N15°W principal horizontal compressive force that developed the San Clemente fault zone as a primary shear as well as other major northwesterly striking faults. Forces normal to the primary shear faults have been small since Miocene time, thus allowing the development of brecciated zones related to simple shear. It is considered that the structural model postulated for this region can be used as a model for interpreting the origin of the Continental Borderland.

VI. SEDIMENT TRANSPORT AND DEPOSITION

PRIMARY SEDIMENTARY STRUCTURES

Primary sedimentary structures are averaged by the resolution of a reflection-profile method. Consequently, the internal structure resulting from the predominant sedimentary process will be recorded principally on the records (Moore, 1966.) A fundamental assumption made by Moore is that the reflections from strata of turbidity-current deposits will characterize topographically low areas by showing apparent truncation of the sediments against topographic highs or even gentle slopes. Sediments of hemipelagic origin will not blanket sharp or irregular highs uniformly, particularly in areas of pronounced currents. These sediments will drape over the more gental highs with no sharp truncation of strata in areas of slow currents. Turbidity-current sediments that show curvature by compaction may be differentiated from the hemipelagic type by the direction and magnitude of curvature and the retention of truncation against the topographic highs. These properties of hemipelagic and turbidite sediments are clearly illustrated by the seismic profiles of Hamilton (1967).

Moore (1966) postulated a relatively insignificant contribution of sediment from hemipelagic origin compared to that by turbidity currents. Probably no more than 15% of the total thickness of Continental Borderland post-orogenic basin sediments is of hemipelagic origin.

San Clemente Island Block Area

Major post-orogenic sediment fill, which forms the valley floor adjacent to the San Clemente Escarpment, is well-defined on the seismic profiles. It appears to be continuously bedded within units defined by the two and possibly three unconformities (Figure 17b). Some trough zones have been partially to completely filled by sediment (Figure 15); some have overflowed to form a continuation with the broader basin areas. An exception is the apparently bare trough formed by a N35°W-striking fault immediately off the escarpment to the southeast of Pyramid Head (Profile 26, Figure 15). Differences in elevation of some of the troughs are noted in Figure 15. The troughs apparently act as sediment traps and often as the paths for dispersal of terrigenous material derived from the slopes of the island block.

Near-horizontal deposits in the basin and trough areas off the east side of the island are considered to be partly of turbidity-current origin. Interpretation of the study area seismic profiles, unpublished data on cores (Figure 47) taken by the U. S. Naval Civil Engineering Laboratory (NCEL), Port Hueneme, California, and analysis of other cores of the area by Gaal (1966) are the bases for this conclusion. Five-foot cores, taken along the San Clemente fault zone and analyzed by NCEL, contain essentially horizontal layers of sand and silt graded upward into clay and containing sharply defined lower contacts. Other coarse to very coarse sand layers contain shell debris, mineral grains, and small rock fragments suggesting other than a hemipelagic or pelagic origin. Foraminifera in some of the more

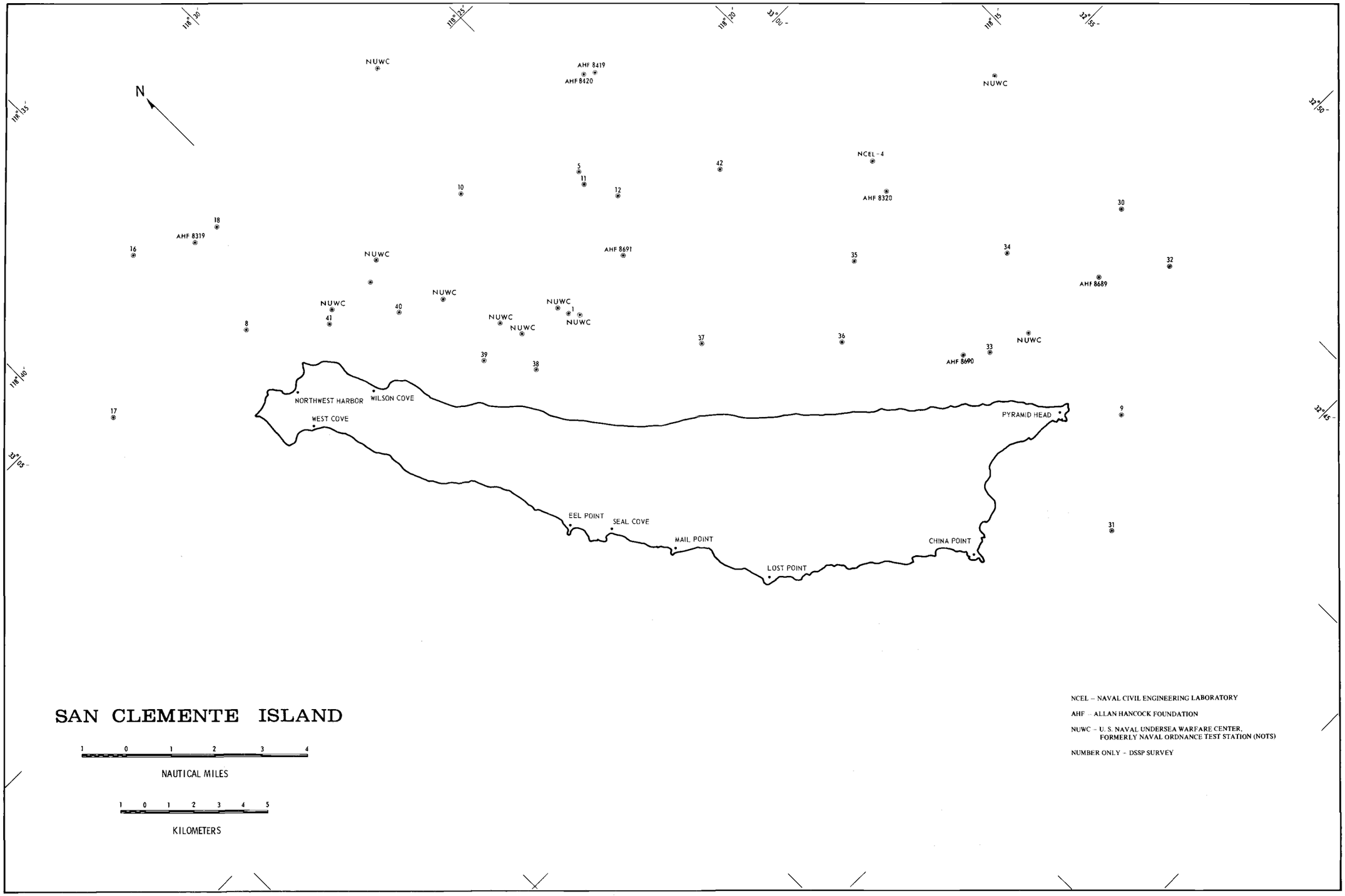

Figure 47. Core location map.

well-defined, coarser sand layers are a mixture of both shallow and deep water species (Warne, 1967). One core (AHF 8320 in Figure 47 and Appendix VI) contained graded bedding of sand and silt layers with very abundant mica, which is suggestive of displaced shallow water sediments. Doubtless, some of the coarse, shelly sand layers taken at the base of the escarpment may have resulted from submarine slides. However, the sand and silt layers with sharply defined bases grading upward into clay suggest deposition by turbidity currents.

By contrast, evidence for leveed sea-floor channels (Menard, 1955; Hamilton, 1967) is not apparent in any of the reflection profiles to suggest that turbidity currents have been recently active. Some channel-like sea-floor depressions contained in the profiles are presumed to be caused by recent fault activity. Conceivably, some of these features may have been maintained by turbidity-current flows, and lack of profile resolution has masked any evidence for levees.

Disproportional sediment-layer thicknesses such as those adjacent to the escarpment suggest fan or apron deposits resulting from recurrent faulting along the island block with subsequent sand or turbidity-current flows.

SEDIMENT TRANSPORT AND DEPOSITION

Elevation and Structural Control

Some conclusions as to the probable evolution of post-orogenic deposition can be drawn from bathymetry and the surface distribution of Unit X. The following sediment transport and depositional

distribution is proposed to satisfy the structure and bathymetric conditions inferred by the seismic-reflection-profile data.

The northeasterly structural and bathymetric saddle between the island and the Emery Seaknoll is represented in Figure 48 by opposing directions of postulated sediment transport. The directions of sediment transport are based on elevation differences and structural control for turbidity-current or sand flows and slides off the escarpment and the Emery Seaknoll. The greater volume of post-orogenic sediments off the northeastern one-half of the island (Figure 16) indicates that much of the sediment flowing from the escarpment and the Seaknoll has been transported to the northwest of the saddle. The elevation in the area of the intersection of cross-section lines I, J, and K (Figure 48) and that of most of the cross-section lines to the southeast is shown to be considerably higher than along cross sections B, C, D, and E. Apparently much of the sediment derived from the slopes off the southeastern end (Pyramid Head) of the island block has been carried to the southeast, as indicated by a southeastern elevation plunge along cross sections G, H, and L. A later structural cutoff of transport to the south is suggested by the higher elevation at the northern ends of cross sections H and L and the intersection of cross sections I, J, and K.

A change of sediment transport direction from northwest to north-northeast is noted along the main San Clemente fault zone at the intersection of seismic Profile 2 and cross-section line B (Figures 1 and 48). Apparently, much of the present sediment transport in this

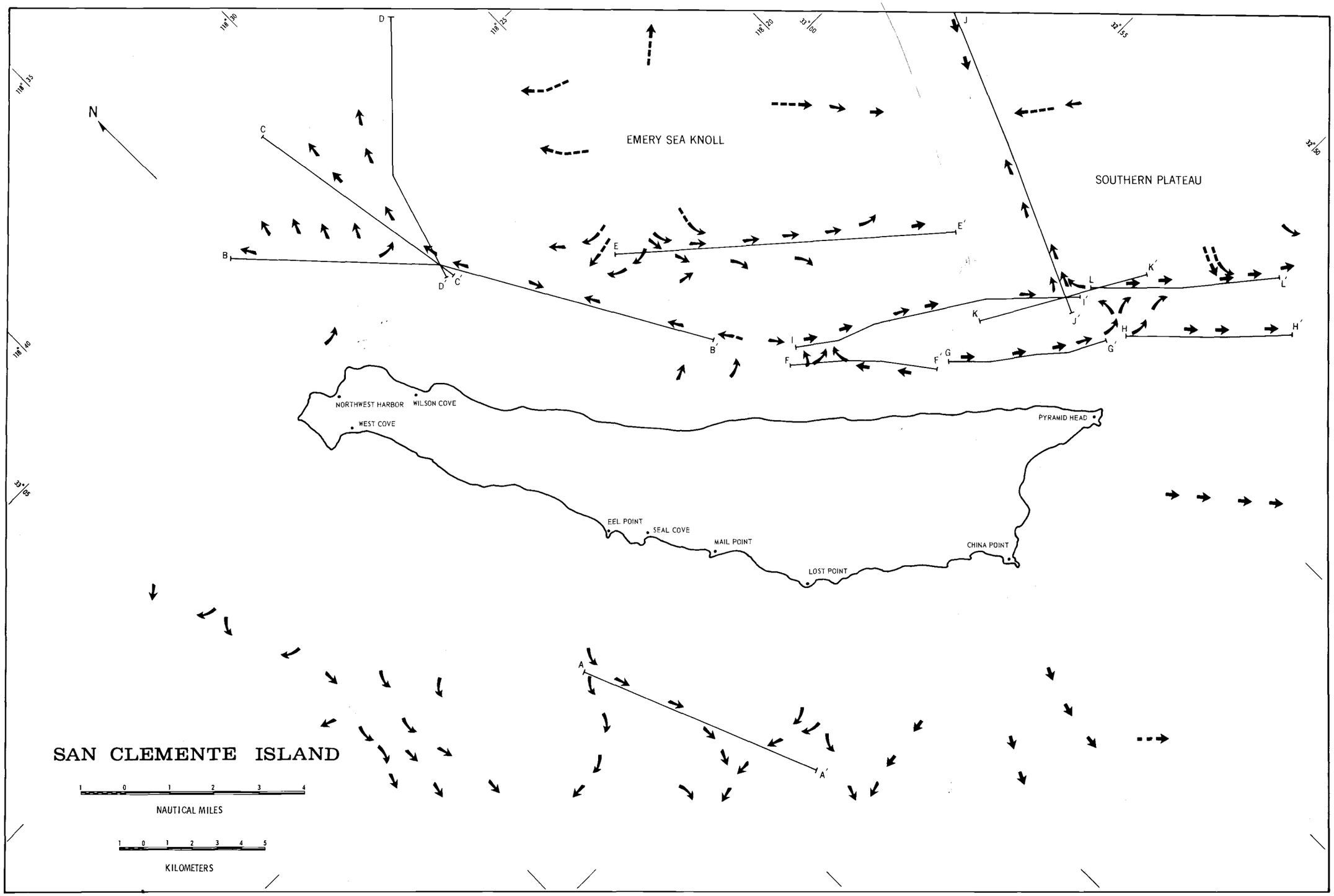
N
118° 30
118° 25
118° 20
33° 00
33° 55
118° 35
118° 40
33° 05
EMERY SEA KNOLL
SOUTHERN PLATEAU
NORTHWEST HARBOR
WILSON COVE
WEST COVE
PYRAMID HEAD
EEL POINT
SEAL COVE
MAIL POINT
CHINA POINT
LOST POINT
A
A′
B
B′
C
C′
D
D′
E
E′
F
F′
G
G′
H
H′
I
I′
J
J′
K
K′
L
L′
SAN CLEMENTE ISLAND
1 0 1 2 3 4
NAUTICAL MILES
1 0 1 2 3 4 5
KILOMETERS

area is to the northeast from the basin area off Wilson Cove, where it then terminates in the Santa Catalina Basin.

At the present time, it is unlikely that any sediment from the island block is carried to the Santa Catalina Basin via the area between the Emery Seaknoll and the Southern Plateau. Some sediment may be transported off the west side of the Southern Plateau and southward into the "Rift" Valley, but elevation differences suggest that major sediment transport from the island source must be to the structural depression between the Emery Seaknoll and the Southern Plateau.

The lack of sediment in the trough southeast of Pyramid Head is attributed to either fault control that cut off the main supply from the island or to faulting so recent that an appreciable volume of sediment has not yet developed. The latter appears more likely since some smaller depressed areas containing fill are now cut off and elevated above surrounding low areas.

Slope conditions and shape of deposits indicate that most of Unit X along the west side of the island block consists of a series of fan deposits (Figures 16, 48, and 49a) that are, for the most part, structurally controlled. Most of these deposits appear to terminate at the principal fault-controlled trough paralleling the west side of the island block.

The structural ridge about 8 kilometers off Mail Point is assumed to have diverted earlier canyon-derived sediment southwesterly to the San Nicolas Basin. Subsequent fill to the north of this high, and possibly structural change, has allowed a more recent southerly transport from the canyon (Figures 16, 23, and 48, cross section A-A').

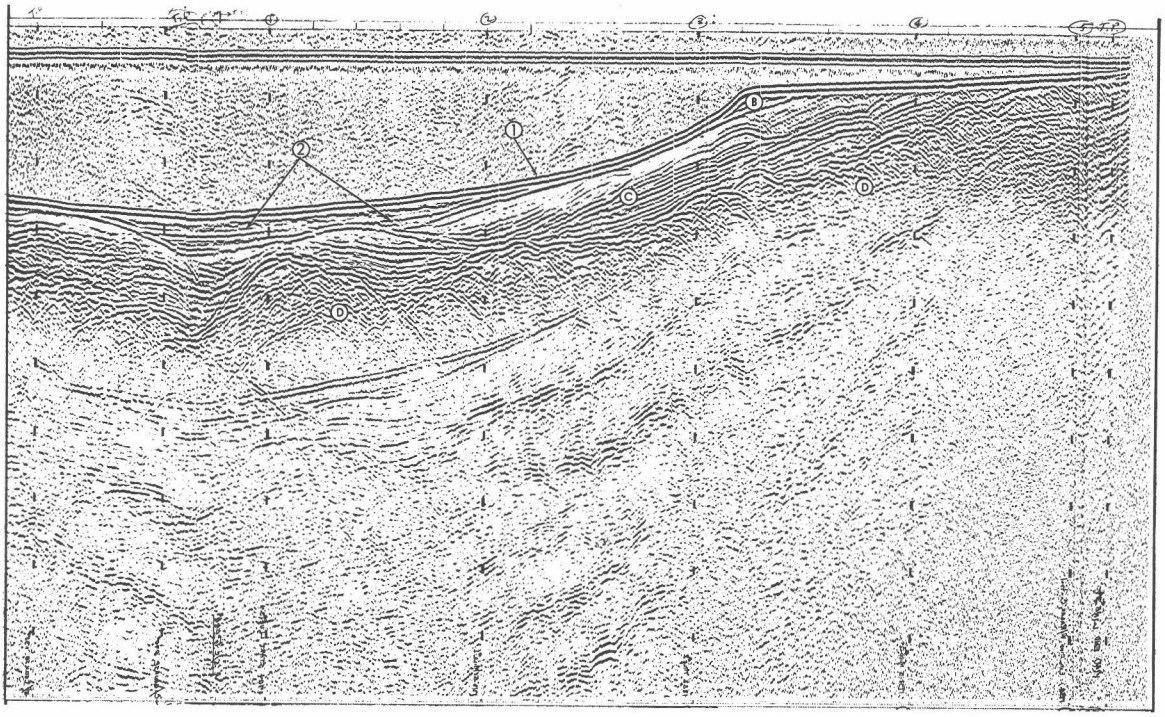

(a)

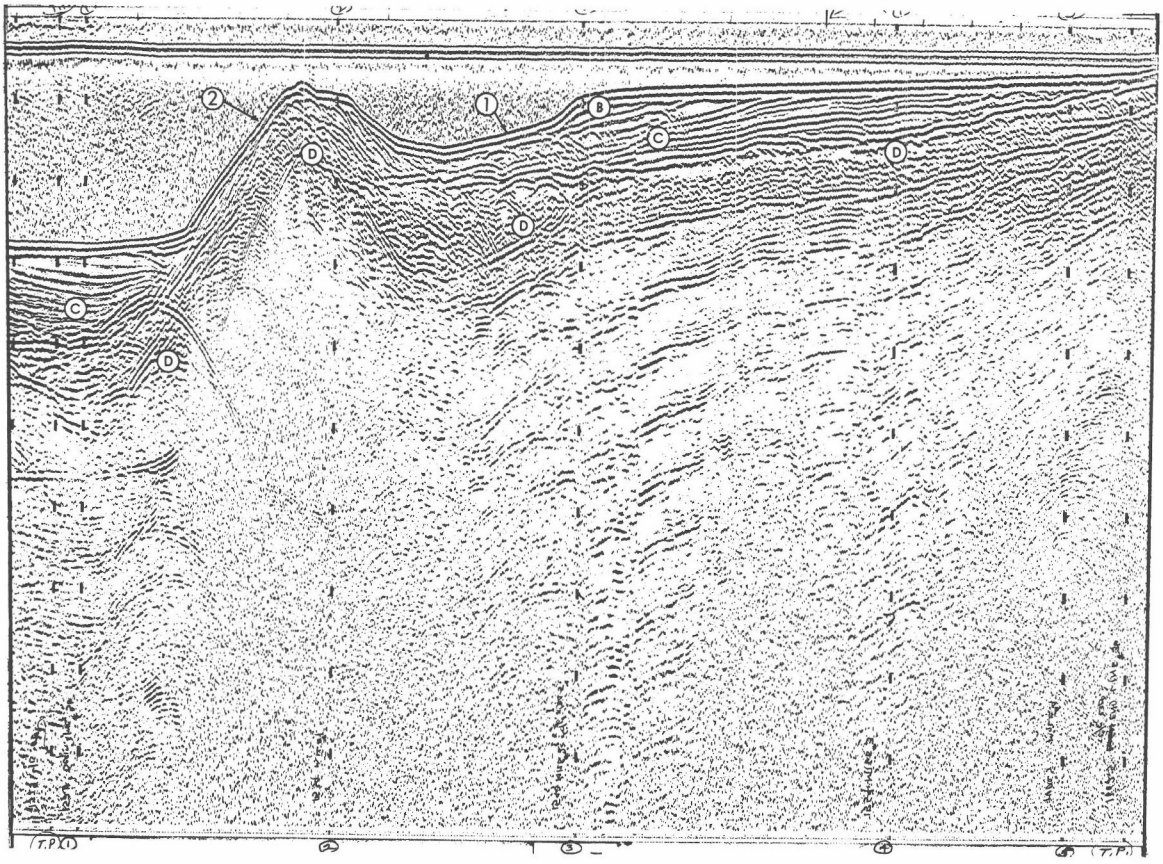

(b)

Rate of Deposition

Calculations for the uncompacted thickness of Continental Borderland post-orogenic sediment have been made by Moore (1966). Moore's method is predicated on corrections for the compaction that has occurred within sediment intervals.

An appraisal of the maximum average rate of deposition per unit of time of the post-orogenic sediments in the studied area is made by the present author using the thickest section (550 meters) off Wilson Cove. The total thickness of this section is corrected to approximately 700 meters of uncompacted sediments. The depositional rates calculated by Moore (1966) and Emery and Bray (1962) for Continental Borderland areas range between 3.8 to 185 centimeters per 1,000 years and 5 to 180 centimeters per 1,000 years, respectively. The present study shows a maximum rate of about 70 centimeters per 1,000 years based on the assumption of one million years by Moore for the total time of deposition for post-orogenic sediments. The average is estimated at approximately 30 centimeters per 1,000 years. This estimate is more in accordance with the finding of Emery and Bray who estimated rates up to 39 centimeters per 1,000 years in far offshore basins, a rate much greater than that estimated by Moore. However, assuming that the span of Pleistocene time is approximately 1.5 to 2.0 million years and that most of the post-orogenic sedimentation occurred during this Epoch (Moore, 1966), a maximum average rate of deposition would then lie between 35 and 47 centimeters per 1,000 years. On this basis, an estimated average rate of deposition is 17 centimeters per 1,000 years.

VII. GEOLOGIC HISTORY

REGIONAL OROGENIC HISTORY

Pre-Cretaceous structural history of the Continental Borderland is very vague due to the lack of data (Emery, 1960). Scarcity of pre-Miocene Tertiary strata is believed by Emery to be due to erosion of the Continental Borderland that existed as a topographic high during early Tertiary time. Further uplift during Oligocene again reduced the areas of deposition. Emery reasoned that downwarping during most of Miocene time accounts for the widespread occurrence of Miocene sedimentary rocks over much of the Continental Borderland. Extensive vulcanism occurred during Middle and Late Miocene, as shown by exposures along the coast (Shelton, 1954) and on nearly all of the islands and sea-floor highs (Emery, 1954, 1960). Accompanying diastrophism is believed to account for much of the present general physiography of the Continental Borderland. However, evidence indicates some continued or recurrent block faulting during Pliocene and Pleistocene. Emery (1960) cited examples of marine terraces 1,000 feet or more above sea level and suggested that those on San Clemente Island may be of mid-Pleistocene age. Emery (1958, 1960) suggested that a broad southerly regional downwarping took place during late structural history of the Borderland region. Also, the lowest of the terraces (considered Pleistocene) on the shelf is shown to be about 250 feet deep near Los Angeles and about 400 feet deep far to the south and west. Cohen et al. (1963) stated that tectonic movements have affected the San Benito Islands, Baja California, during the

Pleistocene as shown by tilt in different directions of three levels of terraces on these islands.

According to Shepard and Emery (1941) and Emery (1960), the major development of the Continental Borderland occurred during Miocene time. Major diastrophism took place in the Middle Miocene, accompanied by voluminous vulcanism. This was followed by minor tectonism in Late Miocene and Pliocene. Later, a mid-Pleistocene orogeny took place, followed by intermittent deformation to the present time with Pleistocene to Recent regional warping and faulting. During Pleistocene time the Continental Borderland topography was essentially as at present, but some of the blocks moved individually and the sea level fluctuated a few hundred feet.

SAN CLEMENTE ISLAND BLOCK

A chronological interpretation of Middle Tertiary to Recent geologic history is proposed for the San Clemente Island block (Figure 50) as follows:

(a) A regional, broad, low land area existed in the Oligocene (Emery, 1960) from which the ancestral San Clemente Island block was to be formed as a result of block faulting.

(b) The primordial San Clemente Island block developed from voluminous lava flows during the Middle Miocene. The mass of volcanic rocks comprising the upper part of the present island block attests to the magnitude of these flows. Early flows have a more basic composition (basalt-andesite) than the final flow stages. Intermediate (dacite) and acid

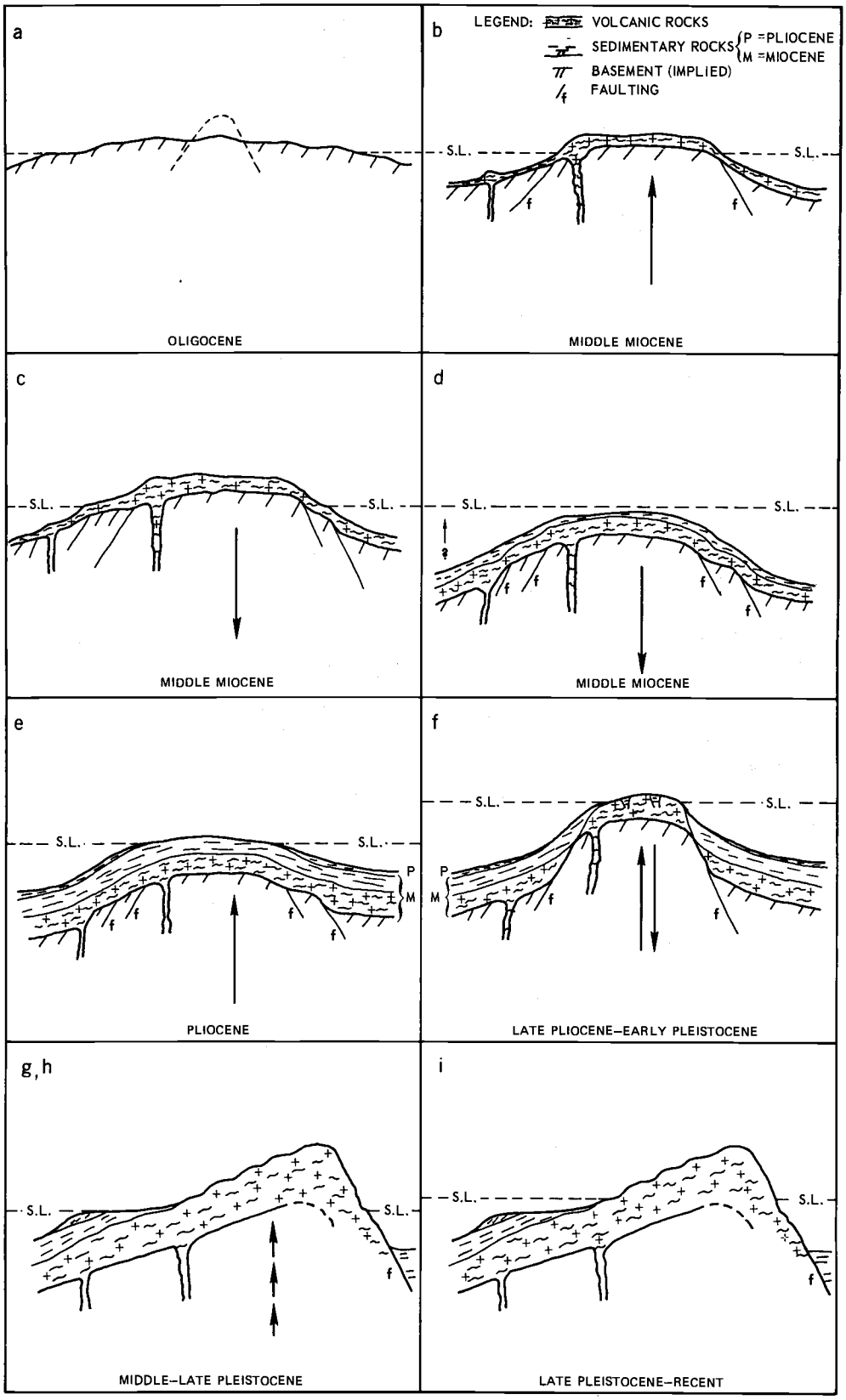
a
OLIGOCENE
b
LEGEND:
VOLCANIC ROCKS
SEDIMENTARY ROCKS
P =PLIOCENE
M =MIOCENE
BASEMENT (IMPLIED)
FAULTING
S.L.
S.L.
f
f
MIDDLE MIOCENE
c
S.L.
S.L.
MIDDLE MIOCENE
d
S.L.
S.L.
?
f
f
f
f
MIDDLE MIOCENE
e
S.L.
S.L.
P
M
f
f
f
f
PLIOCENE
f
S.L.
S.L.
P
M
f
f
LATE PLIOCENE–EARLY PLEISTOCENE
g,h
S.L.
S.L.
f
MIDDLE–LATE PLEISTOCENE
i
S.L.
S.L.
f
LATE PLEISTOCENE–RECENT

(rhyolite) types prevail in the later flows. The presence of large phenocrysts throughout the flows, the platey nature of some of the exposed lavas, the vesicular nature at the tops and bottoms of individual flows, the presence of tuffs and pumices, and the apparent lack of pillow lavas (Olmsted, 1958; Lamar et al., 1967) indicated that at least the upper 1,200 feet of the flows were formed above sea level.

(c) Subsidence and temporary stand(s) of sea level occurred as evidenced by possible terracing on the offshore, subbottom volcanic rock surface (Unit D) along the west side of the island (Figure 23). A hiatus between the Miocene volcanic and sedimentary rocks (Unit C) also suggests lengthy subaerial exposure and shallow water during this event.

(d) Further subsidence and foundering took place during Middle Miocene (Luisian). This barely engulfed the island block, resulting in the deposition of a basal coarse-grained sand containing volcanic rock detritus as shown at the base of the remnants of Miocene sediments on the island. This was followed by continued subsidence with deposition of marine silts and sands, diatom oozes, and calcareous muds. Some local intercalation of volcanic eruptives and marine sedimentary deposits occurred during the later development of Miocene sedimentation (Olmsted, 1958).

(e) The block probably remained submerged into early Pliocene time. This was possibly followed by some block emergence or shoaling with Pliocene sediment deposition along the flanks

of the block and in the surrounding basins. Emery (1960) reported Pliocene mudstone recovered from the northeast submarine slope of the island. According to Gaal (1966), Pliocene (?) sandstone was recovered at the base of a core taken in the area of the "Rift" Valley. During this epoch, a north-south horizontal compressive force developed (or recurred) across the Borderland region with a possible reactivation of forces associated with the East Pacific Rise about 4 million years B. P. (Moore and Buffington, 1968). Initial development of the present San Clemente Island fault zone (probably from an earlier rupture) took place that outlined the island block much as it exists today.

(f) Further uplift of the island block took place during Late Pliocene-Early Pleistocene. This was accompanied by extensive erosion and denudation of the Miocene (and possibly some Pliocene) marine deposits on the emerged island block. Some Miocene (Luisian) rocks preserved by faulting on the island and those described as Unit C immediately offshore remain as remnants. Some of the rocks lying above the lower of two unconformities within Unit C north of Eel Ridge Canyon may represent post-Luisian Miocene or Pliocene rocks that are no longer present on the island. Considerable aerial exposure of the island block is evidenced by the pronounced unconformity on the surface of the offshore Miocene sedimentary rocks to depths in excess of 180 meters. Considerable tectonism occurred (reactivation of faults, primarily), as shown by the

preservation of several thicker zones of Unit C within depressions caused by fault offsets of the offshore Miocene volcanic rocks. These deposits cannot be attributed entirely to deposition in Unit D depressions caused by pre-Unit C erosion or faulting. Uplift of the island block is attributed to the horizontal north-south compressive force which resulted in intermittent wrench-fault movement along the San Clemente fault zone and the development of the shear and tensile fault pattern based upon a modified version of the structural model proposed by Moody and Hill (1956). Finally, the island crustal block subsided to where sea level was about at the 1,500-foot (450 meter) elevation. At this time, part of Unit B was probably deposited in the canyons, gullies, and fault depressions on the unconformity at the surface of Units C and D. Deposition of some of the sediments comprising Unit X also occurred throughout this event.

(g) Intermittent uplift of the island crustal block occurred during the Middle to Late Pleistocene. The intermittent stands permitted the sea to carve many, if not all, of the present island terraces from the present 450-meter elevation to the present sea level. Development of the fault-controlled terrestrial and submarine canyons (particularly on the west side of the island) was possibly contemporaneous with and subsequent to the development of the island terraces. Some of the present structural nature of the island block had developed by the end of the Pleistocene. Considerable

post-orogenic marine sedimentation had also evolved, represented by some of the deposits along the flanks of the island block and in the adjacent basins. Renewed or increased north-south horizontal compression developed a shear couple encompassing the San Clemente Island crustal block. This may also be the case for other Continental Borderland crustal blocks that are now bordered by prominent northwesterly striking lateral faults. This tectonism probably developed in response to a further opening of the Gulf of California.

(h) A eustatic lowering of the sea level took place during the Late Pleistocene to approximately 120 meters below the present sea level. This resulted in wave truncation of Unit C and the further deposition of material in low areas on the post-orogenic surface. Concomitant with the period of low sea level was the development of a major wave-cut terrace with progradation at the seaward end to complete the development of Unit B. Rounded boulders recovered at 100 meters of depth, some containing pholad borings, strongly suggest the intertidal environment. Much of the remainder of Unit X was deposited during this event.

(i) The transgression of the sea during Holocene time took place with temporary regressions possibly occuring during the earlier part of the transgression. This event was concomitant with further fault activity which offset the submerged terrace at many localities around the island. The island crustal block was tilted slightly to the west by continued lateral-fault

activity in response to the opening of the Gulf of California. Much of Unit A was deposited on the offshore terrace island block slopes and basin areas. Younger eolian sand and alluvial deposits were formed on the island (Olmsted, 1958).

VIII. CONCLUSIONS

The structural geology of the San Clemente Island block is resolved by the analysis of continuous acoustic reflection profiles and sea-floor samples. A tectonic model and the geologic history for the San Clemente Island block area are developed and related to the origin of the Continental Borderland. The more important aspects of this study are summarized below:

(1) Bathymetry, as interpreted from the seismic profiles, differs from that shown on published charts. Better definition of structural trends shown by elongate topographic highs and depressions permits a more sophisticated analysis of bathymetric data than has been possible previously.

(2) Five sediment and rock units from Middle Miocene to Recent are defined, (Units A, B, C, D, and X). Unit A is a sediment cover of Recent and possibly Late Pleistocene age. Unit B represents a post-Miocene, probably Pliocene-Pleistocene, accumulation of debris derived mainly from the island's canyons. Microfossils from marine limestone outcrops have established a Middle Miocene age for Unit C. Unit D is considered to be the offshore equivalent of the Miocene volcanic rocks exposed on the island. Unit X is a slope-(fan and apron) and basin-deposit equilvalent of Units A and B.

(3) In most areas, the offshore fault pattern is related to that on the island. The main exception is the San Clemente

fault zone, delineated along the east side of the island by the San Clemente Escarpment.

(4) Both faulting and erosion are responsible for a major unconformity underlying Units B and X. Anomalous isopachous trends of the sedimentary units and structure contour trends on Unit D and the major unconformity substantiate the offshore fault pattern. A terrace on Unit D, possibly wave-cut, suggests a hiatus between Units C and D.

(5) A canyon off Eel Point is the result of pivotal faulting not evident on the island. The canyon lies within a transition zone between different structural trends north and south of the canyon.

(6) The structural pattern of the island block conforms to the wrench-fault system hypothesized by Moody and Hill (1956), modified by general north-south tensile fracturing. The tensile fracturing may be related to (a) lateral extension, (b) upward bowing of the island block, (c) a shear couple, or (d) a combination of these. The strong trend of tensional faulting suggests that some rotational stress-strain mechanism such as a shear couple has been active.

(7) The San Clemente fault zone is considered the primary right-lateral wrench fault in the area.

(8) The San Clemente "Rift" Valley to the southeast of the island is postulated to have resulted from "cross-strike separation" related to right-lateral movement along the gradual curvature

of the San Clemente Fault in the general region of the "Rift" Valley.

(9) A major offshore terrace around the island, which is most prominent along the west side of the island, is postulated to have been cut during Late Pleistocene-Holocene time as a consequence of eustatic lowering of sea level. This terrace, about 120 meters below sea level along the west side of the island and about 90 meters below sea level along the east side of the island, demonstrates tilt of the island block by Recent tectonism. Faulting, along with a combination of southwesterly and northwesterly tilting, has locally affected the level of the terrace. The net tilt to the west is probably associated with an upward bowing of the island block in response to lateral compression under a shear couple encompassing the island block.

(10) A steep magnetic gradient off the San Clemente Escarpment is probably the consequence of a combined effect of (a) the margin of the mass of volcanic flows, (b) a postulated deep basic mass related to a large positive anomaly off West Cove, and (c) major faulting.

(11) Statistical analyses of earthquake epicenters in the northern Continental Borderland indicate that part of the San Clemente fault zone is associated with recent, intermittent fault activity of a possible cyclical nature. These analyses also suggest that the northwesterly fault trends of the Continental Borderland mark the primary direction for recent, intermittent stress releases in this region.

(12) The lack of strong primary folding of the island block infers the lack of a large component of compression normal to the primary shear fracture. It is proposed that a variable, but small compressional component of force normal to the primary shear direction has resulted in the development of horsts and grabens along the San Clemente fault zone.

(13) Very little horizontal rotation of the north-south primary stress direction has occurred since the inception of the faults interpreted.

(14) Fault-trace curvatures along the San Clemente-Agua Blanca fault zone are attributed to extensions of the fault zone at various periods of time in the structural development of the Continental Borderland.

(15) Repetitive fault movement (14 above) is considered responsible for the development of the San Clemente block by lateral shear, with such movement suggested for the development of other upthrown crustal blocks in the Borderland. The basins of the region are postulated to have resulted from tensile release at the end of the primary wrench faults during various times of their development.

(16) East-west spreading by tension is not considered to be a major cause for the structural origin of much of the Borderland. The northern Continental Borderland is thought to be a "vertically laminated" single crustal plate where movement has occurred along the series of primary wrench faults that act in combination as shear couples. This mechanism has

developed the present structural nature of the northern Borderland crustal plate. Furtheremore, these faults have moved in an en echelon fashion with ultimate release of the crustal plate by lateral movement along the major east-west faults bordering the north and south of the crustal plate.

(17) North-south compression probably took place during and since Pliocene time as a consequence of convection cell (postulated by Menard, 1960) movement reflected in the en echelon transform faulting on the East Pacific Rise entering the Gulf of California. These transform faults have translated their movement in the northwest-striking series of parallel to subparallel wrench faults of the Borderland.

(18) It is concluded that, based on an originally horizontal attitude the present dip of the island volcanic rocks and a constant rate of tilt, the total westward dip of the island block could have taken place within the latter part of Pleistocene time. An average rate of throw at the eastern side of the island is about 1/3 meter per 1,000 years.

(19) A major lithostructural division, based upon that proposed by Moore (1966), differentiates pre-orogenic (Units C and D) from post-orogenic (Unit X) deposits. The post-orogenic sediments are believed to have followed certain major transportation channels by means of turbidity currents, sand flows, and slides, and to have been deposited in basin lows developed by faulting and folding. Fans and aprons of post-orogenic

sediments have been developed in some slope areas, particularly off the west side of the island.

(20) A maximum rate of deposition for post-orogenic sediments in the studied area is estimated to be between 35 and 47 centimeters per 1,000 years, with an estimated average rate of about 17 centimeters per 1,000 years.

BIBLIOGRAPHY

Alberding, H. 1957. Application of principles of wrench-faulting tectonics of Moody and Hill to northern South America. Bulletin of the Geological Society of America 68:785-790.

_____ 1958a. Wrench-fault tectonics: a reply. Bulletin of the Geological Society of America 69:931-932.

_____ 1958b. Wrench-fault tectonics: a reply. Bulletin of the Geological Society of America 69:937-939.

Allen, C. R. 1967. Seismological Laboratory, California Institute of Technology. Personal communication. Pasadena, California.

Allen, C. R., P. St.-Amand, C. F. Richter and J. M. Nordquist. 1965. Relationship between seismicity and geologic structure in the southern California region. Bulletin of the Seismological Society of America 55:753-797.

Allen, C. R., L. T. Silver and F. G. Stehl. 1960. Agua Blanca fault--a major transverse structure of northern Baja California, Mexico. Bulletin of the Geological Society of America 71:457-482.

Anderson, E. M. 1951. The dynamics of faulting. 2d ed. Edinburgh, Oliver and Boyd. 206 p.

Austin, C. F. 1966. Manned undersea structure--the Rock-site concept. China Lake, California. 42 p. (U. S. Naval Ordnance Test Station. NOTS TP 4162)

_____ 1967. Geologist, Naval Weapons Center. Personal communication. China Lake, California.

Bagnall, P. S. 1964. Wrench faulting in Cyprus. Journal of Geology 72:327-345.

Bartow, J. A. 1966. Deep submarine channel in Upper Miocene, Orange County, California. Journal of Sedimentary Petrology 36:700-705.

Beloussov, V. V. 1962. Basic problems in geotectonics. New York, McGraw-Hill. 809 p.

Benioff, H. 1958. Circum-Pacific orogeny. Publications of the Dominion Observatory (Ottawa) 20:395-402.

Benioff, H. 1962. Movements on major transcurrent faults. In: Continental drift, ed. by S. K. Runcorn. New York, Academic. p. 103-134. (International Geophysics Series. Vol. 3)

Berggren, W. A., J. D. Phillips, A. Bertels and D. Wall. 1967. Late Pliocene-Pleistocene stratigraphy in deep sea cores from the south-central North Atlantic. Nature 216:253-255.

Billings, M. P. 1954. Structural geology. 2d ed. New York, Prentice-Hall. 514 p.

_____ 1960. Diastrophism and mountain building. Bulletin of the Geological Society of America 71:363-398.

Bird, W. E. 1967. Geophysicist, Continental Oil Company. Personal communication. Ventura, California.

Bradley, W. C. 1958. Submarine abrasion and wave-cut platforms. Bulletin of the Geological Society of America 69:967-974.

Burton, C. K. 1965. Wrench faulting in Malaya. Journal of Geology 73: 781-798.

Butler, L. W. 1964. Geology of a submarine valley on the continental slope off Baja California, Mexico. Master's thesis. San Diego, San Diego State College. 100 numb. leaves.

Chinnery, M. A. 1966. Secondary faulting. I. Theoretical aspects. II. Geological aspects. Canadian Journal of Earth Sciences 3:163-190.

Clarke, A. M. et al. 1961. A marine geophysical survey of the undersea coalfields of Northumberland, Cumberland and Durham. The mining Engineer, no. 15, p. 197-212.

Clements, T. and K. O. Emery. 1947. Seismic activity and topography of the sea floor off southern California. Bulletin of the Seismological Society of America 37:307-313.

Cohen, L. H. et al. 1963. Geology of the San Benito Islands, Baja California, Mexico. Bulletin of the Seismological Society of America 74:1355-1370.

Cotton, C. A. 1956. Geomechanics of New Zealand mountain building. New Zealand Journal of Science and Technology, sec. B, 38:187-200.

_____ 1957. An example of transcurrent-drift tectonics. New Zealand Journal of Science and Technology, sec. B, 38:939-942.

Curray, J. R. 1960. Sediment and history of Holocene transgressions, continental shelf, northwest Gulf of Mexico. In: Recent sediments, northwest Gulf of Mexico, ed. by F. P. Shepard et al. Tulsa, Oklahoma, American Association of Petroleum Geologists. p. 221-266.

_____ 1961. Late Quaternary sea level; a discussion. Bulletin of the Geological Society of America 72:1707-1712.

_____ 1964. Transgressions and regressions. In: Papers in marine geology, Shepard commemorative volume, ed. by R. L. Miller. New York, Macmillan. p. 175-203.

_____ 1965. Late Quaternary history, continental shelves of the United States. In: The Quaternary of the United States, ed. by H. E. Wright, Jr. and D. G. Frey. Princeton, New Jersey, Princeton University. p. 723-735.

Curray, J. R. and D. G. Moore. 1964. Pleistocene deltaic progradation of continental terrace, Costa De Nayarit, Mexico. In: Marine geology of the Gulf of California, ed. by T. H. van Andel and G. G. Shor, Jr. Tulsa, Oklahoma. p. 193-215. (American Association of Petroleum Geologists. Memoir 3)

Emery, K. O. 1952. Continental shelf sediments of southern California. Bulletin of the Geological Society of America 63:1105-1108.

_____ 1954. General geology of the offshore area, southern California. In: Geology of southern California, ed. by R. H. Jahns. Sacramento. p. 107-111. (California. Division of Mines. Bulletin 170)

_____ 1958. Shallow submerged marine terraces of southern California. Bulletin of the Geological Society of America 69:39-60.

_____ 1960. The sea off southern California. New York, Wiley. 366 p.

_____ 1961. Submerged marine terraces and their sediments. Zeitschrift für Geomorphologie, sup., 3:2-29.

Emery, K. O. and E. E. Bray. 1962. Radiocarbon dating of California basin sediments. Bulletin of the American Association of Petroleum Geologists 46:1839-1856.

Emiliani, C. 1955. Pleistocene temperatures. Journal of Geology 63: 538-578.

Emiliani, C. and R. F. Flint. 1963. The Pleistocene record. In: The sea, ed. by M. N. Hill. Vol. 3. The earth beneath the sea. New York, Interscience. p. 888-927.

Emiliani, C. and F. D. Milliman. 1966. Deep-sea sediments and their geologic record. Earth-Science Reviews 1:105-132.

Emiliani, C. et al. 1961. Paleotemperature analysis of the Plio-Pleistocene section of Le Castella, Calabria, Southern Italy. Bulletin of the Geological Society of America 72:679-688.

Ericson, D. B., M. Ewing and G. Woolin. 1963. Pliocene-Pleistocene boundary in deep-sea sediments. Science 139:727-737.

_____ 1964. The Pleistocene epoch in deep-sea sediments. Science 146:723-732.

Folk, R. L. 1962. Spectral subdivision of limestone types. In: Classification of carbonate rocks. Tulsa, Oklahoma. p. 62-85. (American Association of Petroleum Geologists. Memoir 1)

Freund, R. 1965. A model of the structural development of Israel and adjacent areas since Upper Cretaceous times. Geological Magazine 102:189-205.

Gaal, R. A. P. 1966. Marine geology of the Santa Catalina basin area. Ph.D. thesis. Los Angeles, University of Southern California. 266 numb. leaves.

Garfunkel, Z. 1966. Problems of wrench faults. Tectonophysics 3 457-473.

Guilcher, A. 1963. Continental shelf and slope (continental margin). In: The sea, ed. by M. N. Hill. Vol. 3. The earth beneath the sea. New York, Interscience. p. 281-311.

Gutenberg, B. 1941. Mechanism of faulting in southern California, indicated by seismograms. Bulletin of the Seismological Society of America 31:263-302

_____ 1943. Earthquakes and structure in southern California. Bulletin of the Geological Society of America 54:499-526.

Hafner, W. 1951. Stress distributions and faulting. Bulletin of the Geological Society of America 62:373-398.

Hamilton, E. L. 1959. Thickness and consolidation of deep-sea sediments. Bulletin of the Geological Society of America 70:1399-1424.

_____ 1967a. Marine geologist, U.S. Naval Undersea Warfare Center. Personal communication. San Diego, California.

_____ 1967b. Marine geology of abyssal plains in the Gulf of Alaska. Journal of Geophysical Research 72:4189-4213.

Hamilton, W. 1961. Origin of the Gulf of California. Bulletin of the Geological Society of America 72:1307-1318.

Harrison, J. C. and R. E. von Huene. 1965. The surface-ship gravity meter as a tool for exploring the geologic structure of continental shelves. Ocean Science and Ocean Engineering 1:414-431.

Harrison, J. C. et al. 1966. Bouger gravity anomalies and magnetic anomalies off the coast of southern California. Journal of Geophysical Research 71:4921-4941.

Hatherton, T. 1968. Through the looking glass: a comparative study of New Zealand and California. Nature 220:660-663.

Hays, J. D. and N. D. Opdyke. 1967. Antarctica radiolaria, magnetic reversals, and climatic change. Science 158:1001-1011.

Heezen, B. C. 1963. Turbidity currents. In: The sea, ed. by M. N. Hill. Vol. 3. The earth beneath the sea. New York, Interscience. p. 742-771.

Hill, M. L. 1954. Tectonics of faulting in southern California. In: Geology of southern California, ed. by R. H. Jahns. Sacramento. p. 5-13. (California. Division of Mines. Bulletin 170)

Hill, M. L. and T. W. Dibblee, Jr. 1953. San Andreas, Garlock and Big Pine faults, California. Bulletin of the Geological Society of America 64:443-458.

Holzman, J. E. 1952. Submarine geology of Cortes and Tanner Banks. Journal of Sedimentary Petrology 22:97-118.

Hoskins, H. and S. T. Knott. 1961. Geophysical investigation of Cape Cod Bay, Massachusetts, using the continuous seismic profiles. Journal of Geology 69:330-340.

Hubbert, M. K. 1951. Mechanical basis for certain familiar geologic structures. Bulletin of the Geological Society of America 62:355-372.

Isacks, B., J. Oliver and L. R. Sykes. 1968. Seismology and the new global tectonics. Journal of Geophysical Research 73:5855-5899.

Jahns, R. H. 1954. Geology of the peninsular range province, southern California and Baja California. In: Geology of southern California, ed. by R. H. Jahns. Sacramento. p. 29-52. (California. Division of Mines. Bulletin 170)

Johannsen, A. 1931. A descriptive petrography of the igneous rocks. Vol. 1. Introduction, textures, classifications, and glossary. Chicago, University of Chicago. 318 p.

Kingma, J. T. 1958. Possible origin of piercement structures, unconformities, and secondary basins in the eastern geosyncline, New Zealand. New Zealand Journal of Geology and Geophysics 1:269-274.

_____ 1959. The tectonic history of New Zeland. New Zealand Journal of Geology and Geophysics 2:1-55.

Krause, D. C. 1965. Tectonics, bathymetry, and geomagnetism of the southern continental borderland west of Baja California, Mexico. Bulletin of the Geological Society of America 76:617-650.

Krumbein, W. C. and F. J. Pettijohn. 1938. Manual of sedimentary petrography. New York, D. Appleton-Century. 549 p.

Lamar, D. L., P. M. Merifield and M. L. Stout. 1967. Engineering geology of rocks in core hole, Eel Point, San Clemente Island, California. China Lake, California. 18 p. (Naval Weapons Center. NWC TP 4487)

Larson, R. L., H. W. Menard and S. M. Smith. 1968. Gulf of California: a result of ocean-floor spreading and transform faulting. Science 161:781-783.

Leighton, M. W. and C. Pendexter. 1962. Carbonate rock types. In: Classification of carbonate rocks. Tulsa, Oklahoma. p. 33-62. (American Association of Petroleum Geologists. Memoir 1)

Lensen, G. J. 1958a. A method of graben and horst formation. Journal of Geology 66:579-587.

_____ 1958b. Rationalized fault interpretation. New Zealand Journal of Geology and Geophysics 1:307-317.

_____ 1958c. Note on the compressional angle between intersecting transcurrent clockwise and anti-clockwise faults. New Zealand Journal of Geology and Geophysics 1:533-540.

_____ 1959. Secondary faulting and transcurrent splay faulting at transcurrent fault intersections. New Zealand Journal of Geology and Geophysics 2:729-734.

_____ 1960. Principal horizontal stress directions as an aid to the study of crustal deformation. Publications of the Dominion Observatory (Ottawa) 24:389-397.

Lincoln, J. V. 1966. Geomagnetic and solar data. Journal of Geophysical Research 72 (9):2467.

Lincoln, J. V. 1967a. Geomagnetic and solar data. Journal of Geophysical Research 72:2981.

_____ 1967b. Geomagnetic and solar data. Journal of Geophysical Research 72:3522.

Martin, B. D. 1963. Rosedale Channel--evidence for Late Miocene submarine erosion in Great Valley of California. Bulletin of the American Association of Petroleum Geologists 47:441-456.

McKinstry, H. E. 1953. Shears of the second order. American Journal of Science 251:401-414.

Maxwell, J. C. and D. U. Wise. 1958. Wrench-fault tectonics: a discussion. Bulletin of the Geological Society of America 69:927-928.

Menard, H. W. 1955. Deep-sea channels, topography, and sedimentation. Bulletin of the American Association of Petroleum Geologists 39:236-255.

_____ 1960. The East Pacific Rise. Science 132:1737-1746.

_____ 1962. Correlation between length and offset of very large wrench faults. Journal of Geophysical Research 67:4096-4098.

_____ 1964. Marine geology of the Pacific. New York, McGraw-Hill. 271 p.

Merifield, R. M. and D. L. Lamar. 1967. Engineering geology of the central San Clemente Island. China Lake, California. 16 p. (Naval Weapons Center. NWC TP 4469)

Mitchell, E. D., Jr. and F. H. Lipps. 1965. Fossil collecting on San Clemente Island. Pacific Discovery 18 (3):2-8.

Moody, J. D. 1962. Wrench fault tectonics. Mines Magazine 52:22-26.

Moody, J. D. and M. J. Hill. 1956. Wrench-fault tectonics. Bulletin of the Geological Society of America 67:1207-1246.

_____ 1958. Wrench-fault tectonics: a response. Bulletin of the Geological Society America 69:929-930.

_____ 1964. Moody and Hill system of wrench-fault tectonics: a reply. Bulletin of the American Association of Petroleum Geologists 48:112-122.

Moore, D. G. 1966. Structure, litho-orogenic units and post-orogenic basin fill by reflection profiling--California Continental Borderland. Ph.D. thesis. Netherlands, University of Groningen. 151 numb. leaves. (San Diego, U.S. Navy Electronics Laboratory)

Moore, D. G. 1967. Geologist, U. S. Navy Electronics Laboratory. Personal communication. San Diego, California.

Moore, D. G. and E. C. Buffington. 1968. Transform faulting and growth of the Gulf of California since the Late Pliocene. Science 161:1238-1241.

Morgan, W. J. 1968. Rises, trenches, great faults, and crustal blocks. Journal of Geophysical Research 73:1959-1982.

Nettleton, L. I. 1954. Regionals, residuals, and structures. Geophysics 19:1-22.

_____ 1962. Gravity and magnetics for geologists and seismologists. Bulletin of the American Association of Petroleum Geologists 46:1815-1838.

Nevin, C. M. 1949. Principles of structural geology. New York, Wiley. 410 p.

Olmsted, F. H. 1958. Geologic reconnaissance of San Clemente Island, California. U.S. Geological Survey Bulletin 1071-B:55-68.

Opdyke, N. D. et al. 1966. Paleomagnetic study of Antarctica deep-sea cores. Science 349:349-357.

Prucha, J. J. 1964. Moody and Hill system of wrench-fault tectonics: discussion. Bulletin of the American Association of Petroleum Geologists. 48:106-111.

Richter, C. F. 1958. Elementary seismology. San Francisco, Freeman. 768 p.

Roberson, M. I. 1964. Continuous seismic profile survey of Oceanographer, Gilbert, and Lydonia Submarine Canyons, Georges Bank. Journal of Geophysical Research 69

Rod, E. 1958. Application of principles of wrench-fault tectonics of Moody and Hill to northern South America (discussion). Bulletin of the Geological Society of America 69:933-935.

Rusnak, G. A. and R. L. Fisher. 1964. Structural history and evolution of Gulf of California. In: Marine geology of the Gulf of California, ed. by T. H. van Andel and G. G. Shor, Jr. Tulsa, Oklahoma. p. 144-156. (American Association of Petroleum Geologists. Memoir 3)

St.-Amand, P. 1958. Circum-Pacific orogeny. Publications of the Dominion Observatory (Ottawa) 20 (2):403-411.

St.-Amand, P. 1961. The role of lateral faulting in circum-Pacific orogeny--Is the Pacific rotating? (Abstract) In: Proceedings of the Ninth Pacific Science Congress, Bangkok, Thailand, 1957. vol. 12, Bangkok.

St.-Amand, P. and C. R. Allen. 1960. Strike-slip faulting in northern Chile. (Abstract) Bulletin of the Geological Society of America 71:1965.

Shelton, J. S. 1954. Miocene volcanism in coastal southern California. In: Geology of southern California, ed. by R. H. Jahns. Sacramento. p. 31-36. (California. Division of Mines. Bulletin 170)

Shepard, F. P. 1952. Composite origin of submarine canyons. Journal of Sedimentary Petrology 60:84-96.

_____ 1955. Nomenclature based on sand-silt-clay ratios. Journal of Sedimentary Petrology 24:151-158.

_____ 1961. Sea level rise during the past 20,000 years. Zeitschrift für Geomorphologie, sup., 3:30-35.

_____ 1963a. Submarine geology. 2d ed. New York, Harper. 557 p.

_____ 1963b. Thirty-five thousand years of sea level. In: Essays in marine geology in honor of K. O. Emery. Los Angeles, University of Southern California. p. 1-10.

_____ 1965. Types of submarine valley. Bulletin of the American Association of Petroleum Geologists 49:304-310.

Shepard, F. P. and R. F. Dill. 1966. Submarine canyons and other sea valleys. Chicago, Rand-McNally. 381 p.

Shepard, F. P. and K. O. Emery. 1941. Submarine topography off the California coast: canyons and tectonic interpretation. New York. 171 p. (Geological Society of America. Special Paper 31)

Shepard, F. P. and H. E. Seuss. 1956. Rate of post-glacial rise of sea level. Science 123:1082-1083.

Shor, G. G., Jr. and R. W. Raitt. 1958. Seismic studies in the southern California Continental Borderland. In: [Proceedings of the] 20th Congreso Geologico Internacional, Mexico City, 1956. Session 9. Vol 2. Geofisica aplicada. Mexico City, 1958. p. 243-259.

Smith, G. I. 1962. Large lateral displacement on Garlock fault, California. Bulletin of the American Association of Petroleum Geologists 46:85-104.

Smith, P. J. 1967. Paleontologist, U.S. Geological Survey. Personal communication. Menlo Park, California.

Smith, W. S. T. 1898. A geological sketch of San Clemente Island. In: 18th annual report of the U. S. Geological Survey. Part II. Washington, D. C. p. 459-496.

Sonder, R. A. 1947. Discussion of shear patterns of the earth's crust by F. A. Vening Meinesz. Transactions of the American Geophysical Union 28:939-945.

Stride, A. H. 1963. The geology of some continental shelves. In: National Institute of Oceanography, collected reprints. Vol. 11. Surrey, England, Wormley, Godalming. p. 77-88.

Suggate, R. P. 1960. The interpretation of progressive fault displacement of flights of terraces. New Zealand Journal of Geology and Geophysics 3:364-374.

Sugimura, A. and T. Matsuda. 1965. Altera fault and its displacement vectors. Bulletin of the Geological Society of America 76:509-522.

Sverdrup, H. U., M. W. Johnson and R. H. Fleming. 1942. The oceans. New York, Prentice-Hall. 1087 p.

Sykes, L. R. 1968. Seismological evidence for transform faults, sea-floor spreading and continental drift. In: Proceedings of NASA symposium, history of the earth's crust, ed. by R. A. Phinney. Princeton, New Jersey, Princeton University. (In press)

Uchupi, E. 1961. Submarine geology of the Santa Rosa-Cortes Ridge. Journal of Sedimentary Petrology 31:534-545.

U.S. Naval Ordnance Test Station. 1963. Condensed San Clemente Island survey handbook. Rev. of IDP 1219. China Lake, California. 60 p.

van Andel, T. H. and P. L. Sachs. 1964. Sedimentation in the Gulf of Paria during the Holocene transgression; a subsurface acoustic reflection study. Journal of Marine Research 22:30-50.

Vedder, J. C. Geologist, U.S. Geological Survey. Personal communication. Menlo Park, California.

von Huene, R. E. 1967. Geologist, U.S. Geological Survey. Personal communication. Menlo Park, California.

von Huene, R. E. and J. B. Ridlon. 1965. Offshore gravity and magnetic anomalies in the Santa Barbara Channel, California. China Lake, California. 52 p. (U.S. Naval Ordnance Test Station. NOTS TP 3917)

von Huene, R. E. et al. 1967. Geologic interpretation of seismic profiles in Prince William Sound, Alaska. Bulletin of the Geological Society of America 78:259-268.

Warme, J. E. 1967. Geologist, Rice Institute. Personal communication. Houston, Texas.

West, S. S. 1950. Dependence of seismic wave velocity upon depth and lithology. Geophysics 15:653-662.

Wood, H. O. 1947. Earthquake in Southern California with geologic relations. Bulletin of the Seismological Society of America 37:107-157, 217-258.

APPENDICES

APPENDIX I. SUMMARY OF CRUISES OFF SAN CLEMENTE ISLAND

Ship and date	Displacement and length	Scientific crew	Remarks
M/V Defiance 3-5 July 1966	196 tons 136 feet	A. C. Hill[a] J. B. Ridlon[b] D. W. Scholl[c] R. von Huene[c]	Reconnaissance Survey of 58 numbered profiles around the island. Good data and navigational control. Good sea conditions.
M/V Duchess 30 July-9 Aug 1966	..... 25 feet	P. Crampton[d] J. R. Curray[d] W. B. Huckabay[d] J. W. Vernon[d] J. B. Ridlon[b] D. W. Scholl[c]	Detailed Survey off Eel and Lost Points. 59 survey lines plus 8 north of Eel Point. Most data good. Eel Point profiles too highly exaggerated.
Tug YTM-759 21-22 Dec 1966	330 tons 105 feet	L. Brady[b] K. Maxwell[b] A. Nelson[b] J. B. Ridlon[b] G. Stevenson[b]	Recovery of two sedimentary rock samples and a volcanic rock sample by the CURV vehicle.

[a]Geotech Division, Teledyne Industries, Inc., Garland, Texas.
[b]Naval Undersea Research and Development Center, Pasadena, California (formerly the U. S. Naval Ordnance Test Station).
[c]U. S. Geological Survey, Menlo Park, California (formerly with the U. S. Naval Ordnance Test Station).
[d]General Oceanographic Inc., North Hollywood, California.

APPENDIX II. SURVEY METHODS

INSTRUMENTATION

The Reconnaissance Survey was made using a 30- to 120-kilojoule sparker system of the Geotech Division of Teledyne Industries, Inc., Garland, Texas. The basic principles of the sparker system are illustrated in Figure 51. This system employs one to four sets of spark cables towed approximately 45 meters off the stern of a ship for releasing seismic energy (30 kilojoules per cable set) into the water at an equal time rate of discharge. The spark discharge produces a vapor and plasma bubble that couples acoustically with the water around the discharge. This sound source is selected to produce a repeatable pulse containing a broad spectrum that is rich in low frequencies. Omnidirectional low-frequency (mainly 100 to 250 hertz) acoustic energy is developed from the spark discharge followed by the growth and subsequent collapse of the spark bubble. The sea-floor and subsea-floor reflected acoustic signals are picked up by a linear hydrophone array towed approximately 225 meters astern of the survey ship, amplified, and recorded graphically by a facsimile recorder.

In this survey, a 20- to 205-hertz band-pass interval was selected for recording the best balance between depth penetration and resolution of rock structures. A 4-second firing rate was employed in association with a 2-second sweep rate on a modified Raytheon Model (PFR) facsimile recorder with a Geotech Model 26140 signal programmer. Each firing was actuated synchronously at the beginning of each sweep of the recorder that printed across 38-centimeter electrosensitive paper.

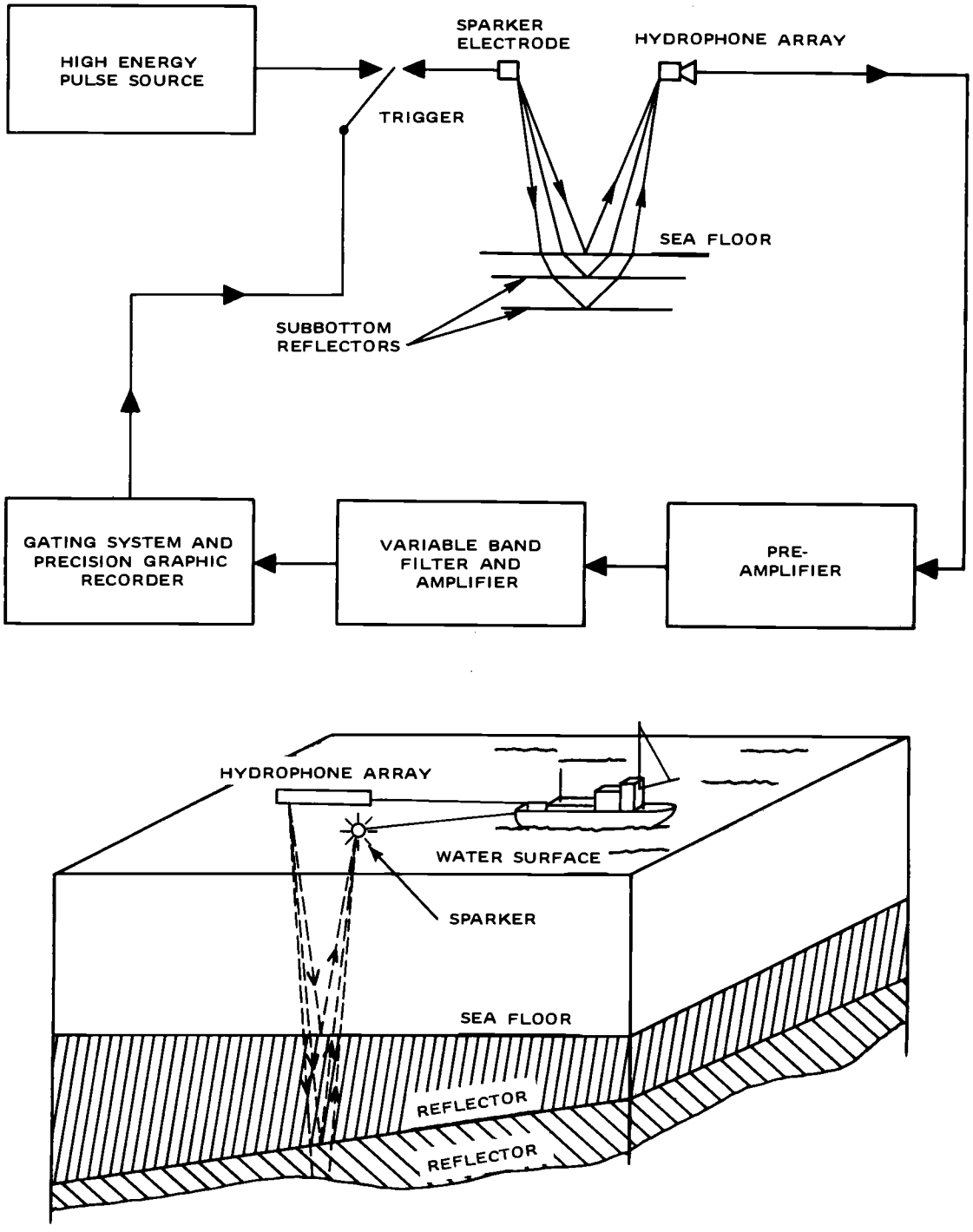

Figure 51. Sparker survey principle.

The Detailed Survey was conducted with seismic profiling equipment operated by the General Oceanographics, Inc., North Hollywood, California. This system is basically the same as that used for the Reconnaissance Survey but uses less power, 750 to 3,000 joules, that allows detailed resolution of upper rock structure. A repetition discharge rate of 1/2 second was coordinated with a 1/4-second sweep interval on a modified Gift (GDR) facsimile recorder. Octave frequency selection varied from 230 to 1,250 hertz, depending upon desired penetration and resolution.

The CURV, operated by personnel from the Naval Undersea Warfare Center, Pasadena, California (now the Naval Undersea Research and Development Center), was used to retrieve submarine rock-strata outcrop samples. This vehicle is designed to operate to a depth of 2,000 feet and is capable of recovering an object weighing a maximum of 1 ton. The vehicle uses a support ship from which it is lowered upon reaching the general area of search. It is equipped with a high resolution sonar, a television camera, a 35-millimeter camera, two mercury vapor lights, and a hydraulically operated recovery claw. The vehicle and equipment are remotely controlled from the support ship at a console equipped with vehicle controls, a sonar analyzer and display, a television monitor, and a compass.

The aeromagnetic instrument used for the measurement of the earth's total intensity field is a Varian airborne, direct-reading, battery-operated, proton precession magnetometer (V-4937-A), with an airborne type of proton sensor. This equipment measures and records the absolute value and changes in the absolute value of the earth's total magnetic

field intensity. Tuning of this instrument covers the range of 20,000 to 100,000 gammas. Readout is made on a chart recorder with a 0 to 99 trace, covering a 5-digit magnetic field intensity significant figure.

NAVIGATION

Both surveys used the Western Electric M-33 fire-control, X-band radar located at three positions on the island for navigational control (Figure 1). This radar uses an automatic X-Y coordinate plotter system and has a specification position accuracy of ±4.5 meters up to several kilometers of range. A radar-beacon transponder was placed aboard the survey craft for the detailed survey. An average transponder delay, measured in microseconds and related to a distance correction of 165 ± 2.7 meters, was compensated for in the radar. Two-way radio communication provided for time and distance synchronization of the facsimile recorder with the radar tracking.

Figure 52 gives an indication of the accuracy of the Detailed Survey. Errors are believed to result mostly from (1) lack of simultaneous marking of events between the radar and the profiling recorder; (2) drafting of the X-Y radar plot; and (3) slope corrections. It is noted, however, that 80% of the crossings have less than a 3-meter difference of depth; 50% have less than 1-meter difference. It is doubtful that much error is attributable to the radar. The individual cumulative error curves for the Lost and Eel Point Grids show that the distance from the radar is not a major error factor; the Lost Point Grid, farther from the radar, contains less cumulative error per difference of depth reading over most of the curve. By inference,

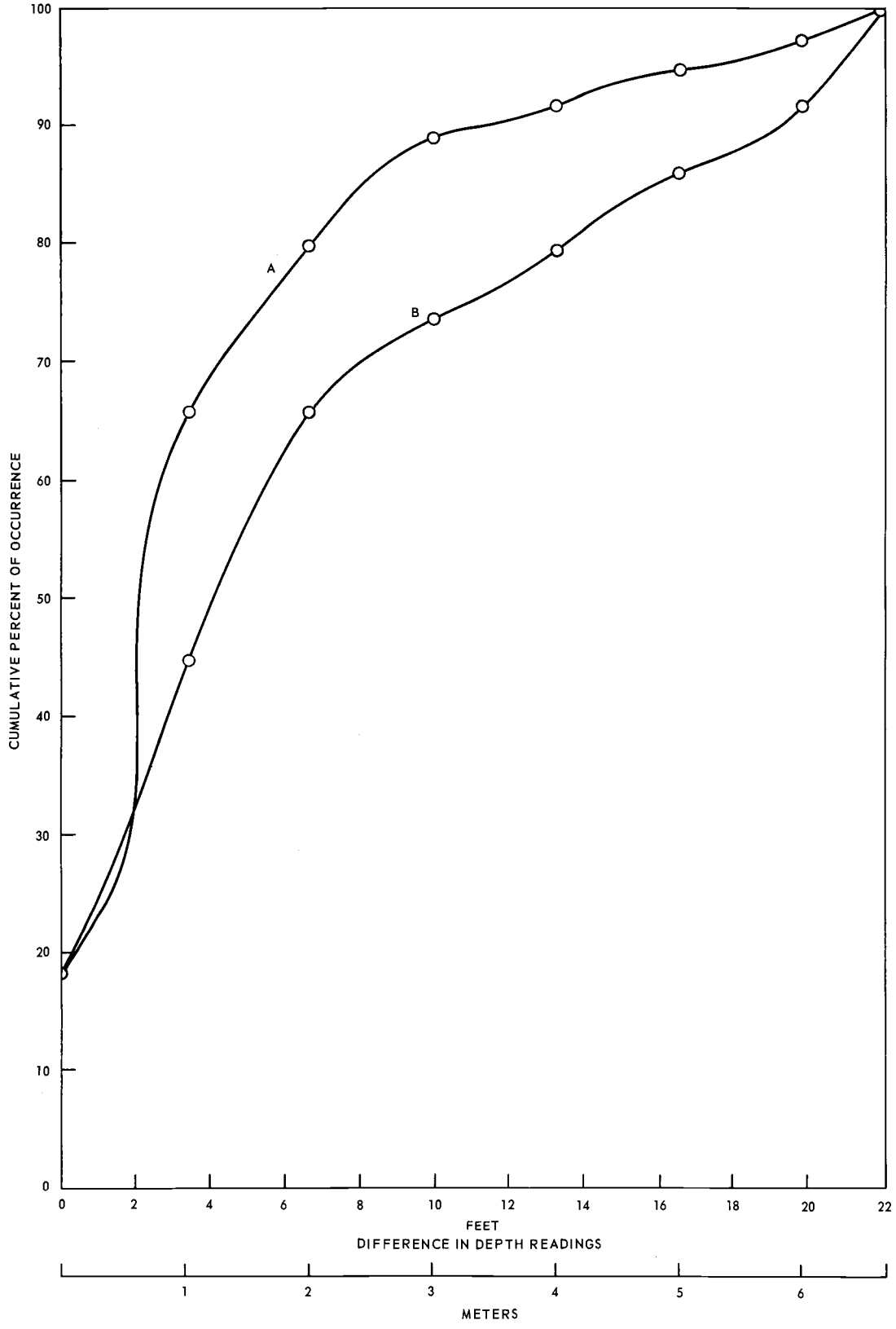
100
90
80
70
60
50
40
30
20
10
0
A
B
CUMULATIVE PERCENT OF OCCURRENCE
0
2
4
6
8
10
12
14
16
18
20
22
FEET
DIFFERENCE IN DEPTH READINGS
1
2
3
4
5
6
METERS

the Reconnaissance Survey is considered relatively accurate in navigational positioning.

The CURV's ship's radar fixed the position of the ship for each recovered outcrop sample. Further sample-position control was provided by the azimuth, dip, and amount of released cable from the ship. CURV instrumentation located on the ship supplied the azimuth of the vehicle relative to the ship. Operation of the CURV was made from the seagoing tug YTM-759, with engines stopped and the tug held as close to position as possible by means of towing by a torpedo recovery boat.

Flight on the aeromagnetic survey was maintained as close as possible to 3,000 feet elevation in a Cessna-180 aircraft; elevation control and positioning were directed by the X-33 fire-control radar located at the highest elevation on the island.

FIELD PROCEDURES

Maximum clarity of geologic features is attained by traverses in the direction of the dip of any strata. Therefore, most lines for both surveys were laid normal to the island shoreline on the assumption that any submarine strata would be dipping away from the island. Profile lines at right angles to those normal to the island were made within the Detailed Survey to identify true dip from apparent dip and provide depth checks of the crossings. Further, profiles at right angles to other profiles often tend to distinguish more clearly the features under study.

CURV operation was primarily over the submarine terrace about 1 to 2 nautical miles from shore at Eel and Lost Points. Subsequent to

the CURV sampling, five dart cores ranging from 2 to 4 feet in length were taken off Eel Point by Global Marine Exploration Company of Los Angeles, California, to further investigate the bottom sediments. Positions for all recovered samples are shown in Figure 2.

APPENDIX III. INTERPRETATION OF SEISMIC RECORDS

GENERAL PROFILE INTERPRETATION

The recording of sea-floor and subsea-floor horizons on a profile displays a continuously correlated pattern of travel times related to those horizons along a given ship's track. Figure 53 is a sample profile showing many features characteristic of continuous seismic reflection profiles. The top edge of the records is the zero line that corresponds to the time of the spark discharge. Close below and parallel to this zero line is the direct arrival signal that has come through the water from the sparking device to the hydrophones. This return is shown as three parallel lines, the uppermost representing the spark discharge that is followed by returns from the growth and collapse of the bubble (bubble plasma). Such a return is normally recorded from most major subsea-floor reflection horizons except where proximity to another horizon causes masking of part of the return signal. Resulting parallel lines from a single reflection horizon may also be caused by a return of the same signal by other than a direct path from source to the reflecting interface. An example of this is the addition of a water-surface reflection that is phase-inverted and displaced in time (Hoskins and Knott, 1961). This parallelism is also believed to be caused more by amplitude excursions resulting from restriction of the bandwidth in electronic filtering and normally occurs as three or four excursions from a 1-octave filter (Moore, 1966; von Huene *et al.*, 1967).

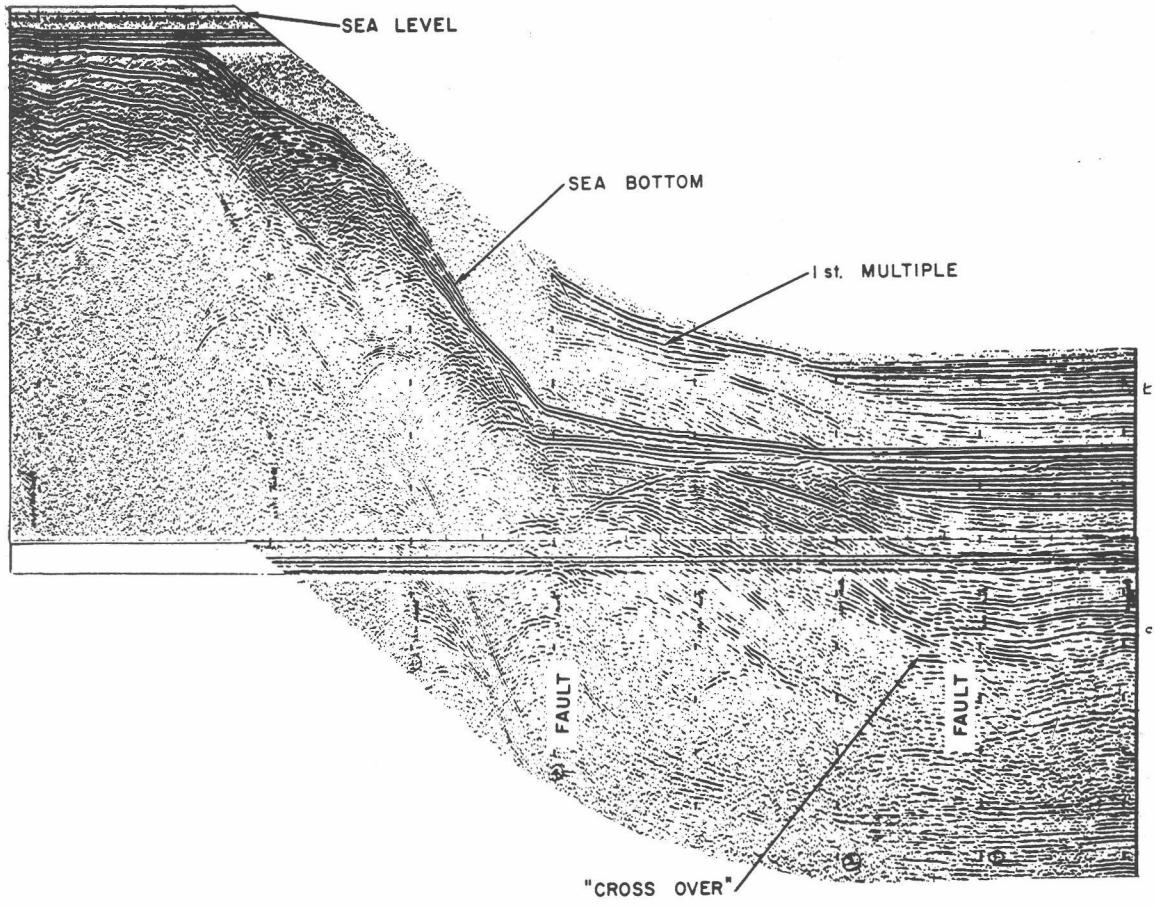

Figure 53. Profile 1 of Reconnaissance Survey showing basic features of continuous seismic-reflection profiles.

At the line of the sea floor in Figure 53 are the reflections from unconsolidated sediments. Below this are reflections from surfaces (sometimes shown as unconformable) of older, consolidated strata represented by parallel reflections extending to various depths. The extremely interlacing hyperbolic pattern below the parallel reflectors is referred to as the acoustic basement in this study; the pattern is interpreted as volcanic rocks that are the equivalent to those comprising the island's land surface.

One of the problems of profile interpretation is that of multiples. This phenomenon occurs as a result of strong reflectors returning to the water-air interface and traveling down again with enough energy to make a second or more round trip. Multiples are often readily seen as equivalents in whole multiple unit distances measured along the vertical scale of the record (Figure 53). The multiple also has twice the slope of the first return. Interpretation becomes complex when multiples overlap subsea-floor reflections on the record. Difficulties of interpretation are generally overcome by a comparison of the shapes of different echo sequences in a given profile accompanied by accurate measurements of travel-time relationships.

Since the sparker sound source is omnidirectional, reflections may be received from any direction. Consequently, it is very possible for a signal to be received from a reflector not directly below the source. Thus, unwanted signals may also occur in the form of side echoes that result from the sound energy being reflected from bathymetric and subsea-floor highs not directly below the sound source

and hydrophone array. This type of return may arrive either earlier or later than those from surfaces directly below.

Resolution is related to the signal length and frequency. Determination of the reflector-layer thickness is limited by the duration and shape of the pulse. Towing the sound source and receiver at approximately 4.5 meters of depth is a common practice for compromise between the requirements of signal and receiving effectiveness and resolution. Consideration of this towing requirement was made during the San Clemente Island surveys.

GEOLOGIC CONSIDERATIONS

Geological analysis of profiles involves four principal steps: (1) basic lithologic interpretation of the acoustic units; (2) correction of the apparent unit thicknesses and depths by the use of known, calculated, or estimated interval velocity of the geologic unit; (3) calculation of true dip and strike from the apparent dip and strike on the profiles after removal of the vertical profile exaggeration; and (4) interpretation of faults and other tectonic features.

It must be recognized that profile reflections represent horizons of acoustic impedance contrasts and are probably keyed to changes of rock types. Also, the vertical scale is a measure of acoustic travel times of the various reflections. The recorder indicated depths that are related to the velocity of sound in water at 1,463 m/sec. Velocities will vary mainly with temperature in water and the physical properties of the rock. Therefore, one of the greatest inherent errors that may be introduced in profile interpretation is that of conversions of

depths or thicknesses of acoustic (rock) units from the records. In this study, interval velocities used for depth and thickness correction were based upon other studies, laboratory sample measurements, and the use of the velocity effect (Roberson, 1964), a mathematical relationship based on the difference between sound velocity in water and the subsea-floor strata at outcrop localities (discussed later).

Vertical exaggeration does not ordinarily become a problem in most records up to a 10 to 15:1 ratio. However, distortions become a much greater exaggeration. This is particularly noticeable in defining dips and changes in the attitude of the strata. Furthermore, it magnifies the error in selecting depth points on the records. Correction for vertical exaggeration was made by the construction of a simple geometric diagram on a transparent overlay. The diagram is drawn with angles based on a 1:1 vertical-to-horizontal ratio for the particular profile exaggeration and placed over the profile for the correction of the slop in question.

Corrections must be made in reading the depths to steep-dipping reflections, since the first return from any horizon by an omni-directional signal will be represented by the time over the shortest distance from the signal source to that horizon. Dips of less than 5 to 10 degrees result in minor corrections. Slope corrections for water depth were made for all submarine slopes greater than 5 degrees on each of the Detailed Survey profiles.

Water depths were averaged at each track intersection. These are listed under Appendix IV.

Subsequent to a correction for the vertical profile exaggeration, an apparent true dip and strike of sedimentary units may be derived by use of stereographic projection from two apparent dips and strikes taken from seismic profile intersections. However, error in the true dip of subsea-floor strata may result from the difference between the rock-unit-interval velocity and that recorded on the profile record. This is particularly true in cases of thinning or thickening of the rock unit in question. A hypothetical case is shown by a simple wedge diagram in Figure 54. Angle A is the dip as shown on the record. A velocity interval correction for the thickness at point X (C + c) results in a larger angle of dip B. The degree of error of dip will depend upon the degree of change in unit thickness over a given horizontal distance. Consequently, the true dip as calculated directly from two apparent dips at profile intersections is actually an apparent true dip or acoustic maximum slope. The actual slope can be calculated only if the velocity of sound in the overlying material is known. Calculation of the true dip becomes tenuous in the case of much rapid horizontal variability in the thickness of the unit in question. In this study, most dips encountered are small and therefore the limit of error between the acoustic maximum slope and the actual true dip of the reflecting horizon is considered to be small. Apparent true dips were calculated for all profile intersections.

Care should be taken in reading strata dip too close to its outcrop on a relatively steep-dipping sea floor, since the velocity effect between the water column and the rock strata may result in a noticeable bend of the reflectors downward toward the outcropping.

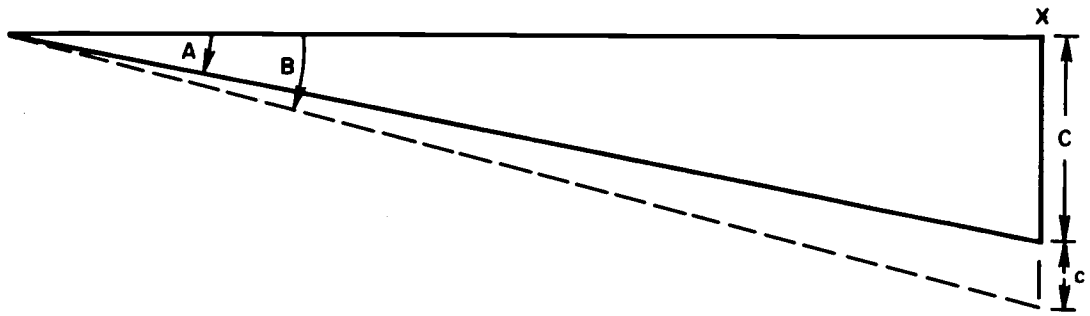

Figure 54. Error of dip resulting from difference between the rock-unit-interval velocity and that recorded on the profile record. A is profile record dip (after vertical exaggeration correction), B is true dip, C is unit thickness recorded on profile record, and c is interval velocity correction.

Interpretation of faulting on seismic profile records is often difficult. Exception to this difficulty is shown where there is obvious displacement of parallel reflectors shown on the records. According to Moore (1966) bedding or fault planes are rarely recorded by echo-ranging techniques on very steep slopes (greater than about 15 degrees). Thus, faults usually must be interpreted from structural offsets and abrupt lithologic changes. In this study, one case is recorded that may possibly represent a fault plane (see Eel Ridge Canyon section) with an apparent 20-degree dip.

One criterion for the recognition of faults is given by Clarke et al. (1961) and is referred to as the low-angle crossover effect. This is a hyperbolic-pattern effect that is often accompanied by a change in dip of the reflectors at the crossover point. This phenomenon is noticed in many of the reconnaissance records; an example is shown in Figure 53. However, care must be taken in the interpretation, as point sources and edges of reflectors diffract or radiate back the impinging signals in all directions and may thus develop hyperbolic patterns by other than a fault feature.

Other problems in fault interpretation develop when (1) different reflectors on either side of a fault may be placed opposite each other and appear to be continuous, particularly when the reflectors are close together, and (2) large vertical exaggeration on the profile records tends to influence a fault interpretation of what might normally be an onlap of sediments at an unconformity.

A method for an approximate determination of interval velocity is referred to as the velocity effect (Roberson, 1964). This is shown

graphically in Figure 55. Where outcrops occur at relatively steep-dipping slopes (such as in canyons), the reflections from a horizontal reflector in the rock will tend to bend downward as the horizon approaches the outcrop. At a point farther down the slope the acoustic signal must travel a greater distance in water. Since the travel time in the rock is greater than in the water, the travel time to the reflector increases with thinning of the rock above the reflector. For horizontal bedding the velocity effect is a function of the velocity in the rock and the water, and the thickness of the rock layer. A simple formula was derived by Roberson (1964) for interval velocity calculation by the velocity effect method as follows:

$$V_s = V_w(t_3 - t_1)/(t_2 - t_1)$$

where V_s is the velocity in the sediment or rock, V_w the velocity in seawater, t_1 the travel time in sea water to the top of the layer, t_2 the travel time in sea water and in rock to the bottom of the layer, and t_3 the travel time in seawater to the bottom of the layer.

In this study, a water velocity of 1,488 m/sec was used in the calculations for V_w.

SAN CLEMENTE ISLAND PROFILES

In this study, selected acoustic units are believed to represent significant geologic units. These units, in turn, are inferred to be sections of sedimentary or igneous rocks and generally unconsolidated, surficial sediments. The terms horizon and reflector, used in this paper, indicate the interface involving acoustical reflections.

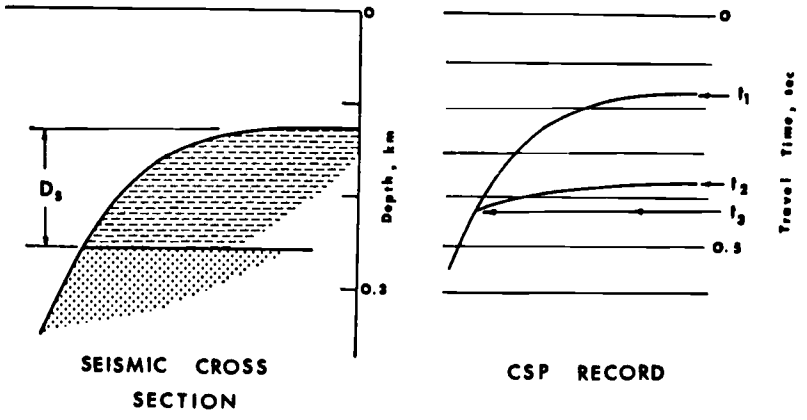

Figure 55. CSP record and the constructed cross section showing the velocity effect and the parameters used in the velocity calculations (from Roberson (1964)).

Correlation between adjacent survey lines is based on (1) the association of related geomorphic or physiologic features, (2) seismic reflection characteristics, (3) nature of unit contacts or sequence of beds, (4) thickness of units, and (5) fault or probable fault trends. Interpretation has been refined by the correction of slopes, stratigraphic dips, and unit thicknesses.

Interpretive line drawings of some of the pertinent profiles (Figures 8 and 22) are shown for clarity of the major structure and lithologic features in the area of study. Vertical exaggeration is noted on each drawing along with symbols referring to various features designated in the interpretation.

Emery (1960) cites criteria for fault origin of sea-floor scarps as straightness, offsets, height, steepness, step-like profiles, and linear depressions at the base. Fault, or probable fault interpretation in the area studied is based upon the following considerations: (1) general bathymetric trends, (2) subsea-floor structural similarities, (3) linearity of features on a plan view map, (4) trend of the island faulting, (5) general structural grain or pattern, (6) abrupt change in lithology (such as from sediments to volcanic rocks that often show as a pocket of sediments or graben fill), (7) low-angle crossover effect, (8) offsets of scarps, and (9) definite break in reflector traces.

In all cases interpretation was based upon a combination of the factors mentioned above. Thus, a number of fault indications may be plotted by marking the points on a structure or geologic map from the corresponding occurrences that appear to display similar characteristics on the profile records.

Various minor changes in the continuity of the reflectors were noticed on the records of both surveys, particularly those of the Detailed Survey. Some of these changes are referred to in this study as lineations. In many cases the alignment of the linear traces with bathymetric offsets was far too good for mere coincidence. The alignment of such features on a map indicates that they are possibly minor normal faults, strike-slip faults, fracture zones, slight distortion of the strata, differential erosional trends (possibly within a fracture or minor fault zone), or undulating flow banding in the volcanic rocks. Where these features tended to be extensive, and particularly to line up with the trends of known island faults, they were interpreted as faults. This interpretation was also given to those lineations that strongly indicate in one or more profiles that they were more likely to be faults.

In most areas, differentiation of post- from pre-orogenic strata was not difficult. However, definition of Unit B was only possible for the Reconnaissance Survey by the use of special playback equipment for the rerun of tapes made on this survey. The rerun filter setting (118 to 245 hertz) resulted in better resolution on the profile records.

There is no information known by the author on interval velocity for Unit B. The interval-velocity correction factor for this unit is derived by inference. Several studies of the geology in the southern California region indicate that the Middle Pliocene was a period of considerable orogeny, with accompanying erosion and deposition during Late Pliocene and Early Pleistocene time. Canyon or submarine channel cut and fills of Late Miocene-Pliocene have been described by

Bartow (1966) and Martin (1963) for Orange County and the area near Bakersfield, California. A compilation of Pliocene interval velocities for the San Joaquin Valley, California, averages 2.08 km/sec (West, 1950). General considerations of the above indicate a probable interval sound velocity ranging between 2.00 and 2.20 km/sec. It is tentatively assumed that Unit B is equivalent to the type and age of the deposits described above. Therefore, an interval-velocity correction factor of 1.4 is considered reasonable for this section; this factor is used to compile the isopach map in Figure 13.

Velocity and porosity determinations have been made on the least weathered portions of the CURV-recovered samples of Unit C by the Chevron Research Corporation, La Habra, California. The results show a velocity range of 3.68 to 4.08 km/sec and an average porosity of 34% for this part of Unit C.

Hamilton (1959) has made an excellent compilation of the relationship between the velocity of elastic compressional waves and the physical properties of sediment and rock. His determinations of velocity on lithified foraminiferal limestone of Cretaceous to Early Tertiary, recovered from Pacific guyots, indicate that such a limestone containing a porosity of 30% normally has a velocity of about 3.50 km/sec. It is noted here that porosity variations greatly outweigh other physical properties in the control of sound velocity. Thin sections of the rock samples from Unit C indicate a porosity of about 25 to 30% for these rocks. This implies a range of 3.50 to 3.70 km/sec. However, Unit C is thought to be lithologically related to the Miocene sedimentary rocks on the island because of proximity and age. The island Miocene

rocks are predominantly clastics containing a variable amount of calcitic cementing agent (Olmsted, 1958), although some siliceous and volcanic materials are also present. On this basis, it is assumed that the average velocity of Unit C is considerably lower than a complete sequence of carbonate rocks.

Variations of velocities of different age rocks with depth have been compiled by Hamilton (1959). The average burial of the Unit C rocks in the area studied is approximately 300 to 350 meters. From Hamilton's curve for Tertiary (post-Eocene) rocks, this depth gives a velocity range of between 2.20 and 2.25 km/sec.

The seismic refraction studies of Shor and Raitt (1958) across the Continental Borderland include the crustal blocks comprising Santa Barbara Island and Tanner Bank, the latter approximately 35 nautical miles southwest of San Clemente Island. These authors calculated a velocity of 2.5 and 2.4 km/sec, respectively, for the uppermost acoustic zone at these localities. This zone includes sediments ranging from Recent to well down into the Tertiary. In a study of Tanner Bank and adjacent Cortes Bank to the west, evidence was found of only Miocene volcanic and sedimentary rocks in 66 bottom samples (Holzman, 1952). The seismic velocity zone at Tanner Bank mentioned above is shown in a cross section by Shor and Raitt (1958) to continue across the northern tip of San Clemente Island; the thickness in these areas (100 meters or less) is well within the average thickness for Unit C. A correction factor based on the velocities derived by Shor and Raitt ranges between 1.60 and 1.67.

Two interval velocities in the general area of interest have been provided by Continental Oil Company, Ventura, California (Bird, 1967). These show ranges from 2.22 to 2.28 km/sec and 1.98 to 2.12 km/sec. The highest of the first range is more representative of the average Miocene interval velocity for southern California and the Continental Borderland (Moore, 1967).

Five measurements of interval velocity, based on the velocity effect (Roberson, 1964) were made on three Profiles (lines 8, 11, and 13) of the Eel Point Grid at the north side of Eel Ridge Canyon (Table 7). Here, the reflectors of Unit C show apparent outcroppings that are nearly horizontal.

TABLE 7. INTERVAL VELOCITY CORRECTION FACTORS DERIVED BY THE VELOCITY EFFECT METHOD.

Profile no.	Interval velocity, km/sec	Correction factor
8	2.29	1.57
11	2.20	1.51
11	2.35	1.61
11	2.25	1.54
13	2.32	1.59
Average	2.28	1.56

A weighted summation of the interval velocity ranges based upon all available data gives a range of 2.26 to 2.32 km/sec for Unit C. An average of this range is 2.28 km/sec, resulting in a correction factor of 1.56. This factor was used for compiling the isopach maps for Unit C.

The limits of profile resolution, density of profiles, and error limits for interval velocity correction factors are the considerations for the isopach map intervals of the various geologic units in the reconnaissance survey.

All profile depth and thickness data were programmed in the UNIVAC 1108 computer (Appendix IV). Velocity correction factors used for Units B and C are based on an average for these units. Correction factors for Units A and X are based on Moore's curve (1966) derived from interval velocities calculated by the wide angle reflection method for post-orogenic sediments. A comparison is made between the calculations for Unit X sediment thickness based on Moore's curve and that derived from the equation of Houtz and Ewing (see Hamilton, 1967b, p. 4211) for determining sediment layer thickness:

$$h = V_o(e^{at} - 1)/a$$

where

h = sediment layer thickness in meters

V_o = sound speed at the sediment surface in meters per second (taken from Figure 18 of Moore, 1966)

e = the base of natural logarithms

a = the linear vertical sound-velocity gradient within the sediment (taken at average of 1.0 sec^{-1})

t = sound travel time in seconds (one way) within the sediment

A 5% greater thickness (about 30 meters for the greatest thickness of Unit X) is noted by using the Houtz and Ewing formula method.

WATER SOUND VELOCITY DATA

Water column sound velocity corrections (Figure 56) were made for the Reconnaissance Survey profile data using a composite of three stations along the east side of the island for the profiles in this area, and a single station located off Seal Cove for the profiles along the west side of the island (Figure 56). Depth intervals of 20 meters were programmed into the computer for this corection. Extrapolation of the curves was made for depths below that covered by the sound velocity survey.

The detailed area bathymetric map is compiled from direct readings taken from the profile records. These readings are based upon an average velocity of sound in water of 1,463 m/sec. From the sound velocity data the approximate average water velocity for the maximum depths (400 to 500 meters) present in the Eel and Lost Point Grid areas is 1,488 m/sec. The difference between the maximum uncorrected readings and that corrected for velocity is considered negligible for the amount of data control for these depths. The limit of error is 2% or approximately 2 meters at the depths over the submerged terrace. This error is considered to be within the order of determination controlled by instrumental characteristics, profile depth reading, drafting, and slope correction.

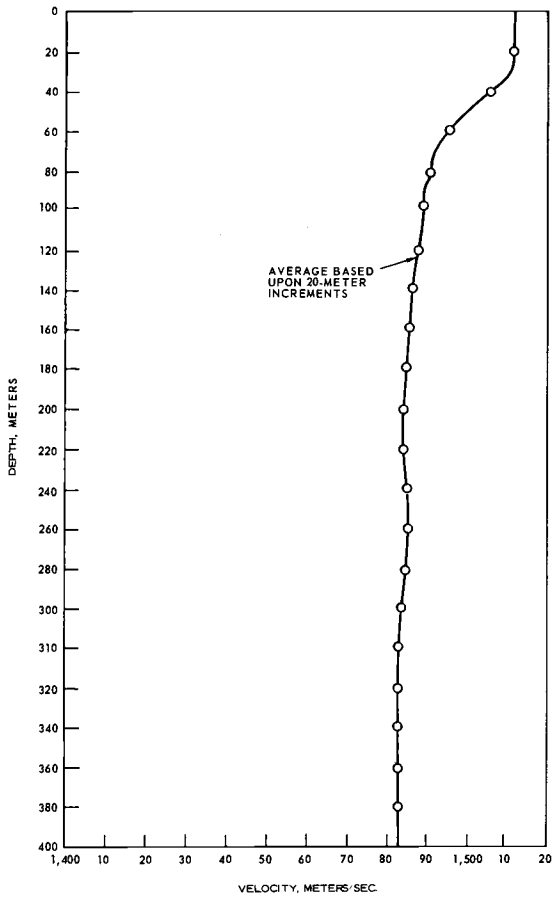
DEPTH, METERS
0
20
40
60
80
100
120
140
160
180
200
220
240
260
280
300
310
320
340
360
380
400
AVERAGE BASED UPON 20-METER INCREMENTS
1,400 10 20 30 40 50 60 70 80 90 1,500 10 20
VELOCITY, METERS/SEC

(a)

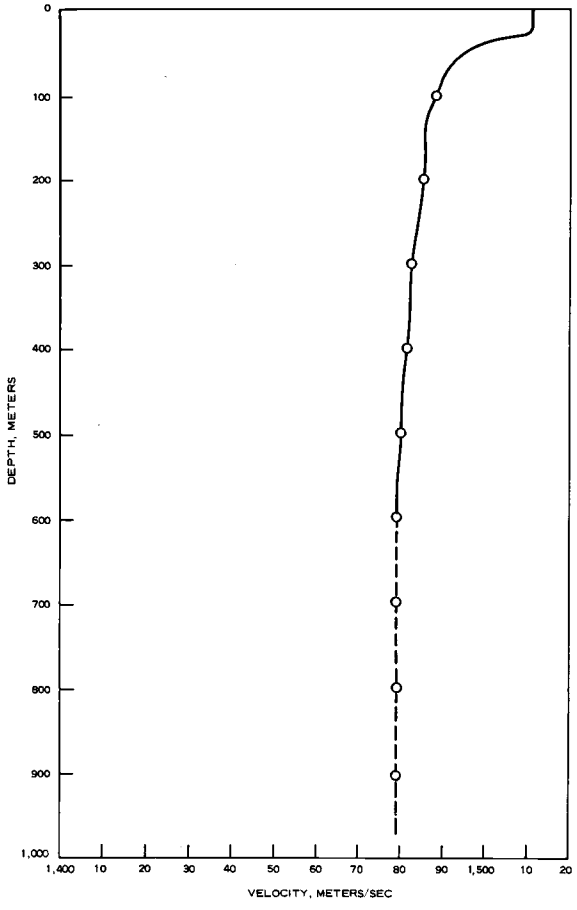
DEPTH, METERS
0
100
200
300
400
500
600
700
800
900
1,000
1,400 10 20 30 40 50 60 70 80 90 1,500 10 20
VELOCITY, METERS/SEC

(b)

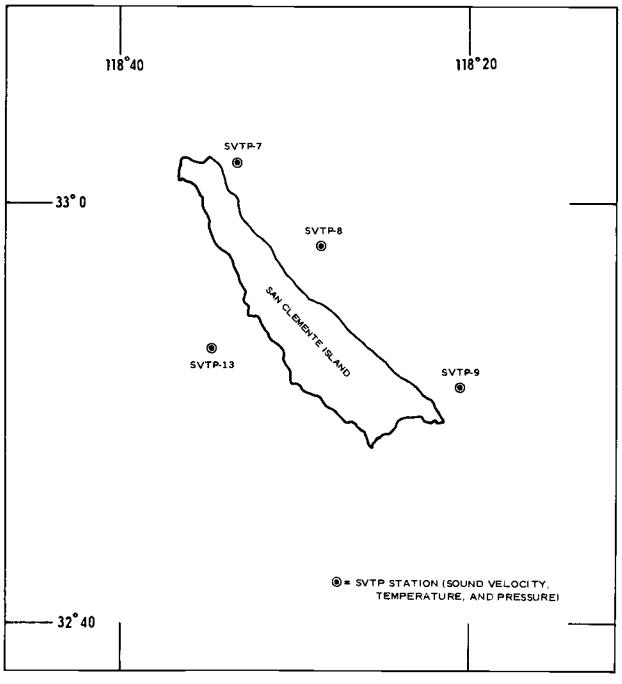
118°40
118°20
33° 0
32° 40
SVTP-7
SVTP-8
SAN CLEMENTE ISLAND
SVTP-13
SVTP-9
⊙= SVTP STATION (SOUND VELOCITY, TEMPERATURE, AND PRESSURE)

(c)

APPENDIX IV. DEPTH AND THICKNESS DATA

DETAILED SURVEY AREA

Station no.	Water depth, m	Corrected thickness of Unit A, m	Corrected thickness of Unit B, m	Corrected thickness of Unit C, m	Depth to Unit D, m
			Line II		
1751.5	173	0	32	169	374
1752.5	132	0	63	180	375
001754	118	0	38	195	351
001757	108	0	0	178	286
001800	98	0	0	114	212
001804	84	0	0	0	84
001805	76	0	0	0	76
001809	38	0	0	0	38
			Line BB-II		
1741.5	220	0	0	0	220
001745	233	0	0	0	233
001750	224	0	0	0	224
			Line BB		
001710	32	0	0	0	32
001715	49	0	0	0	49
001720	58	0	0	0	58
001721	59	0	0	0	59
001725	78	0	0	0	78
1728.5	94	0	0	0	94
001730	99	0	0	78	177
001734	110	0	0	181	291
001735	113	0	0	202	315
001736	117	0	0	221	338
001737	121	0	28	201	350
001738	132	0	48	186	366
001740	207	0	12	153	372

Station no.	Water depth, m	Corrected thickness of Unit A, m	Corrected thickness of Unit B, m	Corrected thickness of Unit C, m	Depth to Unit D, m
			Line BB-CC		
001700	31	0	0	0	31
1702.5	35	0	0	0	35
001705	31	0	0	0	31
001707	30	0	0	1	31
001708	31	0	0	0	31
			Line CC		
001632	137	0	47	?	?
001633	121	0	27	?	?
001634	115	0	0	?	?
001635	109	0	0	?	?
001640	99	0	0	?	?
001645	90	0	0	107	197
164525	84	0	0	75	159
001650	71	0	0	0	71
1655.5	39	0	0	0	39
			Line CC-EE		
1558.5	248	0	0	?	?
001600	251	0	0	?	?
001607	236	0	0	?	?
001610	216	0	0	?	?
001615	216	0	0	?	?
001620	231	0	0	?	?
001625	210	0	0	?	?
1627.5	222	0	0	?	?
001630	179	0	0	?	?
163125	161	0	0	?	?
			Line EE (north)		
1531	36	0	0	0	36
1535	57	7	0	0	64
1536	65	7	0	0	72
1537	71	12	0	0	83
1539	87	0	0	0	87
1542	96	0	0	68	164
1545	103	0	0	189	292
1549	111	0	19	?	?

Station no.	Water depth, m	Corrected thickness of Unit A, m	Corrected thickness of Unit B, m	Corrected thickness of Unit C, m	Depth to Unit D, m
			Line EE (north) (contd.)		
1550	114	0	38	?	?
1551	116	0	55	?	?
1552	120	0	68	?	?
1553	125	0	72	?	?
1554	155	0	46	?	?
1555	182	0	19	?	?
1558	249	0	0	?	?
			Line AA		
0942.5	77	0	0	0	77
000945	60	14	0	0	74
000950	53	0	0	0	53
000955	49	0	0	0	49
000956	53	0	0	0	53
000957	60	0	0	31	91
000958	60	0	0	0	60
000959	71	0	0	41	112
001000	75	0	0	91	166
1002.5	81	0	0	62	143
001005	84	0	0	73	157
1007.5	83	0	0	65	148
001010	84	0	0	66	150
1012.5	82	0	0	52	134
001015	81	0	0	23	104
001020	71	0	0	0	71
001025	64	0	0	0	64
001030	73	0	0	0	73
1032.5	78	0	0	25	103
001035	84	0	0	11	95
1037.5	84	0	0	30	114
001040	84	0	0	30	114
1042.5	85	0	0	19	104
001045	88	0	0	19	107
1047.5	87	0	0	16	103
001050	89	0	0	22	111
1052.5	87	0	0	34	121
001055	85	10	0	43	138
001057	84	14	0	59	157
001058	82	16	0	41	139
001100	77	20	0	53	150

Station no.	Water depth, m	Corrected thickness of Unit A, m	Corrected thickness of Unit B, m	Corrected thickness of Unit C, m	Depth to Unit D, m
Line AA (contd.)					
1102.5	71	22	0	37	128
001105	60	25	0	19	104
001106	57	12	0	0	69
001107	45	0	0	0	45
001108	29	0	0	0	29
001109	32	0	0	0	32
001110	41	0	0	0	41
001111	45	0	0	0	45
001112	46	6	0	0	52
001113	47	12	0	0	59
1114.5	48	12	0	0	60
1116.5	63	0	0	0	63
1117.0	72	13	0	0	85
112025	93	0	0	35	128
1122.5	106	0	0	0	106
1123.5	110	0	36	39	185
001125	114	0	70	62	246
001127	123	0	112	101	336
001128	155	0	94	157	406
001130	227	0	33	167	427
001132	269	0	0	164	433
001135	300	0	0	135	435
001140	359	0	0	57	416
001145	391	0	0	41	432
Eel Point Grid					
A1	60	6	0	0	66
B1	51	21	0	0	72
C1	39	37	0	0	76
A2	64	21	0	3	88
B2	59	23	0	6	88
C2	46	38	0	9	93
A3	78	26	0	34	138
B3	74	21	0	46	141
C3	64	28	0	66	158
D3	45	0	0	0	45
E3	42	0	0	0	42
F3	39	11	0	0	50
G3	40	6	0	0	45
H3	41	20	0	0	61

Station no.	Water depth, m	Corrected thickness of Unit A, m	Corrected thickness of Unit B, m	Corrected thickness of Unit C, m	Depth to Unit D, m
Eel Point Grid (contd.)					
I3	40	0	0	0	40
J3	44	0	0	0	44
K3	57	19	0	14	90
DD3	41	0	0	0	41
3.5F	43	14	0	0	57
3.5G	47	13	0	0	60
3.5H	53	9	0	0	62
3.5I	51	8	0	0	59
3.5J	48	0	0	0	48
3.5K	73	0	0	19	92
A4	87	14	0	70	171
B4	82	15	0	83	180
C4	85	12	0	103	200
D4	63	0	0	0	63
E4	49	0	0	0	49
F4	51	12	0	0	63
G4	56	10	0	0	66
H4	66	8	0	0	74
I4	70	10	0	0	80
J4	78	0	0	0	78
K4	87	0	0	43	130
DD4	48	0	0	0	48
EE4	51	0	0	0	51
A5	98	14	0	113	225
B5	100	5	0	105	210
C5	124	0	0	127	251
D5	117	0	0	0	117
E5	65	0	0	0	65
F5	70	7	0	0	77
G5	77	11	0	0	88
H5	87	0	0	0	87
I5	93	0	0	17	110
J5	108	0	9	16	133
K5	102	0	36	93	231
DD5	85	0	0	0	85
EE5	71	0	0	0	71
A6	112	8	0	145	265
B6	163	0	0	113	276
C6	173	0	0	107	280
D6	178	0	10	45	233
E6	114	0	0	0	114

Station no.	Water depth, m	Corrected thickness of Unit A, m	Corrected thickness of Unit B, m	Corrected thickness of Unit C, m	Depth to Unit D, m
Eel Point Grid (contd.)					
F6	101	0	0	0	101
G6	89	0	0	0	89
H6	103	0	0	23	126
I6	111	0	12	19	142
J6	111	0	49	42	202
K6	112	0	78	82	272
DD6	151	0	32	64	247
EE6	112	0	0	0	112
A7	127	0	9	159	295
B7	200	0	0	129	329
C7	248	0	0	85	333
D7	238	0	0	101	339
E7	170	0	64	95	329
F7	135	0	94	88	317
G7	127	0	39	57	223
H7	117	0	25	63	205
I7	116	0	110	71	297
J7	126	0	107	81	314
K7	180	0	45	114	339
DD7	202	0	51	76	329
EE7	152	0	81	85	318
A8	148	0	0	211	359
B8	235	0	0	112	347
C8	274	0	0	106	380
D8	296	0	0	68	364
E8	251	0	33	92	376
F8	233	0	44	102	379
G8	213	0	30	135	378
H8	183	0	19	105	307
I8	190	0	56	128	374
J8	223	0	59	131	413
K8	247	0	18	151	416
DD8	276	0	13	81	370
EE8	247	0	26	99	372
A9	141	0	25	240	406
B9	242	0	0	129	371
C9	291	0	0	92	383
D9	324	0	0	55	379
E9	294	0	0	108	402
F9	284	0	12	114	410
G9	276	0	3	141	420

Station no.	Water depth, m	Corrected thickness of Unit A, m	Corrected thickness of Unit B, m	Corrected thickness of Unit C, m	Depth to Unit D, m
Eel Point Grid (contd.)					
H9	254	0	0	193	447
I9	251	0	30	159	440
J9	280	0	34	121	435
K9	301	0	0	150	451
DD9	310	0	0	78	388
EE9	259	0	0	114	403
A10	176	0	0	233	409
B10	209	0	0	212	421
C10	281	0	0	124	405
D10	333	0	0	64	397
E10	324	0	0	88	412
F10	321	0	0	107	428
G10	310	0	0	142	452
H10	291	0	0	196	487
I10	295	0	17	188	500
J10	309	0	0	194	503
K10	342	0	0	152	494
DD10	340	0	0	64	404
EE10	324	0	0	94	418
A11	201	0	0	233	434
B11	216	0	0	229	445
C11	282	0	0	137	419
D11	333	0	0	74	407
E11	348	0	0	89	437
F11	349	0	0	109	458
G11	317	0	0	172	489
H11	304	0	0	204	508
I11	323	0	0	188	511
J11	326	0	0	194	520
K11	356	0	0	154	512
DD11	358	0	0	61	419
EE11	356	0	0	86	442
A12	230	0	0	218	448
B12	239	0	0	213	452
C12	287	0	0	141	428
D12	330	0	0	103	433
E12	368	0	0	72	440
F12	365	0	0	91	456
G12	342	0	0	136	478
H12	329	0	0	171	500
I12	341	0	0	170	511

Station no.	Water depth, m	Corrected thickness of Unit A, m	Corrected thickness of Unit B, m	Corrected thickness of Unit C, m	Depth to Unit D, m
Eel Point Grid (contd.)					
J12	346	0	0	173	519
K12	351	0	0	179	530
DD12	359	0	0	77	436
EE12	376	0	0	64	440
A13	267	0	0	215	482
B13	275	0	0	212	487
C13	287	0	0	196	483
D13	360	0	0	84	444
E13	383	0	0	86	469
F13	376	0	0	99	477
G13	351	0	0	169	520
H13	352	0	0	171	523
I13	359	0	0	176	535
J13	377	0	0	148	525
K13	366	0	0	191	557
DD13	365	0	0	95	460
EE13	404	0	0	58	462
Line FF					
1210	93	5	0	4	102
1211	80	12	0	0	92
1212	74	14	0	0	88
1213	66	6	0	0	72
1214	49	0	0	0	49
1215	35	0	0	0	35
1205	111	0	87	81	279
1204	115	0	102	71	288
1200.5	201	0	55	100	356
1200	223	0	37	109	369
Line FF-GG					
001217	31	0	0	0	31
01220	32	0	0	0	32
001225	34	0	0	0	34
001227	36	0	0	0	30
Line GG					
1230	27	0	0	0	27
1235	59	0	0	0	59
1236	66	17	0	0	83

Station no.	Water depth, m	Corrected thickness of Unit A, m	Corrected thickness of Unit B, m	Corrected thickness of Unit C, m	Depth to Unit D, m
			Line GG (contd.)		
1237	73	6	0	0	79
1237½	74	10	0	0	84
1238	78	18	0	0	96
1239	85	6	0	0	91
1240	90	0	0	18	108
1245	105	0	0	111	216
			Line GG-HH		
1310	338	0	0	0	338
1315	373	0	0	0	373
1320	398	0	0	0	398
1325	434	0	0	0	434
1327	438	0	0	0	438
1330	448	0	0	0	448
			Line HH		
1331	448	0	0	0	448
1335	415	0	0	0	415
1338	374	0	0	0	374
1341	334	0	0	54	388
1344	234	0	19	145	398
1348	138	0	61	200	399
1351	113	0	58	185	356
1355	106	0	0	185	291
1400	96	0	0	121	217
1405	84	0	0	0	84
1410	48	0	0	0	48
1412¼	32	0	0	0	32
			Line HH-GG-FF		
1412.5	31	0	0	0	31
1415	33	0	0	0	33
1420	43	13	0	0	56
1421	44	16	0	0	60
1422	46	18	0	0	64
1423	46	8	0	0	54
1424	49	18	0	0	67
1425	49	14	0	0	63

Station no.	Water depth, m	Corrected thickness of Unit A, m	Corrected thickness of Unit B, m	Corrected thickness of Unit C, m	Depth to Unit D, m
			Line HH-GG-FF		
1426	54	13	0	0	67
1427	58	20	0	0	78
1428	64	20	0	0	84
1429	68	14	0	0	82
1430	71	7	0	0	78
Pt. K	73	6	0	0	79
1432	80	14	0	0	94
1433	79	14	0	0	93
1435	53	0	0	0	53
1436	63	8	0	0	71
1437	60	0	0	0	60
1440	65	4	0	0	69
1441	68	14	0	0	82
1442	72	12	0	0	84
1443	73	22	0	0	95
1444	77	11	0	0	88
1445	79	8	0	0	87
1446	82	19	0	0	101
1447	75	8	0	0	93
1448	75	22	0	50	152
1449	80	20	0	8	108
1450	79	14	0	5	98
1451	74	18	0	37	129
1452	58	7	0	0	65
			Extension #6 to GG		
001440	115	0	89	66	270
1445	110	0	84	71	265
1450	107	0	63	100	270
1455	105	0	19	133	257
1436	124	0	69	98	291
			Extension #6 to HH		
1102	106	0	24	143	273
1104	105	0	19	142	266
1107	104	0	29	143	276
1112	101	0	16	156	273
1114	101	0	0	163	264
1117	100	0	0	166	266
1119.5	95	0	0	145	240

Station no.	Water depth, m	Corrected thickness of Unit A, m	Corrected thickness of Unit B, m	Corrected thickness of Unit C, m	Depth to Unit D, m
			Extension #5 to GG		
1506	97	0	0	66	163
1510	102	0	35	44	177
1515	104	0	49	62	215
1520	103	0	47	67	217
1518	104	0	46	73	223
			Lost Point Grid		
L1	31	0	0	0	31
L2	45	0	0	0	45
L3	57	0	0	0	57
L4	74	0	0	0	74
L5	89	5	0	55	149
L6	96	0	0	119	215
L7	102	0	0	154	256
L8	106	0	25	167	298
L9	111	0	60	173	344
L10	117	0	91	166	374
L11	186	0	25	162	373
L12	253	0	0	118	371
L13	309	0	0	60	369
Begn L	31	0	0	0	31
End L	383	0	0	0	383
M1	32	0	0	0	32
M2	43	0	0	0	43
M3	53	0	0	0	53
M4	69	0	0	0	69
M5	86	8	0	40	134
M6	96	0	0	106	202
M7	99	0	0	144	243
M8	103	0	0	190	293
M9	110	0	36	174	320
M10	121	0	66	169	356
M11	207	0	0	152	359
M12	272	0	0	94	366
M13	335	0	0	43	378
Begn M	376	0	0	16	392
End M	37	0	0	0	37
N2	32	0	0	0	32
N3	51	0	0	0	51
N4	67	0	0	0	67

Station no.	Water depth, m	Corrected thickness of Unit A, m	Corrected thickness of Unit B, m	Corrected thickness of Unit C, m	Depth to Unit D, m
Lost Point Grid (contd.)					
N5	85	0	0	0	85
N6	94	0	0	72	166
N7	99	0	0	120	219
N8	101	0	0	151	252
N9	111	0	29	169	309
N10	124	0	80	140	344
N11	220	0	0	120	340
N12	275	0	0	78	353
N13	317	0	0	54	371
Begn N	32	0	0	0	32
Eng N	373	0	0	40	413
02	37	0	0	0	37
03	55	4	0	0	59
04	69	10	0	0	79
05	83	10	0	0	93
06	93	0	0	65	158
07	99	0	0	99	198
08	104	0	0	136	240
09	111	0	43	127	281
010	128	0	99	93	320
011	223	0	15	83	321
012	272	0	0	66	338
013	313	0	0	35	348
Begn 0	357	0	0	12	369
End 0	31	0	0	0	31
02.5	46	0	0	0	46
P2	40	0	0	0	40
P3	53	0	0	0	53
P4	66	0	0	0	66
P5	83	11	0	15	109
P6	92	2	0	50	144
P7	99	0	0	78	177
P8	105	0	0	120	225
P9	111	0	35	125	271
P10	140	0	59	127	310
P11	188	0	15	123	326
P12	229	0	0	111	340
P13	266	0	0	80	346
Begn P	36	0	0	0	36
End P	324	0	0	17	341
2.5P	45	0	0	0	45

Station no.	Water depth, m	Corrected thickness of Unit A, m	Corrected thickness of Unit B, m	Corrected thickness of Unit C, m	Depth to Unit D, m
Lost Point Grid (contd.)					
Q1	31	0	0	0	31
Q2	40	0	0	0	40
Q3	51	0	0	0	51
Q4	59	0	0	0	59
Q5	86	6	0	2	94
Q6	93	0	0	53	146
Q7	98	0	0	92	190
Q8	104	0	0	132	236
Q9	110	0	17	143	270
Q10	118	0	59	116	293
Q11	143	0	57	119	319
Q12	218	0	0	110	328
Q13	255	0	0	87	342
Begn Q	256	0	0	84	340
End Q	29	0	0	0	29
R1	29	0	0	0	29
R2	43	5	0	0	48
R3	56	13	0	0	69
R4	67	0	0	0	67
R5	85	7	0	3	95
R6	96	0	0	43	139
R7	99	0	0	73	172
R8	103	0	0	99	202
R9	112	0	0	129	241
R10	118	0	37	116	271
R11	141	0	60	106	307
R12	222	0	0	111	333
R13	274	0	0	56	330
Begn R	29	0	0	0	29
End R	307	0	0	23	330
S1	32	0	0	0	32
S2	42	0	0	0	42
S3	60	0	0	0	60
S4	75	8	0	0	83
S5	90	7	0	14	111
S6	97	4	0	45	146
S7	101	0	0	86	187
S8	106	0	0	118	224
S9	111	0	0	140	251
S10	118	0	42	110	270
S11	167	0	41	96	304

Station no.	Water depth, m	Corrected thickness of Unit A, m	Corrected thickness of Unit B, m	Corrected thickness of Unit C, m	Depth to Unit D, m
			Lost Point Grid (contd.)		
S12	244	0	0	101	345
S13	292	0	0	55	347
Begn S	344	0	0	14	358
End S	30	0	0	0	30
T1	34	0	0	0	34
T2	45	0	0	0	45
T3	64	0	0	0	64
T4	85	9	0	8	102
T5	92	5	0	45	142
T6	98	0	0	49	147
T7	99	0	0	73	174
T8	106	0	0	116	222
T9	112	0	0	132	244
T10	118	0	45	110	273
T11	182	0	18	85	285
T12	246	0	0	101	347
T13	295	0	0	73	368
Begn T	36	0	0	0	36
End T	335	0	0	70	405
End 13	295	0	0	105	400
			Extension #13		
1422.5	290	0	0	105	395
1425.5	286	0	0	95	381
1428.5	280	0	0	9	289
1432.5	137	0	0	0	137
1434	124	0	0	0	124
1437	252	0	0	0	252
1458	379	0	0	0	379
1459	335	0	0	0	335
1500	271	0	0	0	271
1503	143	0	0	0	143
1504.5	129	0	0	0	129
1506	150	0	0	0	150
1509	225	0	0	52	277
1512	210	0	0	93	303
1515	155	0	30	95	280
1518	115	0	37	123	275
1519	114	0	0	133	247
1520	114	0	0	147	261

Station no.	Water depth, m	Corrected thickness of Unit A, m	Corrected thickness of Unit B, m	Corrected thickness of Unit C, m	Depth to Unit D, m
Extension #13 (contd.)					
1521	113	0	0	145	258
1524	109	0	0	119	228
1527	105	0	0	101	206
1530	105	0	0	83	188

RECONNAISSANCE SURVEY AREA

Station No.	Water depth, m	Corrected thickness of Unit B, m	Corrected thickness of Unit X, m	Corrected thickness of Unit C, m	Depth to Unit D, m
			LINE 27A		
CROSSING	83.1	.0	.0	.0	83.1
BEGIN LINE 27A	84.5	.0	.0	91.3	175.8
1/10	81.2	.0	.0	136.9	218.2
2/10	78.3	.0	.0	182.6	260.9
3/10	75.4	.0	.0	187.2	262.5
4/10	66.6	.0	.0	173.5	240.1
5/10	65.2	.0	.0	.0	65.2
6/10	65.2	.0	.0	111.8	177.0
7/10	68.1	.0	.0	75.3	143.4
8/10	71.0	.0	.0	98.1	169.1
9/10	71.0	.0	.0	143.8	214.8
END LINE 27A	72.5	.0	.0	219.1	291.6
			LINE 27		
END LINE 27	84.5	.0	.0	.0	84.5
1/3	93.3	.0	.0	41.1	134.4
2/3	100.6	.0	.0	157.5	258.1
MILE 3	105.3	.0	.0	273.9	379.2
1/5	108.2	.0	.0	303.6	411.8
2/5	109.7	.0	.0	408.5	518.2
3/5	112.6	38.9	.0	470.2	621.7
4/5	200.2	20.5	.0	447.3	668.1
MILE 2	262.4	.0	.0	442.8	705.2
1/5	310.1	.0	.0	429.1	739.2
2/5	333.8	.0	.0	447.3	781.2
3/5	360.5	.0	.0	438.2	798.7
4/5	381.4	.0	.0	447.3	838.7

MILE 1	393.4	.0	.0	451.9	845.3
1/5	402.2	.0	.0	442.8	845.0
2/5	416.8	.0	.0	447.3	864.1
3/5	446.4	.0	.0	438.2	884.6
4/5	476.7	.0	.0	433.6	910.3
BEGIN LINE 27	509.0	.0	.0	392.6	901.6

LINE 28

START LINE 28	65.2	.0	.0	95.9	161.0
1/5	75.4	.0	.0	159.8	235.2
2/5	83.1	.0	.0	294.4	377.5
3/5	84.5	.0	.0	397.1	481.7
4/5	87.5	.0	.0	447.3	534.8
MILE 1	90.4	.0	.0	502.1	592.5
1/5	96.2	.0	.0	547.8	644.0
2/5	102.1	.0	.0	543.2	645.3
3/5	105.3	.0	.0	547.8	653.1
4/5	109.7	55.3	.0	547.8	712.7
MILE 2	173.5	32.8	.0	497.6	703.8
1/5	220.9	.0	.0	547.8	768.7
2/5	262.4	.0	.0	529.5	791.9
3/5	295.1	.0	.0	529.5	824.6
4/5	339.7	.0	.0	515.8	855.5
MILE 3	384.3	.0	.0	506.7	891.0
1/5	416.8	.0	.0	502.1	918.9
2/5	446.4	.0	.0	511.2	957.6
3/5	467.6	.0	.0	524.9	992.5
4/5	494.0	.0	.0	524.9	1019.0
MILE 4	520.7	.0	.0	524.9	1045.6
END LINE 28	550.6	.0	.0	511.2	1061.8

LINE 29

END LINE 29	90.4	.0	.0	171.2	261.6
1/5	93.3	.0	.0	178.0	271.3
2/5	94.8	.0	.0	301.3	396.0
3/5	96.2	.0	.0	356.0	452.3
4/5	97.7	.0	.0	502.1	599.8
MILE 3	100.6	.0	.0	504.4	605.0
1/5	102.1	28.7	.0	515.8	646.6
2/5	114.1	57.4	.0	524.9	696.4
3/5	182.3	36.9	.0	511.2	730.4
4/5	236.0	.0	.0	534.1	770.0

MILE 2	286.3	.0	.0	524.9	811.2
1/5	330.9	.0	.0	497.6	828.5
2/5	369.7	.0	.0	502.1	871.8
3/5	405.1	.0	.0	493.0	898.1
4/5	428.8	.0	.0	474.7	903.6
MILE 1	458.8	.0	.0	470.2	928.9
1/5	494.0	.0	.0	474.7	968.8
2/5	526.6	.0	.0	488.4	1015.0
3/5	553.5	.0	.0	465.6	1019.1
4/5	583.1	.0	.0	461.0	1044.1
BEGIN LINE 29	606.8	.0	.0	447.3	1054.2
29 TO 28 (0)	613.0	.0	.0	442.8	1055.8
1/4	603.9	.0	.0	451.9	1055.8
2/4	595.1	.0	.0	456.5	1051.6
3/4	595.1	.0	.0	470.2	1065.3
T.P. TO 28	595.1	.0	.0	506.7	1101.8

LINE 29A

BEGIN LINE 29A	79.8	.0	.0	89.0	168.8
1/5	75.4	.0	.0	68.5	143.9
2/5	69.5	.0	.0	45.6	115.2
3/5	61.8	.0	.0	.0	61.8
4/5	55.9	.0	.0	.0	55.9
END LINE 29A	54.5	.0	.0	.0	54.5

LINE 30

START LINE 30	63.7	.0	.0	.0	63.7
1/4	66.6	.0	.0	.0	66.6
2/4	72.5	.0	.0	.0	72.5
3/4	75.4	.0	.0	.0	75.4
MILE 1	83.1	.0	.0	25.1	108.2
1/5	88.9	.0	.0	102.7	191.6
2/5	91.8	.0	.0	198.6	290.4
3/5	93.3	.0	.0	273.9	367.2
4/5	94.8	.0	.0	312.7	407.5
MILE 2	97.7	14.3	.0	360.6	472.6
1/5	102.1	45.1	.0	388.0	535.1
2/5	105.3	57.4	.0	388.0	550.6
3/5	146.9	55.3	.0	358.3	560.5
4/5	206.3	4.1	.0	378.9	589.3

MILE 3	236.0	.0	.0	401.7	637.7
1/5	261.0	.0	.0	417.7	678.6
2/5	283.0	.0	.0	465.6	748.6
3/5	318.9	.0	.0	447.3	766.2
4/5	345.5	.0	.0	483.9	829.4
MILE 4	372.6	.0	.0	447.3	819.9
1/5	402.2	.0	.0	497.6	899.8
2/5	434.7	.0	.0	479.3	914.0
3/5	517.8	.0	.0	420.0	937.7
4/5	532.7	.0	.0	493.0	1025.7
END LINE 30	553.5	.0	.0	543.2	1096.7

LINE 31

END LINE 31	93.3	.0	.0	41.1	134.4
1/5	94.8	.0	.0	43.4	138.1
2/5	96.2	.0	.0	27.4	123.6
3/5	84.5	.0	.0	.0	84.5
4/5	99.2	.0	.0	168.9	268.1
MILE 4	99.2	.0	.0	146.1	245.2
1/5	99.2	.0	.0	45.6	144.8
2/5	96.2	.0	.0	45.6	141.9
3/5	78.3	.0	.0	.0	78.3
4/5	75.4	.0	.0	.0	75.4
MILE 3	78.3	.0	.0	.0	78.3
1/5	93.3	.0	.0	45.6	139.0
2/5	99.2	.0	.0	41.1	140.2
3/5	93.3	.0	.0	.0	93.3
4/5	111.1	57.4	.0	77.6	246.1
MILE 2	129.0	69.6	.0	182.6	381.3
1/5	197.3	6.1	.0	362.9	566.4
2/5	236.0	.0	.0	461.0	697.0
3/5	280.1	.0	.0	502.1	782.2
4/5	342.6	.0	.0	524.9	867.6
MILE 1	387.6	.0	.0	561.5	949.0
1/5	405.1	.0	.0	529.5	934.7
2/5	424.1	.0	.0	477.0	901.1
3/5	446.4	.0	.0	465.6	912.0
4/5	467.6	.0	.0	493.0	960.5
END LINE 31	476.7	.0	.0	511.2	987.9
31 TO 30 (0)	520.7	.0	.0	552.3	1073.0
1/3	538.6	.0	.0	534.1	1072.6
2/3	562.3	.0	.0	556.9	1119.2
T.P. TO 30	580.2	.0	.0	584.3	1164.5

LINE 32

BEGIN LINE 32	94.8	.0	.0	43.4	138.1
1/5	99.2	.0	.0	45.6	144.8
2/5	105.3	.0	.0	59.3	164.6
3/5	109.7	.0	.0	143.8	253.5
4/5	112.6	6.1	.0	264.8	383.5
MILE 1	114.1	34.8	.0	244.2	393.1
1/5	115.5	63.5	.0	232.8	411.8
2/5	164.7	41.0	.0	251.1	456.7
3/5	209.2	.0	.0	251.1	460.3
4/5	253.7	.0	.0	205.4	459.1
MILE 2	280.1	.0	.0	187.2	467.2
1/5	313.0	.0	.0	182.6	495.6
2/5	333.8	.0	.0	173.5	507.3
3/5	351.8	.0	.0	123.2	475.0
4/5	364.9	.0	.0	102.7	467.6
MILE 3	363.5	.0	.0	82.2	445.6
1/3	350.3	.0	.0	79.9	430.2
2/3	379.9	.0	.0	79.9	459.8
END LINE 32	394.9	.0	.0	79.9	474.8

LINE 33

BEGIN LINE 33	362.0	.0	19.1	123.2	504.3
1/5	336.8	.0	.0	123.2	460.0
2/5	300.9	.0	.0	86.7	387.7
3/5	261.0	.0	.0	79.9	340.9
4/5	233.0	.0	.0	100.4	333.5
MILE 1	216.5	.0	.0	125.5	342.1
1/5	204.8	.0	.0	143.8	348.6
2/5	188.5	.0	.0	168.9	357.4
3/5	173.5	45.1	.0	187.2	405.7
4/5	155.7	49.2	.0	232.8	437.6
MILE 2	124.7	79.9	.0	178.0	382.6
1/5	119.9	69.6	.0	219.1	408.7
2/5	115.5	36.9	.0	239.6	392.0
3/5	112.6	.0	.0	239.6	352.3
4/5	109.7	.0	.0	130.1	239.8
MILE 3	102.1	.0	.0	95.9	197.9
1/4	97.7	.0	.0	34.2	131.9
2/4	83.1	.0	.0	.0	83.1
3/4	72.5	.0	.0	.0	72.5
MILE 4	57.4	.0	.0	.0	57.4
END LINE 33	48.6	.0	.0	.0	48.6

LINE 34

35 TO 34 (1/2)	399.3	.0	.0	278.4	677.7
BEGIN LINE 34	409.5	.0	69.3	178.0	656.8
MILE 1	402.2	.0	61.9	86.7	550.8
1/5	392.0	.0	54.5	91.3	537.7
2/5	381.4	.0	50.0	159.8	591.2
3/5	372.6	.0	50.0	196.3	618.9
4/5	360.5	.0	47.1	173.5	581.1
MILE 2	345.5	.0	26.4	182.6	554.5
1/5	328.0	.0	17.6	200.8	546.4
2/5	308.6	.0	.0	235.1	543.7
3/5	280.1	.0	.0	255.6	535.7
4/5	241.8	20.5	.0	223.7	486.0
MILE 3	201.7	45.1	.0	189.4	436.2
1/5	129.0	86.0	.0	210.0	425.0
2/5	115.5	84.0	.0	187.2	386.7
3/5	111.1	38.9	.0	198.6	348.6
4/5	108.2	.0	.0	200.8	309.1
MILE 4	105.3	.0	.0	136.9	242.2
1/5	102.1	.0	.0	95.9	197.9
2/5	94.8	.0	.0	84.4	179.2
3/5	91.8	.0	.0	43.4	135.2
4/5	87.5	.0	.0	27.4	114.8
MILE 5	83.1	.0	.0	.0	83.1
END LINE 34	75.4	.0	.0	.0	75.4
34 TO 33 (1/2)	81.2	.0	.0	.0	81.2

LINE 35

BEGIN LINE 35	66.6	.0	.0	.0	66.6
1/3	78.3	.0	.0	18.3	96.6
2/3	83.1	.0	.0	45.6	128.7
MILE 1	87.5	.0	.0	95.9	183.3
1/5	93.3	.0	.0	155.2	248.5
2/5	97.7	.0	.0	171.2	268.9
3/5	102.1	.0	.0	187.2	289.2
4/5	106.8	.0	.0	226.0	332.7
MILE 2	109.7	.0	.0	221.4	331.1
1/5	114.1	49.2	.0	273.9	437.1
2/5	121.4	79.9	.0	273.9	475.1
3/5	164.7	53.3	.0	283.0	501.0
4/5	200.2	43.0	.0	148.4	391.6
MILE 3	179.3	.0	.0	.0	179.3
1/10	152.8	.0	.0	.0	152.8
1/5	164.7	.0	.0	.0	164.7
2/5	261.0	.0	.0	.0	261.0
3/5	289.2	.0	50.0	95.9	435.1
4/5	313.0	.0	56.0	118.7	487.6
MILE 4	333.8	.0	58.9	127.8	520.6
END LINE 35	360.5	.0	56.0	114.1	530.6

LINE 36

BEGIN LINE 36	416.8	.0	58.9	159.8	635.5
1/5	409.5	.0	54.5	63.9	527.9
2/5	387.6	.0	.0	.0	387.6
3/5	246.3	.0	.0	.0	246.3
4/5	127.6	.0	.0	.0	127.6
MILE 2	134.9	.0	.0	.0	134.9
1/5	209.2	.0	.0	.0	209.2
2/5	230.1	.0	.0	82.2	312.3
3/5	213.6	14.3	.0	114.1	342.1
4/5	190.0	14.3	.0	114.1	318.5
MILE 3	134.9	81.9	.0	136.9	353.8
1/5	122.8	65.5	.0	127.8	316.2
2/5	117.0	38.9	.0	143.8	299.7
3/5	114.1	.0	.0	168.9	283.0
4/5	111.1	.0	.0	150.6	261.8
MILE 4	108.2	.0	.0	143.8	252.0
1/5	105.3	.0	.0	136.9	242.2
2/5	100.6	.0	.0	132.4	233.0
3/5	97.7	.0	.0	102.7	200.4
4/5	93.3	.0	.0	63.9	157.2
MILE 5	90.4	.0	.0	45.6	136.0
END LINE 36	81.2	.0	.0	.0	81.2

LINE 39

40 to 39 (1/2)	66.6	.0	.0	.0	66.6
BEGIN LINE 39	50.1	.0	.0	.0	50.1
1/5	53.0	.0	.0	.0	53.0
2/5	63.7	.0	.0	.0	63.7
3/5	76.9	.0	.0	.0	76.9
4/5	90.4	.0	.0	.0	90.4
MILE 1	97.7	.0	.0	34.2	131.9
1/5	100.6	.0	.0	63.9	164.5
2/5	105.3	.0	.0	91.3	196.6
3/5	108.2	.0	.0	132.4	240.6
4/5	109.7	.0	.0	130.1	239.8
MILE 2	114.1	32.8	.0	109.6	256.4
1/5	122.8	63.5	.0	84.4	270.8
2/5	144.0	77.8	.0	59.3	281.1
3/5	223.9	8.2	.0	59.3	291.4
4/5	262.4	.0	.0	54.8	317.2
1/10	274.2	.0	.0	.0	274.2
MILE 3	238.9	.0	.0	.0	238.9
1/5	182.3	.0	.0	.0	182.3
2/5	132.0	.0	.0	.0	132.0
3/5	201.7	.0	.0	.0	201.7
4/5	320.3	.0	.0	.0	320.3
MILE 4	396.4	.0	.0	77.6	474.0
END LINE 39	402.2	.0	32.3	132.4	566.9
39 TO 36 (1/2)	406.6	.0	45.6	219.1	671.3

LINE 40

41 TO 40 (1/2)	654.6	.0	.0	319.5	974.1
BEGIN LINE 40	617.4	.0	45.6	305.8	968.8
1/5	595.1	.0	47.1	474.7	1116.9
2/5	565.2	.0	47.1	520.4	1132.7
3/5	535.7	.0	44.1	479.3	1059.1
4/5	513.4	.0	45.6	488.4	1047.4
MILE 2	484.0	.0	66.3	593.4	1143.7
1/5	491.1	.0	44.1	661.9	1197.1
2/5	469.4	.0	51.5	570.6	1091.5
3/5	439.1	.0	57.4	493.0	989.5
4/5	416.8	.0	58.9	342.4	818.1
MILE 3	394.9	.0	54.5	246.5	695.9
1/5	364.9	.0	57.4	127.8	550.2
2/5	342.6	.0	50.0	.0	392.6
3/5	305.7	.0	.0	.0	305.7
4/5	261.0	.0	.0	.0	261.0
MILE 4	201.7	18.4	.0	73.0	293.2
1/5	130.5	73.7	.0	84.4	288.7
2/5	121.4	38.9	.0	102.7	263.0
3/5	115.5	.0	.0	109.6	225.1
4/5	108.2	.0	.0	86.7	194.9
MILE 5	105.3	.0	.0	68.5	173.8
1/5	102.1	.0	.0	50.2	152.3
2/5	99.2	.0	.0	32.0	131.1
3/5	90.4	.0	.0	.0	90.4
4/5	69.5	.0	.0	.0	69.5
MILE 6	72.5	.0	.0	.0	72.5
END LINE 40	63.7	.0	.0	.0	63.7

LINE 41

41 TO 42 (1/2)	68.1	.0	.0	.0	68.1
BEGIN LINE 41	53.0	.0	.0	.0	53.0
1/5	57.4	.0	.0	.0	57.4
2/5	68.1	.0	.0	.0	68.1
3/5	72.5	.0	.0	.0	72.5
4/5	84.5	.0	.0	.0	84.5
MILE 2	96.2	.0	.0	47.9	144.2
1/5	100.6	.0	.0	109.6	210.2
2/5	105.3	.0	.0	136.9	242.2
3/5	109.7	.0	.0	152.9	262.6
4/5	112.6	24.6	.0	155.2	292.4
MILE 3	115.5	53.3	.0	152.9	321.7
1/5	130.5	75.8	.0	150.6	356.9
2/5	209.2	.0	.0	182.6	391.8
3/5	271.3	.0	.0	121.0	392.3
4/5	307.1	.0	.0	77.6	384.7

MILE 4	345.5	.0	.0	.0	345.5
1/5	390.5	.0	.0	.0	390.5
2/5	421.2	.0	24.9	.0	446.1
3/5	443.5	.0	53.0	105.0	601.4
4/5	464.6	.0	58.9	269.3	792.9
MILE 5	482.5	.0	56.0	360.6	899.1
1/5	502.8	.0	56.0	420.0	978.7
2/5	520.7	.0	53.0	442.8	1016.5
3/5	543.0	.0	42.6	493.0	1078.6
4/5	565.2	.0	26.4	529.5	1121.2
MILE 6	583.1	.0	17.6	356.0	956.7
1/3	602.5	.0	1.5	214.5	818.5
2/3	624.7	.0	.0	182.6	807.3
END LINE 41	642.6	.0	.0	200.8	843.4

LINE 42

43 to 42 (0)	580.2	.0	.0	.0	580.2
1/4	587.5	.0	.0	.0	587.5
2/4	602.5	.0	13.2	.0	615.6
3/5	617.4	.0	27.9	82.2	727.5
T.P. TO 42	603.9	.0	47.1	301.3	952.3
BEGIN LINE 42	568.2	.0	70.8	479.3	1118.2
1/5	550.6	.0	85.7	392.6	1028.9
2/5	526.6	.0	103.6	264.8	894.9
3/5	502.8	.0	100.6	54.8	658.2
4/5	470.8	.0	11.7	.0	482.5
MILE 2	424.1	.0	.0	.0	424.1
1/5	381.4	.0	.0	.0	381.4
2/5	335.3	.0	.0	34.2	369.5
3/5	290.7	.0	.0	91.3	382.0
4/5	247.8	28.7	.0	91.3	367.8
MILE 3	204.8	43.0	.0	107.3	355.1
1/5	134.9	106.5	.0	109.6	351.0
2/5	122.8	106.5	.0	105.0	334.3
3/5	119.9	102.4	.0	45.6	268.0
4/5	114.1	65.5	.0	73.0	252.7
MILE 4	111.1	32.8	.0	91.3	235.2
1/5	108.2	.0	.0	86.7	194.9
2/5	102.1	.0	.0	50.2	152.3
3/5	90.4	.0	.0	.0	90.4
4/5	78.3	.0	.0	.0	78.3
MILE 5	66.6	.0	.0	.0	66.6
END LINE 42	63.7	.0	.0	.0	63.7

LINE 43

43 TO 44·(1/2)	60.3	.0	.0	.0	60.3
BEGIN LINE 43	51.5	.0	.0	.0	51.5
1/5	63.7	.0	.0	.0	63.7
2/5	69.5	.0	.0	.0	69.5
3/5	83.1	.0	.0	.0	83.1
4/5	99.2	.0	.0	77.6	176.8
MILE 2	109.7	51.2	.0	73.0	233.9
1/5	117.0	96.3	.0	57.1	270.3
2/5	134.9	108.6	.0	61.6	305.1
3/5	187.1	98.3	.0	38.8	324.2
4/5	246.3	71.7	.0	22.8	340.9
MILE 3	283.0	.0	.0	79.9	362.9
1/5	310.1	.0	.0	.0	310.1
2/5	335.3	.0	.0	.0	335.3
3/5	364.9	.0	.0	.0	364.9
4/5	387.6	.0	.0	.0	387.6
MILE 4	405.1	.0	.0	.0	405.1
1/5	450.0	.0	41.2	.0	491.2
2/5	470.8	.0	79.7	.0	550.5
3/5	491.1	.0	76.7	155.2	723.1
4/5	510.5	.0	69.3	182.6	762.4
MILE 5	532.7	.0	44.1	95.9	672.7
END LINE 43	550.6	.0	20.5	59.3	630.5

LINE 44

45 TO 44 (0)	461.7	.0	23.5	100.4	585.6
1/2	451.5	.0	54.5	68.5	574.4
T.P. TO 44	476.7	.0	58.9	22.8	558.4
BEGIN LINE 44	491.1	.0	47.1	18.3	556.5
1/5	491.1	.0	44.1	.0	535.2
2/5	479.6	.0	44.1	.0	523.7
3/5	491.1	.0	26.4	.0	517.5
4/5	479.6	.0	26.4	.0	506.0
MILE 2	470.8	.0	17.6	.0	488.4
1/5	461.7	.0	.0	.0	461.7
2/5	439.1	.0	.0	.0	439.1
3/5	419.7	.0	.0	.0	419.7
4/5	394.9	.0	.0	68.5	463.4
MILE 3	372.6	.0	.0	91.3	463.9
1/5	345.5	.0	.0	121.0	466.5
2/5	330.9	.0	.0	132.4	463.3
3/5	278.6	.0	.0	178.0	456.7
4/5	231.6	26.6	.0	187.2	445.4

MILE 4	167.6	65.5	.0	173.5	406.6
1/4	117.0	61.4	.0	175.7	354.2
2/4	105.3	8.2	.0	139.2	252.7
3/4	93.3	.0	.0	63.9	157.2
END LINE 44	78.3	.0	.0	.0	78.3

LINE 45

46 TO 45 (0)	63.7	.0	.0	.0	63.7
1/2	33.5	.0	.0	.0	33.5
T.P. TO 45	57.4	.0	.0	.0	57.4
BEGIN LINE 45	50.1	.0	.0	.0	50.1
1/5	68.1	.0	.0	.0	68.1
2/5	84.5	.0	.0	.0	84.5
3/5	93.3	.0	.0	.0	93.3
4/5	109.7	.0	.0	38.8	148.5
MILE 2	134.9	49.2	.0	59.3	243.4
1/5	213.6	.0	.0	175.7	389.4
2/5	269.9	.0	.0	180.3	450.2
3/5	298.0	.0	.0	182.6	480.6
4/5	308.6	.0	.0	178.0	486.6
MILE 3	317.4	.0	.0	175.7	493.1
1/5	348.8	.0	17.6	123.2	489.7
2/5	362.0	.0	57.4	63.9	483.3
3/5	378.5	.0	56.0	63.9	498.3
4/5	390.5	.0	61.9	59.3	511.7
MILE 4	402.2	.0	58.9	57.1	518.2
1/4	416.8	.0	44.1	79.9	540.8
2/4	428.8	.0	35.3	98.1	562.2
3/4	443.5	.0	23.5	105.0	571.9
END LINE 45	461.7	.0	8.8	111.8	582.3

LINE 46

46 TO 47 (1/2)	499.9	.0	.0	168.9	668.8
BEGIN LINE 46	461.7	.0	.0	148.4	610.1
1/5	440.5	.0	.0	168.9	609.4
2/5	424.1	.0	.0	159.8	583.9
3/5	405.1	.0	.0	166.6	571.8
4/5	390.5	.0	.0	166.6	557.1
MILE 2	372.6	.0	.0	159.8	532.4
1/5	351.8	.0	.0	146.1	497.8
2/5	330.9	.0	.0	132.4	463.3
3/5	348.8	.0	.0	82.2	431.0
4/5	342.6	.0	.0	68.5	411.1

MILE 3	315.9	.0	.0	86.7	402.7
1/5	313.0	.0	.0	79.9	392.9
2/5	295.1	.0	.0	73.0	368.1
3/5	298.0	.0	.0	57.1	355.1
4/5	286.3	.0	.0	41.1	327.4
MILE 4	256.6	.0	.0	63.9	320.5
1/4	209.2	.0	.0	68.5	277.7
2/4	134.9	.0	.0	136.9	271.8
3/4	105.3	.0	.0	148.4	253.6
END OF LINE 46	83.1	.0	.0	91.3	174.4

LINE 47

48 TO 47 (0)	54.5	.0	.0	.0	54.5
1/2	53.0	.0	.0	.0	53.0
T.P. TO 47	48.6	.0	.0	.0	48.6
BEGIN LINE 47	48.6	.0	.0	.0	48.6
1/5	60.3	.0	.0	.0	60.3
2/5	71.0	.0	.0	.0	71.0
3/5	83.1	.0	.0	.0	83.1
4/5	93.3	.0	.0	29.7	123.0
MILE 2	100.6	.0	.0	52.5	153.1
1/5	105.3	.0	.0	79.9	185.2
2/5	109.7	8.2	.0	257.9	375.8
3/5	114.1	34.8	.0	289.9	438.7
4/5	117.0	59.4	.0	292.1	468.5
MILE 3	121.4	79.9	.0	296.7	498.0
1/5	146.9	61.4	.0	164.3	372.7
2/5	194.4	4.1	.0	178.0	376.5
3/5	223.9	.0	.0	148.4	372.2
4/5	247.8	.0	.0	134.7	382.5
MILE 4	283.0	.0	.0	114.1	397.1
1/5	310.1	.0	.0	141.5	451.6
2/5	342.6	.0	.0	171.2	513.8
3/5	372.6	.0	.0	182.6	555.2
4/5	399.3	.0	.0	164.3	563.6
MILE 5	428.8	.0	.0	175.7	604.6
1/3	455.9	.0	.0	203.1	659.0
2/3	485.5	.0	.0	191.7	677.2
END LINE 47	514.9	.0	8.8	178.0	701.7

LINE 48

49 TO 48 (0)	758.6	.0	.0	365.2	1123.8
1/4	761.6	.0	33.8	34.2	829.6
2/4	755.7	.0	.0	18.3	774.0
3/4	669.2	.0	.0	114.1	783.4
T.P. TO 48	624.7	.0	.0	159.8	784.5
BEGIN LINE 48	535.7	.0	.0	159.8	695.4
1/5	505.8	.0	.0	91.3	597.0
2/5	464.6	.0	.0	121.0	585.6
3/5	439.1	.0	.0	125.5	564.6
4/5	402.2	.0	.0	148.4	550.6
MILE 2	375.5	.0	.0	166.6	542.1
1/5	335.3	.0	.0	171.2	506.5
2/5	300.9	.0	.0	178.0	479.0
3/5	268.4	.0	.0	205.4	473.8
4/5	227.2	16.4	.0	239.6	483.2
MILE 3	176.4	45.1	.0	319.5	541.0
1/5	127.6	84.0	.0	442.8	654.3
2/5	115.5	51.2	.0	337.8	504.5
3/5	112.6	.0	.0	285.3	397.9
4/5	108.2	.0	.0	166.6	274.8
MILE 4	105.3	.0	.0	68.5	173.8
1/5	99.2	.0	.0	20.5	119.7
2/5	93.3	.0	.0	.0	93.3
3/5	84.5	.0	.0	.0	84.5
4/5	75.4	.0	.0	.0	75.4
END LINE 48	63.7	.0	.0	.0	63.7

LINE 49

50 TO 49 (0)	57.4	.0	.0	.0	57.4
1/2	54.5	.0	.0	.0	54.5
T.P. TO 49	54.5	.0	.0	.0	54.5
BEGIN LINE 49	54.5	.0	.0	.0	54.5
1/5	66.6	.0	.0	.0	66.6
2/5	76.9	.0	.0	.0	76.9
3/5	84.5	.0	.0	.0	84.5
4/5	87.5	.0	.0	.0	87.5
MILE 2	99.2	.0	.0	45.6	144.8
1/5	105.3	.0	.0	125.5	230.8
2/5	111.1	.0	.0	264.8	375.9
3/5	117.0	8.2	.0	292.1	417.3
4/5	122.8	63.5	.0	255.6	442.0

MILE 3	158.6	73.7	.0	303.6	535.9
1/5	231.6	34.8	.0	372.0	638.4
2/5	295.1	4.1	.0	547.8	846.9
3/5	350.3	.0	.0	673.3	1023.6
4/5	405.1	.0	.0	725.8	1130.9
MILE 4	458.8	.0	.0	620.8	1079.6
1/4	517.8	.0	.0	575.2	1092.9
2/4	577.3	.0	.0	575.2	1152.4
3/4	639.7	.0	.0	547.8	1187.4
END LINE 49	699.1	.0	.0	456.5	1155.6

LINE 50

51 TO 50 (0)	809.7	.0	.0	718.9	1528.6
1/4	906.3	.0	14.7	639.1	1560.0
2/4	909.2	.0	44.1	588.8	1542.1
3/4	900.4	.0	73.8	534.1	1508.2
T.P. TO 50	898.9	.0	81.2	524.9	1505.1
BEGIN LINE 50	849.8	.0	35.3	545.5	1430.5
1/5	820.2	.0	.0	566.0	1386.2
2/5	737.8	.0	.0	579.7	1317.5
3/5	654.6	.0	.0	593.4	1248.0
4/5	583.1	.0	.0	566.0	1149.1
MILE 2	514.9	.0	.0	534.1	1048.9
1/5	455.9	.0	.0	511.2	967.1
2/5	405.1	.0	.0	474.7	879.9
3/5	345.5	.0	.0	451.9	797.4
4/5	292.2	.0	.0	465.6	757.8
MILE 3	238.9	20.5	.0	342.4	601.7
1/5	149.8	57.4	.0	232.8	440.0
2/5	117.0	.0	.0	232.8	349.8
3/5	111.1	.0	.0	150.6	261.8
4/5	105.3	.0	.0	114.1	219.4
MILE 4	96.2	.0	.0	59.3	155.6
1/4	93.3	.0	.0	27.4	120.7
2/4	87.5	.0	.0	27.4	114.8
3/4	79.8	.0	.0	.0	79.8
END LINE 50	66.6	.0	.0	.0	66.6

LINE 51

BEGIN LINE 51	54.5	.0	.0	.0	54.5
1/3	68.1	.0	.0	.0	68.1
2/3	78.3	.0	.0	22.8	101.1
MILE 2	84.5	.0	.0	45.6	130.2
1/5	93.3	.0	.0	68.5	161.8
2/5	97.7	.0	.0	136.9	234.6
3/5	100.6	.0	.0	257.9	358.5
4/5	105.3	.0	.0	260.2	365.5
MILE 3	108.2	.0	.0	164.3	272.5
1/5	111.1	.0	.0	219.1	330.2
2/5	124.7	63.5	.0	253.3	441.5
3/5	188.5	36.9	.0	333.2	558.6
4/5	238.9	26.6	.0	426.8	692.3
MILE 4	283.0	.0	.0	547.8	830.8
1/5	342.6	.0	.0	616.2	958.9
2/5	393.4	.0	.0	698.4	1091.8
3/5	437.6	.0	.0	698.4	1136.0
4/5	491.1	.0	.0	707.5	1198.6
MILE 5	565.2	.0	.0	730.3	1295.6
1/2	639.7	.0	.0	776.0	1415.7
END LINE 51	731.7	.0	.0	771.4	1503.1

LINE 52

BEGIN LINE 52	761.6	.0	.0	543.2	1304.8
1/5	705.0	.0	.0	378.9	1083.9
2/5	639.7	.0	.0	273.9	913.5
3/5	574.3	.0	.0	191.7	766.1
4/5	505.8	.0	.0	136.9	642.7
MILE 2	446.4	.0	.0	68.5	514.9
1/5	381.4	.0	.0	.0	381.4
2/5	333.8	.0	.0	.0	333.8
3/5	280.1	.0	.0	.0	280.1
4/5	227.2	12.3	.0	118.7	358.2
MILE 3	137.8	73.7	.0	130.1	341.7
1/5	119.9	14.3	.0	166.6	300.9
2/5	114.1	.0	.0	123.2	237.3
3/5	109.7	.0	.0	73.0	182.7
4/5	100.6	.0	.0	36.5	137.1
MILE 4	90.4	.0	.0	.0	90.4
1/5	79.8	.0	.0	.0	79.8
2/5	75.4	.0	.0	.0	75.4
3/5	83.1	.0	.0	.0	83.1
4/5	78.3	.0	.0	63.9	142.2

MILE 5	72.5	.0	.0	50.2	122.7
END LINE 52	66.6	.0	.0	36.5	103.1
52 TO 51 (0)	60.3	.0	.0	.0	60.3
1/3	68.1	.0	.0	11.4	79.5
2/3	65.2	.0	.0	.0	65.2
T.P. TO 51	65.2	.0	.0	.0	65.2

LINE 53

BEGIN LINE 53	66.6	.0	.0	.0	66.6
1/5	75.4	.0	.0	.0	75.4
2/5	78.3	.0	.0	.0	78.3
3/5	99.2	.0	.0	43.4	142.5
4/5	106.8	.0	.0	91.3	198.0
MILE 2	112.6	.0	.0	159.8	272.4
1/5	117.0	8.2	.0	223.7	348.9
2/5	136.4	47.1	.0	139.2	322.7
3/5	194.4	41.0	.0	159.8	395.1
4/5	241.8	10.2	.0	166.6	418.7
MILE 3	278.6	.0	.0	223.7	502.3
1/5	315.9	.0	.0	176.0	493.9
2/5	357.6	.0	.0	159.8	517.4
3/5	402.2	.0	.0	136.9	539.2
4/5	443.5	.0	.0	118.7	562.1
MILE 4	479.6	.0	.0	155.2	634.8
1/2	529.8	.0	.0	260.2	790.0
END LINE 53	592.2	.0	.0	255.6	847.8
53 TO 52 (0)	654.6	.0	.0	319.5	974.1
1/2	705.0	.0	.0	401.7	1106.7
T.P. TO 52	772.8	.0	.0	502.1	1274.9

LINE 54

BEGIN LINE 54	599.5	.0	.0	114.1	713.6
1/5	552.1	.0	.0	123.2	675.3
2/5	514.9	.0	.0	91.3	606.1
3/5	491.1	.0	.0	159.8	650.9
4/5	455.9	.0	.0	123.2	579.1
MILE 2	408.0	.0	.0	150.6	558.6
1/5	360.5	.0	.0	191.7	552.3
2/5	313.0	.0	.0	168.9	481.9
3/5	262.4	.0	.0	146.1	408.5
4/5	223.9	14.3	.0	143.8	382.0

MILE 3	185.6	32.8	.0	123.2	341.6
1/5	127.6	77.8	.0	100.4	305.8
2/5	119.9	30.7	.0	125.5	276.2
3/5	114.1	8.2	.0	136.9	259.2
4/5	108.2	.0	.0	114.1	222.3
MILE 4	100.6	.0	.0	136.9	237.6
1/2	96.2	.0	.0	86.7	183.0
54 TO 53 (0)	90.4	.0	.0	.0	90.4
1/2	78.3	.0	.0	.0	78.3
T.P. TO 53	72.5	.0	.0	.0	72.5

LINE 55

BEGIN LINE 55	97.7	.0	.0	.0	97.7
1/5	106.8	.0	.0	41.1	147.8
2/5	109.7	.0	.0	50.2	159.9
3/5	114.1	.0	.0	100.4	214.5
4/5	119.9	32.8	.0	100.4	253.1
MILE 2	129.0	63.5	.0	98.1	290.7
1/5	179.3	41.0	.0	68.5	288.8
2/5	215.1	4.1	.0	100.4	319.6
3/5	247.8	.0	.0	123.2	371.1
4/5	283.0	.0	.0	114.1	397.1
MILE 3	318.9	.0	.0	150.6	469.5
1/5	360.5	.0	.0	155.2	515.7
2/5	408.0	.0	.0	127.8	535.8
3/5	446.4	.0	.0	150.6	597.0
4/5	482.5	.0	.0	86.7	569.3
MILE 4	523.6	.0	.0	100.4	624.1
END LINE 55	574.3	.0	.0	105.0	679.3
55 TO 54 (0)	642.6	.0	.0	155.2	797.8
1/2	633.8	.0	.0	123.2	757.1
T.P. TO 54	632.4	.0	.0	79.9	712.2

LINE 56

BEGIN LINE 56	618.9	.0	.0	109.6	728.4
1/5	559.4	.0	.0	109.6	668.9
2/5	513.4	.0	.0	118.7	632.1
3/5	470.8	.0	.0	100.4	571.2
4/5	434.7	.0	.0	91.3	526.0

MILE 2	408.0	.0	.0	114.1	522.1
1/5	381.4	.0	.0	155.2	536.6
2/5	342.6	.0	.0	136.9	479.6
3/5	310.1	.0	.0	132.4	442.4
4/5	283.0	.0	.0	123.2	406.3
MILE 3	262.4	.0	.0	136.9	399.4
1/5	241.8	.0	.0	136.9	378.8
2/5	218.0	.0	.0	136.9	354.9
3/5	194.4	14.3	.0	189.4	398.2
4/5	134.9	65.5	.0	155.2	355.6
MILE 4	122.8	43.0	.0	166.6	332.5
END LINE 56	117.0	.0	.0	77.6	194.6
56 TO 55 (0)	103.8	.0	.0	29.7	133.5
1/2	94.8	.0	.0	.0	94.8
T.P. TO 55	97.7	.0	.0	.0	97.7

LINE 57 EAST

MILE 7	126.1	.0	.0	.0	126.1
1/5	121.4	.0	.0	.0	121.4
2/5	121.4	22.5	.0	43.4	187.3
3/5	121.4	51.2	.0	132.4	305.0
4/5	122.8	69.6	.0	150.6	343.1
MILE 8	129.0	81.9	.0	159.8	370.7

LINE 57 WEST

BEGIN LINE 57	136.4	129.0	.0	107.3	372.7
1/5	144.0	110.6	.0	82.2	336.7
2/5	173.5	81.9	.0	91.3	346.7
3/5	223.9	45.1	.0	109.6	378.5
4/5	256.6	36.9	.0	159.8	453.2
MILE 1	262.4	14.3	.0	203.1	479.9
1/5	265.5	.0	.0	232.8	498.3
2/5	271.3	.0	.0	214.5	485.9
3/5	275.7	.0	.0	219.1	494.8
4/5	278.6	.0	.0	246.5	525.1
MILE 2	289.2	.0	.0	241.9	531.2
1/5	313.0	.0	.0	219.1	532.1
2/5	338.2	.0	.0	223.7	561.9
3/5	359.1	.0	.0	191.7	550.8
4/5	387.6	.0	.0	196.3	583.9

MILE 3	416.8	.0	.0	159.8	576.6
1/3	450.0	.0	.0	136.9	586.9
2/3	514.9	.0	.0	86.7	601.6
END LINE 57	553.5	.0	.0	77.6	631.1
57 TO 56 (0)	620.3	.0	.0	59.3	679.7
1/2	614.5	.0	.0	73.0	687.5
T.P. TO 56	635.3	.0	.0	82.2	717.4

Station No.	Water depth, m	Corrected thickness of Unit X, m	Depth to pre-orogenic layer, m
	LINE 57		
MILE 5	783.3	.0	783.3
1/4	952.6	.0	952.6
2/4	1104.3	.0	1104.3
3/4	1156.1	44.1	1200.2
MILE 4	1185.7	73.8	1259.5
1/4	1215.3	73.8	1289.1
2/4	1230.2	81.2	1311.5
3/4	1230.2	96.1	1326.4
MILE 3	1237.6	66.3	1303.9
1/4	1237.6	73.8	1311.3
2/4	1245.2	96.1	1341.3
3/4	1252.5	126.1	1378.7
MILE 2	1252.5	171.5	1424.0
1/4	1245.2	186.7	1431.9
1/2	1245.2	209.6	1454.9
3/4	1245.2	217.3	1462.5
MILE 1	1252.5	217.3	1469.8
1/4	1237.6	234.1	1471.6
2/4	1237.6	243.2	1480.8
3/4	1237.6	271.3	1508.8
END 57	1237.6	290.5	1528.0

LINE 58

MILE 0	305.3	.0	305.3
1/4	405.8	.0	405.8
2/4	615.9	.0	615.9
3/4	826.5	.0	826.5
MILE 1	988.8	.0	988.8
1/4	1153.2	.0	1153.2
2/4	1178.4	96.1	1274.5
3/4	1193.3	88.7	1282.0
MILE 2	1193.3	81.2	1274.6
1/4	1200.7	58.9	1259.6
2/4	1208.0	81.2	1289.2
3/4	1222.9	103.6	1326.6
MILE 3	1237.6	141.2	1378.8
1/4	1245.2	194.4	1439.6
2/4	1245.2	300.2	1545.4
3/4	1245.2	310.1	1555.3
MILE 4	1237.6	320.0	1557.6
1/4	1237.6	320.0	1557.6
2/4	1237.6	310.1	1547.6
3/4	1237.6	290.5	1528.0
END 58	1237.6	280.8	1518.4
58 TO 57 (0)	1230.2	280.8	1511.1
1/2	1237.6	261.8	1499.4
T.P. TO 57	1237.6	280.8	1518.4

LINE 1

1/4	315.7	.0	315.7
2/4	354.2	.0	354.2
3/4	461.1	.0	461.1
MILE 5	591.3	.0	591.3
1/4	730.0	.0	730.0
2/4	934.7	.0	934.7
3/4	1050.9	.0	1050.9
MILE 4	1119.2	73.8	1193.0
1/4	1141.5	300.2	1441.7
2/4	1171.1	171.5	1342.6
3/4	1178.4	126.1	1304.5
MILE 3	1193.3	96.1	1289.5
1/4	1200.7	96.1	1296.8
2/4	1208.0	111.1	1319.1
3/4	1222.9	126.1	1349.1

MILE 2	1237.6	156.3	1393.9
1/4	1237.6	217.3	1454.9
2/4	1237.6	280.8	1518.4
3/4	1230.2	340.2	1570.5
MILE 1	1230.2	340.2	1570.5
1/4	1230.2	340.2	1570.5
2/4	1230.2	330.1	1560.3
3/4	1230.2	320.0	1550.3
BEGIN LINE 1	1230.2	320.0	1550.3

LINE 2

MILE 1	483.5	.0	483.5
1/4	632.0	.0	632.0
2/4	837.1	.0	837.1
3/4	1017.0	.0	1017.0
MILE 2	1074.7	133.7	1208.3
1/4	1111.6	320.0	1431.6
2/4	1133.9	576.5	1710.3
3/4	1163.4	436.1	1599.5
MILE 3	1178.4	290.5	1468.8
1/4	1193.3	194.4	1387.7
2/4	1208.0	126.1	1334.1
3/4	1222.9	118.6	1341.6
MILE 4	1230.2	148.8	1379.0
1/3	1230.2	186.7	1417.0
2/3	1230.2	217.3	1447.6
MILE 5	1227.3	265.6	1492.9
1/4	1227.3	304.1	1531.5
2/4	1227.3	294.3	1521.7
3/4	1227.3	294.3	1521.7
END LINE 2	1227.3	304.1	1531.5

LINE 3

BEGIN 3 (LINE)	63.4	.0	63.4
1/3	154.2	.0	154.2
2/3	247.4	.0	247.4
MILE 4	354.2	.0	354.2
1/4	487.9	.0	487.9
2/4	617.4	.0	617.4
3/4	746.4	.0	746.4

MILE 3	897.7	.0	897.7
1/4	1059.7	36.7	1096.5
2/4	1104.3	234.1	1338.3
3/4	1133.9	458.5	1592.3
MILE 2	1163.4	481.3	1644.7
1/4	1178.4	458.5	1636.9
2/4	1185.7	414.1	1599.8
3/4	1193.3	350.5	1543.8
MILE 1	1200.7	252.5	1453.1
1/4	1215.3	186.7	1402.0
2/4	1222.9	118.6	1341.6
3/4	1222.9	96.1	1319.1
END LINE 3	1222.9	103.6	1326.6
3 TO 4 (0)	1215.3	96.1	1311.4
1/3	1215.3	73.8	1289.1
2/3	1208.0	103.6	1311.6
T. P. TO 4	1208.0	194.4	1402.3

LINE 4

5 TO 4 (0)	43.9	.0	43.9
1/3	75.1	.0	75.1
2/3	84.3	.0	84.3
T.P. TO 4	85.8	.0	85.8
BEGIN 4	99.0	.0	99.0
1/2	284.8	.0	284.8
MILE 1	468.5	.0	468.5
1/4	638.2	.0	638.2
2/4	795.4	.0	795.4
3/4	964.6	.0	964.6
MILE 2	1087.8	.0	1087.8
1/4	1129.5	145.7	1275.2
2/4	1150.3	379.7	1530.0
3/4	1168.2	525.7	1693.8
MILE 3	1174.0	492.8	1666.8
1/4	1179.9	425.0	1604.9
2/4	1185.7	352.5	1538.2
3/4	1193.3	290.5	1483.8
MILE 4	1199.2	248.7	1447.9
1/2	1205.1	234.1	1439.1
END LINE 4	1209.4	218.8	1428.3

LINE 5

END LINE 5	82.9	.0	82.9
1/4	94.6	.0	94.6
2/4	161.5	.0	161.5
3/4	241.5	.0	241.5
MILE 5	293.6	.0	293.6
1/4	383.9	.0	383.9
2/4	588.4	.0	588.4
3/4	756.7	.0	756.7
MILE 4	946.7	.0	946.7
1/4	1150.3	.0	1150.3
2/4	1151.7	123.1	1274.9
3/4	1159.0	356.7	1515.7
MILE 3	1163.4	481.3	1644.7
1/4	1168.2	269.4	1437.5
2/4	1171.1	127.6	1298.7
3/4	1175.5	.0	1175.5
MILE 2	1102.8	.0	1102.8
1/4	1052.4	.0	1052.4
2/4	1067.4	.0	1067.4
3/4	1101.3	.0	1101.3
MILE 1	1111.6	.0	1111.6
1/4	1114.8	.0	1114.8
2/4	1147.3	29.4	1176.7
3/4	1126.5	35.3	1161.8
START LINE 5	1052.4	.0	1052.4
5 TO 6 (0)	969.0	.0	969.0
1/3	999.1	.0	999.1
2/3	986.6	.0	986.6
T.P. TO LINE 6	971.9	.0	971.9

LINE 6

BEGIN LINE 6	91.9	.0	91.9
1/3	182.3	.0	182.3
2/3	232.7	.0	232.7
MILE 1	354.2	.0	354.2
1/4	416.5	.0	416.5
2/4	569.0	.0	569.0
3/4	755.2	.0	755.2
MILE 2	879.8	.0	879.8
1/4	1102.8	.0	1102.8
2/4	1157.6	75.3	1232.8
3/4	1162.0	254.3	1416.3

MILE 3	1166.7	230.4	1397.1
1/4	1166.7	183.7	1350.4
2/4	1160.5	114.1	1274.6
3/4	1144.4	58.9	1203.3
MILE 4	1105.7	56.0	1161.7
1/4	1061.2	.0	1061.2
2/4	1019.9	.0	1019.9
3/4	1007.9	.0	1007.9
MILE 5	1004.9	.0	1004.9
1/4	1012.3	24.9	1037.2
2/4	1018.4	24.9	1043.4
3/4	1007.9	.0	1007.9
END LINE 6	1012.3	.0	1012.3

LINE 7

1/4	91.6	.0	91.6
END LINE 7	99.0	.0	99.0
1/3	158.6	.0	158.6
2/3	320.1	.0	320.1
MILE 4	374.7	.0	374.7
1/4	498.1	.0	498.1
2/4	600.1	.0	600.1
3/4	793.9	.0	793.9
MILE 3	957.0	.0	957.0
1/4	1091.1	.0	1091.1
2/4	1178.4	66.3	1244.7
3/4	1178.4	226.8	1405.2
MILE 2	1172.5	142.7	1315.3
1/4	1163.4	81.2	1244.6
2/4	1136.8	41.2	1177.9
3/4	1105.7	.0	1105.7
MILE 1	1064.4	.0	1064.4
1/4	1028.7	.0	1028.7
2/4	1007.9	.0	1007.9
3/4	996.2	.0	996.2
BEGIN LINE 7	996.2	23.5	1019.6
1/2	967.6	.0	967.6

LINE 8

9 TO 8 (0)	93.1	.0	93.1
1/2	78.5	.0	78.5
T.P. TO LINE 8	81.4	.0	81.4
BEGIN LINE 8	161.5	.0	161.5
1/3	241.5	.0	241.5
2/3	332.2	.0	332.2
MILE 1	410.6	.0	410.6
1/4	510.2	.0	510.2
2/4	706.2	.0	706.2
3/4	851.7	.0	851.7
MILE 2	1017.0	.0	1017.0
1/4	1128.0	.0	1128.0
2/4	1162.0	76.7	1238.7
3/4	1171.1	163.9	1335.0
MILE 3	1172.5	27.9	1200.4
1/4	1099.9	.0	1099.9
2/4	1040.7	.0	1040.7
3/4	1012.3	.0	1012.3
MILE 4	1007.9	.0	1007.9
1/3	996.2	.0	996.2
2/3	993.2	.0	993.2
END LINE 8	990.3	.0	990.3

LINE 9

END LINE 9	124.2	.0	124.2
1/3	255.1	.0	255.1
2/3	348.3	.0	348.3
MILE 4	431.1	.0	431.1
1/4	510.2	.0	510.2
2/4	691.6	.0	691.6
3/4	820.6	.0	820.6
MILE 3	1009.3	.0	1009.3
1/4	1126.5	.0	1126.5
2/4	1150.3	154.8	1305.1
3/4	1163.4	163.9	1327.3
MILE 2	1171.1	73.8	1244.8
1/4	1168.2	14.7	1182.8
2/4	1156.1	.0	1156.1
3/4	1144.4	.0	1144.4
MILE 1	1135.3	.0	1135.3
1/4	1126.5	.0	1126.5
2/4	1123.6	.0	1123.6
3/4	1076.1	.0	1076.1

BEGIN LINE 9	1043.6	.0	1043.6
9 TO 10 (0)	1045.1	.0	1045.1
1/2	1064.4	.0	1064.4
9 TO 10 (1)	1055.3	.0	1055.3
1/2	1094.0	.0	1094.0
T.P. TO 10	1119.2	47.1	1166.3

LINE 10

11 TO 10 (0)	179.4	.0	179.4
1/3	134.8	.0	134.8
2/3	105.2	.0	105.2
T.P. TO LINE 10	93.1	.0	93.1
BEGIN LINE 10	90.2	.0	90.2
1/4	134.8	.0	134.8
2/4	261.0	14.7	275.6
3/4	335.1	29.4	364.5
MILE 1	412.1	.0	412.1
1/4	459.7	.0	459.7
2/4	608.8	.0	608.8
3/4	744.9	.0	744.9
MILE 2	909.4	.0	909.4
1/4	1073.2	.0	1073.2
2/4	1094.0	157.8	1251.9
3/4	1116.3	99.1	1215.4
MILE 3	1138.2	47.1	1185.3
1/4	1156.1	51.5	1207.6
2/4	1145.9	60.4	1206.3
3/4	1147.3	53.0	1200.3
MILE 4	1145.9	54.5	1200.3
1/3	1143.0	51.5	1194.5
2/3	1138.2	47.1	1185.3
END LINE 10	1130.9	44.1	1175.0

LINE 11

END LINE 11	302.4	.0	302.4
1/2	404.3	70.8	475.1
MILE 4	471.4	26.4	497.8
1/4	549.6	38.2	587.8
2/4	620.3	.0	620.3
3/4	752.3	.0	752.3

MILE 3	854.6	.0	854.6
1/4	1022.8	29.4	1052.2
2/4	1025.7	93.1	1118.9
3/4	1030.1	.0	1030.1
MILE 2	1059.7	.0	1059.7
1/4	1071.8	.0	1071.8
2/4	1102.8	8.8	1111.6
3/4	1141.5	61.9	1203.4
MILE 1	1148.8	81.2	1230.0
1/4	1141.5	61.9	1203.4
2/4	1138.2	50.0	1188.3
3/4	1138.2	58.9	1197.2
MILE 0	1135.3	44.1	1179.4
1/4	1129.5	17.6	1147.1
2/4 BEGIN LINE 11	1116.3	.0	1116.3

LINE 12

13 TO 12 (0)	189.6	.0	189.6
1/3	179.4	.0	179.4
2/3	188.1	.0	188.1
T. P. TO 12	216.4	.0	216.4
BEGIN LINE 12	323.0	48.5	371.6
1/2	446.1	78.2	524.3
MILE 1	543.7	41.2	584.9
1/4	591.3	.0	591.3
2/4	707.7	.0	707.7
3/4	857.5	.0	857.5
MILE 2	1012.3	.0	1012.3
1/4	1019.9	32.3	1052.2
2/4	1027.2	.0	1027.2
3/4	1033.1	.0	1033.1
MILE 3	1055.3	.0	1055.3
1/4	1086.4	.0	1086.4
2/4	1141.5	.0	1141.5
3/4	1144.4	94.6	1239.1
MILE 4	1144.4	85.7	1230.1
1/2	1144.4	79.7	1224.1
END LINE 12	1138.2	70.8	1209.0

LINE 13

END LINE 13	302.4	42.6	345.0
MILE 4	450.5	48.5	499.0
1/4	552.5	20.5	573.0
2/4	642.6	.0	642.6
3/4	749.3	.0	749.3
MILE 3	897.7	.0	897.7
1/4	982.2	32.3	1014.5
2/4	996.2	.0	996.2
3/4	1012.3	.0	1012.3
MILE 2	1040.7	.0	1040.7
1/4	1084.9	17.6	1102.5
2/4	1126.5	209.6	1336.2
3/4	1147.3	194.4	1341.7
MILE 1	1147.3	195.9	1343.2
1/4	1150.3	179.1	1329.4
2/4	1151.7	162.4	1314.1
3/4	1150.3	145.7	1296.0
MILE 0	1145.9	132.2	1278.0
BEGIN LINE 13	1144.4	118.6	1263.0
13 TO 14 (0)	1147.3	112.6	1260.0
1/2	1156.1	136.7	1292.8
T.P. TO 14	1162.0	150.3	1312.2

LINE 14

15 TO 14 (0)	78.5	.0	78.5
1/4	78.5	.0	78.5
2/4	82.9	.0	82.9
3/4	101.9	.0	101.9
T.P. TO 14	119.8	.0	119.8
BEGIN LINE 14	231.3	.0	231.3
1/3	354.2	.0	354.2
2/3	475.8	35.3	511.0
MILE 1	579.2	35.3	614.5
1/4	666.4	45.6	711.9
2/4	742.0	.0	742.0
3/4	801.2	20.5	821.8
MILE 2	830.9	11.7	842.6
1/4	840.0	.0	840.0
2/4	979.3	.0	979.3
3/4	1067.4	44.1	1111.5
MILE 3	1071.8	24.9	1096.7
1/4	1105.7	29.4	1135.1
2/4	1141.5	133.7	1275.2
3/4	1150.3	139.7	1290.0

MILE 4	1156.1	145.7	1301.9
1/3	1159.0	166.9	1326.0
2/3	1162.0	173.0	1335.0
END LINE 14	1163.4	162.4	1325.8

LINE 15

END LINE 15	139.2	.0	139.2
1/2	296.5	.0	296.5
MILE 4	415.0	.0	415.0
1/4	556.9	.0	556.9
2/4	675.1	54.5	729.6
3/4	765.8	11.7	777.5
MILE 3	798.3	.0	798.3
1/4	825.0	94.6	919.6
2/4	822.1	.0	822.1
3/4	905.1	.0	905.1
MILE 2	955.5	41.2	996.7
1/4	1007.9	29.4	1037.2
2/4	1064.4	23.5	1087.9
3/4	1135.3	29.4	1164.7
MILE 1	1159.0	115.6	1274.7
1/4	1153.2	225.0	1378.2
2/4	1159.0	228.6	1387.7
3/4	1168.2	232.2	1400.4
BEGIN LINE 15	1172.5	214.2	1386.8
T.P. TO 15	1182.8	182.2	1364.9
1/2	1191.9	160.9	1352.8
16 TO 15 (0)	1191.9	115.6	1307.5

LINE 16

1/2	75.1	.0	75.1
T.P. TO 16	75.1	.0	75.1
BEGIN LINE 16	170.3	.0	170.3
1/2	314.2	.0	314.2
MILE 1	464.1	.0	464.1
1/4	564.6	67.8	632.4
3/8	614.4	97.6	712.1
2/4	641.1	5.9	647.0
3/4	614.4	.0	614.4

MILE 2	731.4	.0	731.4
1/4	866.7	8.8	875.5
3/8	893.4	58.9	952.3
2/4	893.4	5.9	899.2
3/4	902.1	.0	902.1
MILE 3	985.1	23.5	1008.6
1/8	985.1	23.5	1008.6
1/4	996.2	.0	996.2
2/4	1028.7	.0	1028.7
3/4	1116.3	.0	1116.3
MILE 4	1156.1	.0	1156.1
1/3	1174.0	.0	1174.0
2/3	1188.6	56.0	1244.6
END LINE 16	1187.2	126.1	1313.3

LINE 17

END LINE 17	212.0	.0	212.0
MILE 5	449.0	.0	449.0
1/4	511.7	82.7	594.4
2/4	539.3	108.1	647.4
3/4	523.4	.0	523.4
mile 4	505.4	.0	505.4
1/4	632.0	.0	632.0
2/4	810.0	.0	810.0
3/4	914.2	5.9	920.0
7/8	920.0	58.9	978.9
MILE 3	914.2	.0	914.2
1/4	893.4	.0	893.4
2/4	946.7	.0	946.7
3/4	1022.8	.0	1022.8
MILE 2	1073.2	.0	1073.2
1/4	1171.1	.0	1171.1
2/4	1200.7	53.0	1253.7
3/4	1212.4	97.6	1310.0
MILE 1	1230.2	112.6	1342.9
1/4	1245.2	106.6	1351.8
2/4	1252.5	84.2	1336.7
3/4	1256.9	94.6	1351.5
BEGIN LINE 17	1265.7	112.6	1378.3
1/2	1265.7	124.6	1390.3

LINE 18

19 TO 18 (0)	90.2	.0	90.2
1/4	81.4	.0	81.4
2/4	96.0	.0	96.0
3/4	94.6	.0	94.6
T.P. TO 18	99.0	.0	99.0
BEGIN LINE 18	216.4	.0	216.4
1/2	400.0	.0	400.0
MILE 1	558.7	.0	558.7
1/4	614.4	67.8	682.3
2/4	573.4	.0	573.4
3/4	605.9	.0	605.9
MILE 2	701.8	60.4	762.2
1/4	792.5	23.5	815.9
2/4	881.3	38.2	919.5
3/4	912.4	70.8	983.2
MILE 3	908.0	.0	908.0
1/4	890.4	.0	890.4
2/4	967.6	.0	967.6
3/4	1067.4	.0	1067.4
MILE 4	1156.1	.0	1156.1
1/4	1191.9	.0	1191.9
2/4	1227.3	.0	1227.3
5/8	1245.2	14.7	1259.9
3/4	1252.5	11.7	1264.2
MILE 5	1227.3	.0	1227.3
1/3	1227.3	.0	1227.3
2/3	1245.2	.0	1245.2
END LINE 18	1259.8	23.5	1283.3

LINE 19

BEGIN LINE 19	207.6	.0	207.6
MILE 4	394.1	.0	394.1
1/4	520.5	.0	520.5
2/4	605.9	17.6	623.5
5/8	623.2	50.0	673.3
3/4	623.2	.0	623.2
MILE 3	681.0	.0	681.0
1/4	762.9	.0	762.9
2/4	835.2	10.3	845.5
3/4	869.6	26.4	896.0
MILE 2	896.3	23.5	919.7
1/4	943.8	23.5	967.3
3/8	954.0	24.9	979.0
2/4	957.0	.0	957.0
3/4	976.3	.0	976.3

MILE 1	1010.8	.0	1010.8
1/4	1002.0	.0	1002.0
2/4	1025.7	.0	1025.7
3/4	1052.4	.0	1052.4
END LINE 19	1099.9	.0	1099.9
1/2 TURN	1120.7	14.7	1135.3
19 TO 20 (0)	1096.9	.0	1096.9
1/2	1040.7	.0	1040.7
T.P. TO 20	999.1	.0	999.1

LINE 20

1/2	93.1	.0	93.1
T.P. TO 20	122.7	.0	122.7
BEGIN LINE 20	191.1	.0	191.1
1/3	299.5	.0	299.5
2/3	395.6	.0	395.6
MILE 1	529.2	.0	529.2
1/4	623.2	88.7	711.9
2/4	632.0	.0	632.0
3/4	713.9	.0	713.9
MILE 2	801.2	.0	801.2
1/4	894.8	.0	894.8
2/4	949.6	32.3	982.0
3/4	976.3	61.9	1038.2
MILE 3	983.6	35.3	1018.9
1/4	940.9	.0	940.9
2/4	940.9	.0	940.9
3/4	957.0	.0	957.0
MILE 4	949.6	.0	949.6
1/2	946.7	.0	946.7
END LINE 20	954.0	.0	954.0

LINE 21

BEGIN LINE 21	91.6	.0	91.6
1/2	161.5	.0	161.5
MILE 4	336.6	.0	336.6
1/4	477.2	.0	477.2
2/4	605.9	.0	605.9
3/4	721.2	5.9	727.0
7/8	718.3	14.7	732.9

MILE 3	752.3	.0	752.3
1/4	822.1	.0	822.1
2/4	912.4	.0	912.4
3/4	946.7	41.2	987.9
MILE 2	982.2	106.6	1088.8
1/4	988.0	91.7	1079.7
2/4	925.9	.0	925.9
3/4	914.2	.0	914.2
MILE 1	914.2	.0	914.2
1/4	937.6	.0	937.6
2/4	925.9	.0	925.9
3/4	939.4	.0	939.4
END LINE 21	949.6	11.7	961.4
21 TO 22 (0)	958.4	32.3	990.7
1/2	949.6	33.8	983.4
T.P. TO 22	937.6	.0	937.6

LINE 22

23 TO 22 (0)	97.5	.0	97.5
1/2	90.2	.0	90.2
T.P. TO 22	201.3	.0	201.3
BEGIN LINE 22	278.5	.0	278.5
1/2	391.2	.0	391.2
MILE 1	566.0	.0	566.0
1/4	697.4	.0	697.4
2/4	801.2	.0	801.2
3/4	840.0	79.7	919.7
MILE 2	887.5	76.7	964.2
1/4	923.0	70.8	993.8
2/4	927.3	111.1	1038.5
3/4	937.6	191.3	1128.9
MILE 3	946.7	160.9	1107.6
1/4	957.0	44.1	1001.1
2/4	961.3	.0	961.3
3/4	973.4	.0	973.4
MILE 4	958.4	.0	958.4
1/2	957.0	.0	957.0
END LINE 22	934.7	.0	934.7

LINE 23

END LINE 23	101.9	.0	101.9
1/2	116.9	.0	116.9
MILE 4.5	219.3	.0	219.3
1/3	303.9	.0	303.9
2/3	383.9	.0	383.9
MILE 4	498.1	.0	498.1
1/4	615.9	.0	615.9
2/4	697.4	.0	697.4
3/4	739.1	.0	739.1
MILE 3	816.2	.0	816.2
1/4	851.7	.0	851.7
2/4	884.2	.0	884.2
3/4	910.9	.0	910.9
MILE 2	925.9	56.0	981.8
1/4	940.9	148.8	1089.6
2/4	964.6	173.0	1137.6
3/4	967.6	185.2	1152.8
MILE 1	973.4	163.9	1137.3
1/4	982.2	73.8	1055.9
2/4	982.2	35.3	1017.4
3/4	897.7	.0	897.7
BEGIN LINE 23	882.8	.0	882.8
23 TO 24 (0)	872.5	.0	872.5
1/3	860.5	.0	860.5
2/3	851.7	.0	851.7
T.P. TO 24	842.9	.0	842.9

LINE 24

25 TO 24 (0)	335.1	.0	335.1
1/3	315.7	.0	315.7
2/3	283.4	.0	283.4
T.P. TO 24	261.0	.0	261.0
BEGIN LINE 24	268.3	.0	268.3
1/4	357.1	.0	357.1
2/4	478.7	.0	478.7
3/4	532.2	.0	532.2
MILE 1	651.4	.0	651.4
1/8	756.7	.0	756.7
1/4	765.8	.0	765.8
2/4	819.1	.0	819.1
3/4	868.1	58.9	927.0
MILE 2	884.2	5.9	890.1
1/4	920.0	.0	920.0
2/4	957.0	44.1	1001.1
3/4	971.9	118.6	1090.6

MILE 3	982.2	170.0	1152.2
1/4	999.1	97.6	1096.7
2/4	967.6	.0	967.6
3/4	899.2	.0	899.2
MILE 4	878.4	.0	878.4
1/2	860.5	.0	860.5
END LINE 24	845.8	.0	845.8

LINE 25

END LINE 25	300.9	.0	300.9
1/2	395.6	.0	395.6
MILE 4	588.4	.0	588.4
1/4	819.1	.0	819.1
3/8	890.4	.0	890.4
2/4	845.8	.0	845.8
3/4	860.5	.0	860.5
MILE 3	920.0	58.9	978.9
1/4	928.8	50.0	978.8
2/4	958.4	35.3	993.7
3/4	1002.0	17.6	1019.6
MILE 2	1022.8	64.9	1087.7
1/4	1022.8	133.7	1156.5
2/4	1027.2	171.5	1198.7
3/4	1030.1	156.3	1186.5
MILE 1	1022.8	.0	1022.8
1/4	897.7	.0	897.7
2/4	845.8	.0	845.8
3/4	840.0	.0	840.0
BEGIN LINE 25	827.9	.0	827.9
25 TO 26 (0)	830.9	.0	830.9
1/4	857.5	.0	857.5
2/4	881.3	.0	881.3
3/4	923.0	.0	923.0
T.P. TO 26	952.6	.0	952.6

LINE 26

BEGIN LINE 26	600.1	.0	600.1
1/2	649.9	.0	649.9
MILE 1	804.2	.0	804.2
1/5	946.7	.0	946.7
2/5	1194.8	.0	1194.8
3/5	1015.5	.0	1015.5
4/5	952.6	.0	952.6
7/8	958.4	64.9	1023.3
MILE 3	946.7	47.1	993.8
1/4	937.6	.0	937.6
2/4	937.6	.0	937.6
3/4	1002.0	.0	1002.0
MILE 4	1055.3	85.7	1141.0
1/4	1058.3	112.6	1170.9
2/4	1061.2	88.7	1149.9
3/4	1061.2	50.0	1111.2
MILE 5	1061.2	14.7	1075.8
1/3	1037.5	.0	1037.5
2/3	1002.0	.0	1002.0
END LINE 26	973.4	.0	973.4

APPENDIX V. GEOPHYSICAL METHODS

MAGNETIC SURVEY

Total magnetic intensity in the study area was measured using flight lines 1 nautical mile apart and mostly normal to the island (Figure 37). Figure 38 was drawn by graphic subtraction of the earth's smoothed magnetic field from the measured field based on the interpretation of the smoothed total intensity for this region by Krause (1965). Magnetic storm and diurnal corrections were considered impractical because of the contour interval used and the minor data differences at crossing by a southeast to northwest flight over the length of the island. No magnetic storms occurred during the surveys (Lincoln, 1966, 1967a, 1967b). Figure 39 was drawn by use of the empirical grid-residual system (Nettleton, 1954). A center-point-and-one-ring method was used with a 4-nautical-mile ring and 2-nautical-mile grid, selected to emphasize anomalies that may indicate structure or anomalous rock masses.

SEISMIC DATA

Epicenter data from January 1934 through August 1967 obtained from the California Institute of Technology Seismological Laboratory, Pasadena, California (C. R. Allen, 1967), covers shocks within a 90-kilometer radius of 32°55'N, 118°30'W ("zero" position on San Clemente Island). This radius was arbitrarily selected for statistical purposes to encompass the major part of the northern Continental Borderland within a given radius of the island. Seismic zoning for a total of 489 shocks was compiled

as a function of frequency of occurrence, magnitude, unit area, and distance from the island.

APPENDIX VI. DEPTHS AND POSITION DATA FOR CORES AND BOTTOM SAMPLES

DEEP SUBMERGENCE SYSTEMS PROJECT AND GAAL (1966) SAMPLES

Sample no.	Depth, meters	Position	
		North	West
Deep Submergence Systems Project			
1	1134.0	32°58.6'	118°28.5'
5	960.0	33°00.7'	25.7'
8	252.0	33°03.4'	34.9'
9	95.0	32°48.2'	20.1'
10	1198.0	33°03.2'	28.3'
11	969.0	33°00.4'	25.8'
12	1077.0	32°59.7'	25.4'
16	1244.0	33°06.4'	35.6'
17	247.0	33°04.2'	39.0'
18	1218.0	33°05.5'	33.5'
30	1181.0	32°51.5'	16.2'
31	223.0	32°46.5'	22.5'
32	997.0	32°49.8'	16.4'
33	613.0	32°51.3'	21.4'
34	915.0	32°52.6'	19.2'
35	1134.0	32°54.9'	22.2'
36	658.0	32°53.8'	24.0'
37	860.0	32°56.0'	26.6'
38	521.0	32°58.4'	30.2'
39	219.0	32°58.4'	31.0'
40	860.0	33°01.3'	31.7'
41	302.0	33°02.2'	33.2'
42	995.0	32°58.5'	118°23.0'

Sample no.	Depth, meters	Position	
		North	West
	Gaal (1966)		
AHF8319	1227.8	33°05.6'	118°34.2'
AHF8320	1260.4	32°55.5'	20.3'
AHF8419	728.0	33°02.0'	23.5'
AHF8420	785.0	33°02.2'	23.8'
AHF8421	530.2	33°02.2'	31.7'
AHF8689	999.4	32°50.8'	17.9'
AHF8690	781.5	32°51.7'	22.0'
AHF8691	1150.9	32°58.7'	26.4'
NOTS-6	1157.0	33°05.5'	27.5'
NOTS-7	505.4	33°02.4'	32.9'
NOTS-8	1101.3	32°57.7'	28.4'
NOTS-9	757.9	32°51.0'	20.3'
NOTS-15	1045.8	32°55.6'	16.1'
NCEL-4	1258.6	32°56.2'	118°20.0'

DETAILED SURVEY SAMPLES

Sample no.	Depth, meters	Position	
		North	West
	SCUBA		
8	45	32°54.2'	117°32.7'
9	30	54.7'	32.9'
10	35	54.2'	32.4'
15	40	50.0'	29.6'
33	30	59.6'	35.3'
36	20	33°00.6'	35.9'
39	20	33°01.2'	117°36.6'

Sample no.	Depth, meters	Position	
		North	West
	SNAPPER		
B4	80	32°55.5'	117°33.9'
B8	230	55.1'	34.7'
B12	230	54.8'	35.6'
D5	130	55.1'	33.8'
D7	250	54.8'	34.3'
D10	340	54.6'	34.9'
F5	70	54.7'	33.6'
F7	140	54.5'	34.1'
F12	355	54.1'	35.1'
H6	105	54.1'	33.7'
H10	290	53.8'	34.4'
J4	80	54.1'	32.9'
J9	280	53.6'	33.9'
J12	345	53.3'	34.6'
Mail Point	100	52.5'	32.4'
L13	315	50.4'	33.1'
M6	95	50.9'	31.5'
M10	120	50.5'	32.2'
O4	70	50.9'	30.8'
O8	105	50.4'	31.6'
O12	275	50.0'	32.4'
Q6	95	50.3'	30.9'
Q10	120	49.8'	31.8'
Q13	255	49.4'	32.5'
S4	75	50.1'	30.3'
S8	105	49.7'	31.1'
S12	250	49.3'	32.0'
Dome	125	32°48.1'	117°31.4'